CONTEXT VERSUS CONTENT: CONTRIBUTIONS OF THE HIPPOCAMPUS AND CORTICAL ORGANIZATION TO SPATIOTEMPORAL MEMORY

AUBREY MARISSA DEMCHUK
Bachelor of Science (Honours), University of Alberta, 2008
Master of Science, University of Lethbridge, 2015

A thesis submitted
in partial fulfillment of the requirements for the degree of

DOCTOR OF PHILOSOPHY

in

NEUROSCIENCE

Department of Neuroscience
University of Lethbridge
LETHBRIDGE, ALBERTA, CANADA

CONTEXT VERSUS CONTENT:
CONTRIBUTIONS OF THE HIPPOCAMPUS AND CORTICAL ORGANIZATION TO SPATIOTEMPORAL MEMORY

AUBREY MARISSA DEMCHUK

Date of Defence: May 18, 2023

Dr. Bruce L. McNaughton *Supervisor*	*Professor*	*Ph.D.*
Dr. Robert J. Sutherland *Thesis Examination Committee Member*	*Professor*	*Ph.D.*
Dr. Majid Mohajerani *Thesis Examination Committee Member*	*Associate Professor*	*Ph.D.*
Dr. Francesco Battaglia *External Examiner* *Radboud Universiteit Nijmegen* *Nijmegen, Netherlands*	*Professor*	*Ph.D.*
Dr. Trushar Patel *Internal External Examiner*	*Associate Professor*	*Ph.D.*
Dr. Robbin Gibb *Chair, Thesis Examination Committee*	*Associate Professor*	*Ph.D.*

ABSTRACT

During learning, the hippocampus is proposed to link the distributed components of neocortical memory representations to a spatiotemporal framework. However, the continued involvement of the hippocampus after memory consolidation is debated. Moreover, the relative encoding of spatial context (descending 'where' information) versus sensory content (ascending 'what' information), and how cortical architecture supports these interactions, remains poorly understood. Thus, *in vivo* two-photon microscopy of genetically encoded Thy1-GCaMP6s calcium indicator mice was used to longitudinally image cortical volumes from retrosplenial and motor cortices during behaviour both before and after bilateral lesions of the dorsal hippocampus. While the global spatial context remained constant throughout training and imaging, two familiar obstacles were added, interchanged, or removed from a cued treadmill to decouple sensorimotor activity from location-specific activity. The results support that (1) the online binding of unreliable sensory attributes to a coherent spatial framework remains mediated by the hippocampus in pre-operatively familiar environments, (2) the descending suppression of cortical responses by the hippocampus obeys hierarchical interareal and interlaminar gradients opposite to the flow of ascending sensory inputs, (3) motor cortices exhibit weak columnar spatial tuning, and (4) probabilistic cell dynamics drive the temporal drift of memory representations. Altogether, even in familiar environments, the hippocampus appears to actively integrate current sensory information with an internal model of the environment and propagate top-down predictions throughout the cortical hierarchy to improve the efficiency of ongoing information processing.

ACKNOWLEDGEMENTS

First, thank you to my supervisor, Dr. Bruce McNaughton, and to my committee members, Dr. Majid Mohajerani and Dr. Robert Sutherland, for your comments, criticisms, and general discussion throughout this project. Your combined expertise in this field has been an invaluable asset throughout my decade-long journey from geneticist to neuroscientist. Also, thank you to Dr. Francesco Battaglia, Dr. Trushar Patel, and Dr. Robbin Gibb for taking the time to facilitate my thesis examination (and a special thanks to Dr. Patel for enthusiastically co-authoring a *completely* unrelated paper about protein nanocompartments with me during the early stages of my Ph.D. program).

I owe a colossal debt of gratitude to my many colleagues at the Canadian Centre for Behavioural Neuroscience (CCBN) whose collaborations were essential to the success of this project: HaoRan Chang for lending your analytical expertise, patiently teaching me MATLAB, and for always being a suspiciously eager collaborator; Dr. Ingrid De Miranda Esteves and Dr. Jianjun Sun for each sharing your individual surgical expertise (and a special thank you to Ingrid for frequent data discussions); Adam Neumann and Dr. Maurice Needham for (what felt like 24/7) microscopy support; Dr. Samsoon Inayat for developing the aversive air stimulus system; Di Shao for assistance with genotyping; Karim Ali for Suite2p support; Dr. Flavio Donato (University of Basel, Switzerland) and Dr. Isabelle Gauthier for helping me pilot *in utero* retroviral microinjection surgeries (that didn't even make it into this thesis!); Karen Dow-Cazal for gavaging numerous pregnant mice (which also didn't make it into this thesis!); the animal care staff for providing mouse husbandry services; Jennifer Tarnowsky for administrative support; and the rest of my CCBN family—particularly Dr. Sergey Chekov, Zak Stinson, Vicky Ivan, and Dr. Rui Pais—for

keeping my sanity in check with coffee breaks, all-you-can-eat sushi, “lab meetings”, a few soggy cycling adventures, and sardonic conversation. Of course, I am also grateful to my tiny murine comrades for keeping me company throughout the COVID-19 pandemic and for making the ultimate sacrifice in the name of scientific advancement.

Outside of the lab, words cannot express the extent of my gratitude to my partner, Jeff Harker, who graciously dealt with a lot of “life maintenance” for the both of us over the last few years. “Lub” you. I also owe thanks to my closest non-academic friends for keeping me on two wheels and reminding me that everything happens because of astrological destiny (*obviously*), not because of hard work or scientific reason. Finally, thank you to my family for fostering my scientific curiosity and for always thinking I’m the smartest person in every room.

Funding Acknowledgements: This program was funded by a Natural Sciences and Engineering Research Council of Canada (NSERC) Canadian Graduate Studentship (CGS-D3) and institutional scholarships from the University of Lethbridge. Research costs were supported by a number of grants awarded to Dr. Bruce L. McNaughton: NSERC grant RGPIN-2017-03857, Canadian Institutes of Health Research (CIHR) grants PJT156040, and PJT173523, National Institutes of Health (NIH) grants RF1NS132041 and RF1NS121764, and Compute Canada Resource Allocation grant MCI-401.

TABLE OF CONTENTS

LIST OF TABLES

LIST OF FIGURES

LIST OF ABBREVIATIONS

AMPA	α-amino-3-hydroxy-5-methyl-4-isoxazole propionic acid
ANOVA	Analysis of variance
AP	Anterior-posterior
CA1-3	*Cornu Ammonis* subfield 1-3
D5W	Dextrose 5% in water
DV	Dorsal-ventral
IEG	Immediate-early gene
L1-6 / LI-VI	Layer 1-6
LEC	Lateral entorhinal cortex
LTP	Long-term potentiation
M	Mean
M1	Primary motor cortex
M2	Secondary motor cortex
MEC	Medial entorhinal cortex
ML	Medial-lateral
NMDA	N-methyl-D-aspartate
PBS	Phosphate buffered saline
PFA	Paraformaldehyde
ROI	Region of interest
RSC	Retrosplenial cortex
S1	Primary somatosensory cortex
SEM	Standard error of the mean
SD	Standard deviation
SOM	Somatostatin
SWR	Sharp wave ripple
V1	Primary visual cortex

1. GENERAL INTRODUCTION

The hippocampus as a cognitive map

Pioneering studies of amnesic human patients have established that medial temporal lobe damage profoundly impairs declarative memory. In particular, loss of the hippocampus compromises the acquisition and recall of recent autobiographical events (episodic memory), new knowledge (semantic memory), and coherent spatial memories (Maguire et al., 2006; Penfield & Milner, 1958; Rosenbaum et al., 2005; Scoville & Milner, 1957). These seminal human studies subsequently spurred a multitude of lesion studies in animal models (e.g. in rodents: Kim & Fanselow, 1992; Morris et al., 1982), which have collectively reinforced that the hippocampus is functionally critical to the encoding and consolidation of context-dependent memories (for review see Ferbinteanu et al., 2006).

Episodic memories—embodying the "what", "where", and "when" components of lived events and experiences—allow us to recollect and mentally navigate past moments from our own lives (Tulving, 1972). Supporting the spatiotemporal aspects of episodic memory at the cellular level, the hippocampus boasts both "place" cells (O'Keefe, 1976; O'Keefe & Dostrovsky, 1971; Wilson & McNaughton, 1993) and "time" cells (Kraus et al., 2013; MacDonald et al., 2011; Pastalkova et al., 2008; Umbach et al., 2020). These cells fire in self-organized sequences to represent specific locations within a particular environment and brief intervals of passing time, respectively. During active navigation of an environment, the spatial code produced by place cells reflects the integration of multimodal sensory information stemming from motor efference copy, optic flow, proprioception, and vestibular inputs (McNaughton et al., 1989; Muller & Kubie, 1987;

O'Keefe & Speakman, 1987; Pereira et al., 2007; Quirk et al., 1990; Save et al., 1998) that together support path integration (for reviews see McNaughton et al., 1996, 2006). In conjunction with learned spatial boundaries, goals, or landmark locations, the hippocampus ultimately calibrates these egocentric (idiothetic) self-motion cues with the allocentric (world-centered) representation of a given environment (for review see Wang et al., 2020). Altogether, the discovery and characterization of place cells supported that the hippocampus is the locus of an internal representation of external space or a "cognitive map" (O'Keefe & Nadel, 1978; Tolman, 1948).

Complementary learning systems in the hippocampus and neocortex

In seminal studies of human patients with hippocampal damage, retrograde amnesia was observed to be temporally graded such that remote—but not recent—declarative memories remained intact (e.g. Penfield & Milner, 1958; Scoville & Milner, 1957). This finding suggested that the hippocampus was only a temporary store for episodic memories and inspired the prevailing theory that memory consolidation occurs in two stages (Buzsáki, 1989; Marr, 1971; McClelland et al., 1995; Squire & Alvarez, 1995; Treves & Rolls, 1994). First, during behaviour, the hippocampus rapidly receives and links ascending sensory information from the neocortex to a spatiotemporal framework—a neural "index code"—that is unique to each experience (Nadel & Willner, 1980; Teyler & DiScenna, 1986). During the second stage of memory consolidation, which occurs during subsequent slow-wave sleep or quiet wakefulness, the hippocampal index code is thought to facilitate the coordinated retrieval of the distributed components of the neocortical representation. This process is proposed to drive a progressive redistribution of synaptic weights in the neocortex, imparting long-lasting changes to cortical connectivity even without continued

training (Takehara-Nishiuchi & McNaughton, 2008; Figure 1.1). In support of this theory, the sequences of neural activity that occur during awake behaviour have been shown to be simultaneously "replayed" in both the hippocampus (Kudrimoti et al., 1999; Skaggs & McNaughton, 1996; Wilson & McNaughton, 1994) and the neocortex (Euston et al., 2007; Ji & Wilson, 2007; Peyrache et al., 2009; Qin et al., 1997). Ultimately, the interplay between the hippocampus and the cortex is thought to enable the latter to gradually extract broader statistical regularities or stimulus generalities (i.e. semantic "schemas") across overlapping episodes (Marr, 1970; McClelland et al., 1995). This theoretical framework has been recently updated to reflect that neocortical learning might not always be slow *per se* but, rather, the rate of memory consolidation may depend on the amount of relevant prior knowledge that is available to augment the interleaving of new associations within existing schemas (McClelland, 2013; Tse et al., 2007, 2011; van Kesteren et al., 2012).

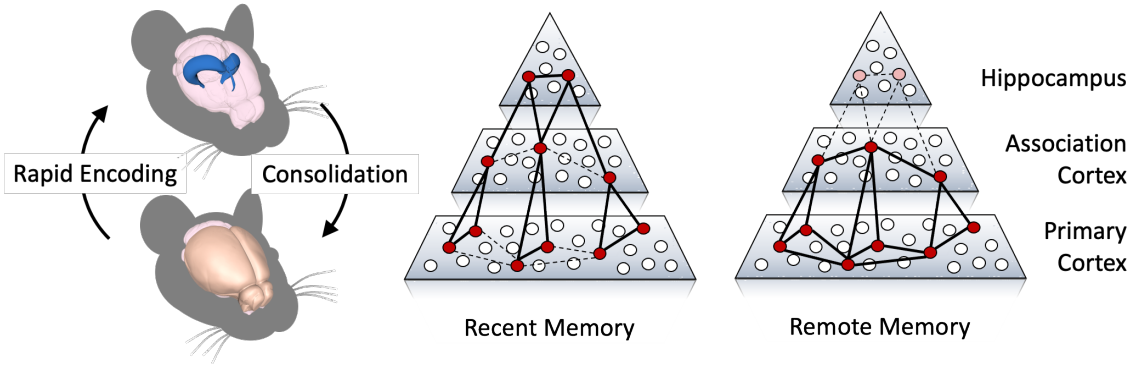

Figure 1.1: Hippocampal-neocortical interactions during memory encoding and retrieval according to the standard model of systems consolidation. During learning, distributed sensory inputs from the neocortex (gold) converge on the hippocampus (blue) where a spatiotemporal "index code" is rapidly generated. After initial encoding, spontaneous or cued reactivation of an incomplete pattern of cortical activity can engage the hippocampal index, which reinstates a complete memory representation in the cortex and drives consolidation processes. Over time, cortical connections become sufficiently strengthened such that remote memory retrieval becomes independent of the hippocampus. Figure created with the Scalable Brain Atlas (Bakker et al., 2015; Lein et al., 2007).

In recent years, genetic tagging and optogenetic manipulation of hippocampal cell ensembles have validated a number of predictions made by hippocampal indexing theory. First, the subset of neurons in the hippocampus, neocortex, and amygdala that are active during context-dependent fear conditioning are also more likely to be reactivated during post-learning sleep and subsequent retrieval (Ghandour et al., 2019; Reijmers et al., 2007; Tayler et al., 2013). Second, direct inhibition (Tanaka et al., 2014) or reactivation (Ghandour et al., 2019; Liu et al., 2012; Robinson et al., 2020) of a hippocampal ensemble can impair or induce memory recall, respectively. For instance, Liu et al. (2012) demonstrated that reactivation of hippocampal dentate gyrus neurons, initially active during fear conditioning, was sufficient to induce freezing behavior in the relevant context. Finally, synthetic associative memories can be generated by the coincident activation of neuronal ensembles that represent elements of distinct experiences (Garner et al., 2012; Ohkawa et al., 2015; Ramirez et al., 2013). As an example, when activated dentate gyrus neurons from an unconditioned context were later optically reactivated during fear conditioning in a different context, a "false" memory was formed and subjects showed freezing behaviours in the unconditioned context where a foot shock never occurred (Ramirez et al., 2013).

Further supporting that memory consolidation is orchestrated by the hippocampus, the coordinated replay of behaviourally-relevant activity patterns coincides with brief, high frequency network oscillations called hippocampal sharp wave ripples (SWRs; Buzsáki, 1986; Kudrimoti et al., 1999). Disruption of hippocampal SWRs after spatial learning impairs subsequent task performance (Ego-Stengel & Wilson, 2010; Girardeau et al., 2009; Jadhav et al., 2012) and cortical ensembles relating to recent learning are more likely to be reactivated concurrently with SWRs (Peyrache et al., 2009). Notably, hippocampal SWRs

and replay events do not strictly precede and spontaneously initiate neocortical replay events (Karimi Abadchi et al., 2020; Rothschild et al., 2017). Instead, there is evidence of a cortical-hippocampal-cortical loop surrounding SWR complexes such that pre-SWR cortical activity can precede and predict patterns of hippocampal reactivation, which, in turn, also predicts subsequent post-SWR cortical reactivation (Rothschild et al., 2017). These findings are consistent with yet another prediction made by hippocampal indexing theory: spontaneous or cued reactivation of a partial cortical memory representation should be sufficient to trigger pattern completion in the hippocampus which, consequently, initiates reinstatement of the complete cortical memory representation (Marr, 1971; McClelland et al., 1995; Rolls, 2013; refer to Figure 1.1).

Hippocampus-dependent recall of remote episodic memories

According to the standard model of systems consolidation, cortical memory representations are assumed to be gradually strengthened until they are functionally independent of the hippocampus (refer to Figure 1.1). While this theory is heavily influenced by seminal observations of human patients that exhibited temporally-graded loss of declarative memories after medial temporal lobe damage (Kirwan et al., 2008; Penfield & Milner, 1958; Scoville & Milner, 1957; but see Steinvorth et al., 2005), a dissociation may exist between the hippocampal-dependence of semantic and episodic memories. Numerous other studies of human patients with bilateral hippocampal damage have typically confirmed a temporally-graded loss of semantic memories but, conversely, reported flat impairments in the retrieval of both recent and remote autobiographical memories (e.g. Cermak & O'Connor, 1983; Damasio et al., 1985; Tulving et al., 1988; for review see Nadel & Moscovitch, 1997). In these patients, any surviving autobiographical

memories notably lacked spatiotemporal specificity and resembled little more than generalized knowledge. Moreover, amnesic patients also exhibit deficits in coherently narrating imagined scenarios such that episode descriptions are typically composed of fragmented elements that lack a holistic context, much like their descriptions of past events (Hassabis et al., 2007; Race et al., 2011). Functional imaging studies have confirmed that the hippocampus remains engaged during recall of both recent and remote autobiographical memories (Addis et al., 2004; Gilboa et al., 2004; Maguire et al., 2001; Ryan et al., 2001; Viard et al., 2007) but hippocampal activation declines as a function of memory age for retrieval of semantic knowledge (Harand et al., 2012; Smith & Squire, 2009). Thus, the online binding of context-dependent memory elements and the coherent retrieval of detailed episodic memories may be enduringly dependent on an intact hippocampus. Nevertheless, these results do not preclude the possibility that a large amount of time, experience, or emotional salience might enable detailed contextual memories to become independent of the hippocampus (Teng & Squire, 1999).

In rodents, there are numerous examples of temporally-graded retrograde amnesia following hippocampal damage where remote memories are spared, particularly after contextual fear conditioning (Anagnostaras et al., 1999; Kim & Fanselow, 1992; Maren et al., 1997; but see Sparks et al., 2011) and in the social transmission of food preferences (Clark et al., 2002; Ross & Eichenbaum, 2006; Winocur, 1990; but see Thapa et al., 2014). However, complete and dorsal lesions of the hippocampus more often result in ungraded retrograde amnesia after spatial learning (Bolhuis et al., 1994; Clark et al., 2005; Martin et al., 2005; Mumby et al., 1999; Sutherland et al., 2001). Moreover, episodic memories can transition into a more generalized form that becomes independent of the hippocampus but this occurs at the expense of context-specificity (Wiltgen et al., 2010; Wiltgen & Silva,

2007; Winocur et al., 2007). Thus, regardless of the interval of time separating training and recall, an intact hippocampus may also remain essential for performing spatial tasks and/or for composing a coherent cognitive map.

Implications of cortical organization for memory

The neocortex can be divided into mesoscale regions based on distinct contributions to sensory perception, motor control, decision-making, attention, spatial memory, and other specialized cognitive functions. During information processing, the projection topology between these functional modules is hierarchically organized (Felleman & Van Essen, 1991; Schwindel & McNaughton, 2011). Sensory information is initially relayed by the thalamus to unimodal primary sensory areas of cortex. Secondary and other supplemental sensory cortices subsequently provide additional processing before transmitting the information to higher association areas for multimodal integration with subcortical inputs, altogether supporting higher level cognition. Ultimately, this highly processed information converges on the hippocampus, which is reciprocally connected with association cortices, enabling both conjunctive indexing of ascending sensory information and, in turn, descending control over memory consolidation and retrieval (refer to Figure 1.1).

Despite the clear functional delineation of these various cortical regions, the majority of the neocortex has a relatively uniform anatomy and stereotyped circuitry, suggesting a common underlying computational basis for all cognitive processes (Douglas et al., 1989; Douglas & Martin, 2004; Harris & Mrsic-Flogel, 2013; Thomson & Lamy, 2007). In general, the neocortex consists of six distinct horizontal laminae that differ in thickness, cell morphology, cell density (Keller et al., 2018), patterns of gene expression (Belgard et al., 2011), cell physiology (Senzai et al., 2019), and connectivity with other

layers and functional regions (Douglas & Martin, 2004; Markram et al., 2015; Weiler et al., 2008). Spanning layers II-VI, this horizontal architecture is also intersected by a modular vertical circuitry called "minicolumns" that are thought operate in parallel within larger "macrocolumns" (Mountcastle, 1997). Together, this cortical organization provides a scaffold for the hierarchical interareal and interlaminar interactions of feed-forward or "bottom-up" sensory inputs originating in the thalamus and primary cortices with feedback or "top-down" contextual information from the hippocampus and higher-level cortices. However, while both the horizontal and vertical circuitry are largely evolutionarily preserved across mammalian cortices (Buxhoeveden & Casanova, 2005; Nieuwenhuys, 1994; Rakic, 2009; Shepherd & Rowe, 2017), the contribution of these distinct anatomical divisions to the computational capacity of the brain remains poorly understood.

Overview of study objectives

The continued involvement of the hippocampus in remote memory retrieval remains a contentious topic. Moreover, the relative encoding of spatiotemporal context versus sensory content among neocortical cells has been largely unexplored and any interactions between higher-level and lower-level inputs are plausibly mediated by the hierarchical, modular architecture of the cortex. Therefore, this thesis examined the contributions of regional (Chapter 3), laminar (Chapter 4), and columnar (Chapter 5) neocortical topography to spatiotemporal memory representations, with a particular focus on the continued influence of the hippocampus on the context, content, and time-dependent (Chapter 6) coding characteristics of the spatiomotor pathway. To achieve this, *in vivo* two-photon microscopy of genetically encoded calcium indicator mice (Chen et al., 2012) was utilized to longitudinally image neurons spanning superficial layers of retrosplenial cortex (RSC)

and layers II-Va of primary motor (M1) and secondary motor (M2) cortex during behaviour. For comparison to hippocampal place cells, the dorsal CA1 region of the hippocampus was also imaged in a separate cohort of mice according to the same behavioural paradigm. While the global spatial context remained constant throughout training and imaging, two familiar obstacles were added, interchanged, or removed from a cued treadmill to decouple sensorimotor activity from location-specific activity. In addition, the experimental paradigm was replicated for each cortical region of interest after bilateral sham or dorsal hippocampal lesions to examine the level of influence maintained by the hippocampus over cortical spatial representations during recurrent exploration of a familiar environment.

2. MATERIALS AND METHODS

Animals

A total of nineteen adult hemizygous C57BL/6J-Tg(Thy1-GCaMP6s)GP4.3Dkim/J ("Thy1-GCaMP6s"; Jackson Laboratory #024275) mice were used: eleven males and eight females (with initial craniotomies completed by 3-4 months of age). Of those 19 mice, three (2 males and 1 female) were implanted with a hollow cylinder to enable imaging of the CA1 subregion of the hippocampus. The remaining sixteen mice (9 males and 7 females) received a typical cranial window for imaging of cortical regions. Of those latter sixteen mice, ten (6 males and 4 females) received excitotoxic lesions of the dorsal hippocampus and six (3 males and 3 females) received sham lesions after training and pre-lesion imaging. Age-matched littermates were split equally between the sham and lesion groups when possible. Following the initial cranial window surgery, mice were housed individually in standard, plastic rodent cages under constant humidity, temperature, and a twelve hour light/dark cycle. Mice were experimentally manipulated during the light cycle and both food and water were available *ad libitum* throughout the experiment. All procedures were performed in accordance with the Canadian Council on Animal Care guidelines and following protocols approved by the Institutional Animal Care and Use Committee at the University of Lethbridge.

Surgical procedures

Cranial window implantation: Before surgery, mice were administered buprenorphine (0.05 mg/kg, subcutaneous), dexamethasone (2 mg/kg, intramuscular), and 0.5 ml of dextrose 5% in water (D5W) with atropine (0.06 mg/kg, subcutaneous). Mice

were then anesthetized with 1.5% isoflurane and immobilized in a stereotaxic frame with body temperature maintained at 37°C by a regulated heating pad. Lidocaine (0.5%, 7 mg/kg, subcutaneous) was injected under the skin at the incision site. Once the skull was exposed, a custom-made titanium head-plate was fixed to the skull using adhesive cement (Metabond®, Parkell) and dental acrylic (Jet™ Tooth Shade Powder and Liquid, Lang Dental Manufacturing Co.). For imaging of cortical regions, a bilateral craniotomy, 4 mm in diameter, was performed above dorsal cortex (centered at Bregma; AP & ML: +2 mm to -2 mm). The cranial window—composed of a 6 mm diameter round coverslip stacked over two 4 mm diameter coverslips and affixed with optical adhesive (NOA71, Norland)—was implanted over the craniotomy and attached to the skull with Vetbond™ (3M). For imaging of CA1, a 3 mm craniotomy was performed above the right hippocampus (centered at AP: -2.5 mm, ML: -1.5 mm). Cortical tissue was aspirated to a depth of 1 mm and a hollow glass cylinder (1.5 mm long and 3 mm in diameter) capped with a 3 mm coverslip (affixed with optical adhesive; NOA71, Norland) was inserted until the coverslip touched the exposed cortical white matter. The cylinder was then attached to the skull with Vetbond™ (3M; Figure 2.1A). For both cortical and hippocampal windows, dental acrylic was used to create a well around the imaging window and a rubber O-ring was fixed to the outer edge of the of the head-plate to help retain water during immersion of an objective lens. Mice received subcutaneous injections of meloxicam (Metacam®, 1 mg/kg) and enrofloxacin (Baytril®, 10 mg/kg) post-operatively and once daily for an additional three days following the surgery. Mice were allowed to recover for a minimum of two weeks before behavioural training and two-photon microscopy (Figure 2.2A).

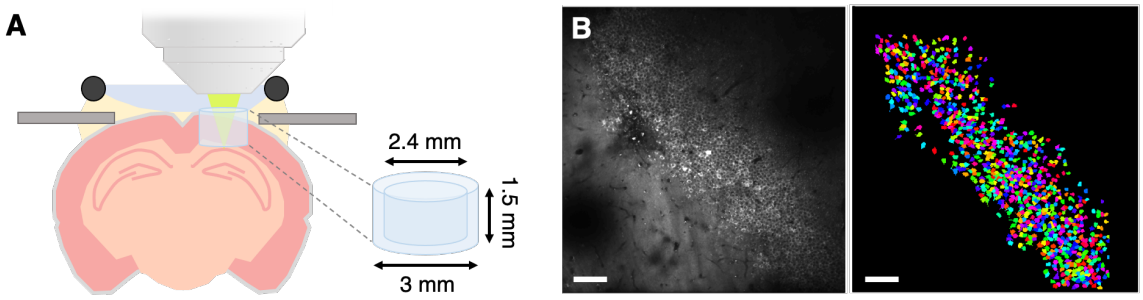

Figure 2.1: Chronic two-photon imaging of dorsal hippocampus. (A) Schematic of dorsal CA1 two-photon imaging preparation and implanted hollow glass cylinder. (B) Example 835 µm x 835 µm mean image (left; contrast-enhanced for clarity) from CA1 and the corresponding Suite2p-detected neurons (right). Scale bar is 100 µm.

Hippocampal excitotoxic and sham lesions: Before surgery, mice were administered phenobarbital (30 mg/kg, intraperitoneal), meloxicam (Metacam®, 1 mg/kg, subcutaneous), dexamethasone (2 mg/kg, intramuscular), and 0.5 ml of D5W with atropine (0.06 mg/kg, subcutaneous). Mice were then anesthetized with 1-1.5% isoflurane, and immobilized in a stereotaxic frame with body temperature maintained at 37°C by a regulated heating pad. A dental drill was used to create four small holes (two per hemisphere) in the dental adhesive surrounding the craniotomy and the skull for injection sites targeting the dorsal hippocampal formation (AP -2.3 mm, ML +/-1.5 mm, DV 1.8 mm and AP -3.2 mm, ML +/-2.5 mm, DV 2.0 mm; the locations of the injection sites are shown in Figure 2.2D). Eight pulses (9.2 nL/pulse for a total of 73.6 nL) of 15 mg/ml N-methyl-D-aspartate (NMDA; Sigma-Aldrich) in 1x phosphate-buffered saline (PBS) was then injected at each site with a Nanoject II auto-nanoliter injector (Drummond Scientific) and a beveled micropipette (20-30 µm tip diameter) with an inter-pulse interval of 15 seconds. For sham lesions, the micropipette was loaded and inserted into the hippocampus at the

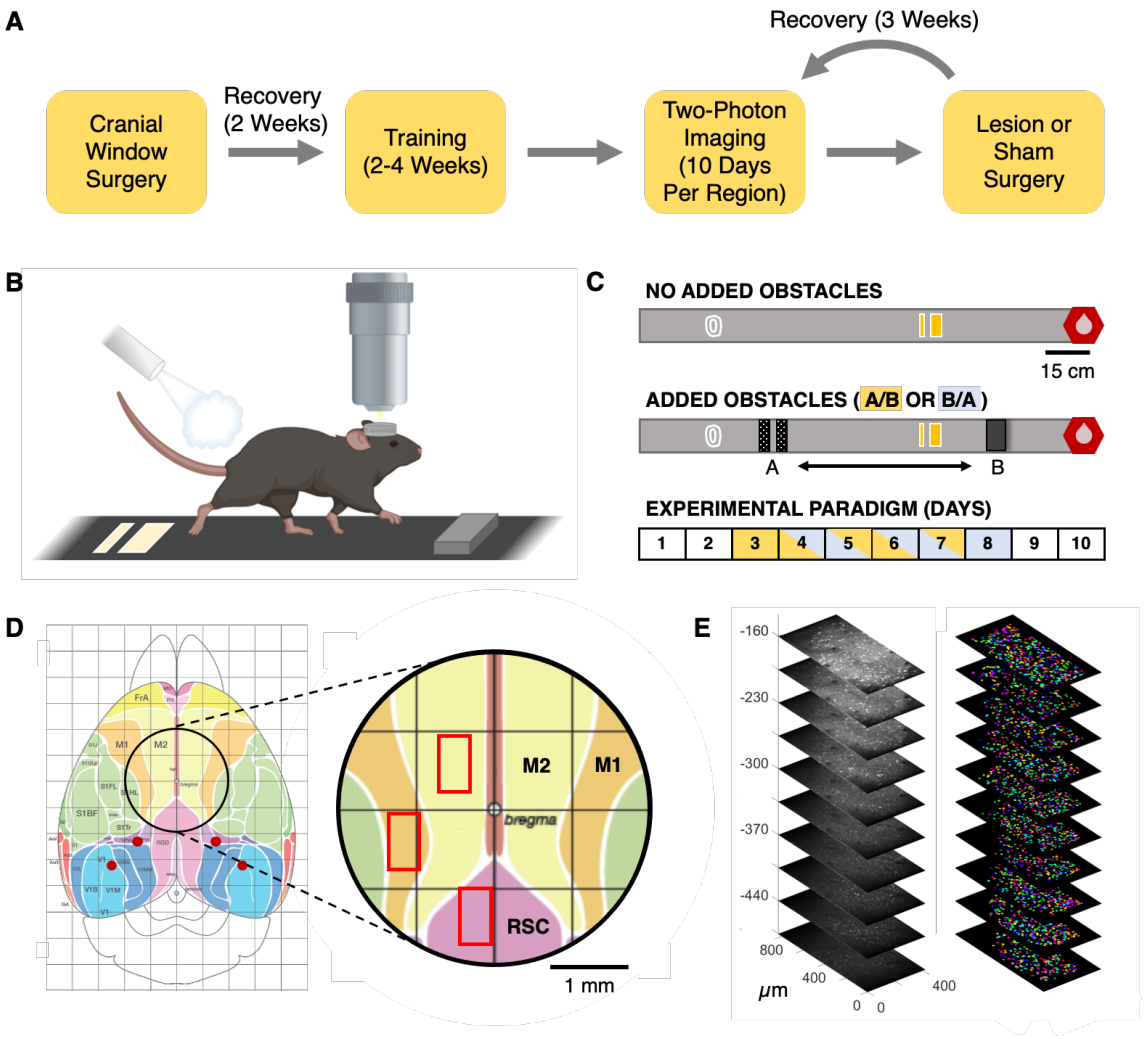

Figure 2.2: Overview of the experimental paradigm and two-photon imaging of the neocortex. (A) Workflow for the surgeries, training, and chronic two-photon imaging. (B) Schematic diagram of a head-fixed mouse on the treadmill belt situated under a two-photon microscope. A mild aversive air stimulus directed at the rump was used to motivate running. Figure created with BioRender.com. (C) The 150 cm treadmill belt had two static cues (reflective tape strips and glue circles) and two interchangeable obstacles (A: rough Velcro strips and B: a raised block) that were added in the indicated positions during the ten-day experimental paradigm (shown below). On days 1-2 and 9-10, mice ran on the familiar treadmill belt without added obstacles. One days 3 and 8, the obstacles were added in orientations A/B and B/A, respectively, but remained static throughout the imaging session. During days 4-7, the obstacles were pseudo-randomly added to the treadmill belt and their position was interchanged mid-way through the session. (D) Cortical regions of interest within the cranial window area and example positions of the 417 μm x 835 μm imaging frames (red rectangles) over RSC, M2, and forelimb M1 (adapted from Kirkcaldie, 2012). NMDA and sham injection sites are shown as red dots. (E) Example maximum intensity projection *z*-stack from M2 spanning ten frames from -160 to -475 μm below the cortical surface (left) and the corresponding Suite2p-detected neurons (right).

injection sites but no pulses were administered. The injection sites were subsequently closed with dental adhesive, and diazepam (5 mg/kg, intraperitoneal) was administered to both sham and lesion animals to prevent seizures. Mice also received injections of meloxicam (Metacam®, 1 mg/kg, subcutaneous) and enrofloxacin (Baytril®, 10 mg/kg, subcutaneous) post-operatively and once daily for an additional three days following the surgery. Mice were allowed to recover for a minimum of 21 days to allow sufficient time for the NMDA to exert its excitotoxic effects (refer to Figure 2.2A). The bilateral and dorsal extent of the hippocampal lesions were qualitatively predicted by nest construction behaviours prior to experiments (see Chapter 8, Supplementary Data).

Behaviour

Training: During the first three days of training, head-fixed mice were acclimatized to a mildly aversive air stimulus and trained to run on a non-motorized treadmill in response to it (Figure 2.2B; see Chapter 8, Supplementary Data). An automated solenoid valve-based system was used to direct a continuous air stream from a regulated compressed air supply towards the rump of the mice (Inayat et al., 2023). During these first three training sessions, progressively longer running distances were required to trigger cessation of the air stimulus, at which point the mice could move freely on the belt without the air stimulus for 15 seconds. After the initial three days, the air stimulus duration was increased such that mice had to run one complete lap of the belt (150 cm) to trigger cessation of the air stimulus, at which point a brake was applied to prevent movement during the 15 second intertrial interval. This brake point occurred whenever a photoelectric sensor (Omron) was triggered by reflective tape attached on the opposite side of the belt, and coincided with delivery of a ~1 µl strawberry-flavoured milk reward dispensed by a solenoid pinch valve (Bio-Chem).

A custom-designed circuit and microcontroller (Arduino Uno, Farnell) were used to control reward delivery, as well as air stimulus onset and offset. Mice were trained daily for a minimum of 2 weeks and until they ran consistently for 20 minutes (the duration of a typical imaging session).

The treadmill belt—used for both training and subsequent experiments—was constructed with a 150 cm length of Velcro (Country Brook) and included two static visuotactile cues, hot glue circles (Figure 2.3A) and reflective tape strips (Figure 2.3B), as well as two separate but identical squares of treadmill material that both joined the ends of the belt and marked where two obstacles would later be attached during experiments (Figure 2.2C, "No Added Obstacles"). Two polyamide wheels (10 cm in diameter) were used to guide the circular treadmill belt, and an optical encoder (Avago Tech) attached to the wheel shaft was used to monitor the belt movement during behaviour.

Experimental paradigm: One region of interest (dorsal CA1, anterior RSC, posterior medial M2, or forelimb M1*; Figure 2.2D) was imaged for ~20 minutes per day for ten consecutive days. On days 1-2 and 9-10, mice ran on the familiar treadmill belt used during training (i.e. no added obstacles). On days 3 and 8, two additional obstacles—rough Velcro strips (obstacle A; Figure 2.3C) and a soft block-like barrier (obstacle B; Figure 2.3D)—were added in orientations A/B, respectively, but remained static throughout these imaging sessions. During days 4-7, obstacles A and B were added in a pseudo-random order to the

---

* It should be noted that, while the imaged region in M1 most closely corresponds with the forelimb region, there is considerable variability observed among rodent species and individual subjects in microstimulation studies (Hall & Lindholm, 1974; Neafsey et al., 1986; Pronichev & Lenkov, 1998; Tennant et al., 2011). Thus, both trunk and hindlimb regions of M1 may be included within this imaging area to some extent.

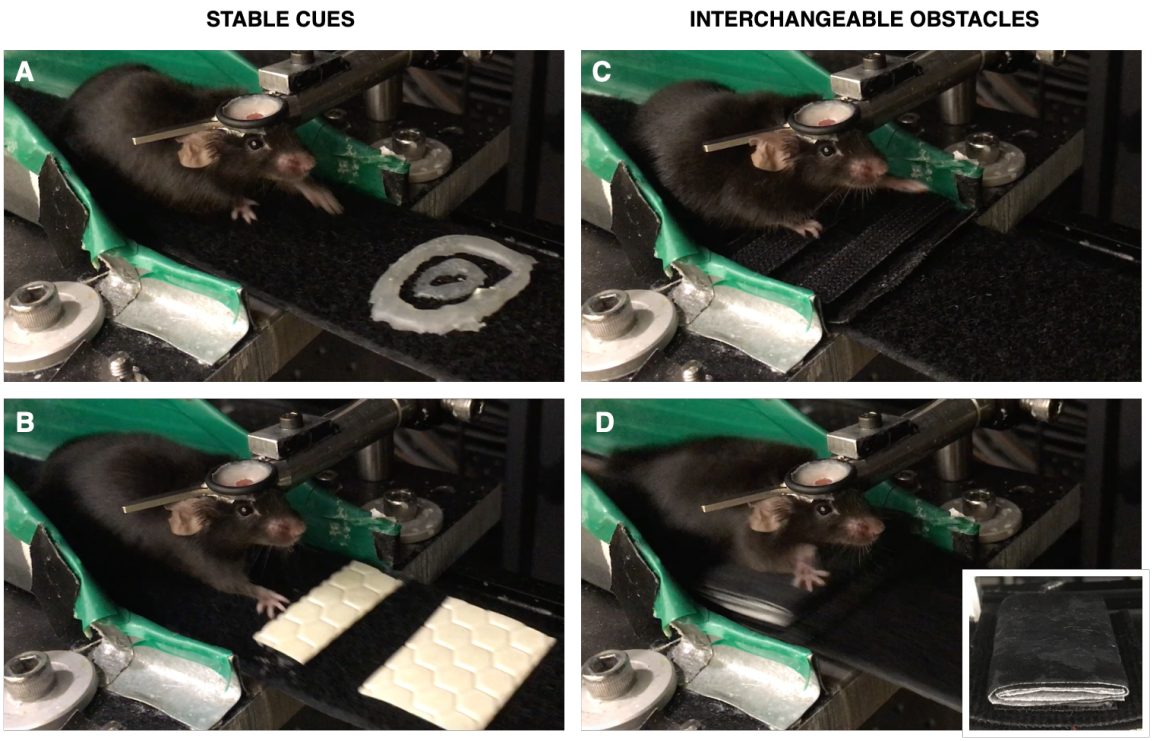

Figure 2.3: Stable visuotactile cues and interchangeable obstacles added to the treadmill belt during the experimental paradigm. The treadmill belt—used for both training and subsequent experiments—was a 150 cm length of soft Velcro that included two static visuotactile cues: (A) hot glue circles and (B) reflective tape strips. During days 3-8 of the experimental paradigm, two obstacles were added to the belt that interchanged positions: (C) rough Velcro strips and (D) a soft block-like barrier (inset shows side view). Note that the Velcro strips were not a purely tactile cue but required a pulling motion during traversal due to friction from the barrier on the opposite side of the belt as it passed through the open braking system. In these images, the objective lens, second headplate stabilizing bar, and the reward delivery system were removed from the apparatus for clarity.

treadmill belt and their positions were interchanged mid-way through the session (refer to Figure 2.2C). As during training, mice had to run one complete lap of the belt to trigger cessation of the air stimulus, at which time the brake was applied, a milk reward was delivered, and there was a 15 second intertrial rest interval. Mice were given a minimum of three days of rest after completion of the ten day paradigm before another cortical region was imaged using the same methods. The order that each region of interest was imaged was varied for each mouse. The imaging paradigm was then repeated after bilateral sham or hippocampal lesions for each region of interest.

Two-photon microscopy

Images were acquired using a Thorlabs Bergamo II multi-photon microscope. A Ti:Sapphire femtosecond pulsed laser (Coherent Chamelion Ultra II)—tuned to an excitatory wavelength of 920 nm—was passed through a 16x water immersion objective (Nikon; NA = 0.8; 80–120 mW output power measured at the sample). Using a galvo-resonant scanner and a piezoelectric oscillator (PI), twelve 836 μm × 418 μm planes, each separated in the *z*-dimension by 35 μm and spanning a total depth of 385 μm across layers II–V of the cortex, were sequentially acquired (Figure 2.2E). Emitted signals were amplified using a GaAsP photomultiplier tube (Hamamatsu) and each frame was digitized to a resolution of 384 x 192 pixels at a sampling rate of 5 Hz. For dorsal CA1, the galvo-resonant scanner was used to acquire a single 835 μm x 835 μm plane, which was digitized to a resolution of 800 x 800 pixels at a sampling rate of 19 Hz (Figure 2.1B). Photosensor and rotation encoder signals were acquired and synchronized with imaging data using a data acquisition system (Axon Instruments Digidata 1322A) and Clampex software (Axon

Instruments). During imaging, a strip of Velcro was wrapped around the body of the objective and lowered to the level of the cranial window to block ambient light.

Histology

During sacrifice, mice were deeply anesthetized with an intraperitoneal injection of sodium pentobarbital (1000 mg/kg) and perfused transcardially with 1x PBS and 4% paraformaldehyde (PFA; Sigma-Aldrich). Following fixation, brains were extracted, post-fixed overnight in 4% PFA, and subsequently cryoprotected in 30% sucrose in 1x PBS with 0.02% sodium azide. Coronal sections (40 μm) were prepared using a sliding microtome (Model 860; American Optical Instrument Co.). Sections were collected in 1x PBS, manually mounted on Superfrost Plus slides (Fisher Scientific), and dried before coverslipping with VECTASHIELD antifade mounting medium (Vector Laboratories).

A NanoZoomer (Hamamatsu Photonics) scanning microscope was then used to acquire images of all coronal sections. For both sham controls and mice with hippocampal lesions, the area of intact hippocampus and subiculum in each hemisphere of each section was measured using the freehand region drawing tool in the NDP.view2 image viewing software (Version 2.3.1; Hamamatsu Photonics). The total volume of intact hippocampus and subiculum per hemisphere was then calculated by multiplying the observed area in each section by the section thickness (40 μm) and summing the resulting volumes across all sections. Mice with lesions that comprised less than 50% of the total mean volume of sham lesioned hippocampii (including both dorsal and ventral regions) were excluded. That is, only mice with complete dorsal lesions were included in post-lesion analyses (Figure 2.4).

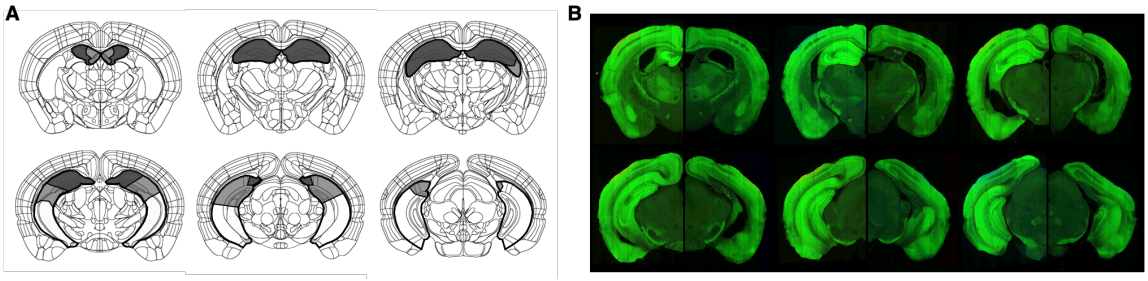

Figure 2.4: Extent of bilateral dorsal hippocampal lesions. (A) Schematic depictions of the maximum extent (shaded grey) and minimum extent (dark grey) of dorsal hippocampal lesions included in the experiment. Note that the dorsal subiculum was also lesioned. Figure adapted from the Allen Mouse Brain Atlas (Allen Brain Institute for Science, 2011; Lein et al., 2007). (B) Example images of a sham control (left hemisphere) relative to a mouse with bilateral dorsal hippocampal lesions (right hemisphere). Images were contrast-enhanced for clarity.

Image processing and analysis

For each brain region of each animal, all imaging sessions were combined across days for automated image registration, cellular region of interest (ROI) detection, and activity extraction. For imaging frames that could be accurately re-aligned before and after surgery, all imaging sessions from that particular region were combined across all days from both pre- and post-surgery conditions for processing. Suite2p (Pachitariu et al., 2016) was used to automatically detect neuronal ROIs (refer to Figures 2.1B and 2.2E) and the extracted fluorescent traces were deconvolved by constrained non-negative matrix factorization (Friedrich et al., 2017; Pnevmatikakis et al., 2016). All automatically-detected cellular ROIs were manually assessed to ensure that neurons were not duplicated, improperly segmented, or misclassified. For all datasets, the most superficial two planes and all flyback frames were excluded from analyses.

Spatially selective cells were identified as previously described (Chang et al., 2020; Esteves et al., 2021) using custom-written MATLAB (The Mathworks; version R2019a)

code (available at https://github.com/LelouchLamperougeVI/pc_analysis). Briefly, two criteria needed to be met for a neuron to be classified as spatially selective. First, the spatial information (SI) conveyed by a neuron about the animal's location needed to exceed the 95th percentile of a shuffled distribution. Spatial information was computed as in Skaggs et al. (1993):

$$\mathrm{SI} = \sum_{i=1}^{N} p_i \frac{f_i}{f} \log_2 \frac{f_i}{f}$$

where the average neuronal activity (f_i) in the i^{th} bin over the total average activity (f), weighted by the occupancy (p_i), was evaluated over $N = 50$ spatial bins (1 bin = 3 cm). The null distribution of SI was obtained by circularly shifting the timecourse vectors of neuronal activities 1000 times by a random factor. Second, the place fields of neurons were identified by conducting a continuous wavelet transform over the spatial tuning curve using a Ricker (Mexican Hat) wavelet. The scales evaluated were $\Sigma = \{1, 2, 3, \ldots, 50\}$ corresponding to the $N = 50$ spatial bins. Local maxima exceeding 3 median absolute deviations from the wavelet coefficients at the lowest scale of the transform ($\sigma = 1$) were identified as potential place fields. If a local maximum fell within the bounds of another maximum at a higher scale (i.e. a wider place field), the candidate with the narrower place field was discarded. The width of a place field was restricted between 5-80% of the length of the environment and the mean activity within a place field had to be 2.5 times higher than the activity outside of place fields. Peak activity during individual trials must also have occurred within the place field in at least a third of the total trials. Cells that exhibited one or more place fields satisfying these criteria were considered to be spatially selective.

For differentiation of cue- and place-tuned cells, analyses were restricted to spatially selective cells with maximum mean normalized activity within the binned locations trailing the interchangeable obstacles. These locations were demarcated by the leading boundary of each obstacle and the area trailing those obstacles that exhibited elevated fractions of place fields relative to days with static cues only (Figure 2.5A). In addition, place fields within these boundaries often changed locations with the interchangeable obstacles (Figure 2.5B) and this area of the treadmill also roughly corresponded to the mean length of a mouse (15 cm; Figure 2.5C). Cue cells were defined as those spatially selective cells that exhibited maximum mean normalized activity across days with added obstacles at the position of one specific moving obstacle, regardless of its location on the track, whereas place cells were defined as spatially selective cells that always exhibited maximum mean normalized activity at the same location on the track, regardless of which obstacle was present (Figure 2.5D).

Lifetime sparsity—a measure of how diffuse the firing of an individual neuron is in the spatial domain—was calculated as in Jung et al. (1994):

$$sparsity = \frac{(\sum_{i=1}^{N} p_i f_i)^2}{\sum_{i=1}^{N} p_i f_i^2}$$

where f_i is the average neuronal activity in the i^{th} bin, weighted by the probability of occupancy (p_i), and evaluated over $N = 50$ spatial bins. Sparsity ranges between 0 and 1, where smaller values indicate narrower spatial tuning profiles (i.e. firing was more sparse).

Population activity was decoded using an independent Bayesian decoding algorithm (Mao et al., 2018; Zhang et al., 1998). Briefly, for every time bin (1 second), the probability (P) of being at a position (x) given the population response of all imaged neurons was estimated as:

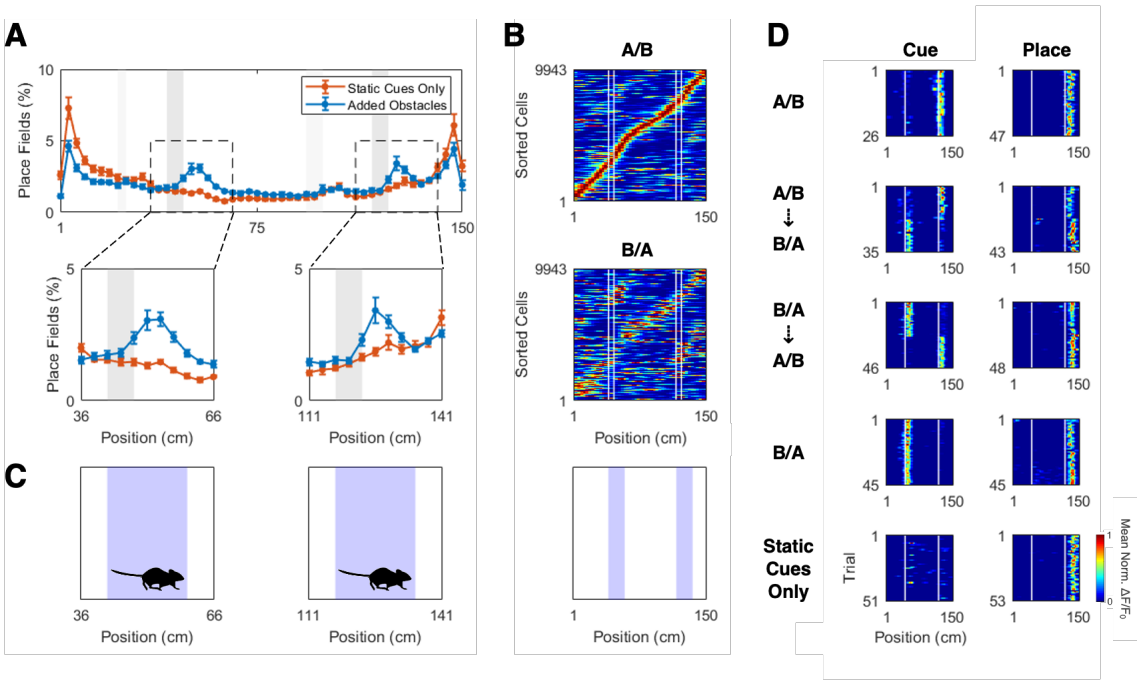

Figure 2.5: Criteria for the classification of spatially selective cells as place- or cue-tuned at the interchangeable obstacle locations. (A) Top: binned distributions of place field locations detected across RSC, M2, and M1 spanning the length of the treadmill belt and averaged across days with static cues only (orange) and days with added obstacles (blue). Error bars are SEM. Gray bars indicate positions of stable cues (light gray) and interchangeable obstacles (dark gray). The outsets highlight an increased representation of fields trailing the obstacle locations (position A on left and position B on right). Note that the position of the forelimb is one bin (3 cm) delayed from where imaging occurs. (B) Spatially selective cells were pooled across M2 of all pre-surgery mice on a cue swap day. Top: spatially selective cells were sorted by the order of maximum mean normalized $\Delta F/F_0$ during trials with obstacles in the A/B position. Bottom: maximum mean normalized $\Delta F/F_0$ during trials with obstacles in the B/A position sorted by the order of maximum mean normalized $\Delta F/F_0$ during trials with obstacles in the A/B position (top). White lines indicate the boundaries of the interchangeable obstacles. (C) The regions of the environment (blue) that were analyzed for activity relating to the interchangeable obstacles for cue and place cell classification analyses, which corresponded to both (A) the locations of increased place fields after the obstacles were added and (B) place field movement during the cue swaps. (D) Representative cue cell and place cell from M2. Normalized mean $\Delta F/F_0$ across laps on example days with the added cues in a stable configuration (A/B or B/A), on cue-swap days (A/B→B/A or B/A→A/B), and a day without the added cues (Static Cues Only). White lines indicate the center positions of the two interchangeable obstacles.

$$P(x|n) = C\left(\prod_{i=1}^{N} f_i(x)^{n_i}\right) exp\left(-\tau \sum_{i=1}^{N} f_i(x)\right)$$

where $f_i(x)$ is the mean deconvolved fluorescence trace over position, n_i is the time-course vector of the i^{th} neuron within a time bin of length τ, N is the number of neurons, and C is a normalizing constant which makes the probability distribution across all positions sum to one. For within-session decoding, odd trials were used for training the model, and even trials were used to evaluate decoding error. Decoded position was defined as the position with the highest probability for any given time bin, and Bayesian decoding error was the absolute value of the difference between true position and decoded position. To account for differences in the number of detected cells across mice, Bayesian decoding analyses were restricted to a random sampling of cells equal to the lowest number of detected cells in any region of interest across mice (n = 267 cells).

For topographical analyses (Chapter 5), neuronal ensembles that exhibited co-activity during running or spontaneous co-activity during intertrial rest were detected using agglomerative clustering as in Chang et al. (2020). Briefly, activity vectors were first smoothed using a Gaussian kernel (σ = 1 second) to reduce temporal noise. Next, the Pearson correlation coefficient (R) between smoothed activity vectors for each pair of neurons was calculated and converted to a distance metric (d = 1-R). Hierarchical clustering was then performed on the upper triangle of the distance matrix using unweighted average distance linkage criterion and a threshold of d < 0.75 for assignment to an ensemble cluster. Ensembles containing fewer than 10 co-active neurons were excluded. Finally, the silhouette coefficient was used to determine how topographically clustered the detected ensembles were (Rousseeuw, 1987). For each detected ensemble (i), the mean Euclidean

distance between neurons within an ensemble (a) was compared to the mean Euclidean distance from the nearest ensemble (b) as follows:

$$s(i) = \frac{b(i) - a(i)}{\max(a(i), b(i))}$$

Silhouette scores range from -1 to 1; a high value indicates compact clustering between neuronal members of an ensemble and separation from neighbouring ensembles, whereas a negative value indicates that ensembles are highly overlapping and poorly clustered.

To quantify the change in mean population activity vector correlation across days (Chapter 6), the decay constant (r) was derived from the following equation:

$$N_t = N_0 e^{-rt}$$

where N_t is the correlation at time t, and N_0 is the correlation between even and odd trials on day 0. For all calculations, t = 4 d was used.

Statistical analyses were performed using MATLAB (The Mathworks; version R2019a) and GraphPad Prism (version 9.4.1). For repeated measures analysis of variance (ANOVA) calculations, sphericity was not assumed and the Geisser-Greenhouse correction was applied, if necessary. In figures, the level of significance is indicated as: *$p < 0.05$, **$p < 0.01$, and ***$p < 0.001$.

3. COHERENT REPRESENTATION OF A FAMILIAR CONTEXT IN THE NEOCORTEX DEPENDS ON AN INTACT HIPPOCAMPUS

3.1 ABSTRACT

During navigation, the neocortex must actively integrate learned spatial context with current sensory experience to guide effectual behaviours. Accordingly, cortical neurons have been shown to exhibit place cell-like activity, and the emergence of uniform cortical spatial representations is dependent on an intact hippocampus. However, the relative encoding of spatial context versus the sensory content of experience, and whether the hippocampus continues to modulate the properties of spatially selective cortical cells in familiar environments, remains poorly understood. Thus, *in vivo* two-photon microscopy of genetically encoded Thy1-GCaMP6s calcium indicator mice was used to chronically image neurons in retrosplenial and motor cortices, both before and after bilateral dorsal hippocampal lesions. While the global spatial context remained constant throughout training and imaging, two familiar obstacles were added, interchanged, or removed from a cued treadmill to decouple sensorimotor activity from location-specific activity. Fractions of both place- and cue-tuned cells were evident at the obstacle locations and these cell types each formed interareal gradients such that higher-level cortical regions exhibited higher fractions of place cells, whereas lower-level regions exhibited higher fractions of cue cells. After bilateral dorsal hippocampal lesions, position-correlated sequences became more cue-tuned in RSC, supporting that the hippocampus dynamically maintains a coherent representation of space in the presence of unreliable cues and descending spatial modulation obeys the interareal hierarchy opposite to the flow of ascending sensory inputs.

3.2 INTRODUCTION

Navigation relies on a cortical spatiomotor pathway

In laboratory tasks, rodents exploit learned associations between goals and landmarks to navigate their environment (e.g. Morris, 1981), a strategy that is likely also employed under naturalistic conditions. As such, volitional behaviour within a familiar environment must rely on an internal representation of external space that is formed during prior experience. In addition, this world-centered cognitive map must also be flexibly translated back into a body-centered spatial coordinate system to robustly guide locomotor output within egocentric space (Wang et al., 2020). Thus, effectual navigational behaviours hinge on descending projections from the canonical hippocampal feedback pathway and downstream association areas, particularly posterior parietal and retrosplenial cortices, which have been demonstrated to encode spatial information in both allocentric and egocentric reference frames (Alexander & Nitz, 2015; Clark et al., 2018; Wilber et al., 2014).

In addition to an internal perception of space, behaviour also relies on active sensory processing to guide movements towards goals and flexibly adapt to unexpected perturbations. Hence, as an animal navigates a familiar environment, the cortex must actively integrate learned spatial context with current sensory experience. Within the spatiomotor pathway, M2 exhibits striking interconnectivity with association, sensory, and motor cortices (Hoover & Vertes, 2007; Olsen et al., 2019; Reep et al., 1990; Yamawaki et al., 2016) and thus is well-positioned to integrate bottom-up sensory signals with top-down spatial predictions for planning and initiating voluntary behaviours. Moreover, although most forms of motor learning do not depend on the hippocampus, learning arbitrary

sensorimotor associations does, and M2 plays an important role in this (Murray et al., 2000; Murray & Wise, 1996; Wise & Murray, 1999). These perceptual and cognitive information streams—in parallel with modulatory signals from the striatum and cerebellum—ultimately converge on the primary output structure of the cortex, M1, which directly interfaces with the brainstem and corticospinal tract to execute behaviour.

Cortical correlate of a spatial map in RSC

The RSC is anatomically situated at the interface between the hippocampal formation and the motor cortices, suggesting a pivotal role for RSC subregions in conveying internal representations of space to cortical sensorimotor networks during navigation. RSC is a major target of projections from both CA1—the primary origin of hippocampal output—as well as the adjacent subiculum and parahippocampal regions, with the RSC granular b (A29c) subregion receiving the bulk of these projections (Cenquizca & Swanson, 2007; van Groen & Wyss, 2003; Wyss & van Groen, 1992). The more dorsally located dysgranular RSC (A30), which is the focus of this study, is primarily reciprocally connected to subiculum (van Groen & Wyss, 1992a), but is also innervated by distal CA1 and parahippocampal regions and exhibits extensive reciprocal connectivity with the entire rostrocaudal extent of RSC granular b (Shibata et al., 2009; Sugar et al., 2011; van Groen & Wyss, 1992a, 2003; Vogt & Miller, 1983). Dysgranular RSC also receives considerable thalamic inputs that originate in the anterior, laterodorsal, and reuniens nuclei (Shibata, 1993; van Groen & Wyss, 1992b, 1992a) and boasts more extensive corticocortical connectivity than other RSC subregions, most notably with visual and motor cortices (Vogt & Miller, 1983; Yamawaki et al., 2016).

Based on this pattern of anatomical connectivity, it is unsurprising that the function

of RSC overlaps with that of the hippocampus. RSC lesions impair performance in both allocentric and egocentric spatial memory tasks (Cooper & Mizumori, 1999; Sutherland et al., 1988; Vann & Aggleton, 2004, 2005; Whishaw et al., 2001), contextual fear-conditioning (Keene & Bucci, 2008a, 2008b), as well as object-location discrimination (Vann & Aggleton, 2002). Moreover, RSC exhibits cellular correlates of spatial encoding: head-direction cells (Chen et al., 1994; Cho & Sharp, 2001), border cells (Alexander et al., 2020; van Wijngaarden et al., 2020), and place cells (Esteves et al., 2021; Mao et al., 2017, 2018). Despite these parallels, the roles of the hippocampus and RSC are not indistinguishable. RSC neurons preferentially respond to behaviourally salient cues that predict reward, encode navigational landmarks, or relate to task demands (Fischer et al., 2020; Smith et al., 2012; Vedder et al., 2017) and, accordingly, post-learning replay events in the RSC are also biased towards the locations of landmarks and rewards (Chang et al., 2020). In addition, artificial stimulation of neural ensembles in RSC can elicit learned context-specific behaviours in the absence of a functional hippocampus (Cowansage et al., 2014) and remote contextual memories continue to remain dependent on the RSC after learning (Corcoran et al., 2011; Katche et al., 2013; Maviel et al., 2004; Todd et al., 2016). Taken together, the RSC is speculated to assume a long-term role in storing allocentric representations of contextual associations, particularly between stable navigational cues within a given environment.

Sensorimotor integration for action planning in M2

A particularly prominent cortical target of both monosynaptic and disynaptic RSC projections is posterior M2, which is located immediately anterior to RSC (Vogt & Miller, 1983; Yamawaki et al., 2016). This region of M2 is also diversely innervated by primary

motor, somatosensory, visual, auditory, olfactory, insular, orbital, posterior parietal, and medial prefrontal cortical afferents (Hoover & Vertes, 2007; Reep et al., 1990; Yamawaki et al., 2016) and is interconnected with various thalamic nuclei (Reep & Corwin, 1999). The efferent targets of M2 are equally diverse (Reep et al., 1987) but, in particular, this multimodal associative region makes conspicuous connections with downstream motor regions. M2 is not only reciprocally connected with neighbouring M1 but also projects to subcortical brain regions associated with motor control including the striatum (Reep & Corwin, 1999), the superior colliculus and oculomotor nuclei in the brainstem (Stuesse & Newman, 1990), and along the corticospinal tract to the spinal cord (Donoghue & Wise, 1982).

Rodent M2, considered a specialized subdivision of medial prefrontal cortex, bears an anatomical and functional resemblance to primate prefrontal cortex, frontal eye field, supplementary motor cortex, and premotor areas (Barthas & Kwan, 2017; Hoover & Vertes, 2007; Reep et al., 1990). Together with the broad diversity of inputs from sensorimotor modalities and the prominent reciprocal connections with RSC and posterior parietal cortex, this homology strongly suggests an associative role for rodent M2 in facilitating the integration of sensory information with descending cognitive inputs for action planning. Accordingly, bilateral inactivation or lesions of M2 cause enduring sensorimotor deficits in cue-guided motor tasks (Passingham et al., 1988; Siniscalchi et al., 2016), without any discernible effects on motor output. Lesion and inactivation studies also highlight a role for M2 in the learning—but not the execution—of skilled movements (Cao et al., 2015) and novel action sequences (Yin, 2009). Notably, neural activity in M2 reliably precedes both forced (Olson et al., 2020) and choice-specific movement initiation (Chen et al., 2017; Guo et al., 2014; Li et al., 2016) and action-tuned cells also encode multiple

context-specific variables including location, orientation, route progress, and the expected value of outcomes (Gremel & Costa, 2013; Olson et al., 2020; Sul et al., 2011). Altogether, M2 appears to broadly support the flexible adaptation of behaviour by mediating sensory-motor transformations during context-dependent action selection and sequence learning.

From plan to action in M1

Sensorimotor information and volitional commands ultimately converge on M1, the primary behavioural output structure of the cortex. Relative to M2, rodent M1 makes far fewer cortico-cortical connections and is predominantly interconnected with primary somatosensory cortex (S1; Aronoff et al., 2010; Mao et al., 2011; Reep et al., 1990). M1 receives additional ascending sensory projections from secondary somatosensory cortex and higher-order sensory thalamic areas, as well as descending inputs from orbital cortex and M2 (Hooks et al., 2013; Suter & Shepherd, 2015; Ueta et al., 2014). Modulatory information from the cerebellum and the basal ganglia is also conveyed to M1 via projections from motor-related thalamic nuclei, including the ventral anterior, ventromedial, and ventrolateral nuclei (Hooks et al., 2013; Kuramoto et al., 2009; Yamawaki et al., 2014). Although rodent M1 projects directly to the corticospinal tract (Donoghue & Wise, 1982), monosynaptic connections to spinal motoneurons largely regress after post-natal development and, instead, interactions are typically routed through the reticular formation in adults (Alstermark et al., 2004; Maeda et al., 2016).

Seminal electrophysiological studies in non-human primates have historically posited that the motor cortex governs low-level movement kinematics, with single cells encoding the force (Evarts, 1968), direction (Georgopoulos et al., 1982), and velocity of movements (Moran & Schwartz, 1999). While the stimulation of M1 neurons has also been

directly linked to muscle activation patterns (Fritsch, 1870; Kakei et al., 1999; Morrow et al., 2007), the role of M1 is not simply to execute basic motor commands. At the population level, the activity of M1 neurons reflects higher-level sensorimotor transformations including preparation for movement (Churchland et al., 2006; Tanji & Evarts, 1976), active sensation (Ferezou et al., 2007; Petreanu et al., 2012), context-dependent adaptation of motor behaviours (Omlor et al., 2019), and the spatiotemporal movement trajectories that underlie complex behaviours (Hatsopoulos et al., 2007; Saleh et al., 2012). Fundamental to these roles, M1 has also been strongly implicated in sensorimotor learning (Huber et al., 2012; Iriki et al., 1989; Pavlides et al., 1993) and is crucial for acquiring stereotyped movement sequences (Kawai et al., 2015). After learning, however, the behavioral consequences of M1 impairments are limited to dexterous movements (Kawai et al., 2015; Lawrence & Kuypers, 1968). In rodents, for example, lesions or inactivation of M1 can hinder skilled reaching for a food pellet (Guo et al., 2015; Whishaw, 2000), manipulation of a joystick (Hwang et al., 2022), or stepping on a rotarod or ladder rungs (Farr et al., 2006). Importantly, these studies emphasize that the absence of input from M1 does not preclude use of the same muscle groups for untrained behaviours, and compensatory mechanisms fail to restore the dexterous movement sequences. Altogether, the primary role of M1 may lie in the learning of novel spatiotemporally stereotyped movement patterns and the task-specific execution of complex, sensory-guided actions.

Study objectives

During navigation, the neocortex must actively integrate learned spatial context with current sensory experience to guide effectual behaviours. Accordingly, descending hippocampal feedback has been shown to influence the functional properties of

cortical neurons. Akin to place cells in the hippocampus, large proportions of neurons in superficial RSC, M2, M1, S1, posterior parietal cortex, medial prefrontal cortex, and primary visual cortex (V1) have recently been shown to exhibit spatially selective activity during navigation (Esteves et al., 2021; Fujisawa et al., 2008; Mao et al., 2017; Saleem et al., 2018; Zielinski et al., 2019). Importantly, the emergence of uniform spatial representations of novel environments in the cortex—including RSC, M2, and M1—is impeded by bilateral lesions of the dorsal hippocampus (Esteves et al., 2021; Mao et al., 2018). Nevertheless, cortical spatial representations of familiar environments largely survive such lesions, a defining characteristic of memory consolidation (Esteves et al., 2023). However, the relative encoding of spatial context versus the sensory content of experience, and whether the hippocampus continues to modulate the properties of spatially selective cortical cells in familiar environments, remains to be determined. To address these questions, *in vivo* two-photon microscopy of genetically encoded Thy1-GCaMP6s calcium indicator mice was used to longitudinally image spatially selective cells in retrosplenial and motor cortices, as well as place cells in hippocampal CA1 for comparison. While the global spatial context remained constant throughout training and imaging, two familiar obstacles were added, interchanged, or removed from a cued treadmill to decouple sensorimotor activity from location-specific activity. In addition, the experimental paradigm was replicated for each cortical region of interest after bilateral sham or dorsal hippocampal lesions to assess the level of influence maintained by the hippocampus over position-correlated neural activity in the spatiomotor pathway.

3.3 RESULTS

Spatially selective cells were ubiquitous in the hippocampus and neocortex

Consistent with previous studies (Esteves et al., 2021; Mao et al., 2017), large proportions of active cells in RSC, M2, and M1 were found to exhibit spatially selective activity and these cells composed position-correlated activity sequences that uniformly tiled the treadmill environment (analogous to place cells in CA1; Figure 3.1A-B; see Table 3.1 for total detected cell counts). The fractions of detected cells that were classified as spatially selective were significantly different across regions among pre-surgery animals (one-way ANOVA & Tukey's test, $F(3,27)=1.189$, $p<0.01$), with M2 exhibiting fewer spatially selective cells than RSC ($p<0.01$) and CA1 ($p<0.05$; Figure 3.1C). Notably, spatially selective cells in CA1 encoded significantly higher median spatial information (one-way ANOVA & Tukey's test, $F(3,27)=15.56$, $p<0.001$; Figure 3.1D) and lower median sparsity indices (one-way ANOVA & Tukey's test, $F(3,27)=12.21$, $p<0.001$; Figure 3.1E) relative to all examined cortical regions. Otherwise, spatially selective cell characteristics were comparable across CA1 and all examined cortical regions of pre-surgery animals including place field distribution (two-sample Chi-square tests & Bonferroni corrected $\alpha=0.01$, $p=0.02$-0.45; Figure 3.1F); median place field width (one-way ANOVA, $F(3,27)=1.336$, $p=0.28$; Figure 3.1G); and the fraction of spatially selective cells exhibiting only one place field (or, conversely, multiple fields; one-way ANOVA, $F(3,27)=1.846$, $p=0.11$; Figure 3.1H. However, CA1 exhibited a significantly elevated fraction of spatially selective cells with only one place field (two-tailed t-test, $p<0.05$) relative to cortical cells when grouped across examined regions (refer to Figure 3.1F).

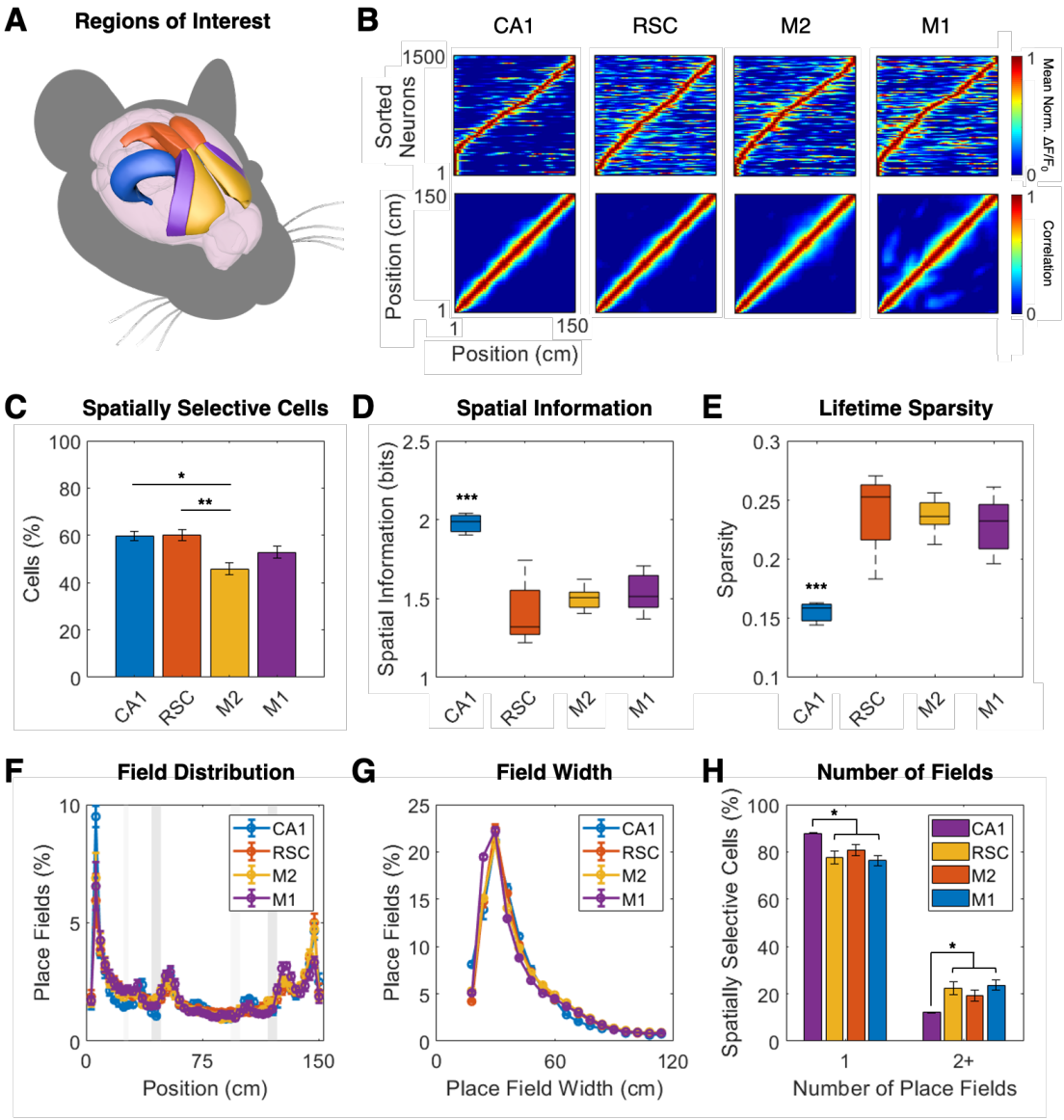

Figure 3.1: Comparison of pre-surgery spatially selective cell characteristics in hippocampal CA1 and cortical regions (RSC, M2, and M1). (A) Regions of interest: hippocampus (blue), RSC (orange), M2 (yellow), and M1 (purple). Figure created with the Scalable Brain Atlas (Bakker et al., 2015; Lein et al., 2007). (B) Top: spatially selective cells were pooled across mice and a random selection of 1500 cells from each region were sorted by the order of maximum mean normalized $\Delta F/F_0$ on a day with static cues only. Bottom: Pearson correlation matrices of sorted cells. (C) Proportions of all detected cells that were classified as spatially selective. (D) Spatial information encoded by spatially selective cells. For all boxplots, line: median; box: 25th and 75th percentiles; whiskers: minimum and maximum values; + signs: outliers. (E) Lifetime sparsity of spatially selective cells. (F) Binned distributions of place field locations across the length of the treadmill belt. Gray bars indicate positions of stable cues (light gray) and interchangeable obstacles (dark gray). (G) Binned distributions of place field widths. (H) Fractions of spatially selective cells with one or more (2+) place fields. For C and F-H, error bars are SEM. For C-H, measures were averaged across all pre-surgery days for each mouse.

Table 3.1: Mean and total number of active cells detected across mice in each hippocampal or cortical region and experimental treatment group. Sample sizes: CA1 (*n*=3), pre-surgery (*n*=11), sham controls (*n*=5), and bilateral lesions of the dorsal hippocampus (*n*=4).

	Pre-Surgery		**Post-Sham**		**Post-Lesion**	
Region	***M* ± *SD***	**Total**	***M* ± *SD***	**Total**	***M* ± *SD***	**Total**
CA1	884 ± 195	2653	-	-	-	-
RSC	1353 ± 626	10823	1909 ± 823	3818	367 ± 134	1468
M2	1453 ± 821	15981	1454 ± 924	7273	707 ± 556	2829
M1	1208 ± 497	10875	1156 ± 713	4623	584 ± 364	1751

Neocortical representations of a familiar environment persisted after hippocampal lesions

The characteristics of spatially selective cells detected in a familiar, cued treadmill environment were next examined in cortical regions before (*n*=11) and after bilateral sham (*n*=5) or dorsal hippocampal lesions (*n*=4; refer to Figure 2.4). It is important to note that there was a main effect of treatment group (one-way ANOVA, $F(2,47)=6.963$, $p<0.01$) on the total number of cells detected per mouse such that significantly fewer cortical cells were active among cortical regions of interest of mice with bilateral dorsal hippocampal lesions relative to both pre-surgery or sham controls (Tukey's test, $p<0.01$; refer to Table 3.1; Figure 3.2A). There was substantial uncontrolled variability in the total number of detected cells between individual mice (and between regions within subjects) due to differences in the extent that blood vessels, the edge of the cranial window, or tissue regrowth obscured individual imaging frames. Nevertheless, the median distance between segmented superficial cells and their nearest three neighbours was also significantly different among treatment groups (one-way ANOVA, $F(2,47)=17.95$, $p<0.0001$), with lesioned mice exhibiting a lower density of detected cells than both pre-surgery (Tukey's test, $p<0.0001$)

and sham controls (Tukey's test, $p<0.001$; Figure 3.2B). This result could not be explained by motor deficits, as running performance on the treadmill was not impaired after sham surgeries or hippocampal lesions relative to pre-surgery performance (one-way ANOVA, $F(2,25)=0.3244$, $p=0.726$; Figure 3.2C). Although inactive cells were not quantified in this study, these findings suggest that complete dorsal hippocampal lesions may impair cortical cell recruitment during navigation of a familiar environment. However, such an effect on cell recruitment has not been reported by other studies that used comparable methods (Esteves et al., 2021, 2023; Mao et al., 2018) and, thus, variability among mice cannot be excluded as the underlying cause of this disparity in detected cells between groups.

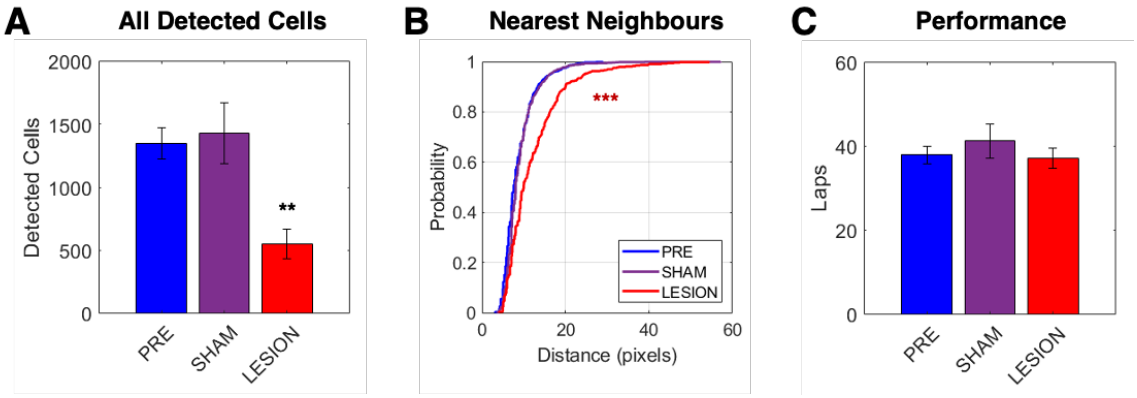

Figure 3.2: Recruitment of cortical cells during navigation of a familiar environment was reduced after bilateral lesions of the dorsal hippocampus. Data was pooled across cortical regions (RSC, M2, and M1) for each treatment group: pre-surgery (PRE; blue), sham controls (SHAM; purple), and mice with bilateral lesions of the dorsal hippocampus (LESION; red). (A) Mean number of active cells detected across mice in each experimental treatment group. Error bars are SEM. (B) Cumulative distributions of distances between detected cells and their three nearest neighbours in each experimental treatment group. (C) Mean number of laps run per ~20 minute experimental session. Error bars are SEM.

Considering that spatially selective cell characteristics were relatively consistent across cortical regions (refer to Figure 3.1), cells detected in RSC, M2, and M1 were grouped together by treatment for many of the subsequent analyses. Consistent with previous findings (Esteves et al., 2021; Mao et al., 2017), spatially selective cells in CA1 and the neocortex formed position-correlated sequences that uniformly tiled the treadmill environment. After bilateral dorsal hippocampal lesions, a spatial representation of the familiar environment persisted in all examined cortical regions. However, addition of the familiar interchangeable obstacles specifically disrupted the uniformity of the cortical spatial representations in the lesioned group at the locations of those cues (Figure 3.3).

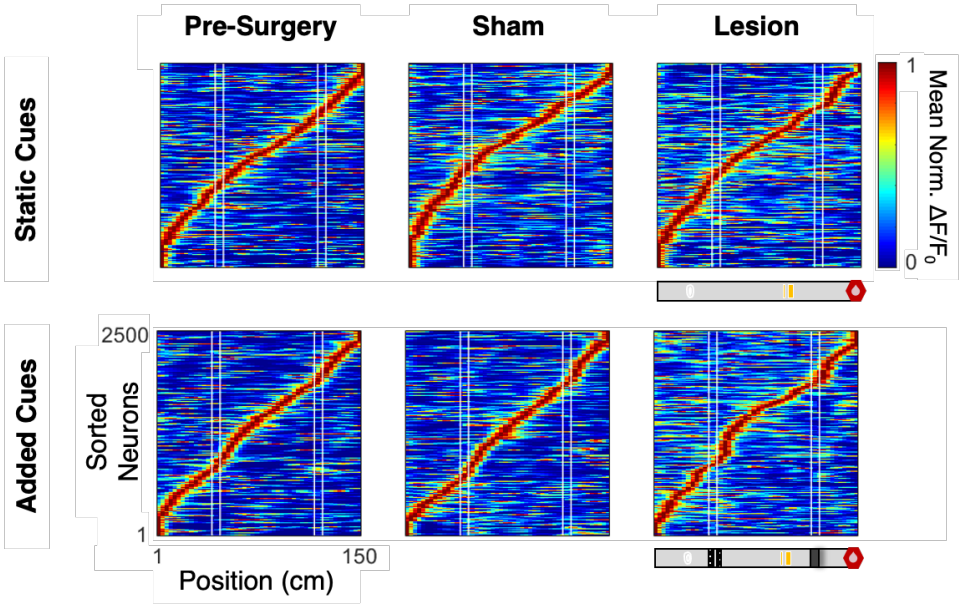

Figure 3.3: Cortical representations of a learned context were preserved after bilateral lesions of the dorsal hippocampus but uniformity was disrupted at unstable cues. Spatially selective cells were pooled across the cortical regions imaged during the last pre-surgery experimental days and the first post-surgery experimental days for each mouse. A random selection of 2500 cells from each treatment group were sorted by the order of maximum mean normalized $\Delta F/F_0$ on the last days before and the first days after sham or lesion surgeries. Static cues only (top panel) corresponds with day 10 (pre-surgery) and day 1 (post-surgery) of the ten-day paradigm, whereas days with added obstacles (bottom panel) correspond with day 8 (pre-surgery) and day 3 (post-surgery). White lines indicate the boundaries of the interchangeable obstacles.

In mice that were introduced to a novel environment, Esteves et al. (2021) demonstrated that bilateral hippocampal lesions significantly decreased both the detected proportion of spatially selective cortical cells and their encoded spatial information relative to sham controls, which was interpreted as a failure to acquire a cortical representation of the novel spatial environment. However, Esteves et al. (2023) reported that spatial tuning was preserved in a pre-operatively learned environment. Similarly, in the current study, there was no effect of lesion on the mean detected proportions of spatially selective cells (two-way repeated measures ANOVA, $F(2,47)=0.5274$, $p=0.59$; Figure 3.4A), the median encoded spatial information (two-way repeated measures ANOVA, $F(2,47)=0.2956$, $p=0.75$; Figure 3.4B), or the median lifetime sparsity (two-way repeated measures ANOVA, $F(2,47)=1.286$, $p=0.29$; Figure 3.4C) across mice, consistent with a learned representation of a familiar environment persisting in the absence of an intact hippocampus. The distribution of place fields across the length of the treadmill belt was proportionate (two-sample Chi-square tests, $p=0.15$-0.54; Figure 3.4D) and there were no significant differences in median place field width (one-way ANOVA, $F(2,47)=0.84$, $p=0.44$; data not shown) between all treatment groups. However, mice with hippocampal lesions demonstrated a significant (~9%) reduction in the proportion of spatially selective cells that exhibited only one place field (and, conversely, a significantly higher proportion of cells with multiple place fields; one-way ANOVA, $F(2,47)=5.122$, $p<0.01$) relative to both pre-surgery and sham controls (Tukey's test, $p<0.05$; Figure 3.4E).

A Bayesian decoder was next trained with the population activity from odd trials and used to decode mouse position from the population activity on even trials for each experimental day. To account for differences in the number of detected cells between sham

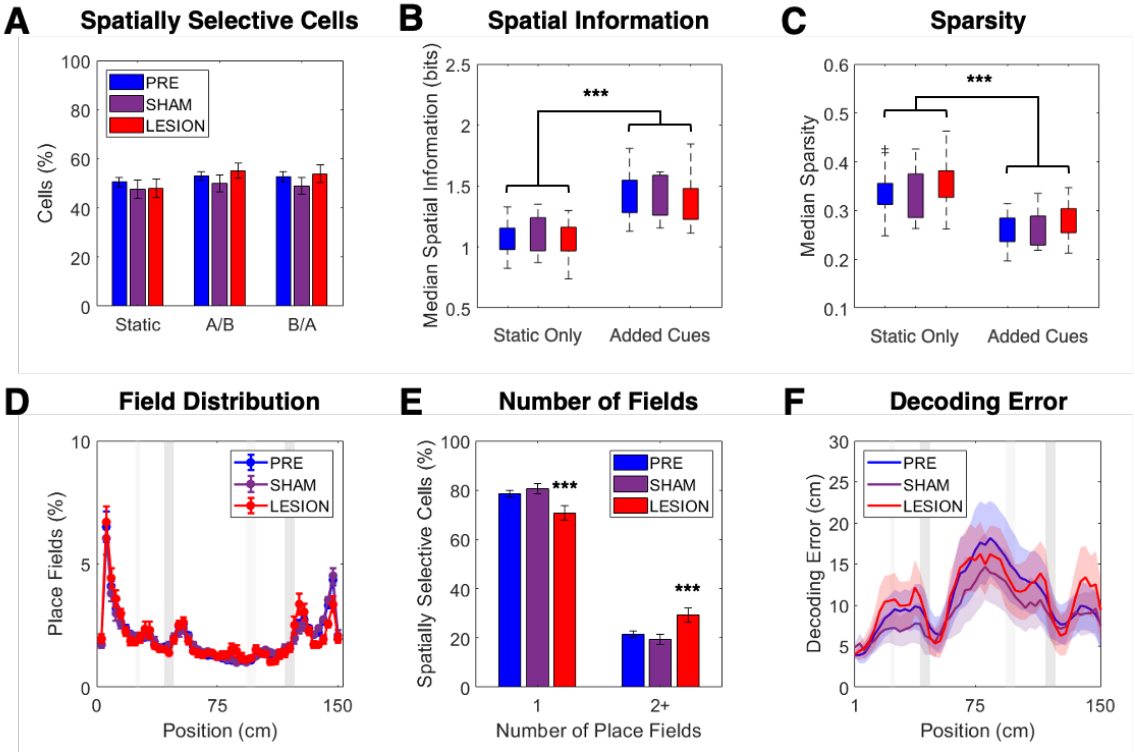

Figure 3.4: Spatially selective cortical cell characteristics were generally stable before and after bilateral sham or dorsal hippocampal lesions. (A) Mean fractions of spatially selective cells detected on days with static cues only (days 1-2 & 9-10) or with obstacles added in either orientation (A/B or B/A). Error bars are SEM. (B) Spatial information encoded by spatially selective cells with only the static cues on the treadmill belt (left; days 1-2 & 9-10) and after addition of the interchangeable obstacles (right; days 3-8). For all boxplots, line, median; box, 25th and 75th percentiles; whiskers, minimum and maximum values; + signs, outliers. (C) Lifetime sparsity of spatially selective cells with only the static cues on the treadmill belt (left; days 1-2 & 9-10) and after addition of the interchangeable obstacles (right; days 3-8). Note that a reduced sparsity index indicates that cells exhibited narrower spatial tuning profiles (i.e. firing became more sparse). (D) Distributions of place field locations across the length of the treadmill belt, averaged across all experimental days. Error bars are SEM. Gray bars indicate positions of stable cues (light gray) and interchangeable obstacles (dark gray). (E) Fractions of spatially selective cells exhibiting one or more (2+) place fields, averaged across all experimental days. Error bars are SEM. (F) Mean Bayesian decoding error across the binned length of the treadmill belt, averaged across all experimental days with added obstacles and across mice in CA1 and each cortical treatment group. Shaded area is SEM. Gray bars indicate positions of stable cues (light gray) and interchangeable obstacles (dark gray).

and hippocampus lesioned mice, the analysis was restricted to a random sampling of cells equal to the lowest number of detected cells in any region of interest across mice (n = 267 cells). The median Bayesian decoding error across the treadmill environment was not significantly different across treatment groups (one-way ANOVA, $F(2,45)=0.4486$, $p=0.64$) and, when averaged across mice, the median decoding error was ~10 cm among pre-surgery controls ($M\pm SD$ = 9.83±5.00 cm), sham lesioned controls ($M\pm SD$ = 8.60±6.51 cm), and hippocampus lesioned mice ($M\pm SD$ = 10.77±3.63 cm; Figure 3.4F). Notably, the decoding error was specifically reduced trailing the locations of the two interchangeable obstacles among cortical regions of all treatment groups. In contrast, CA1 exhibited a significantly smaller median Bayesian decoding error ($M\pm SD$ = 4.12±0.04 cm) relative to cortical regions (two-tailed t-test with Welch's correction, $p<0.0001$).

Spatial representations of a familiar environment were enhanced by added local cues

The fraction of spatially selective cells recruited at any given time in CA1 and all examined cortical regions was not significantly different across cue orientations, including in the absence of the added obstacles (two-way repeated measures ANOVA, $F(1.253,58.90)=3.04$, $p=0.08$; refer to Figure 3.4A). In CA1, the median encoded spatial information (two-tailed t-test, $t(2)=2.139$, $p=0.17$) and lifetime sparsity (two-tailed t-test, $t(2)=0.2413$, $p=0.83$) of spatially selective cells were not significantly different on experimental days with the added interchangeable obstacles (days 3-8) relative to days without the added cues (data not shown). In contrast, spatially selective cells in cortical regions encoded significantly increased median spatial information (two-way repeated measures ANOVA, $F(1,47)=523.7$, $p<0.0001$; refer to Figure 3.4B) and lifetime sparsity

indices were significantly reduced (i.e. firing became more sparse; two-way repeated measures ANOVA, $F(1,47)=353.1$, $p<0.0001$; refer to Figure 3.4C) due to the addition of the interchangeable obstacles. This effect was evident among pre-surgery (Dunn–Šidák, $t(47)=19.87$, $p<0.0001$) and sham (Dunn–Šidák, $t(47)=11.43$, $p<0.0001$) controls, as well as mice with bilateral lesions of the dorsal hippocampus (Dunn–Šidák, $t(47)=11.52$, $p<0.0001$). Although the distribution place fields was selectively elevated trailing the interchangeable obstacle locations during trials with the added obstacles (Figure 3.5), *all* spatially selective cortical cells exhibited reduced sparsity indices and increased encoded spatial information, regardless of place field location.

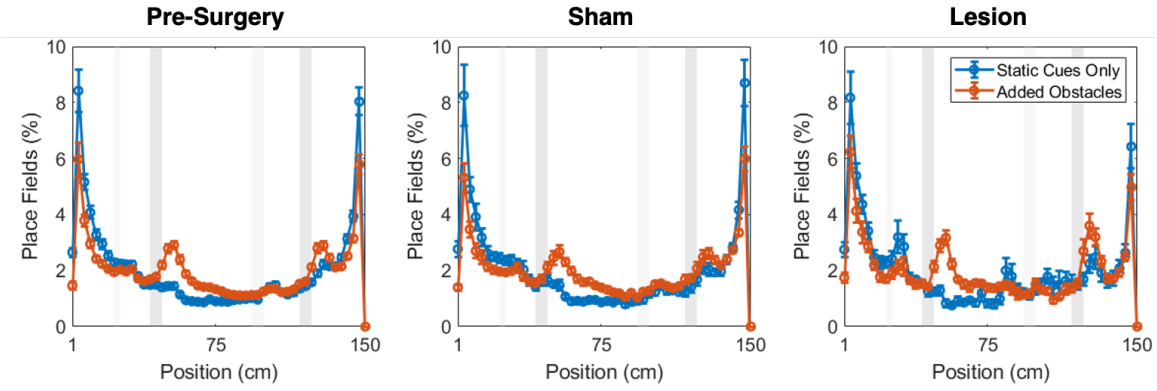

Figure 3.5: Addition of unstable local cues increased the allocation of cortical place fields to those locations. Distributions of place field locations across the length of the treadmill belt with only the static cues on the treadmill belt (blue; days 1-2 & 9-10) and after addition of the interchangeable obstacles (orange; days 3-8) in pre-surgery mice, sham controls and mice with bilateral dorsal hippocampal lesions Gray bars indicate positions of stable cues (light gray) and interchangeable obstacles (dark gray).

Position-correlated sequences contained both place and cue cells in an interareal gradient

By interchanging the two added obstacle positions, cue-specific activity could be dissociated from global location-specific activity, enabling assessment of the relative

encoding of place versus sensorimotor information among spatially selective cells. For differentiation of cue- and place-tuned cells, analyses were restricted to spatially selective cells with maximum mean normalized activity within the binned locations trailing the interchangeable obstacles. These locations were demarcated by the leading boundary of each obstacle and the area trailing those obstacles that exhibited elevated fractions of place fields relative to days with static cues only (refer to Figures 2.5A & 3.5). In addition, place fields within these boundaries often changed locations with the interchangeable obstacles (refer to Figure 2.5B) and this area of the treadmill also roughly corresponded to the mean length of a mouse (15 cm; refer to Figure 2.5C). Cue cells were defined as those spatially selective cells that exhibited maximum mean normalized activity across days with added obstacles at the position of one specific moving obstacle, regardless of its location on the track, whereas place cells were defined as spatially selective cells that always exhibited maximum mean normalized activity at the same location on the track, regardless of which obstacle was present (Figure 3.6A; refer to Figure 2.5D).

Spatially selective cells of pre-surgery mice could possess multiple place fields (an example cue cell with multiple fields is shown in Figure 3.6A) and, interestingly, place and cue cells with either single or multiple fields often exhibited activity modulation by both interchangeable obstacles (Figure 3.6B). On average, the population of place cells exhibited significantly different mean non-normalized peak activity within their place fields before and after the obstacles were interchanged on the treadmill (paired two-tailed t-test, $t(27)=5.6865$, $p<0.0001$) such that there was a ~15-20% reduction in peak activity across days in the presence of the “non-preferred” obstacle. In contrast, the mean peak activity of the cue cell population was not modulated by obstacle location as there was no significant difference between the mean non-normalized peak activity at the preferred obstacle while

positioned at either location (paired two-tailed *t*-test, $t(27)=0.4653$, $p=0.65$). In addition, both cue- and place-tuned cells with single place fields demonstrated significantly elevated mean non-normalized activity at the *non-preferred* obstacle or obstacle location, respectively, relative to baseline non-normalized activity (averaged across all treadmill locations that were at least 30 cm from the interchangeable obstacle locations; paired two-tailed *t*-tests, place: $t(27)=6.5169$, $p<0.0001$, cue: $t(27)=5.1182$, $p<0.0001$). These findings suggest that spatially selective cells in the neocortex undergo firing rate remapping, at least at cued locations in the environment where those cues demonstrate a salient relationship with each other.

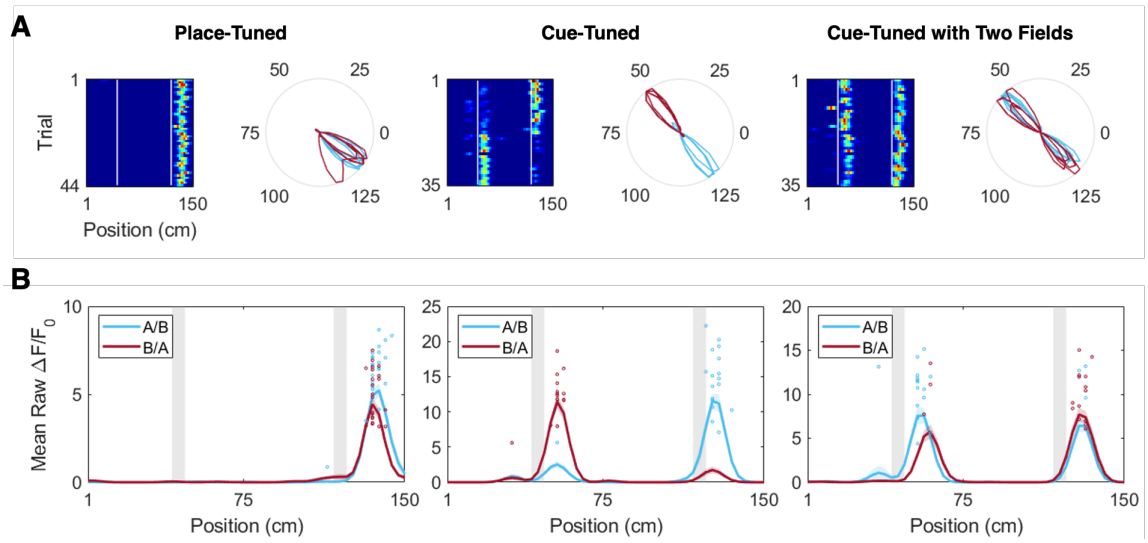

Figure 3.6: Spatially selective cells at the interchangeable obstacle locations included both place- and cue-specific cells. (A) Examples of representative place and cue cells, including a cue-tuned cell that exhibited two fields. Left: normalized mean $\Delta F/F_0$ across laps of an example cue-swap day where the obstacles changed orientations (A/B→B/A) mid-way through the session. White lines indicate positions of interchangeable obstacles. Right: polar plots showing trial-averaged normalized mean $\Delta F/F_0$ for all cue-swap days (days 4-7). (B) Trial-averaged non-normalized mean $\Delta F/F_0$ as a function of position for the cells shown in (A) on an example cue-swap day where the obstacles changed orientations (A/B→B/A) mid-way through the session. Open circles indicate peak activity for each trial within the session. Gray bars indicate positions of interchangeable obstacles.

Across cortical regions in pre-surgery animals, there were significantly different fractions of cue- and place-tuned cells at the locations of the interchangeable obstacles (one-way ANOVA and Tukey's test, $F(3,25)=31.67$, $p<0.0001$; Figure 3.7A). In general, for the regions studied, the proportions of detected place- and cue-tuned cells formed interareal gradients such that higher-level cortical regions exhibited increased fractions of place cells, whereas regions that were lower in the cortical hierarchy exhibited increased fractions of cue cells. Specifically, M1 exhibited significantly higher proportions of cue cells—and, conversely, fewer place cells—relative to M2 ($p<0.01$) and RSC ($p<0.0001$). The fraction of cue cells was also significantly increased in M2 relative to RSC ($p<0.001$). There were no significant differences in the fractions of place and cue cells between CA1 and RSC (two-tailed *t*-test, $t(9)=1.1$, $p=0.30$; data not shown).

Despite differences in relative proportions, place cells at the interchangeable obstacle locations exhibited characteristics that were comparable across cortical regions. There were no significant differences in encoded spatial information (one-way ANOVA, $F(2,25)=2.846$, $p=0.08$; Figure 3.7B), lifetime sparsity (one-way ANOVA, $F(2,25)=1.055$, $p=0.36$; Figure 3.7C), or the number of cells that exhibited multiple place fields (one-way ANOVA, $F(2,25)=0.04$, $p=0.96$; Figure 3.7D). In contrast, cue cells exhibited characteristics that varied consistently across the cortical hierarchy. Compared to cells in motor cortices, cue cells in RSC exhibited significantly lower spatial information (one-way ANOVA, $F(2,25)=0.9163$, $p<0.01$; Tukey's test, M2: $p<0.05$, M1: $p<0.01$; refer to Figure 3.7B) and higher measures of sparsity (one-way ANOVA, $F(2,25)=4.046$, $p<0.05$; Tukey's test, M2: $p=0.14$, M1: $p<0.05$; refer to Figure 3.7C). There was also a trend towards cue cells in RSC being more likely to exhibit multiple place fields but this effect was not

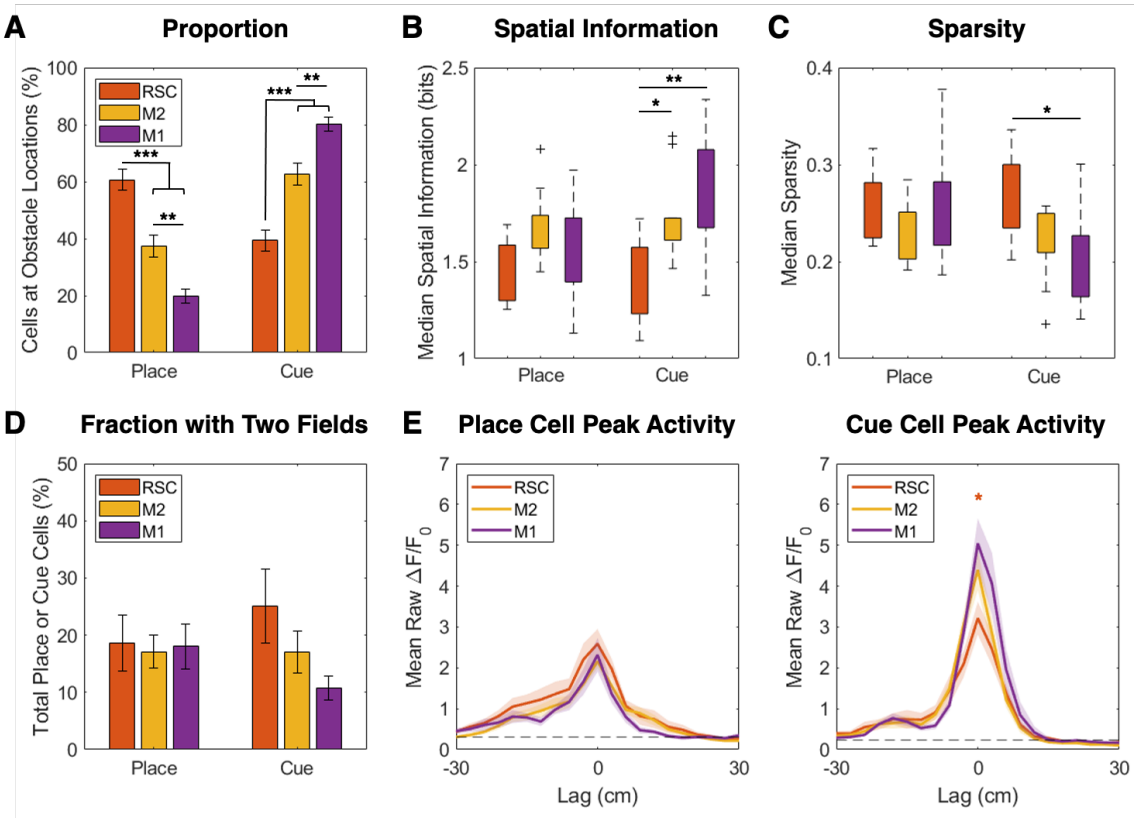

Figure 3.7: Lower cortices exhibited elevated fractions of cue cells with higher spatial information. (A) Mean proportions of place- versus cue-tuned cells at the locations of the interchangeable obstacles in RSC (orange), M2 (yellow), and M1 (purple) of pre-surgery mice. Error bars are SEM. (B) Median spatial information encoded by place versus cue cells. (C) Median lifetime sparsity indices for place versus cue cells. For all boxplots: line, median; box, 25th and 75th percentiles; whiskers, minimum and maximum values; + signs, outliers. (D) Mean fractions of total place or cue cells that exhibited multiple place fields. Error bars are SEM. (E) Aligned peak non-normalized $\Delta F/F_0$ of place cells (left) and cue cells (right) with maximum mean normalized $\Delta F/F_0$ at one of the interchangeable obstacle locations. Shaded area is SEM.

significant (one-way ANOVA, $F(2,25)=2.653$, $p=0.09$; Figure 3.7D). Consistent with increased spatial information among cue cells of lower cortices, the peak trial-averaged, non-normalized activity of cue cells—but not place cells—was also significantly higher in M1 relative to RSC (two-way repeated measures ANOVA & Dunn–Šidák, $F(2,25)=5.470$, $p<0.05$; Figure 3.7E). There was also a main effect of cell type such that cue cells in M2 and M1 exhibited significantly elevated peak non-normalized activity relative to place-tuned cells (two-way repeated measures ANOVA & Dunn–Šidák, $F(1,25)=51.37$, $p<0.0001$; refer to Figure 3.7E), suggesting that cue cells in these regions have higher firing rates at their preferred obstacle than place cells at their preferred location. In contrast, there was no difference between the peak activity of cue- and place-tuned cells in RSC ($p=0.50$).

Spatially selective cells in RSC exhibited increased cue tuning after hippocampal lesions

After sham surgeries, the main effect of region on the relative fractions of cue and place cells persisted (two-way ANOVA & Tukey's test, $F(2,41)=20.94$, $p<0.0001$; refer to Figure 3.7A) such that RSC exhibited significantly lower proportions of cue cells relative to M2 ($p<0.05$) and M1 ($p<0.01$). However, after bilateral lesions of the dorsal hippocampus, this effect was abolished (M2: $p=0.84$, M1: $p=0.14$) and RSC tended to exhibit higher proportions of cue-tuned cells relative to sham and pre-surgery controls, though the effect of lesion was not significant (two-way ANOVA, $F(2,41)=2.405$, $p=0.10$; Figure 3.8A). Notably, there was a significant interaction between treatment group and cell type (two-way repeated measures ANOVA, $F(2,11)=5.56$, $p<0.05$) on median spatial information such that cue-tuned RSC cells of lesioned mice encoded significantly higher spatial information relative to cue-tuned cells of both pre-surgery and sham controls

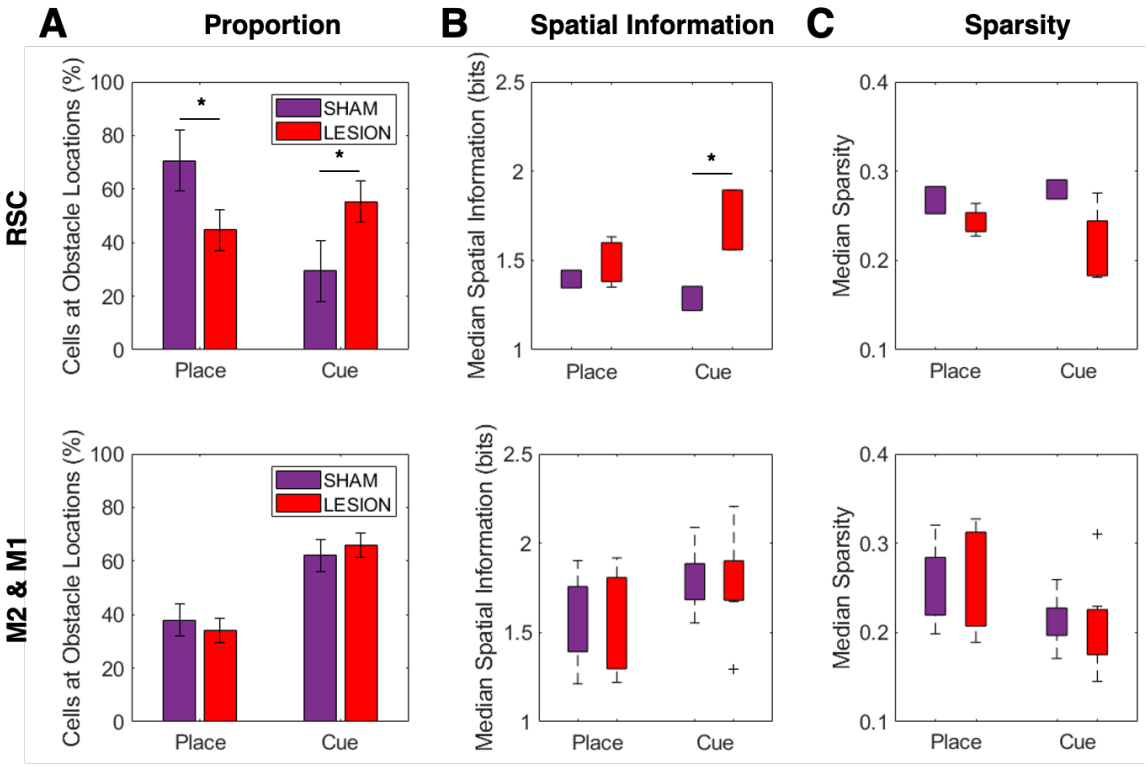

Figure 3.8: After bilateral lesions of the dorsal hippocampus, RSC exhibited increased fractions of cue-tuned cells that encoded significantly higher spatial information, analogous to motor cortices of control mice. Cells in M2 and M1 exhibited similar characteristics and were combined for clarity. (A) Fractions of place- and cue-specific cells detected at the locations of the interchangeable obstacles in RSC and motor cortices of sham controls (purple) and hippocampus-lesioned mice (red). (B) Median encoded spatial information and (C) median lifetime sparsity of place- and cue-tuned cells of mice with sham or bilateral lesions of the dorsal hippocampus. Note that a reduced sparsity index indicates that cells exhibited narrower spatial tuning profiles (i.e. firing became more sparse). For all boxplots: box, 25th and 75th percentiles; whiskers, minimum and maximum values; + signs, outliers.

(Tukey's test, $p<0.05$; Figure 3.8B). This interaction was not evident for median lifetime sparsity (two-way repeated measures ANOVA, $F(2,11)=1.864$, $p=0.20$; Figure 3.8C). The increase in encoded spatial information was consistent with observations of substantially elevated non-normalized population activity in RSC at the interchangeable obstacle locations after hippocampal lesions (coefficient of variation (*SD/M*), sham: 9.52%, lesion: 27.32%; Figure 3.9A), which was at least partially a consequence of increased peak activity of cue cells with single fields after hippocampal lesions (two-way repeated measures ANOVA, interaction: $F(1,4)=8.524$, $p<0.05$; Dunn–Šidák, cue: $t(4)=6.039$, $p<0.01$, place: $t(4)=0.6945$, $p=0.77$; Figure 3.9B). Interestingly, bilateral lesions of the dorsal hippocampus also abolished the ramping activity observed among place cells of sham controls (Figure 3.9B) and a larger proportion of spatially selective cells exhibited multiple place fields, although this lesion effect was not significant (two-way repeated measures ANOVA, $F(1,4)=3.142$, $p=0.15$; Figure 3.9C). Thus, elevated activity at the interchangeable obstacle locations in RSC could also be partially explained by an increased fraction of spatially selective cells with multiple fields at the obstacle locations, as well as greater spatial clustering of cue-specific activity (i.e. reduced ramping and spatial uniformity; refer to Figure 3.3).

In motor cortices, the fraction of cue-tuned cells detected at obstacle locations was consistently higher than that of place-tuned cells (two-way repeated measures ANOVA & Tukey's test, $F(2,99)=184.5$, $p<0.001$; refer to Figure 3.7A) and there was no effect of hippocampal lesions on the relative fractions of cue- and place-tuned cells (one-way ANOVA, $F(2,33)=1.087$, $p=0.35$; Figure 3.8A). There was also a consistent main effect of cell type on encoded spatial information (two-way repeated measures ANOVA,

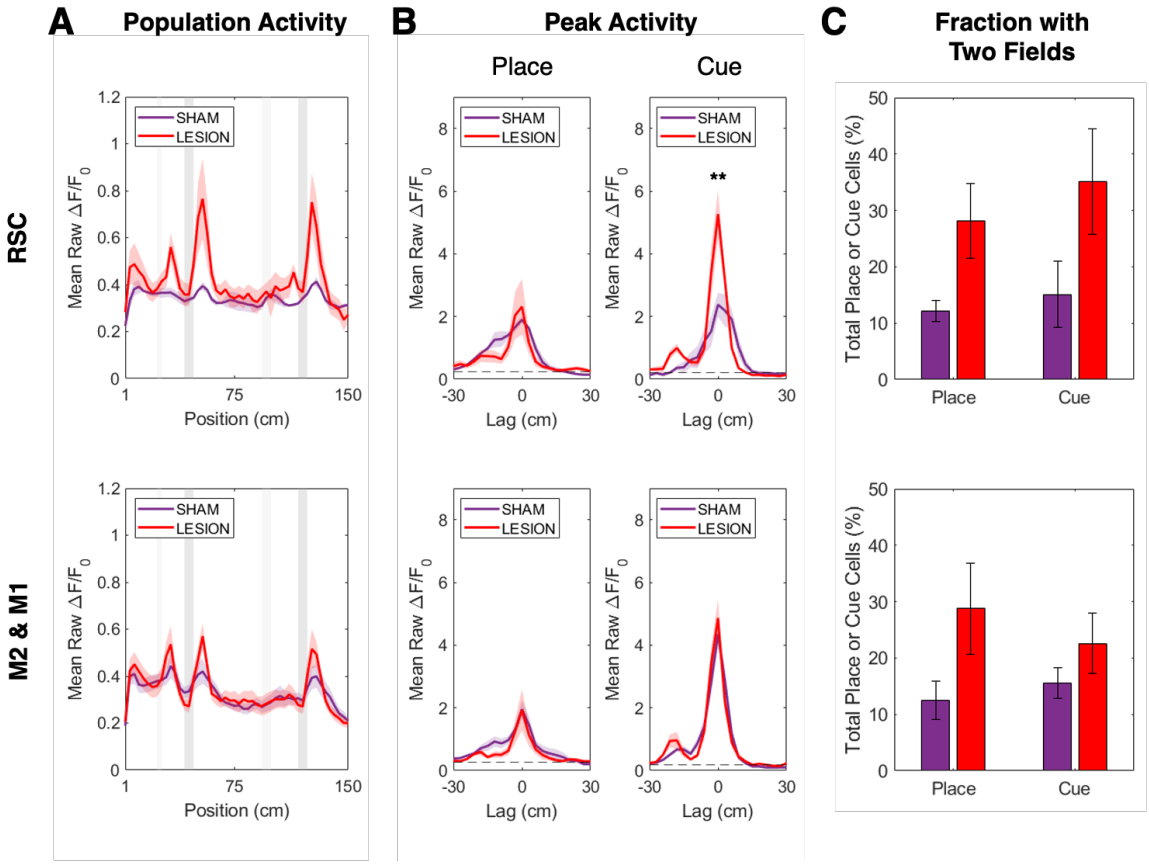

Figure 3.9: After bilateral lesions of the dorsal hippocampus, cue-tuned cells exhibited significantly elevated activity in RSC. Cells in M2 and M1 exhibited similar characteristics and were combined for clarity. (A) Mean non-normalized $\Delta F/F_0$ of all detected cells in RSC and motor cortices after sham (purple) or bilateral lesions of the dorsal hippocampus (red). Shaded area is SEM. Gray bars indicate positions of stable cues (light gray) and interchangeable obstacles (dark gray). (B) Aligned peak non-normalized $\Delta F/F_0$ of place cells (left) and cue cells (right) with maximum mean normalized $\Delta F/F_0$ at one of the interchangeable obstacle locations. Shaded area is SEM. Note the loss of ramping activity among place cells after bilateral lesions of the dorsal hippocampus. (C) Fractions of total place or cue cells detected at the interchangeable obstacle locations that exhibited two place fields on cue-swap days. Error bars are SEM.

$F(1,33)=29.37$, $p<0.0001$) and lifetime sparsity (two-way repeated measures ANOVA, $F(1,33)=39.15$, $p<0.0001$) such that cue-tuned cells in motor cortices encoded elevated spatial information (refer to Figure 3.7B & 3.8B) and exhibited lower sparsity indices (refer to Figure 3.7C & 3.8C) after sham lesions. However, unlike RSC, there was no effect of lesion group on median encoded spatial information (two-way repeated measures ANOVA, $F(2,33)=0.1103$, $p=0.90$; Figure 3.8B) or median lifetime sparsity (two-way repeated measures ANOVA, $F(2,33)=0.0433$, $p=0.96$; Figure 3.8C) among place- and cue-tuned cells in motor cortices. Nevertheless, non-normalized population activity was moderately elevated at the interchangeable obstacle locations after bilateral lesions of the dorsal hippocampus (coefficient of variation (*SD/M*), sham: 18.09%, lesion: 26.17%; Figure 3.9A), which—in contrast to RSC—was not a consequence of increased peak activity at the preferred firing locations of place or cue cells with single fields (two-way repeated measures ANOVA, $F(2,11)=2.326$, $p=0.14$; Figure 3.9B). Instead, this less pronounced change in population activity at the obstacle locations was likely primarily attributable to greater spatial clustering of cue-specific activity (i.e. reduced ramping and spatial uniformity; refer to Figure 3.3) and the observed trend towards increased fractions of place and cue cells exhibiting multiple place fields after bilateral lesions of the dorsal hippocampus (however, as in RSC, this lesion effect was not significant; two-way repeated measures ANOVA, $F(1,14)=3.498$, $p=0.08$; Figure 3.9C).

3.4 DISCUSSION

This study sought to disentangle the relative context and content encoding of spatially selective cells in the neocortex and assessed the continued influence of hippocampal modulation on cortical spatial representations of a familiar environment. Consistent with previous studies, large proportions of active cells in RSC, M2, and M1 were found to exhibit position-correlated activity (Esteves et al., 2021; Mao et al., 2017). Within each region, these cells yielded a uniform spatial map of the familiar environment that persisted after bilateral lesions of the dorsal hippocampus, a finding that was concurrently validated by Esteves et al. (2023) and provides cellular evidence in support of the standard model of systems consolidation. Movement of two familiar obstacles within the bounds of the familiar track, however, revealed regionally-variant subpopulations of place- and cue-tuned cells. In M2 and M1, spatially selective cells were more likely to be cue-tuned, shifting their preferred firing locations in coordination with the locations of the moving obstacles. In contrast, the majority of spatially selective cells in dysgranular RSC of pre-surgery or sham controls were found to be place-specific; they did not change their preferred location of firing with the manipulated cues. Bilateral lesions of the dorsal hippocampus, however, significantly increased the fraction of spatially selective cells in RSC that exhibited cue-tuning—and those cue cells exhibited peak activity and spatial characteristics that were more comparable to cue cells observed in lower cortices—suggesting that the balance between sensorimotor and contextual information was shifted in favour of ascending sensory information. Thus, at the population level, these findings support that position-correlated representations in the cortex encode both context and content information, the balance of which remains dependent on feedback from the hippocampus in RSC.

In the hippocampus, place cells tend to remained fixed to a particular location and undergo firing rate remapping amid changing spatial cues (Leutgeb et al., 2005). Nevertheless, a subpopulation of cue-tuned cells was detected in distal CA1, which is consistent with previous reports of a fraction of CA1 cells following unstable but behaviourally-relevant landmarks (Gothard et al., 1996; Knierim et al., 1995). The detection of cue-tuned cells in CA1 may also be attributable to the distal location of imaging. Across the transverse and radial axes of CA1, pyramidal neurons exhibit anatomical heterogeneity in projections from the entorhinal cortex that mirrors observed differences in activity patterns during spatial and non-spatial tasks. Along the transverse (proximodistal) axis, neurons in proximal CA1 (neighbouring CA2) preferentially receive spatial information from medial entorhinal cortex (MEC), whereas neurons in distal CA1 (towards dorsal subiculum) primarily receive non-spatial information from lateral entorhinal cortex (LEC; Burke et al., 2011; Henriksen et al., 2010; Ito & Schuman, 2012; Steward, 1976; Tamamaki & Nojyo, 1995). Furthermore, across the radial axis, MEC preferentially excites the deep sublayer of pyramidal neurons (adjacent to stratum oriens) in proximal CA1, while LEC preferentially targets superficial neurons (adjacent to stratum radiatum) in distal CA1 (Masurkar et al., 2017; Mizuseki et al., 2011). These interactions within distal CA1 could translate to a subset of superficial cells that are stably tuned to relevant local cues amid place cells that are more flexibly modulated in response to behaviourally-salient features—including rewards and navigational landmarks—than place cells in proximal CA1 (Danielson et al., 2016; Geiller et al., 2017).

Accordingly, the similarity in the relative fractions of place- and cue-tuned cells between distal CA1 and the RSC of intact animals may be a direct consequence of anatomical interconnectivity. However, in the absence of an intact hippocampus, a striking

fraction of spatially selective cells in the RSC transitioned from place- to cue-specific at the locations of the interchangeable obstacles. Thus, the hippocampus appears to be essential for either updating or stabilizing the global spatial representation in the presence of unreliable sensory information. In fact, the post-learning function of the RSC may not strictly lie in storing an allocentric representation of space, but rather in transforming between the allocentric and egocentric spatial coordinate frames to both guide self-referenced behaviour and, in return, transmit relevant ascending information to update the view-invariant model of the environment (Alexander & Nitz, 2015; Byrne et al., 2007; Clark et al., 2018). The marked shift from place- to cue-specific tuning and loss of spatial coherence at the obstacle locations may reflect the local imbalance between global contextual and local sensory inputs, with RSC responses being principally driven by locomotor information and optic flow in the absence of spatiotemporal inputs from the hippocampus (Mao et al., 2020; Yamawaki et al., 2016).

It is important to note that the dorsal subiculum, which mediates the majority of the interactions between CA1 and dysgranular RSC, was also lesioned in this study. CA1-projecting subiculum cells have been shown to form alternative non-canonical circuits from the visual cortex to the hippocampus both directly and indirectly via the perirhinal cortex (Sun et al., 2019). These cells specifically modulate the responses of place cells to displaced objects, which may indicate that the dorsal subiculum is critical for directly updating object location in allocentric space. Thus, after lesions of the dorsal hippocampus and subiculum, the transition of spatially selective RSC cells from place- to cue-specific at obstacle locations may indeed reflect a loss of coherence between sensory information and the internal representation of space.

In the motor cortices, the balance of tuning among spatially selective cells was consistently biased towards the added obstacles, likely because ascending sensory input predominates in these regions. Even in the absence of an intact hippocampus, spatial information was reliably greater among cue-tuned cells and Bayesian decoding error was lower at the interchangeable obstacle locations, indicating that cue information is locally accessible in the cortex and confers egocentric spatial localization. In terms of both place fields and population activity, there was a marked overrepresentation of the unstable obstacles relative to the stable cues, particularly in M1. In the hippocampus, the fraction of place cells, density of place fields, and spatial resolution are also locally increased at the locations of rewards or goals (Danielson et al., 2016; Dupret et al., 2010; Gauthier & Tank, 2018; Hollup et al., 2001; Sato et al., 2020), aversive stimuli (Okada et al., 2017), and salient sensory cues (Bourboulou et al., 2019; Burke et al., 2011; Hetherington & Shapiro, 1997; Sato et al., 2020; Wiener et al., 1989). Therefore, it is likely that either the increased physical demands of the interchangeable obstacles or the instability of their positions enhanced their salience and the attentional state of the animals, increasing spatial resolution in the motor cortices at those locations (Kentros et al., 2004). Alternatively (or as an additional consequence of differences in attentive state; Alink & Blank, 2021), there may be repetition or expectation suppression of responses to the predictable *stable* cues, a phenomenon that is frequently reported in functional imaging studies of sensory cortices (Henson et al., 2000; Richter et al., 2018; Summerfield et al., 2008; Todorovic et al., 2011). In addition, rodent hippocampal place cells tend not to orient their place fields to unstable environmental cues (Knierim et al., 1995) and the RSC preferentially encodes permanent landmarks in humans (Auger et al., 2012, 2015) and behaviourally significant or context-identifying cues in rats (Smith et al., 2012; Vedder et al., 2017). Thus, the increased activity

at the unreliable cue locations in lower cortices may reflect reduced top-down modulation and a greater reliance on local sensory inputs for initiating behavioural responses. Notably, this explanation is also congruent with the reduction in uniformity of cortical spatial representations and the overabundance of cue-tuned cells at the interchangeable obstacle locations in RSC after hippocampal lesions, despite the persistence of a generally stable representation of the underlying familiar environment.

In addition to the reduced spatial uniformity of position-correlated sequences at the interchangeable obstacle locations, the ramping activity of cortical place cells was also specifically disrupted by bilateral dorsal hippocampal lesions. These findings suggest that, even after extensive experience in the environment, cortical place cells in intact animals continued to receive top-down contextual modulation that enabled anticipation of salient segments of the learned environment. In another study that examined superficial cells in V1, learning-induced ramping activity in anticipation of a visual stimulus offset (and the coincident timing of an aversive shock) was similarly abolished after post-learning inactivation of RSC (Makino & Komiyama, 2015). Notably, the RSC is directly innervated by both excitatory (Sugar et al., 2011; Wyss & van Groen, 1992) and inhibitory (Miyashita & Rockland, 2007; Yamawaki et al., 2019) projections from CA1 and is likely a pivotal structure for relaying hippocampal output to lower cortical regions. Thus, in addition to a role in facilitating episodic memory retrieval, these findings add to a growing body of evidence that the hippocampus also governs internal model-based planning and prediction (for review see Barron et al., 2020). For instance, during repeated traversal of an environment, hippocampal place cells exhibit phase precession and backwards expansion of place fields due to the asymmetric synaptic coupling of sequentially activated cells, which manifests as apparent anticipation of forthcoming spatial positions (Lisman &

Redish, 2009; Mehta et al., 1997; Skaggs et al., 1996). Moreover, hippocampal cell assemblies have been shown to spontaneously explore candidate actions both during sleep (Gupta et al., 2010) and ahead of behaviour (Johnson & Redish, 2007; Pfeiffer & Foster, 2013). At the apex of the cortical hierarchy, the hippocampus is well-positioned to both update the internal model of the environment based on current sensory experience and propagate higher-level predictions regarding behavioural outcomes to improve the efficiency of information processing throughout the cortex.

A potential caveat is that position-correlated activity sequences in the cortex may be a consequence of head-fixed imaging preparations that restrict naturalistic head direction, optic flow, and vestibular inputs compared to freely-moving mice. It is certainly possible that repeated traversal of a treadmill environment with restricted sensory modulation might render an overabundance of *seemingly* spatially selective cells or impose a somewhat atypical organization on the spatial map. Nevertheless, a few studies have reported position-correlated cortical activity in freely-moving mice (Haggerty & Ji, 2015; Ji & Wilson, 2007; Long & Zhang, 2021; Nitz, 2009), suggesting that space is a common element of neocortical memory representations. Alternatively, neocortical place cells—particularly in lower sensory cortices—might actually be cue cells that are responsive to uncontrolled sensory cues such as traces of urine, drips of unconsumed strawberry milk, or tactile inconsistencies in the treadmill material. In fact, it may be that top-down inputs are sharpening sensory receptive fields in lower cortical regions and, as a consequence, creating apparent place coding. Thus, some discriminative, bottom-up sensory input may be a prerequisite for spatial representations to form in the cortex. Future studies might test this prediction by comparing development of spatial representations in somatosensory and visual cortices in both tactile and virtual environments. If true, S1 would be expected to

develop spatially selective cells rapidly in a predominantly tactile environment and more slowly in a virtual environment, whereas the opposite would be the case for V1.

Another possible limitation is that some hippocampal lesion effects may have been masked by compensatory mechanisms. The extent of the bilateral lesions completely spanned the *dorsal* hippocampus but left large portions of the ventral hippocampus intact. However, ventral hippocampal compensation seems unlikely because the lesion cohort used by Esteves et al. (2021, 2023) exhibited similar ventral sparing, yet the formation of uniform spatial representations of a novel environment in the cortex was still markedly impaired. Nevertheless, learning impairments after hippocampal lesions or inactivation have been shown to be overcome with repeated conditioning (Kim & Frank, 2009), possibly because alternative learning systems are disinhibited or persistently activated (White & McDonald, 2002), and/or because the memory becomes linked to sensory attributes rather than the holistic context (Matus-Amat et al., 2004). Indeed, overtraining can lead to a natural shift from using flexible, context-dependent behavioural strategies to more habitual responses that rely on fixed motor sequences generated by the dorsal striatum (Packard & McGaugh, 1996; Schmitzer-Torbert, 2007). However, the results of this study highlight changes to the cortical spatial representations only after hippocampal lesions (and not with prolonged training), suggesting that any increased dependence on entrained motor responses with recurrent experience does not come at the expense of descending contextual modulation in intact animals.

Altogether, the results of this study suggest that the top-down modulation of cortical responses by the hippocampus obeys hierarchical interareal gradients opposite to the flow of bottom-up sensory inputs. In addition, while a cortical spatial representation of a familiar environment can persist in the absence of an intact hippocampus, the binding of unstable

sensory attributes to the learned contextual framework is enduringly dependent on descending feedback. Specifically, in familiar environments, the hippocampus may function to actively update the internal model of the environment based on current sensory experience to improve the efficiency of downstream information processing. Thus, these findings lend further support for an ongoing role for the hippocampus in both maintaining a coherent cognitive map and anticipating future behaviours.

4. TOP-DOWN INPUTS SUPPRESS BOTTOM-UP SENSORY SIGNALS IN MOTOR CORTEX DURING NAVIGATION OF A FAMILIAR ENVIRONMENT

4.1 ABSTRACT

In the neocortex, volitional behaviour is governed by the integration of bottom-up sensory inputs with top-down contextual feedback. Across laminae, recent studies have demonstrated that hippocampus-dependent encoding of spatial information is a general feature of superficial neocortex, whereas deep layers may better represent the salient sensory attributes required to drive appropriate behavioural responses. To further explore this putative laminar division of context and content in motor cortices, this study used *in vivo* two-photon microscopy of genetically encoded Thy1-GCaMP6s calcium indicator mice to nearly simultaneously image pyramidal neurons spanning cortical layers II-Va. To assess the relative impact of descending feedback from the hippocampus across the cortical volume, mice with bilateral sham or dorsal hippocampal lesions navigated a pre-operatively familiar treadmill environment that contained both stable and unstable cues. Consistent with context being more strongly represented in superficial layers, fractions of spatially selective cells and their encoded spatial information formed a gradient such that cells closer to the cortical surface were more sparsely and precisely tuned than middle or deep layer cells. After hippocampal lesions, both spatially selective cell recruitment and cue-specific population activity became more homogeneously elevated throughout the cortical volume. These results support the conclusion that, even in learned environments, descending contextual signals from the hippocampus actively suppress ascending sensory inputs in a depth-dependent manner.

4.2 INTRODUCTION

Laminar architecture of the neocortex

The neocortex consists of six horizontal laminae, each composed of distinct cell types that differ in their morphological, physiological, and molecular properties (e.g. Belgard et al., 2011; Markram et al., 2015; Senzai et al., 2019). Despite the broad diversity of excitatory cell subtypes that have been identified, which altogether account for the vast majority of cortical neurons (~85%; Beaulieu, 1993), laminar boundaries can be generally characterized by long-distance projection patterns (Douglas & Martin, 2004; Harris & Shepherd, 2015) and depth-dependent differences in neuron size and density (Keller et al., 2018). The molecular layer, L1, is almost entirely devoid of neuronal cell bodies and, instead, is predominantly occupied by glia and the cell processes extended from somas in other layers. All other cortical laminae residing below L1 are populated by diverse subtypes of intratelencephalic pyramidal neurons that mediate interactions among the cortical hemispheres, the limbic forebrain, and the basal ganglia. Neurons in the external granular layer, L2, and the external pyramidal layer, L3, are the primary target of cortico-cortical afferents, with L3 providing the principal source of cortico-cortical efferent projections. In rodents, these layers are difficult to distinguish by morphology alone and so are often grouped together as L2/3, which, together with L1, constitute the supragranular or "superficial" layers. The internal granular layer, L4, typically contains both pyramidal and spiny stellate cells, and receives the bulk of thalamocortical input. In addition to intratelencephalic neurons, the infragranular or "deep" layers, L5 and L6, are also populated by neurons with projection targets outside of the telencephalon. For direct control of behaviour, the internal pyramidal layer, L5, contains large pyramidal tract neurons in

L5b that project to the brainstem and spinal cord, with collaterals to subcortical regions. Finally, the multiform layer, L6, includes corticothalamic neurons that send projections back to the thalamus.

As a result of these anatomical consistencies, the translaminar flow of feed-forward and feedback information is largely conserved across the various functional regions of the neocortex (Douglas & Martin, 2004; Gilbert & Wiesel, 1983). In primary cortices, granular L4 is considered the first level of processing in the laminar hierarchy—the "input" layer—as it is the principal recipient of sensory information from the thalamus (Bopp et al., 2017). The perisomatic basal dendrites of excitatory neurons in L3 receive the majority of feed-forward ("bottom-up") sensory inputs from L4, whereas the distal apical dendrites of L2/3 and L5a neurons receive feedback ("top-down") inputs from higher-level cortical and thalamic areas via synaptic connections in L1 (Cauller & Connors, 1994; Petreanu et al., 2009; Sermet et al., 2019). L2/3 pyramidal cells primarily exhibit short-range, recurrent connections with an abundance of activity-modifiable synapses that, in concert with horizontal inhibitory signals from neighbouring interneurons, plausibly function as a local associative network (Harris & Shepherd, 2015; Holmgren et al., 2003; Monaghan & Cotman, 1985; Rolls, 2016). L2/3 cells then send a major descending projection to L5—the major "output" layer—which also locally innervates L6. In return, intrinsic feedback is conveyed by ascending projections from L5 to superficial layers and from L6 to L4 (Figure 4.1; Burkhalter, 1989; Gilbert & Wiesel, 1983; Harris et al., 2019).

An apparent exception to this generalized circuit is found within M1, which lacks a cytologically distinct L4. Thus, unlike other primary cortical areas, interlaminar excitatory circuits between M1 pyramidal neurons are largely dominated by descending pathways (Hooks et al., 2011; Weiler et al., 2008). Nevertheless, M1 possesses a thin band of

pyramidal neurons at the laminar zone between L2/3 and L5a that express molecular markers of L4, receive thalamic input, and primarily unidirectionally excite L2/3 neurons, analogous to the archetypal input-output circuits of L4 of sensory cortices (Bopp et al., 2017; Skoglund et al., 1997; Yamawaki et al., 2014).

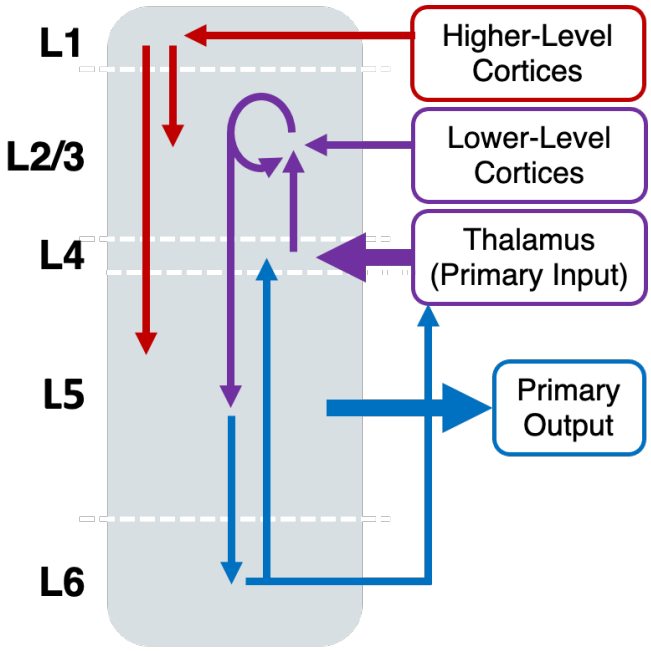

Figure 4.1: Simplified schematic demonstrating intrinsic laminar circuitry and the principal layer-specific targets of ascending (feed-forward) and descending (feedback) interareal inputs to a primary cortical region.

Long-range laminar connectivity within the spatiomotor pathway

Back-projections from the hippocampus, relayed via the subiculum and parahippocampal areas, predominantly innervate the superficial layers of the neocortex (Insausti et al., 1997; McIntyre et al., 1996; Sugar et al., 2011; Swanson & Köhler, 1986; van Groen & Wyss, 1990a, 1990b). Within the RSC, axons from the subiculum terminate

in L1/2 of dysgranular RSC and both CA1 and subiculum target L2/3 of granular RSC, with return projections to the hippocampal formation arising predominantly in L5 (Sugar et al., 2011; van Groen & Wyss, 1990a, 1990b; Vogt & Miller, 1983; Wyss & van Groen, 1992). From the limbic thalamus, axons originating in the anteromedial nucleus terminate in L1 and L4-6 of the dysgranular RSC, whereas those arising in the laterodorsal nucleus innervate L1 and L3-4 (van Groen & Wyss, 1992b, 1992a). In addition, L1 of dysgranular RSC also receives sensory feedback from the visual cortex (van Groen & Wyss, 1992a).

M2 is extensively and reciprocally interconnected with the RSC. RSC axons form monosynaptic connections on all excitatory cell classes spanning L2-6 of M2 and, in return, M2 preferentially targets L2/3 of RSC (Yamawaki et al., 2016). RSC also makes disynaptic connections with M2 via the posterior parietal cortex, which most densely innervates L5 of M2 but also makes widespread connections spanning L2-6 (Olsen et al., 2019). Projections from motor-related thalamic nuclei appear to target both M2 and M1 to a similar extent. The excitatory caudolateral portion of the ventral anterior/ventral lateral complex, conveying cerebellar information, broadly targets L2-5 (Hooks et al., 2013; Kuramoto et al., 2009). On the other hand, the ventral medial thalamus and the inhibitory rostromedial portion of the ventral anterior/ventral lateral complex, which receive strong inputs from the basal ganglia, target apical tuft dendrites within L1 of motor cortices (Cruikshank et al., 2012; Guo et al., 2018; Kuramoto et al., 2009).

M2 and M1 exhibit the archetypal interareal connections that are characteristic of higher and lower order sensory cortices, respectively. From M2, feedback projections make connections within L1 of M1, whereas feedforward efferents from M1 target L2/3 of M2 (Ueta et al., 2014). Ascending sensory-related projections to M1, including those from primary and secondary somatosensory cortex as well as posterior sensory thalamic areas,

preferentially target L2/3 and L5a (Aronoff et al., 2010; Hooks et al., 2013; Mao et al., 2011; Suter & Shepherd, 2015). In contrast, top-down inputs from orbital cortex and M2 largely bypass local associative circuitry and communicate with neurons in L5b and L6, respectively, which project directly to brainstem and thalamus (Hooks et al., 2013).

Discrete context and content sensitivity of cortical laminae

Considering that cortico-cortical communication, efferent projections from the hippocampal formation to association areas, and bottom-up sensory information from the thalamus converge on the supragranular layers, L2/3 may serve to integrate spatiotemporal context with the sensory content of experience. Hippocampus-dependent encoding of spatial information appears to be ubiquitous throughout superficial neocortex (Esteves et al., 2021; Fujisawa et al., 2008; Mao et al., 2017, 2018; Saleem et al., 2018; Zielinski et al., 2019), whereas the deep layers of RSC exhibit a much smaller fraction of place cells (Mao et al., 2017). In vibrissal S1, superficial cells play a sustained role in the integration of locomotor signals with continuous sensory inputs, whereas deep cells have been shown to respond preferentially and transiently to salient tactile perturbations (Ayaz et al., 2019). Moreover, L5 neurons in anterolateral M2 participate in the planning and execution of movement to a greater extent than superficial neurons (Chen et al., 2017) and have been proposed to store the outcome-predicting sensory information required for action selection (Kondo & Matsuzaki, 2021). Altogether, there may be a division of labour between superficial and deep layers such that contextual predictions are better represented in superficial layers while salient sensory attributes, necessary for driving appropriate behavioural responses, dominate in deep layers.

In a study that directly examined the postulated laminar division of context sensitivity in the neocortex, Burke et al. (2005) used immediate-early gene (IEG) expression as a surrogate for recording behaviourally-relevant neural activity *in vivo* across the posterior parietal and insular cortices. Whereas superficial layers exhibited substantial spatial sensitivity in both cortical regions, deep laminae failed to discriminate between spatial contexts, a finding that was later replicated (Takehara-Nishiuchi et al., 2013). However, Takehara-Nishiuchi et al. (2013) revealed that the enhanced distinction of episodes observed in superficial laminae relative to deep laminae was also apparent during re-exposure to the same environment and persisted in the absence of an intact hippocampus, suggesting that laminar differences were not related to direct or indirect contextual input from the hippocampal formation. However, while IEGs play an important role in synaptic plasticity and long-term memory consolidation (Fleischmann et al., 2003; Guzowski et al., 2000), the relationship between neuronal activity and IEG expression is not always straight-forward (Carpenter-Hyland et al., 2010; Guzowski et al., 2006; Kelly & Deadwyler, 2003; Vazdarjanova et al., 2006). As an example, Tanaka et al. (2018) found that only ~25% of place cells expressed c-Fos and that c-Fos-positive place cells exhibited higher mean firing rates, larger place fields, and lower spatial information than their c-Fos-negative counterparts. Thus, IEG studies may fail to adequately explore the laminar relationship between context and content encoding in the cortex.

Study objectives

Layer-specific compartmentalization of spatial context and content coding may be a general feature of the neocortex, perhaps arising as a consequence of intrinsic interactions between top-down and bottom-up inputs. To explore the putative laminar division of

context and content coding in motor cortices, this study used *in vivo* two-photon microscopy of genetically encoded Thy1-GCaMP6s calcium indicator mice to nearly simultaneously image pyramidal neurons spanning cortical layers II-Va. While the global spatial context remained constant throughout training and imaging, two familiar obstacles were added, interchanged, or removed from a cued treadmill to decouple cue-specific activity from location-specific activity. This experimental paradigm was implemented after both bilateral sham or dorsal hippocampal lesions to examine the layer-specific interactions between ascending sensory inputs and descending contextual information and their relative influence on position-correlated neural activity in the spatiomotor pathway.

4.3 RESULTS

Superficial cells exhibited characteristics of higher context selectivity

Two-photon imaging extended from approximately 150 μm to 500 μm below the pial surface in M2 and M1 of mice with bilateral sham (n=4) or dorsal hippocampal lesions (n=3; refer to Figure 2.4). Based on anatomical atlases (Allen Brain Institute for Science, 2011), the boundary between superficial (L2/3) and deep (L5a) layers was expected to be located at a depth of ~400 μm. Corresponding with this approximation, the three z-planes below this division exhibited a higher density of active cells in any given imaging session relative to planes above 400 μm (Figure 4.2A), which is also consistent with evidence of sparse and dense coding strategies in L2/3 and L5, respectively (for reviews see Barth & Poulet, 2012; Petersen & Crochet, 2013). Thus, when segmented cells were grouped by laminae, the visible transition between planes with a low versus high density of active cells was used to both verify the approximate depth of the boundary between superficial and deep layers and align this boundary across mice. Superficial cells were further divided into "upper" and "lower" divisions such that cells from the most superficial three imaging planes 1-3 were classified as upper L2/3 (upper superficial) and cells from planes 4-6 were classified as lower L2/3 (lower superficial). Cells detected in the deepest three imaging planes 8-10 were classified as L5a (deep) and the intermediate plane 7 was excluded to account for variations in the location of the boundary between L2/3 and L5a across mice (refer to Figure 4.2B). When all detected cells were grouped by these laminar divisions, there were significantly fewer deep layer cells recorded from both M2 (two-way ANOVA, $F(1.3,6.6)=8.304$, $p<0.05$) and M1 (two-way ANOVA, $F(1.1,3.2)=14.17$, $p<0.05$) relative

to upper and lower superficial cells, which was likely a consequence of two-photon imaging limitations that arise due to increased light scattering and poor signal contrast at greater cortical depths. However, there was no effect of lesion on the relative fractions of detected cells per laminar division in M2 (two-way ANOVA, $F(1,5)=1.975$, $p=0.22$) or M1 ($F(1,3)=0$, $p=0.99$; Figure 4.3).

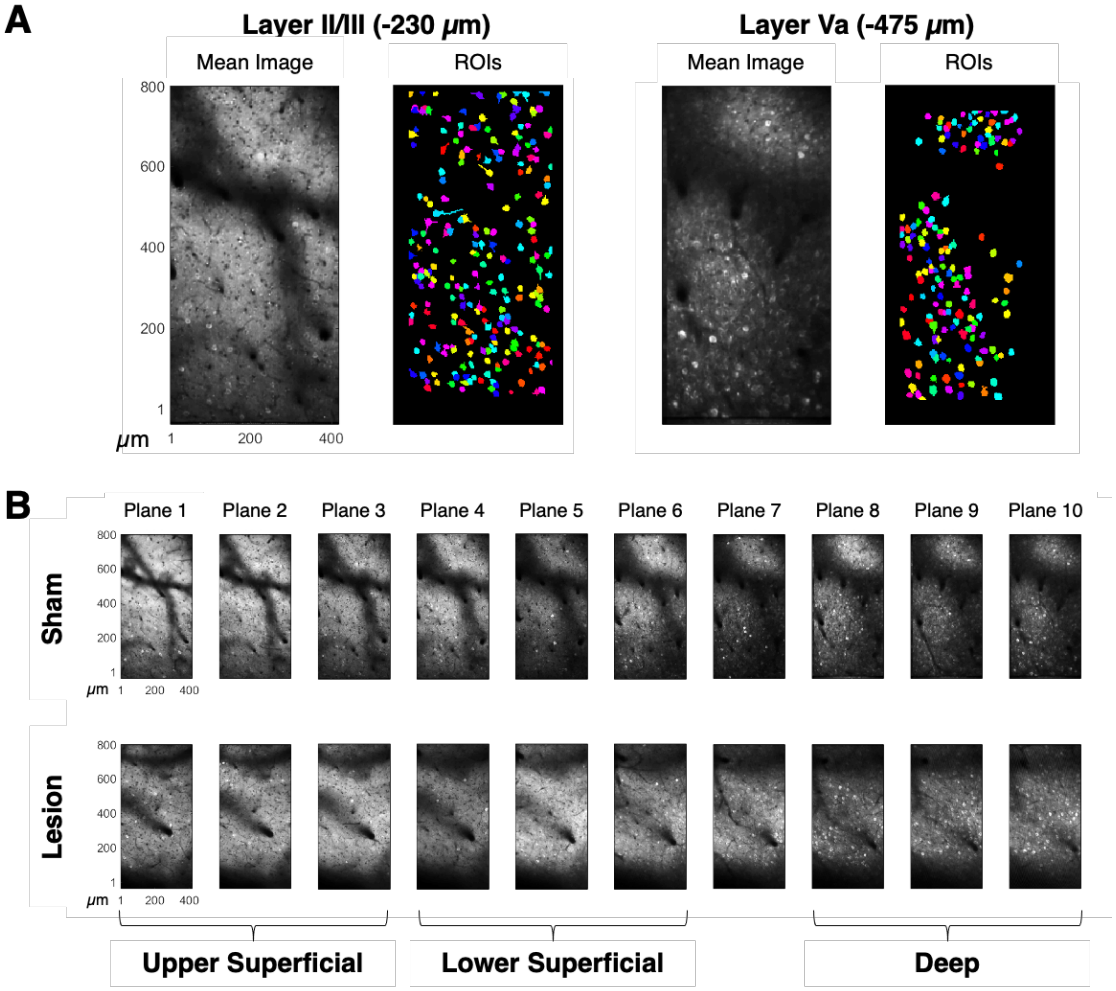

Figure 4.2: Layer 5a exhibited a higher density of active cells relative to layer 2/3. (A) An example mean image (left) and corresponding Suite2p-detected cellular regions of interest (ROIs; right) for an L2/3 *z*-plane (-230 μm) and an L5a *z*-plane (-475 μm) from a sham control. (B) Mean images of all analyzed *z*-planes (spanning approximately -150 to -500 μm below the cortical surface) from an example sham control (top panel) and an example mouse with bilateral dorsal hippocampal lesions (bottom panel). The grouped laminar divisions are delineated. Mean images in (A-B) were contrast enhanced for clarity.

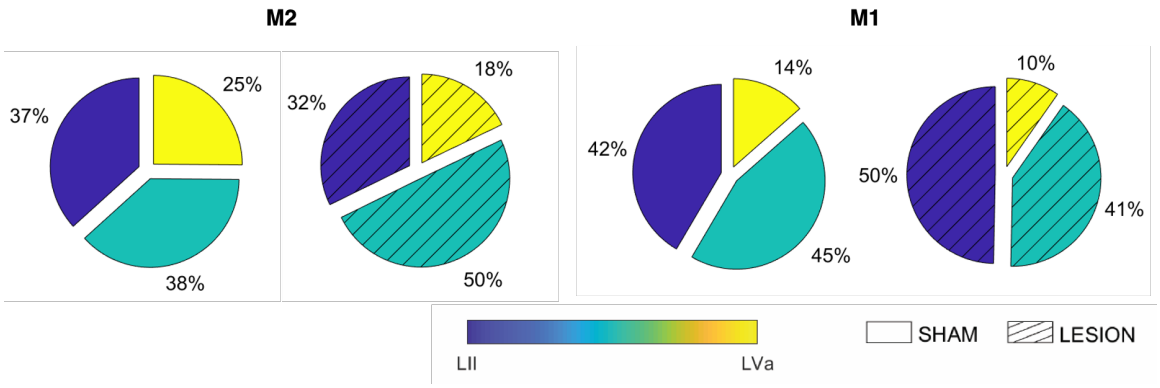

Figure 4.3: Mean fractions of all detected cells, grouped by cortical depth, in M2 and M1 of sham controls and mice with bilateral lesions of the dorsal hippocampus. Superficial L2/3 cells were divided into upper (dark blue) and lower (teal) fractions, whereas deep L5a cells are shown separately (yellow).

Spatially selective cells were detected in both the superficial and deep laminae of motor cortices and, within each laminar division, these cells formed uniform representations of the spatial environment (Figure 4.4A). Spanning the superficial layers of motor cortices, the fractions of spatially selective cells detected in each *z*-plane formed a gradient with the highest proportion in the most superficial plane and lower proportions evident around the boundary between L3 and L5 (Figure 4.4B). Subsets of cue-tuned cells—that is, spatially selective cells with activity patterns that were more closely correlated with obstacle location than contextual space—were evident in both laminar divisions. There was an interaction between cortical region and depth (three-way ANOVA, $F(9,81)=8.4.155$, $p<0.001$), but not lesion group, such that cue-tuned cells were generally underrepresented in deep layers of M1 (Figure 4.4C). Otherwise, the distributions of cue-specific cells were each roughly proportionate to the total population of active spatially selective cells across the cortical depth of M2 and M1 (Figure 4.4B-C).

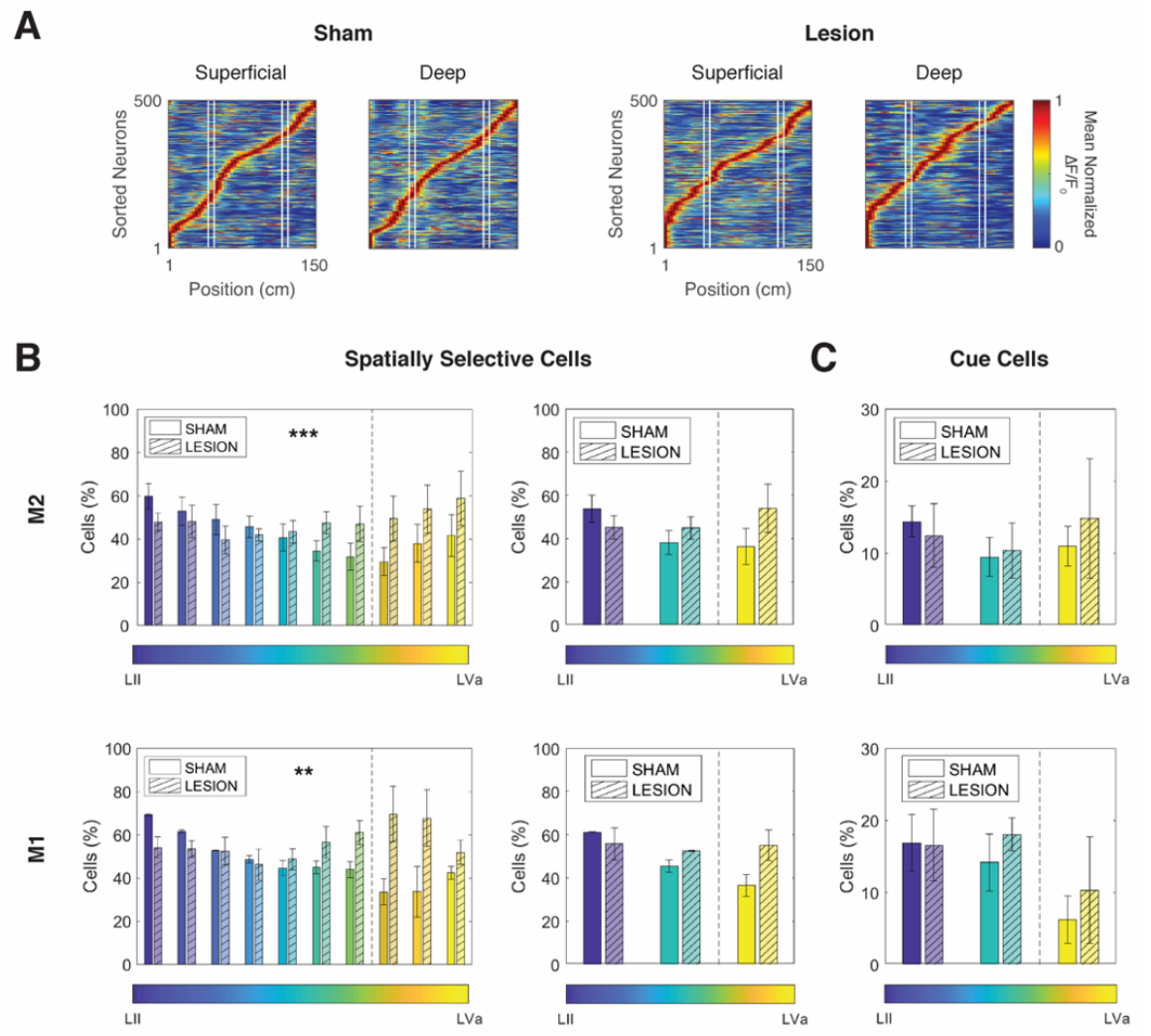

Figure 4.4: Fractions of spatially selective cells formed a gradient across superficial layers that was abolished by hippocampal lesions. (A) Mean normalized activity vectors for spatially selective cells in superficial *z*-planes (left panels) or deep *z*-planes (right panels), averaged across experimental sessions with added obstacles in the A/B orientation and sorted by the order of maximum mean normalized $\Delta F/F_0$. A random selection of 500 spatially selective cells from both M2 and M1 were divided by laminar position and pooled across sham controls (left) or mice with bilateral dorsal hippocampal lesions (right). White lines indicate the boundaries of the interchangeable obstacles. (B) Left: Fraction of all cells detected within each cortical imaging *z*-plane that were classified as spatially selective after sham (solid bars) or bilateral lesions (dashed bars) of the dorsal hippocampus. Right: Fraction of all cells that were classified as spatially selective cells within each laminar subdivision. (C) Proportion of all cells that were classified as cue-tuned within each laminar subdivision. Note the difference in scale between (B) and (C) and that cue-tuned cells fit the criteria for spatially selective and so are also represented in (B). For all plots, the dashed line indicates the approximate boundary between L3 and L5 (~400µm below the cortical surface). Error bars are SEM. Cortical depth of cells is indicated by colour bar.

Consistent with elevated spatial selectivity in superficial layers, cells located in *z*-planes closer to the cortical surface encoded higher spatial information (Figure 4.5A) and exhibited reduced lifetime sparsity indices (Figure 4.5B). These measures each formed a gradient that extended into deep layers, with deep cells encoding the lowest spatial information and exhibiting the highest lifetime sparsity indices. In both M2 and M1 of sham controls, the distributions of spatial information were significantly different among pooled upper superficial, lower superficial, and deep layer cells (two-sample Kolmogorov-Smirnov tests and Bonferroni-corrected α=0.008, p<0.001) and there was a main effect of depth across mice (two-way repeated measures ANOVA, F(1.397,6.986)=9.023, p<0.05) such that the median spatial information was significantly higher in upper superficial cells relative to lower superficial and deep cells (Tukey's test, p<0.001). The distributions of lifetime sparsity were also significantly different between pooled laminar divisions of both M2 and M1 after sham surgeries (two-sample Kolmogorov-Smirnov tests and Bonferroni-corrected α=0.08, p<0.001) but the effect of depth on median sparsity was not significant across mice (two-way repeated measures ANOVA, F(1.109,5.545)=4.581, p=0.08).

The distribution of population activity (averaged across all detected cells at each binned position on the treadmill) was also different across the cortical volume (Figure 4.6A). Cell populations in more superficial imaging *z*-planes exhibited moderately elevated non-normalized activity trailing all cued locations in the environment, a trend that was not evident in deep layers (coefficient of variation (*SD/M*), upper superficial: 21.11%, lower superficial: 18.60%, deep: 14.61%). There was also a main effect of depth (two-way repeated measures ANOVA & Tukey's test, F(1.414,12,72)=13.74, p<0.01) such that the mean trial-averaged, non-normalized peak $\Delta F/F_0$ of spatially selective cells was

significantly higher in upper superficial planes relative to lower superficial and deep planes (p<0.01), and in lower superficial relative to deep planes (p<0.05; Figure 4.6B). Altogether, cells that were located closer to the cortical surface were more likely to be both spatially selective and to exhibit higher cue modulation.

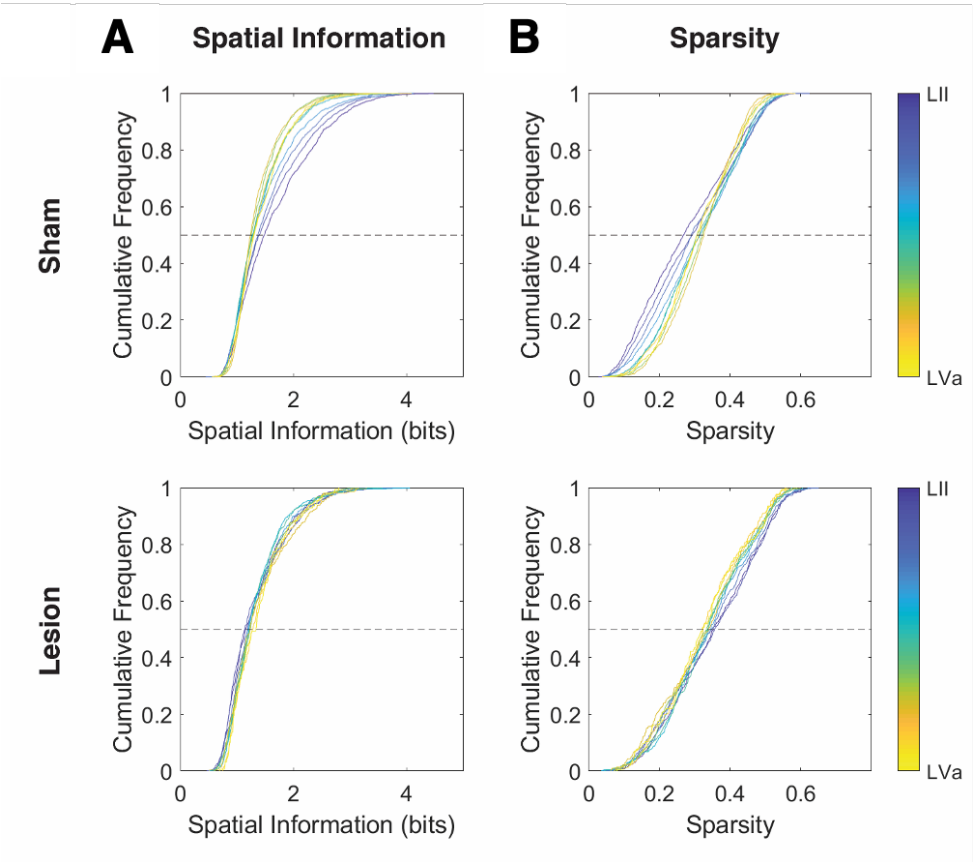

Figure 4.5: Cortical depth-varying gradient of spatial information and lifetime sparsity among spatially selective cells in motor cortices was abolished after hippocampal lesions. Cells were pooled across M2 and M1 of all mice within each treatment group. (A) Cumulative frequency distributions of spatial information encoded by spatially selective cells, averaged across experimental days with added obstacles, after sham (top) or bilateral dorsal hippocampal lesions (bottom). (B) Cumulative frequency distributions of lifetime sparsity indices, averaged across experimental days with added obstacles, after sham (top) or bilateral dorsal hippocampal lesions (bottom). Note that a lower sparsity index indicates that cells exhibited narrower spatial tuning profiles (i.e. firing was more sparse). In all panels, cortical depth of cells is indicated by colour bar.

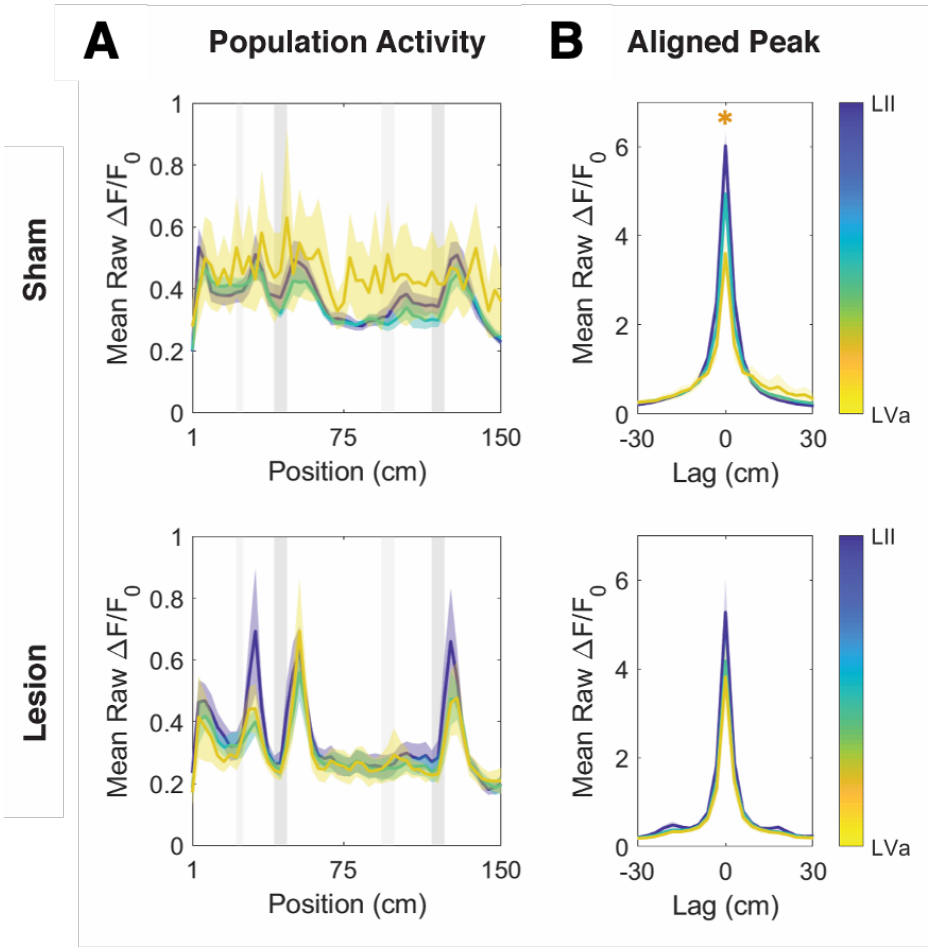

Figure 4.6: Mean non-normalized population activity and peak non-normalized activity of individual cells was more uniform across layers in the absence of an intact hippocampus. Cells were pooled across M2 and M1 of all mice within each treatment group. (A) Mean non-normalized $\Delta F/F_0$ across binned locations on the treadmill of upper superficial (blue), lower superficial (teal), and deep (yellow) cells after sham (top) or bilateral lesions of the dorsal hippocampus (bottom). Shaded area is SEM. Gray bars indicate the positions of the stable cues (light gray) and interchangeable obstacles (dark gray). (B) Aligned peak non-normalized $\Delta F/F_0$ of all upper superficial (blue), lower superficial (teal), and deep (yellow) cells after sham (top) or bilateral lesions of the dorsal hippocampus (bottom). Shaded area is SEM.

Spatially selective activity became more uniform across layers after hippocampal lesions

After bilateral lesions of the dorsal hippocampus, the representations of the spatial environment persisted in both superficial and deep layers, though the uniformity of those spatial representations were similarly disrupted at the interchangeable obstacle locations in

both laminar divisions (refer to Figure 4.4A; refer to Chapter 3). Strikingly, the gradient of spatially selective cell recruitment (refer to Figure 4.4B) was largely abolished. There was a significant interaction between lesion group and cortical depth (three-way ANOVA, $F(9,80)=8.484$, $p<0.0001$) such that the proportion of spatially selective cells increased in middle and deeper layers after bilateral lesions of the dorsal hippocampus, particularly in upper L5a. Moreover, the differences in mean population activity were also largely attenuated such that all grouped layers exhibited homogenously elevated activation at the cued locations (coefficient of variation (*SD/M*), upper superficial: 36.54%, lower superficial: 26.95%, deep: 31.92%; refer to Figure 4.6A) and there were no longer significant differences between the mean trial-averaged, non-normalized peak $\Delta F/F_0$ of spatially selective cells in upper superficial, lower superficial, and deep planes (Tukey's test, $p=0.27$-0.46); refer to Figure 4.6B). In L5a, changes in population activity also corresponded with alterations to the distributions of place fields. Deep layers of sham controls had a relatively uniform distribution of place fields across the cued portion of the environment whereas mice with dorsal hippocampal lesions demonstrated elevated concentrations of place fields at cued locations and a corresponding reduction of place fields at the surrounding non-cued locations (Figure 4.7).

Consistent with more homogenous spatially selective cell recruitment and population activity across layers, the gradients of spatial information (refer to Figure 4.5A) and lifetime sparsity (refer to Figure 4.5B) were also largely abolished after bilateral dorsal hippocampal lesions. Although the distributions of spatial information and lifetime sparsity were still significantly different between pooled upper superficial cells and those of other laminar divisions after hippocampal lesions (two-sample Kolmogorov-Smirnov tests and

Bonferroni-corrected α=0.08, spatial information: p<0.001, sparsity: p<0.01), there were no longer significant differences between lower superficial and deep layers in both M2 (spatial information: p=0.09; sparsity: p=0.07) and M1 (spatial information: p=0.03; sparsity: p=0.07). In addition, and in contrast to sham controls, there was no longer a main effect of depth on median spatial information (two-way repeated measures ANOVA, F(1.294,5.175)=0.1110, p=0.81) or median sparsity (two-way repeated measures ANOVA, F(1.224,4.896)=0.0232, p=0.92) across laminar divisions. In sum, in the absence of an intact hippocampus, the recruitment and spatial characteristics of spatially selective cells were more uniform across the cortical depth relative to sham controls and, in general, the modulation of those cells by cues was enhanced across layers.

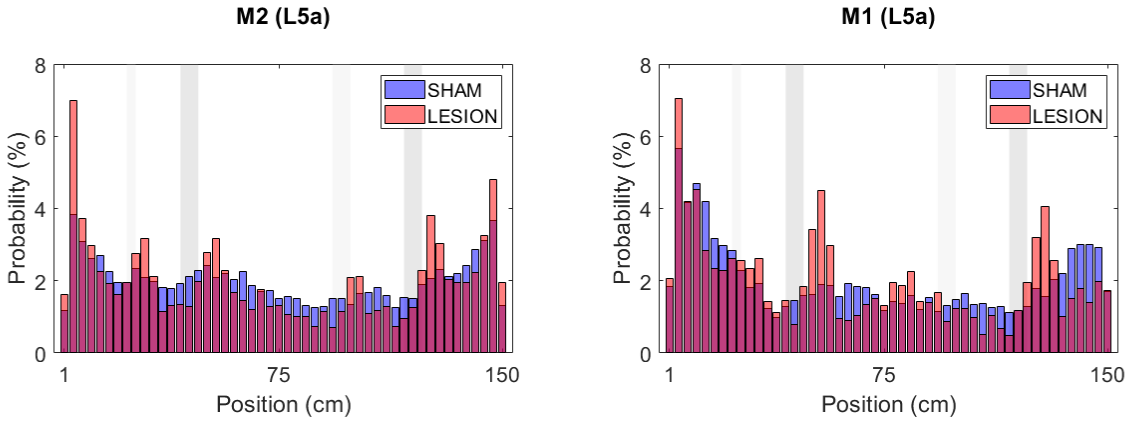

Figure 4.7: Distributions of place fields in L5a were more concentrated at cued locations in the absence of an intact hippocampus. For experimental days 3-8 (with added cues), the locations of place fields from spatially selective cells in L5a of M2 (left) or M1 (right) were pooled across sham controls (purple) or mice with bilateral lesions of the dorsal hippocampus (red). The mean probability of place field occurrence across days is shown. Gray bars indicate the positions of the stable cues (light gray) and interchangeable obstacles (dark gray).

Temporal drift could not explain increased spatial selectivity in superficial layers

Although temporal drift in spatial representations is more comprehensively examined in Chapter 6, Takehara-Nishiuchi et al. (2013) suggested that their observed differences in laminar context selectivity could be the result of differences in representation turnover with time or recurrent experience. That is, superficial layers only *appear* more context-selective because of more rapid changes in excitability or synaptic connectivity relative to deep layers. To assess this possibility, pre-surgery spatially selective cells were pooled across M2 and M1 according to cortical depth (upper superficial, lower superficial, and deep) and the temporal drift in the active spatially selective cell populations, place field positions, and the population correlations were examined across days.

The average turnover of active cells between consecutive days was significantly lower among deep cells ($M\pm SEM$=40.3±1.5%; one-way ANOVA & Tukey's test, $F(2,56)=6.59$, $p<0.01$) relative to upper superficial ($M\pm SEM$=44.4±0.4%; $p<0.05$) and lower superficial cells ($M\pm SEM$=45.3±0.8%; $p<0.01$; Figure 4.8A). Although this appears to support the hypothesis that deep layer cells are more stable, the ~5% difference in active cell turnover between superficial and deep layers is too small to account for the ~15% difference in representation overlap (measured by patterns of IEG expression) observed by Burke et al. (2005). Moreover, the distributions of place field shifts were not significantly different at any cortical depth (p=0.41-1, two-sample Kolmogorov-Smirnov test; Figure 4.8B). The distributions were highly peaked around 0 cm and 55% of all place field drift occurred within 15 cm of the previous place field location, indicating that place fields typically did not randomly relocate.

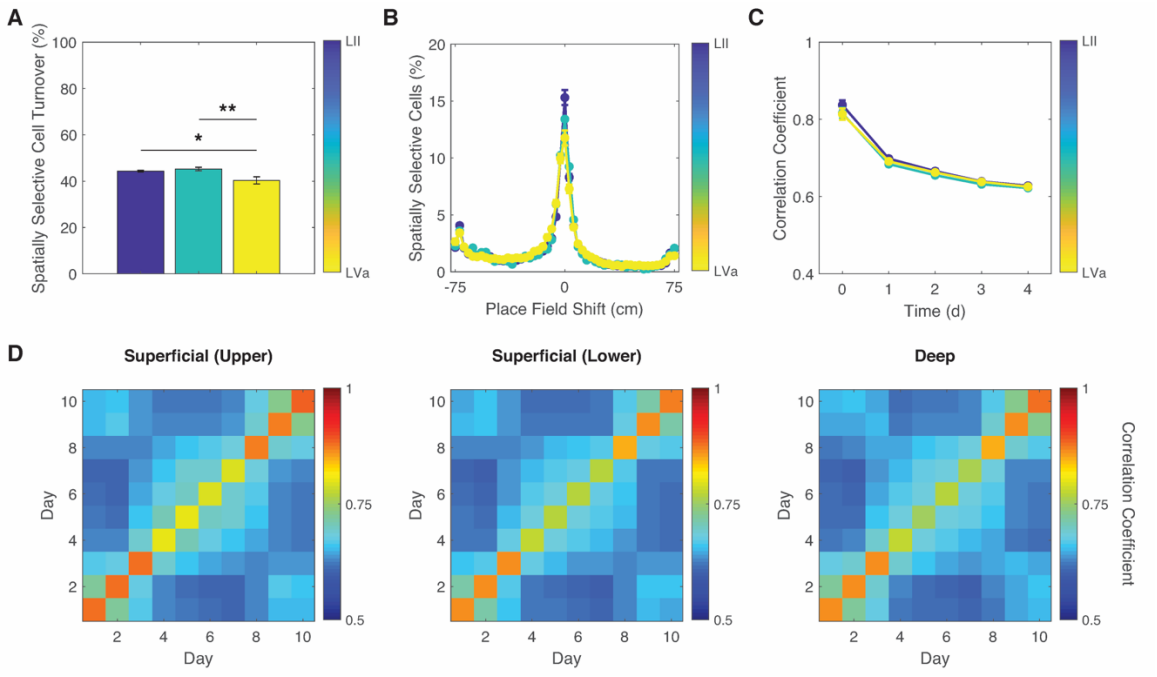

Figure 4.8: Representational turnover over time was weakly elevated in deep layers relative to superficial layers. (A) The proportion of spatially selective cells that gain or lose place fields (i.e. turnover) between consecutive days. Error bars are SEM. (B) The shift in the location of maximum firing of place fields between consecutive days, shown as a proportion of total detected place fields. Error bars are SEM. (C) Rate of decay of mean population activity correlation in the 1-4 days surrounding a context exposure. Error bars are SEM between sliding windows. (D) For each pair of days, the mean normalized activity vectors for each cell were cross-correlated (within a range of +/- 9 cm to account for the majority of place field drift) and averaged to obtain the Pearson's correlation co-efficient for the population. For cue-swap days (4-7), the pre- and post-swap trials were counterbalanced such that half of the neurons were always sampled from orientation A and the other half from orientation B across days. The diagonal represents the mean correlation between odd and even trials within one day.

To examine population activity patterns at each pooled cortical depth across the ten day paradigm, the mean normalized activity vectors for each cell were cross-correlated (within a range of +/- 9 cm to account for the majority of place field drift) and averaged to obtain the Pearson's correlation co-efficient for the population for each pair of days. For cue-swap days (4-7), the pre- and post-swap trials were counterbalanced such that half of the neurons were always sampled from orientation A and the other half from orientation B

across days. Within days, the mean correlation between odd and even trials was used as the starting (t = 0 d) correlation. The decay rate of the mean population activity correlation over four days after each behavioural episode was comparable between upper superficial (r = -0.072), lower superficial (r = -0.068), and deep layers (r = -0.066; Figure 4.8C). Overall, there were no significant differences between superficial or deep layers in the mean population activity vector correlations across all pairs of days (p=0.91, Kruskal-Wallis; Figure 4.8D).

4.4 DISCUSSION

This study examined the layer-specific influence of descending input from the hippocampus on context and content encoding in motor cortices. Consistent with previous findings in RSC (Mao et al., 2017), higher fractions of spatially selective cells were present in the superficial layers of motor cortices relative to middle and deep layers. The distribution of spatially selective cells and their encoded spatial information formed a gradient across the cortical volume such that superficial cells closer to the cortical surface were more sparsely and precisely tuned than those in deep layers. Interestingly, following bilateral lesions of the dorsal hippocampus, the proportion of spatially selective cells increased in upper L5a and the laminar gradients of spatial information and sparsity were abolished. Notably, these depth-dependent increases in relative spatially selective cell recruitment coincide with the location of sensory posteromedial thalamic nuclei inputs to motor cortex, which are concentrated within the upper portion of L5a (Hooks et al., 2013). Moreover, population activity became highly homogenous across layers in hippocampal-lesioned mice, displaying prominent peaks trailing the interchangeable obstacles. These results suggest that descending contextual input from the hippocampus indirectly suppresses the stimulus-evoked recruitment of deep layer cells and sharpens spatial tuning among superficial cells of motor cortices during behaviour in a familiar environment. Importantly, the concept that descending feedback functions to suppress or "explain away" ascending sensory inputs in lower cortices is a central hypothesis of the predictive coding theoretical framework (e.g. Friston, 2005; Rao & Ballard, 1999; Srinivasan et al., 1982). Thus, this study provides further evidence in favour of a dual role for the hippocampus in facilitating the coordinated reinstatement of distributed cortical memory representations

and propagating top-down predictions to improve the efficiency of cortical information processing (Barron et al., 2020).

Considering that there was lower overall recruitment of active cells in lesioned animals (refer to Chapter 3), a potential caveat is that these suppressive effects may have arisen due to decreased recruitment of spatially selective cells in superficial layers and/or a detection bias towards highly active cells. However, these explanations seem unlikely as the relative fractions of active cells detected across laminar divisions of sham and lesioned animals were not significantly different and encoded spatial information was selectively increased in deep layers of lesioned animals relative to controls, a finding that is inconsistent with a generalized recruitment bias towards highly active cells throughout the depth of the cortex. Moreover, such a hippocampal effect on cell recruitment has not been reported by other studies that used comparable methods (Esteves et al., 2021, 2023; Mao et al., 2018) and, thus, uncontrolled variability among mice cannot be excluded as the underlying cause of this disparity in detected cells between experimental groups.

Despite elevated fractions of spatially selective cells in upper superficial layers, there was no evidence of a corresponding increase in the representation of salient sensory cues in deep layers. In fact, cue-tuned cells tended to exhibit higher spatial information (refer to Chapter 3), suggesting that superficial layers may be more cue- than context-tuned. However, this study was limited by the poor signal contrast of green-shifted fluorophores in deep layers and the atypical agranular anatomy of motor cortex. Thus, the results do not preclude the possibility that context and content may be differently represented across L5a and L5b/6, or between the superficial and deep layers of non-motor cortical regions. Even within M2, Chen et al. (2017) similarly found that object place-specific cells were pervasive throughout the cortical volume in posterior medial M2—the area examined in the current

study—but not anterolateral M2. Regional generalizations are further muddied by inconsistencies in the literature regarding the classification of the medial agranular area, which is conventionally defined as part of M2 (Paxinos & Franklin, 2001). Based on microstimulation and anatomical tracing studies, others have argued that posterior medial M2 may actually correspond with vibrissal M1 (Brecht et al., 2004; Hooks et al., 2011). Although posterior medial M2 and M1 displayed subtle differences in cue cell characteristics (refer to Chapter 3), generalizing these regions as M1 might offer the most conservative interpretation of the results. In any case, a laminar division of context and content representation is not a generic feature of the neocortex. Future advances in three-photon imaging (Horton et al., 2013; Ouzounov et al., 2017) and genetically encoded calcium indicators with red-shifted fluorophores (e.g. Dana et al., 2016) may soon improve quantification of deep (L5-6) cell activity for further exploration of how the stereotyped laminar circuitry of the cortex mediates the integration of learned context with current sensory experience.

While M1 may have a unique agranular anatomy relative to other primary cortices, the observed distributions of spatial and sensory-evoked activity are not incongruent with other findings in primary sensory cortices. In a recent study that uncovered a full repertoire of spatial cell types—including place, grid, head direction, border, and conjunctive cells—within layers IV-VI of S1, spatially selective cells were also markedly underrepresented in upper L5 (Long & Zhang, 2021). The authors speculated that L5a may serve to integrate spatial and sensory information, effectively masking the independent impacts of salient inputs within that layer. Notably, this could also explain why the population activity in L5a became biased towards sensory stimuli in the absence of an intact hippocampus.

The observed interactions between top-down and bottom-up inputs in M1, revealed by bilateral lesions of the hippocampus, are also consistent with the findings of recent studies that inactivated RSC and M2 after learning. In mice learning a visually-guided active avoidance task, Makino & Komiyama (2015) found that the activity of L2/3 and L4 neurons in V1 gradually became sparser while the long-range inputs from RSC to L1 were concurrently enhanced. Furthermore, synaptic boutons in L1 and excitatory cells in L2/3 (the location of which corresponded with upper superficial cells in this study) were predominantly responsive to the visual stimulus onset in naïve animals but, with learning, eventually exhibited ramping activity specific for the stimulus *offset* and the coincident timing of an aversive shock. These learning-induced activity dynamics were strikingly abolished after post-learning inactivation of the RSC, leading the authors to conclude that descending inputs from RSC modulate task-dependent responses in V1. In another study, inactivation of M2 was also shown to impair the context-dependent enhancement of learned forelimb movement accuracy in M1 (Omlor et al., 2019). However, the results of the current study imply that these context-dependent signals might actually be higher-level, originating in the hippocampus and distributed through circuits in RSC and M2.

Although resolving the local circuits that facilitate contextual modulation of laminar activity dynamics is beyond the scope of this study, L5 is well-positioned to suppress recruitment of L4 and sharpen spatial tuning in L2. Both feedback projections from higher level cortices and descending input from L2/3 converge on L5, and the net effect of L5 activation is recurrent suppression of L2-4 (Onodera & Kato, 2022). In auditory cortex, optogenetic stimulation of L5 has been shown to sharpen frequency tuning and reduce the amplitude of tone-evoked responses in the superficial layers (Onodera & Kato, 2022), analogous to the effects of hippocampal input in this study. This laminar effect may be

partially mediated by somatostatin-expressing (SOM) interneurons, which exhibit reduced activity in parallel with learning-induced increases in top-down inputs to L1 (Makino & Komiyama, 2015). A subpopulation of SOM interneurons, Martinotti cells, are particularly abundant in L5 and target apical tuft dendrites within L1 (Kawaguchi & Kubota, 1997; Murayama et al., 2009; Silberberg & Markram, 2007). Within L4 and the upper boundary of L5a, another subtype of SOM interneuron (X94; Ma et al., 2006) specifically *disinhibits* L4 principal neurons by inhibiting parvalbumin-expressing fast-spiking interneurons (Xu et al., 2013). Thus, in a familiar environment, a decrease in SOM interneuron activity could simultaneously augment the relative strength of descending contextual inputs and reduce sensory-evoked recruitment of neurons within the thalamocortical recipient layer. On the other hand, in the absence of an intact hippocampus, recruitment of spatially selective principal cells around the boundary of L3/5 was increased and cells in L5a exhibited sharpened tuning to sensory stimuli, which may be the consequence of both enhanced L4 recruitment of parvalbumin-expressing interneurons in L5 (Pluta et al., 2015) and L2/3 activation of SOM interneurons in L5 (Pluta et al., 2019). Therefore, the relative strength of salient ascending inputs may be selectively enhanced by translaminar inhibitory circuits when descending contextual inputs are unavailable (e.g. during learning) and during attentive behaviour (Kok et al., 2012), an effect that may ultimately be facilitated by cholinergic signalling (Hasselmo, 2006; Letzkus et al., 2011; Obermayer et al., 2018; Poorthuis et al., 2014).

Altogether, the laminar organization of the cortex appears to provide a scaffold for the hierarchical retrieval of distributed memory representations throughout the neocortex, which can locally mediate the balance between excitation and inhibition. Hippocampal indices are sparsely coded (Jung & McNaughton, 1993), limiting both the density of direct

hippocampal back-projections to the cortex and the amount of information that can be transmitted. To more efficiently facilitate pattern completion in downstream cortical targets, the sparse hippocampal code is converted to a dense code in the subiculum and the deep layers of entorhinal areas (Barnes et al., 1990; Kim et al., 2012). In turn, the recurrently connected superficial cells of downstream association cortices are well equipped to "unzip" these dense codes, selectively retrieve the local component of a distributed memory representation, and effect output via L5. Interestingly, in contrast to the sparse code observed among cells in L2/3, cells in L5 (particularly thick-tufted pyramidal cells in L5b) also appear to employ a dense coding strategy (for reviews see Barth & Poulet, 2012; Petersen & Crochet, 2013). These output layer cells are highly intrinsically excitable and display elevated spontaneous and sensory-evoked firing rates (de Kock et al., 2007; de Kock & Sakmann, 2009; Hooks et al., 2011; Manns et al., 2004; O'Connor et al., 2010; Sakata & Harris, 2009; Schnepel et al., 2015; Schubert et al., 2001). Thus, descending interlaminar (L2/3→L5) and interareal (L5→L1) feedback circuits may represent recurring instances of the sparse-to-dense and dense-to-sparse code transitions, enabling sequential retrieval of distributed memory representations throughout the neocortical hierarchy. Future studies might employ transient optogenetic inactivation of association cortices—or specifically the output layers of those regions—to directly test this assumption that each tier of the hierarchy remains critical to retrieving sparse, uniform spatial representations in lower cortices.

5. MINICOLUMNAR ARCHITECTURE IS MASKED BY LOCALLY HETEROGENEOUS TUNING IN MURINE MOTOR CORTEX

5.1 ABSTRACT

The neocortex consists of neurons that are organized into distinct vertically-interconnected microcircuits known as “minicolumns”. These columnar modules tend to exhibit highly similar functional properties and thus are proposed to be the fundamental units of cortical operation. However, the functional relevance of minicolumns in rodents is a contentious topic; there are conflicting reports of depth-invariant tuning, mixed minicolumnar architecture, and a complete lack of modularity. To explore the putative role of minicolumnar architecture in motor cortex during spatial navigation, this study used *in vivo* two-photon microscopy of genetically encoded Thy1-GCaMP6s calcium indicator mice to nearly simultaneously image pyramidal neurons spanning cortical layers II-Va of M1. During both running in a familiar treadmill environment and intertrial rest, spatial tuning and co-active cell activity was locally heterogeneous at all cortical depths with no apparent topographical clustering. However, proximate neurons within columnar volumes exhibited significantly higher mean correlation with each other than with a random sampling of cells from outside the column and their mean response properties formed a patchy topography of spatial tuning with relatively distinct boundaries. These results support that a weak functional minicolumnar architecture exists in the rodent cortex, including in non-sensory cortices, perhaps as a result of shared inputs and developmental biases.

5.2 INTRODUCTION

Columnar topography of the neocortex

The horizontal laminar architecture of the neocortex is intersected by a uniform and evolutionarily-preserved vertical circuitry called "minicolumns" that are thought to operate in parallel within larger functional "macrocolumns". Minicolumns are narrow, radially-interconnected microcircuits—roughly 20-60μm in diameter—comprised of a variable quantity of neurons that depends largely on species-specific cortical thickness (Buxhoeveden & Casanova, 2002). The minicolumn consists of a cell-dense linear core of pyramidal neurons and inhibitory interneurons (with associated vertical bundles of axons and apical dendrites) surrounded by a cell-sparse peripheral neuropil space containing glia and basal dendritic arbor (Buxhoeveden & Casanova, 2002; Lorente de Nó, 1938; Mountcastle, 1997; Peters & Sethares, 1996).

Diverse experimental methodologies have demonstrated that the pyramidal cells comprising individual minicolumns exhibit highly similar functional properties, most notably shared receptive fields or "tuning" in sensory cortices. Single unit microelectrode recordings have superimposed distinct peripheral receptive fields on individual minicolumns in the somatosensory cortex (Favorov et al., 1987; Favorov & Whitsel, 1988; Mountcastle, 1957), demonstrated the successive orientation tuning of adjacent minicolumns in the visual cortex (Hubel & Wiesel, 1962, 1968), and provided evidence for minicolumnar frequency mapping in the auditory cortex (Shamma et al., 1993; Sugimoto et al., 1997). Additionally, in a somatosensory nerve regeneration experiment, Kaas et al. (1981) demonstrated that neighbouring minicolumns respond to adjacent and overlapping peripheral receptive fields such that the transition between minicolumns appears to

gradually shift. However, regeneration of transected nerve fibers was often misdirected, resulting in the innervation of abnormal locations of skin and the imposition of new receptive fields on the corresponding minicolumns. This remapping resulted in more abrupt shifts in responses between adjacent minicolumns, supporting the theory that the minicolumn is the smallest identifiable functional unit in the neocortex (Buxhoeveden & Casanova, 2002). Furthermore, coordinated variations in the activity-dependent intrinsic optical and metabolic properties of neurons have confirmed the anatomical size and periodic spatial distribution of minicolumns and suggest that the neurons comprising a minicolumn have synchronized activity (Holthoff & Witte, 1996; Kohn et al., 1997; Tommerdahl et al., 1993). Taken together, the minicolumn is now widely considered the basic computational unit of the mature neocortex (Kaas & Balaram, 2015; Lorente de Nó, 1938; Mountcastle, 1997; Rakic, 1988).

Though minicolumnar architecture was the focus of this study, the functional significance of minicolumns to cortical processing is more apparent in the context of the higher-level macrocolumn. Sometimes referred to "segregates" (Favorov & Whitsel, 1988), "modules" (Hubel, 1982), or simply as "columns" (Mountcastle, 1997), macrocolumns are groupings of 50-80 minicolumns (approximately 300-600μm in diameter) bound together by common input and short-range lateral connections (Mountcastle, 2003). Macrocolumns have been extensively described in the somatosensory cortex (Favorov & Diamond, 1990; Mountcastle, 1957; Powell & Mountcastle, 1959; Woolsey & Van der Loos, 1970) and visual cortex (Blasdel & Salama, 1986; Hubel & Wiesel, 1974, 1977) where sensory input can be topographically mapped. Typically, these clusters of proximate minicolumns have similar response properties and abrupt functional boundaries. In somatosensory cortex, the extent of afferent thalamocortical innervation in layer IV corresponds to macrocolumn

dimensions, supporting that each macrocolumn may serve to process and respond to a subset of related afferent inputs (Favorov et al., 2015; Garraghty & Sur, 1990; Jones et al., 1982; Landry et al., 1987; Landry & Deschênes, 1981; Rausell & Jones, 1995). GABAergic lateral inhibition and recurrent connectivity between the minicolumns comprising the greater macrocolumn then presumably function to enhance feature tuning, distinguish similar inputs, and provide a strong, sparsely distributed pattern of neural activation.

However, the functional relevance of columnar architecture has historically been debated (Horton & Adams, 2005; Jones, 2000; Purves et al., 1992; Swindale, 1990). Unlike minicolumnar cytoarchitecture, which visibly pervades the neocortex, functional macrocolumns are not always distinctly evident and there is substantial heterogeneity among cortical regions and species (Horton & Adams, 2005). In the visual cortex, there are well-characterized examples of "unbounded" macrocolumns where stimulus dimension parameters, such as orientation and spatial frequency, exhibit gradual, continuous feature tuning from one minicolumn to the next such that individual macrocolumns cannot be distinguished by receptive field input (Hubel & Wiesel, 1974; Kaas & Balaram, 2015; Nauhaus et al., 2012). Even distinct functional boundaries (or lack thereof) are highly influenced by synaptic plasticity mechanisms after the underlying minicolumn cytoarchitecture has already been firmly established (Hubel et al., 1977; Merlin et al., 2013). Thus, macrocolumns are somewhat arbitrarily defined and their existence throughout the entire cortex remains merely speculative. Furthermore, mature minicolumns also exhibit a degree of heterogeneity and a "generic" computational function for the minicolumn (that extends beyond feature tuning in sensory cortices) has yet to be experimentally resolved. Though substantial physiological, developmental, computational, and pathological evidence has accrued in support of minicolumns as elementary cortical

processing units, the link between the anatomical organization of the cortex and the physiological role of columnar architecture remains a contentious topic.

Cortical neurogenesis and ontogenetic minicolumns

The relative uniformity of minicolumnar cytoarchitecture across the mature neocortex is established during neurogenesis. Though other mechanisms of cell migration have been identified (Anderson et al., 1997; Austin & Cepko, 1990; O'Rourke et al., 1995; Reid et al., 1995), radial migration of neuronal precursor cells from the embryonic ventricular zone is the dominant mode for structural organization of the developing neocortex (Gressens & Evrard, 1993). During early cortical development, a homogenous population of neuroepithelial cells (neural stem cells) first symmetrically divides and gives rise to radial glial cells, the major class of neuronal progenitors (Cameron & Rakic, 1991; Götz & Barde, 2005). The radial glial cells produced during these first few parent cell divisions extend through the neuronal layers from the apical surface of the ventricular zone to the basal lamina, becoming a scaffold for further structural organization of the cortex (Huttner & Kosodo, 2005; Rakic, 1978, 2003). These cells then undergo asymmetrical mitosis to produce both bipolar migrating neurons and other neural progenitors including short neural precursors (Gal et al., 2006) and intermediate neuronal progenitors (Noctor et al., 2004). New neurons then migrate and are positioned along the elongated radial glial fibre guides in an "inside-out" manner where early-born neurons occupy deep layers and late-born neurons migrate to superficial layers (Noctor et al., 2001, 2004; Rakic, 1988). Altogether, the three-dimensional architecture of the mature neocortex derives largely from three interactions: the sites of radial glial cell origin in the ventricular zone, radial migration

of clonal neuronal precursors along glial scaffolds, and the temporal origin of neuronal precursor cells (Rakic, 1988, 2007).

Recent evidence suggests that the modular *functional* circuitry of the neocortex also arises from these radial ontogenetic units. During early post-natal development, sister excitatory neurons arising from the same parent radial glial cell exhibit strong, transient electrical coupling (He et al., 2015; Yu et al., 2012). This selective electrical communication promotes synchronous firing within ontogenetic columns, which appears to facilitate later development of specific unidirectional chemical synapses between sister neurons but not with adjacent, unrelated cells (Yu et al., 2009, 2012). Furthermore, radially-aligned sister neurons in the superficial layers of the visual cortex have been shown to develop similar orientation selectivity, and this shared functional maturation within the ontogenetic column can be abolished by disruption of early electrical coupling (Li et al., 2012; Ohtsuki et al., 2012). After this gap junction-mediated receptive field formation, the recurrent connections between unrelated (but similarly tuned) minicolumns appear to be primarily established by synaptic plasticity mechanisms (Ko et al., 2013). Taken together, these findings strongly support that ontogenetic minicolumns have an inherent predisposition to coordinated functionality in the adult cortex and are not merely anatomically similar, repetitive arrangements of excitatory neurons.

Computational predictions of modular cortical processing

Neural activity in the neocortex is commonly modeled as an attractor network in which the firing of recurrently connected nodes dynamically evolves towards a stable network state (i.e. a memory; Amari, 1972; Amit, 1989; Rolls & Treves, 1998). The number of stable attractor states in a sparse, uniformly distributed, random pattern of neural activity

increases with the number of modifiable connections but not with the number of functional units (O'Kane & Treves, 1992b, 1992a; Treves, 2005). So, in a network where the nodes are assumed to be individual neurons (as dictated by the "single neuron doctrine"; Barlow, 1972), the maximum interconnectivity and thus the maximum memory capacity of the network is largely limited (Treves, 2005). However, if the nodes are scaled up to *modules* of neurons (i.e. minicolumns) selected for activity by lateral inhibition within small attractor networks (i.e. macrocolumns), and only a fraction of these are simultaneously active (i.e. a sparse distributed representation), the storage capacity of the network is substantially increased (Fulvi Mari, 2004; Fulvi Mari & Treves, 1998; Johansson & Lansner, 2007).

In attractor neural networks modeled on these assumptions, minicolumns operate as competitive "winner-take-all" modules within macrocolumns, which are proposed to process, store, and later retrieve the relevant activity patterns (Lundqvist et al., 2006; Rinkus, 2010). In response to simulated inputs to the macrocolumn, the firing of cells comprising individual minicolumns becomes synchronized and minicolumns enter clear active and inactive states that mimic physiological "UP" and "DOWN" states of firing frequency (Cossart et al., 2003; Lundqvist et al., 2006). When the afferent input is phase-locked to inhibitory oscillations, the system is capable of self-tuning the receptive fields of its minicolumns (Lücke & von der Malsburg, 2004). Moreover, these models exhibit important characteristics of cortical processing including spontaneous pattern activation or reactivation, pattern completion (the retrieval of a complete "memory code" from an incomplete input), and pattern rivalry (the competition between simultaneously stimulated patterns of activity; Lundqvist et al., 2006).

Besides an increased pattern storage capacity, modular neural networks have other fundamental advantages over non-columnar models such as fault tolerance, improved reaction time, and noise robustness. A modular system, especially one that is self-tuning, can tolerate low levels of cell or synaptic loss—from physical damage, improper wiring during neurogenesis, or disease—because of the functional redundancy of a shared receptive field among the many cells comprising a minicolumn (Lücke & von der Malsburg, 2004). In addition, the close physical proximity of similarly tuned minicolumns facilitates the direct inhibition of nearest neighbours by the cells best tuned to the stimulus, which improves the feature discrimination of similar inputs within a macrocolumn. The signal to noise ratio is further improved by the recurrent connectivity of excitatory cells between these minicolumns (especially in layers II/III), which amplifies the firing rate of the best-tuned minicolumns (Bush & Mainen, 2015; Lundqvist et al., 2006). This recurrent connectivity also reduces the latency of pattern completion within the macrocolumn, especially when the codes representing related inputs are highly overlapping (Lücke & von der Malsburg, 2004; Rinkus, 2010). While individual neurons have relatively low firing rates that would presumably delay information processing, the population code derived from minicolumns enables a more rapid, accurate, graded response from the macrocolumn (Lundqvist et al., 2006).

Altogether, abstract attractor neural network models that consider modular cortical architecture appear to out-perform those that rely on single neurons as the basic functional units of cortical activity. Nevertheless, while these small-scale computational models provide a theoretical framework for understanding modular cortical processing, future models will undoubtedly be improved by larger-scale simulations (that better represent the

configuration and spatial extent of a cortical network) and new physiological data (that elaborate on the intricate biological constraints within and between minicolumns).

Minicolumn disorganization in neurological disorders

In further support of the functional significance of columnar architecture, cognitive ability in humans appears to be directly related to minicolumn integrity (Chance et al., 2011; Cruz et al., 2009). Disruptions to minicolumn structure, spacing, connectivity, and modulation have been implicated in numerous neurological disorders including autism spectrum disorders (Casanova et al., 2003, 2006, 2010), Down's syndrome (Buxhoeveden et al., 2002), schizophrenia (Casanova, 2007; Casanova et al., 2005, 2008; Chance et al., 2008; Di Rosa et al., 2009), dyslexia (Casanova et al., 2002), drug addiction (Buxhoeveden et al., 2006), Alzheimer's disease (Buldyrev et al., 2000; Chance, 2006; Chance et al., 2011), and Lewy body dementia (Buldyrev et al., 2000).

Thinning of minicolumns (defined as reduced dendritic spines and arborisation without cell loss) in temporal association cortex is characteristic of normal aging and correlated with mild cognitive impairment (Chance et al., 2006; Cruz et al., 2009). Given that the number of cortical neurons and neuronal density does not change with age, it has been suggested that subtle changes in neuron location and dendritic atrophy could be sufficient to reduce minicolumn fidelity (Cruz et al., 2004, 2008). In Alzheimer's disease and Lewy body dementia, the increasing neural degeneration and incidence of neurofibrillary tangles or Lewy bodies in the cortex is thought to surpass the fault tolerance of the network, significantly disrupt information processing by minicolumn ensembles, and exacerbate the cognitive decline associated with aging (Buldyrev et al., 2000; Chance et al., 2011).

Narrowing of the cell-dense minicolumn core and the peripheral cell-poor neuropil space as a result of neurodevelopmental abnormalities are also linked with several pathologies. In autism spectrum disorders, for example, there are increased numbers of cortical minicolumns (resulting in larger overall brain volumes) and both the peripheral neuropil space and the width of the minicolumn core are significantly diminished compared to unaffected adults (Casanova et al., 2006, 2010). Considering that inhibitory elements are typically present in the surrounding neuropil space and that short-range connections are favoured in higher density tissue, the hypersensitivity associated with autism spectrum disorders can likely be attributed to an imbalance between excitation and inhibition within and between minicolumns (Casanova et al., 2003; Vattikuti & Chow, 2010). These incongruities may originate from a temporal dissociation of radial glial cell migration from the tangential migration of inhibitory cells or, considering the increased number of minicolumns, a prolonged period of symmetrical neuroepithelial cell divisions during neurogenesis (Casanova, 2013; Kornack & Rakic, 1995).

On the opposite end of the cortical disorganization spectrum, *widening* of the minicolumn core and surrounding neuropil space can also impair normal cortical processing. In contrast to autism, children with Down's syndrome tend to have broader neuropil spaces and wider, but less cell-dense, minicolumns than the normal population. The enlargement of minicolumns during development is consistent with accelerated aging, as they are of relatively normal width in the adult brain. However, the adult brain volumes of Down's syndrome patients are significantly smaller than controls and thus the capacity for information processing is diminished due to the overall reduction in both computational units and neuronal complexity (Buxhoeveden et al., 2002).

In addition to anatomical abnormalities, minicolumnar pathologies can also arise from aberrant modulation of relatively normal minicolumn circuitry. Patients with schizophrenia exhibit normal core minicolumnar architecture with region- and layer-specific alterations to neuropil spacing, which suggests that circuitry disturbances occur after formation of the radial glial cell scaffold (Casanova et al., 2005, 2008). Considering the success of treatment with anti-psychotics and dopamine antagonists, the behavioural abnormalities observed after puberty may stem from a single defect in the monoaminergic systems (Casanova, 2007). Furthermore, while schizophrenia is a multifactorial disorder with many genetic and environmental factors that influence susceptibility, many of these risk factors, such as abnormal expression of *Disrupted-in-Schizophrenia-1 (DISC1)*, have been shown to impair monoaminergic innervation during ontogenesis (Niwa et al., 2010). Monoamines are essential to pyramidal cell specification and maturation, and monoaminergic projections constitute a significant component of normal neuropil, serving to modulate glutamatergic and GABAergic output (Casanova et al., 2008; Seamans & Yang, 2004). Thus, aberrant neurotransmission in adult schizophrenics may be attributable to a defective interaction between cortical lamination, monoaminergic innervation, and the maturation of minicolumn interconnections during neurodevelopment (Casanova, 2007; Casanova et al., 2008).

Altogether, minicolumn development, structure, and circuit integrity have been broadly implicated in numerous neurological disorders and even subtle changes to morphology and connectivity can potentially affect normal cortical processing. However, the study of minicolumn pathologies is largely restricted to post-mortem anatomical analyses and computational modelling. Novel animal models of both normal and abnormal

functional cortical architecture are critical to improving future research concerning the gain, progression, and treatment of these various neurological disorders.

Study objectives

Rodents are the most commonly used animal models in neuroscience and biomedical research. However, the functional relevance of minicolumns in rodents—and, therefore, their utility for studying minicolumnar pathologies—remains controversial. In contrast to the distinct columnar tuning observed in cats (Hubel & Wiesel, 1962; Ohki et al., 2005) and primates (Favorov & Whitsel, 1988; Hubel & Wiesel, 1968), the rodent cortex tends to exhibit a locally heterogeneous architecture in both the horizontal (e.g. Bonin et al., 2011) and vertical (e.g. Andermann et al., 2013) dimensions. Moreover, there are conflicting reports of depth-invariant tuning (Li et al., 2012; Ringach et al., 2016), mixed minicolumnar architecture (Kondo et al., 2016), and a complete lack of modularity (Han et al., 2019). To further explore the functional role of minicolumnar architecture during spatial navigation, this study used *in vivo* two-photon microscopy of genetically encoded Thy1-GCaMP6s calcium indicator mice to nearly simultaneously image pyramidal neurons spanning cortical layers II-Va in M1 while mice ran on a familiar treadmill environment. Notably, the fine-scale columnar topography of mouse motor cortex has not previously been investigated and agranular M1 uniquely enables single colour two-photon imaging as deep as L5, which is typically obscured by L4 in archetypal granular sensory regions. The topography of co-active cells and spatially co-tuned cells was examined during both active behaviour and intertrial rest to assess the potential role of modular processing during spatial navigation and locomotor movement.

5.3 RESULTS

Co-active cells were not topographically clustered

Neuronal ensembles—each containing at least ten co-active cells with a minimum pairwise correlation of 0.25—were detected separately for running and for the 15 second intertrial rest epochs in M1 of intact mice (n=7). On any given experimental day, ensemble cells comprised a small proportion of the total detected cells during behaviour (*M*±*SEM:* 17±2%) and intertrial rest (*M*±*SEM*: 9±2%; Figure 5.1A). The mean Pearson correlation of cells within individual intertrial rest ensembles (*M*±*SEM*: 0.42±0.01) was significantly higher than those detected during running (*M*±*SEM*: 0.35±0.01) and a random sampling of non-ensemble cells (*M*±*SEM*: 0.01±0.00; one-way ANOVA & Tukey's test, $F(2,15)=1614$, $p<0.001$; Figure 5.1B). The distributions of ensemble cells throughout the cortical volume were not significantly different between rest or running ensembles (multiple pairwise *t*-tests and two-stage step-up method of Benjamini, Krieger, and Yekutieli with false discovery rate threshold of 0.01, q=0.02-0.89; Figure 5.1C). Whereas co-active cells detected during running were predominantly spatially tuned to the same location(s) on the track, individual rest ensembles consisted of cells with activity patterns during running that corresponded with places or cues, short sequential sections of the treadmill belt, or the entire length of the environment (Figure 5.1D).

Co-active cells spanned cortical layers II-Va during both running (Figure 5.2A) and rest (Figure 5.3A) epochs. Although some select ensemble members were vertically-oriented, the majority of ensemble cells exhibited a "salt and pepper" organization across the lateral (XY) dimensions of the imaging volume (Figures 5.2B and 5.3B). Ensembles were highly overlapping in horizontal (XY) space and not clustered according to activity

during behaviour (Figure 5.2C) or rest (Figure 5.3C). The median silhouette score across all ensembles detected across ten experimental days and pooled across mice was -0.50 for running ensembles and -0.45 for intertrial rest ensembles, indicating that ensembles were highly overlapping and poorly clustered (Figure 5.4).

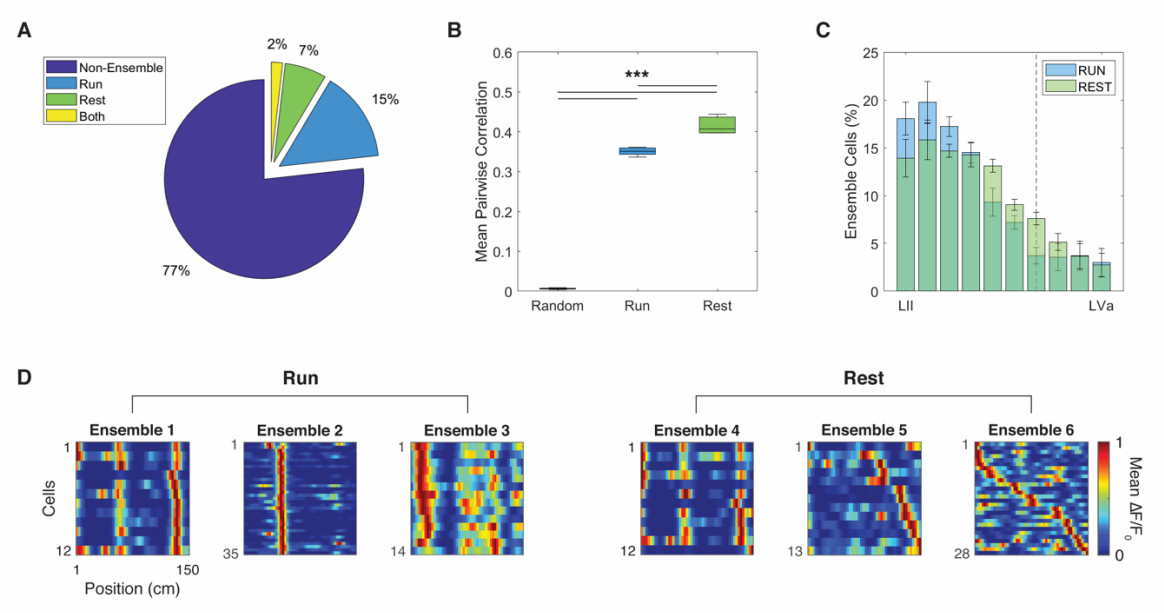

Figure 5.1: Neuronal ensembles that were active during running exhibited different characteristics than intertrial rest ensembles. (A) Mean proportion of all detected cells that were allocated to run or rest ensembles on any given experimental day. (B) Mean pairwise Pearson correlation between neurons comprising run or rest ensembles relative to random samples of neurons from the population. (C) Distribution of ensemble cells by cortical depth during rest and running epochs. Note that the apparent laminar effect is due to impaired detection of cells with increasing cortical depth. (D) Mean normalized $\Delta F/F_0$ of three example ensembles detected during running (1-3) and three ensembles detected during intertrial rest (4-6), each sorted by the location of maximum firing during running.

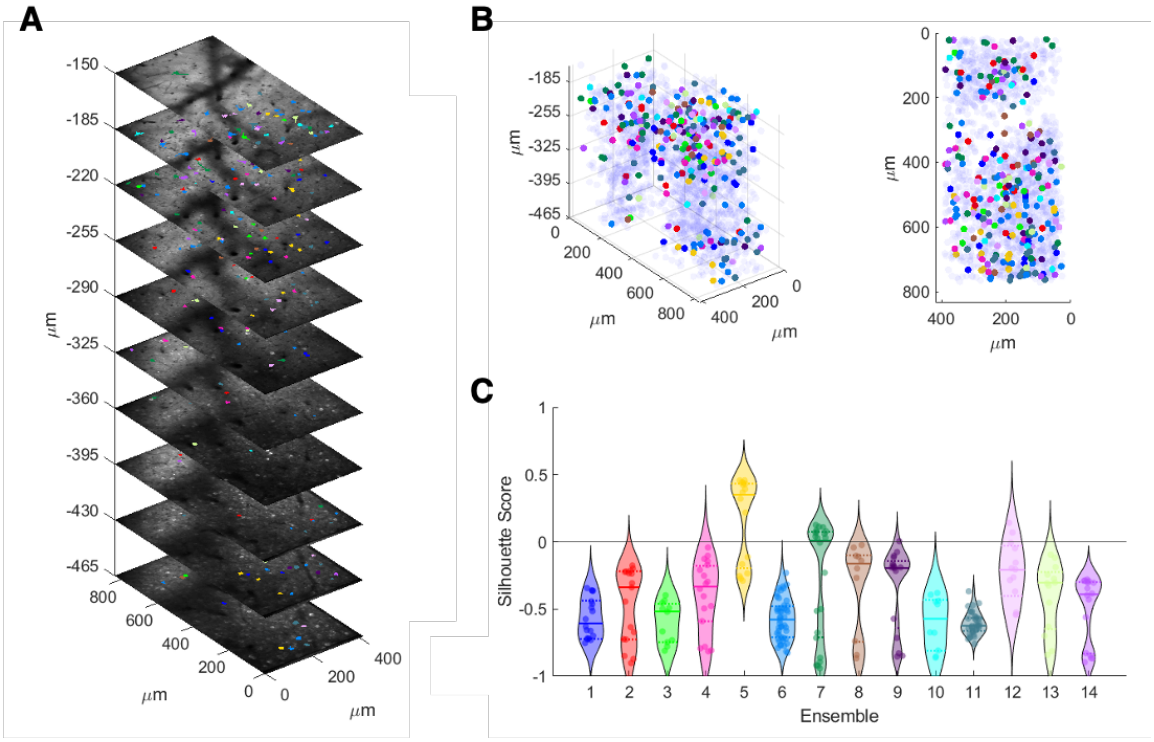

Figure 5.2: Co-active cells detected during running spanned cortical layers II-Va but were not topographically-clustered. Neuronal ensembles—containing at least ten cells with a minimum pairwise deconvolved activity vector correlation of 0.25—were detected during behavioural epochs where instantaneous velocity was greater than 0. (A) Example mean image stack from M1 with running ensemble cell bodies highlighted as different colours. (B) Centroids of coactive cells within individual ensembles from (A) plotted in a 3D volume (left) and as a collapsed *z*-stack (right). (C) Silhouette score for each detected ensemble relative to all other ensembles. Note that negative scores indicate that ensembles were highly overlapping and poorly clustered. For each violin plot, the line indicates the median and the colour corresponds with the cell and centroid colours in (A) and (B), respectively.

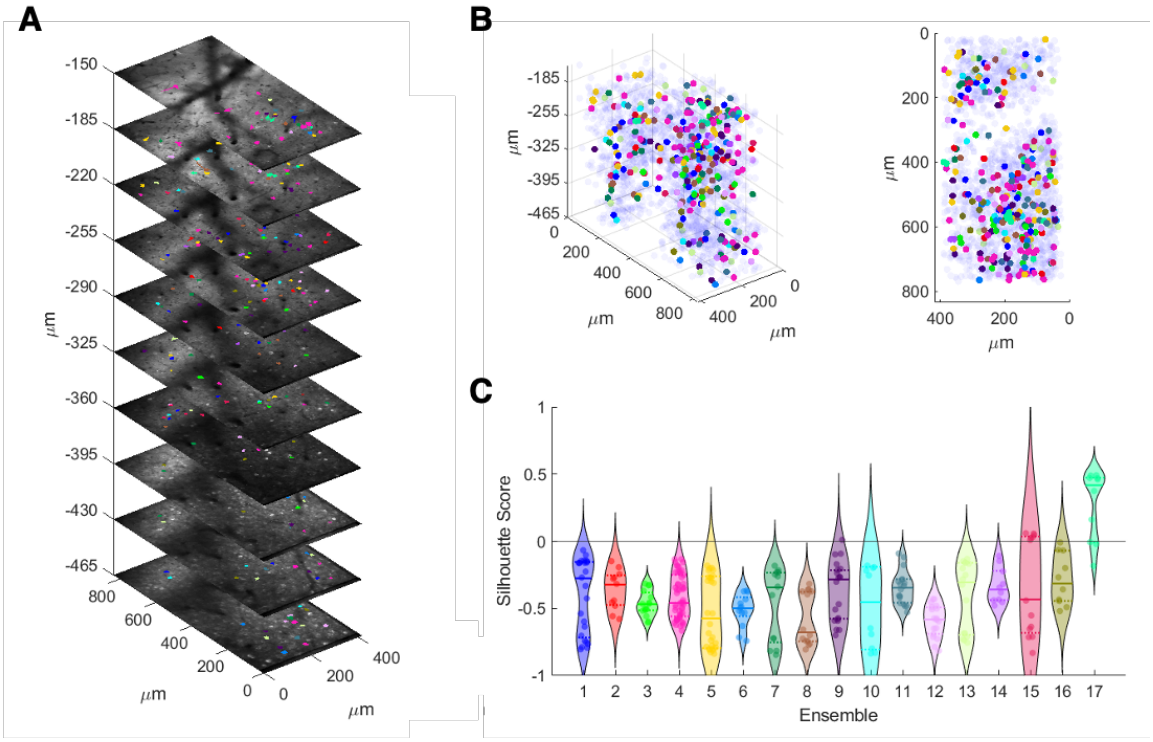

Figure 5.3: Co-active cells detected during intertrial rest spanned cortical layers II-Va but were not topographically-clustered. Neuronal ensembles—containing at least ten cells with a minimum pairwise deconvolved activity vector correlation of 0.25—were detected during intertrial rest epochs where velocity was 0. (A) Example mean image stack from M1 with rest ensemble cell bodies highlighted as different colours. (B) Centroids of coactive cells within individual ensembles from (A) plotted in a 3D volume (left) and as a collapsed *z*-stack (right). (C) Silhouette score for each detected ensemble relative to all other ensembles shown in (A-B). Note that negative scores indicate that ensembles were highly overlapping and poorly clustered. For each violin plot, the line indicates the median and the colour corresponds with the cell and centroid colours in (A) and (B), respectively.

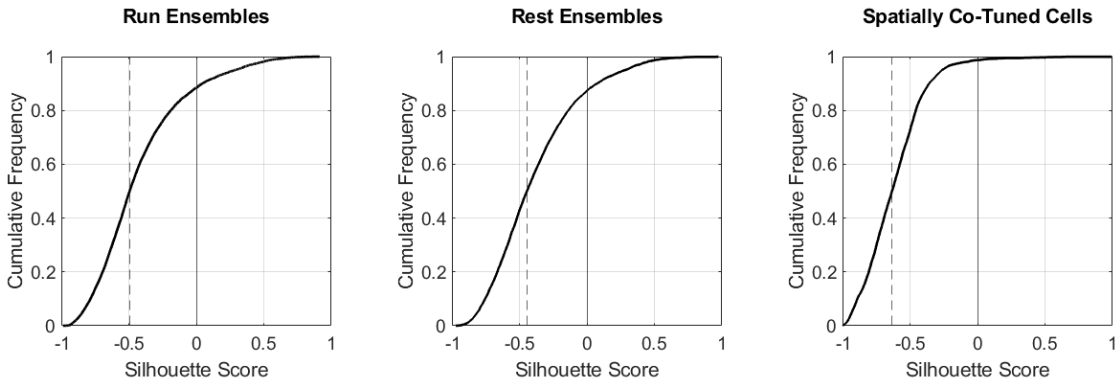

Figure 5.4: Co-active cells and spatially co-tuned cells were not topographically clustered. Cumulative frequency distributions of silhouette scores from running ensembles (left), intertrial rest ensembles (middle), and co-tuned spatially selective cells (right). Silhouette scores from ensembles were pooled across ten experimental days and mice. Silhouette scores from clusters of co-tuned spatially selective cells were pooled across mice. Dashed line indicates median.

It is possible that the cells comprising a minicolumn may not necessarily exhibit significantly correlated co-activity during behaviour as a consequence of sub-threshold stimulation or differences in long-range inputs or lateral inhibitory modulation. Nevertheless, a minicolumn may still be generally co-tuned to a particular stimulus. To address this possibility, all detected cells were clustered by less stringent criteria: the binned location of maximum mean normalized activity during running. As observed with co-active cells, some spatially co-tuned cells were vertically-aligned but, in general, a heterogenous pattern of tuning representation was dominant (Figure 5.5A-B). Spatially co-tuned cells exhibited no topographical clustering with a median silhouette score of -0.64 when pooled across mice (Figure 5.4 & 5.5C).

Finally, the relationship between the lateral proximity and the activity of pairs of neurons was examined. During both rest and running epochs, there was no correlation between horizontal (XY) Euclidean distance and the pairwise deconvolved activity vector

correlation between cells. The least squares regression correlation factor for all pairwise comparisons was approximately 0 (Figure 5.6).

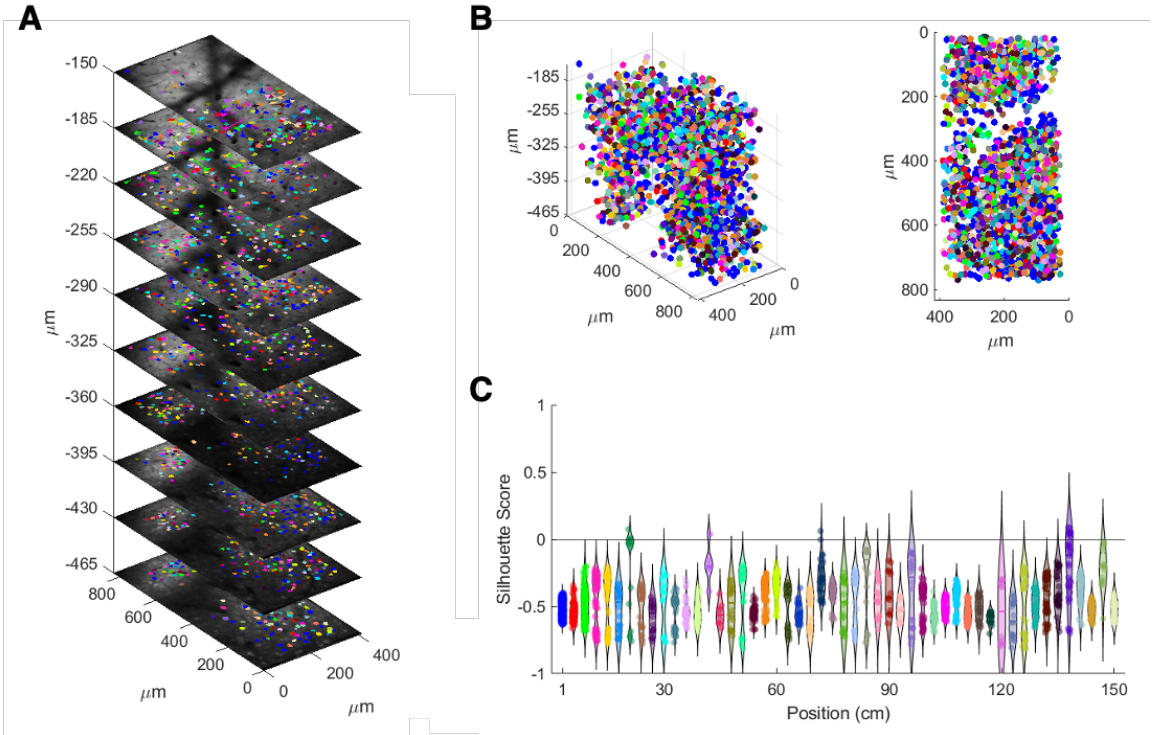

Figure 5.5: Neurons tuned to the same location spanned cortical layers II-Va but were not topographically-clustered. All spatially selective neurons were clustered by their binned (3 cm) location of maximum mean normalized activity during running. (A) Example mean image stack from M1 with spatially co-tuned cell bodies highlighted as different colours. (B) Centroids of co-tuned cells from (A) plotted in a 3D volume (left) and as a collapsed *z*-stack (right). (C) Silhouette score for each spatially co-tuned cluster relative to all other clusters shown in (A-B). Note that negative scores indicate that clusters were highly overlapping and poorly clustered. For each violin plot, the line indicates the median and the colour corresponds with the cell and centroid colours in (A) and (B), respectively.

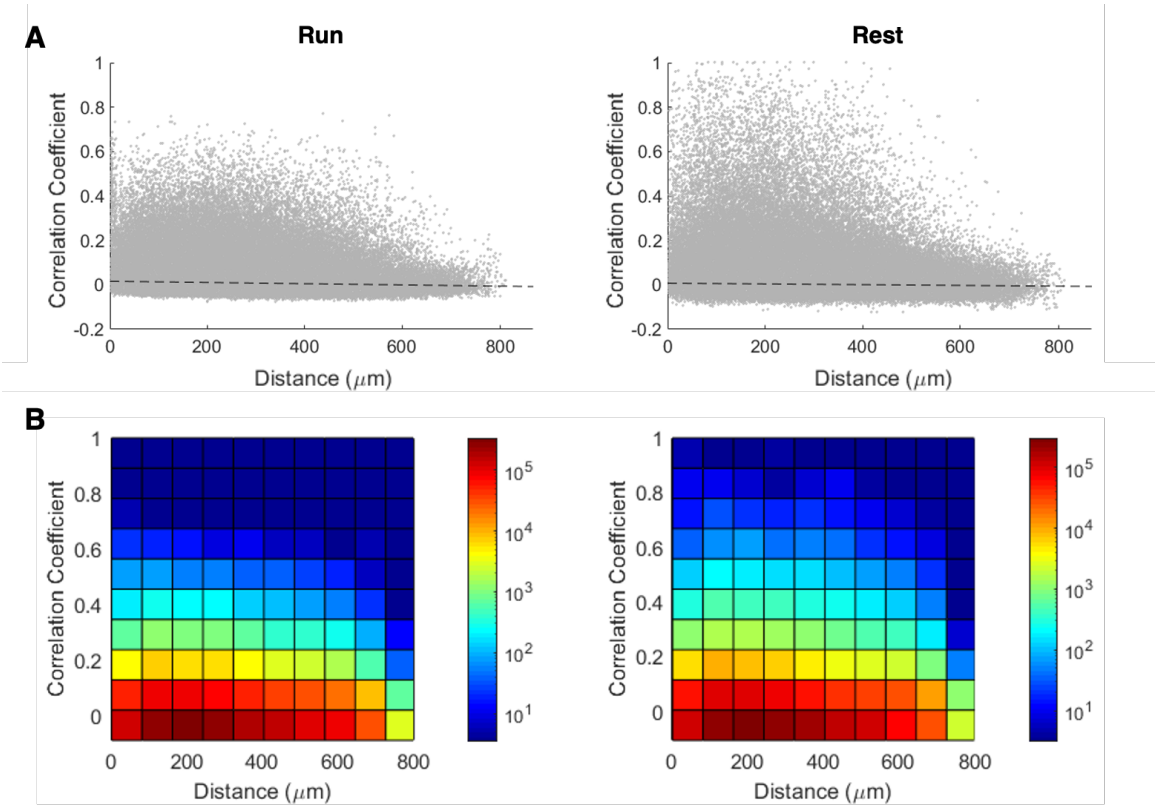

Figure 5.6: No relationship between lateral proximity and activity vector correlation between pairs of neurons in M1 during running or intertrial rest. (A) Comparison of the pairwise lateral (XY) Euclidean distance and the deconvolved activity vector correlation for all detected neurons irrespective of cortical depth. During both running and rest epochs, the slope of the least squares regression line was approximately 0 (dashed line). (B) Bivariate tiled histograms of data shown in (A).

Lack of depth-dependent clustering of response preferences in M1

Other studies have reported that tuning in rodent L4 is more topographically clustered, presumably due to shared thalamic inputs (LeMessurier et al., 2019; Winkowski & Kanold, 2013). To test for depth-specific clustering, the topography of co-active and spatially co-tuned cells was next assessed separately for each *z*-plane. There was no clustering of co-active or co-tuned cells evident at any cortical depth (Figure 5.7A) and the median depth-dependent silhouette score across mice was -0.47 for running ensembles, -

0.41 for intertrial rest ensembles, and -0.60 for spatially co-tuned cells (Figure 5.7B). Moreover, there was no relationship between the lateral (XY) Euclidean distance and the activity vector correlation between pairs of cells within each *z*-plane. During both running and rest epochs, the least squares regression correlation factor for all pairwise comparisons at each cortical depth was approximately 0 (Figure 5.8).

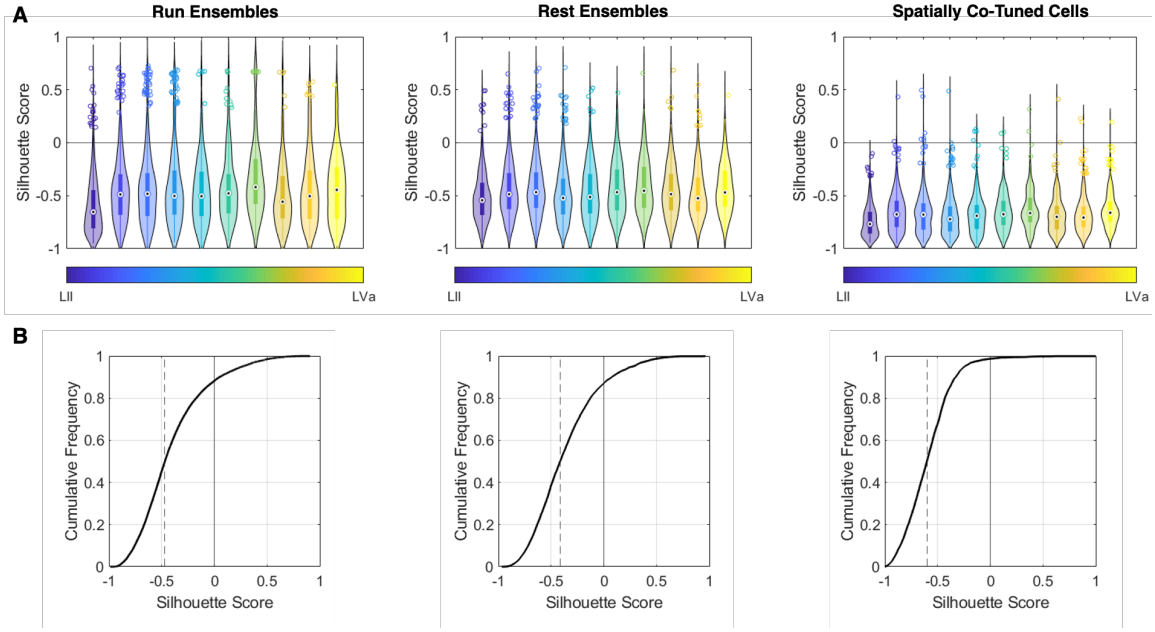

Figure 5.7: Lack of depth-dependent topographical clustering of co-active or co-tuned cells. (A) Silhouette scores for running or rest ensembles and spatially-co-tuned cells from an example animal, pooled across ten experimental days and clustered by cortical depth. Note that negative scores indicate that clusters are highly overlapping and poorly clustered. For each violin plot, the dot indicates the median and the colour corresponds with cortical depth (superficial layers are shown as cool tones and deep layers as warm tones). (B) Cumulative frequency distributions of depth-specific silhouette scores for all detected ensembles or co-tuned cells across ten experimental days and pooled across mice. Dashed line indicates median.

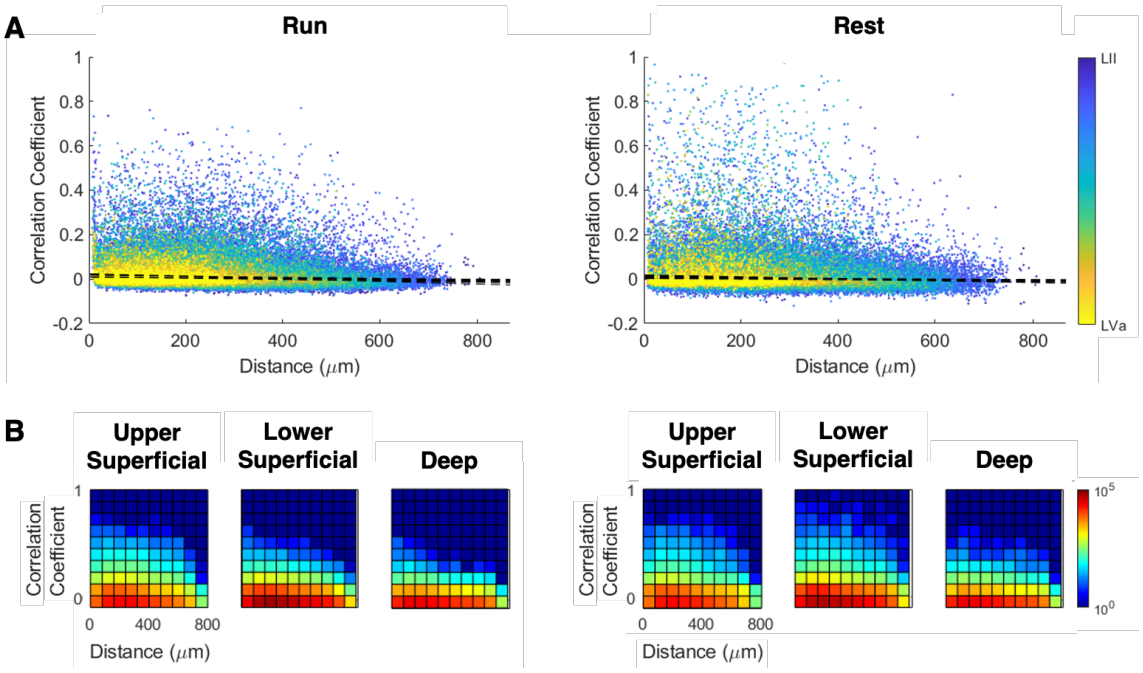

Figure 5.8: No relationship between lateral proximity and activity vector correlation between pairs of neurons at the same cortical depth in M1 during running or intertrial rest. Comparison of the pairwise lateral (XY) Euclidean distance and the deconvolved activity vector correlation for cells within each *z*-plane. Pairwise comparisons are coloured according to cortical depth; superficial layers are shown as cool tones and deep layers as warm tones. During both running and rest epochs, the slopes of the least squares regression lines were approximately 0 for each cortical depth (dashed lines). (B) Bivariate tiled histograms of data shown in (A), grouped by upper superficial, lower superficial, and deep layer divisions.

Proximate neurons within columns exhibited shared response properties

A sliding circular window with a diameter of 30, 50, or 100 µm was next used to examine the correlation between neighbouring neurons throughout the depth of the cortical volume (Figure 5.9A). The mean pairwise correlation between the deconvolved activity traces of neurons within a cylindrical volume was significantly higher than the mean correlation between those same neurons and a random sample of neurons outside the window (Wilcoxon signed rank test on binned data, $p<0.001$; Figure 5.9B). The largest deviation from random chance correlation was observed with a 30 µm diameter sliding

window. However, all larger diameter columns also exhibited increased mean correlation between proximate neurons, likely as a consequence of the smaller scale columnar bias within those populations.

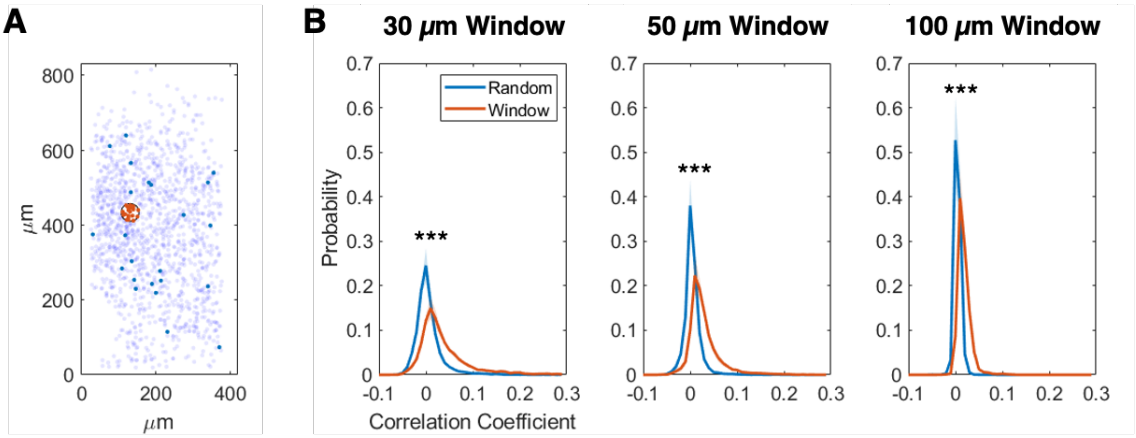

Figure 5.9: Nearest neighbours within a column exhibited higher mean correlation than across columns. (A) Example collapsed *z*-stack of neuronal centroids (light blue) from M1. A circular window (50 μm diameter) surrounds a cluster of nearest neighbours within a column (orange), which were compared to a random sampling of neurons of equal size outside the column (dark blue). (B) A circular sliding window (30, 50, or 100 μm in width) was used to calculate the mean pairwise Pearson correlation between neurons within each column (orange). Random controls (blue) were generated by calculating the mean pairwise correlation of the neurons within each window with a random sampling of neurons outside the column. Shaded area is the SEM across mice. The mean correlation between neurons within a column was significantly higher than with a random sample of cells outside the column.

To assess the preferred response properties of proximate neurons within cylindrical volumes, the mean normalized activity vectors of cells were averaged within a 15 μm radius of each lateral (XY) position in the imaging frame. Despite the heterogeneous arrangement of tuning profiles among neighbouring neurons, the mean response properties of proximate

cells within columnar volumes formed a patchy topography of spatial tuning with relatively distinct boundaries (Figure 5.10).

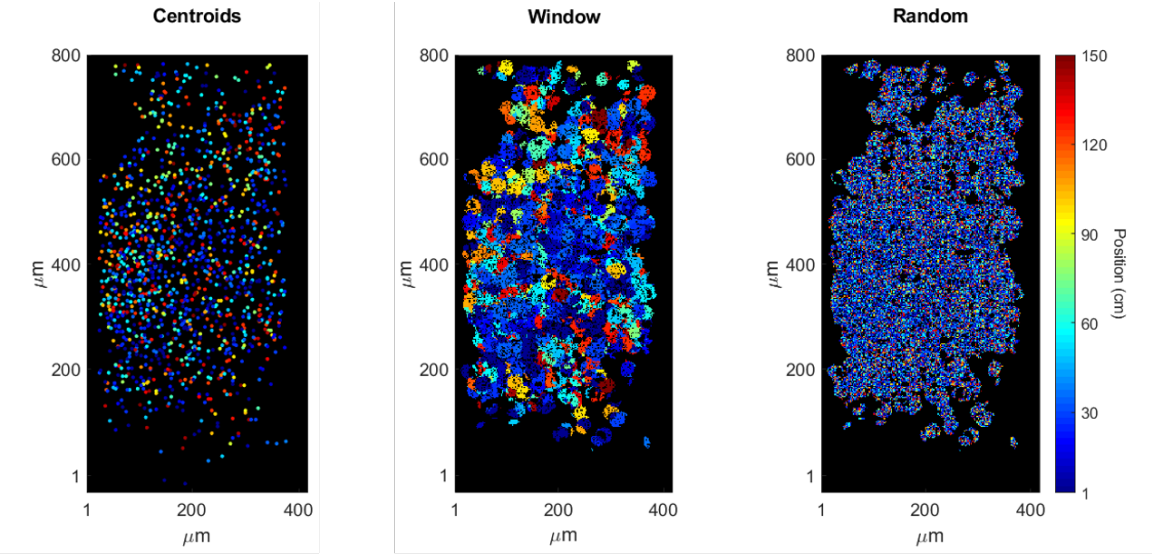

Figure 5.10: Mean spatial tuning of neighbouring cells in M1 revealed a patchy functional architecture. The mean normalized activity vectors of all neuronal centroids from an example mouse (left) were averaged within a 15 µm radius of each lateral (XY) position to determine the mean response properties of proximate cells (center). Random controls (right) were generated by averaging the mean normalized activity vectors of a random sampling of neurons outside the 30 µm diameter column (of equal number to those contained within the column). Colours of centroids (left) and averaged response properties at each lateral position (pixels in center and right panels) correspond with the location of maximum mean normalized activity in the treadmill environment.

5.4 DISCUSSION

This study examined the putative functional role of columnar architecture in rodent motor cortex during active navigation. While individual glutamatergic neurons in layers II-Va of mouse M1 exhibited robust spatial tuning, co-active and spatially co-tuned cells were not topographically clustered. Thus, the results of this study are consistent with other reports of "salt and pepper" orientation selectivity in V1 (Bonin et al., 2011; Girman et al., 1999; Han et al., 2019; Ohki et al., 2005), frequency tuning in auditory cortex (Bandyopadhyay et al., 2010), and whisker representations in barrel cortex (LeMessurier et al., 2019; Sato et al., 2007). Nevertheless, the mean correlation between neighbouring neurons within columnar volumes was significantly higher than with random samples of the larger population, forming a patchy topography of mean preferred spatial tuning. This finding could not be explained by lateral proximity alone, nor proximity as a function of cortical depth, suggesting that there is a small but significant tendency for correlated columnar activity. Notably, this effect was largest for columns with a 30 μm diameter, which corresponds with previous measurements of minicolumn width in mice (Escobar et al., 1986; Lev & White, 1997; White & Peters, 1993).

Considering that apical dendrite bundles are approximately 30 μm in width in M1 (Lev & White, 1997), a potential caveat is that spatially-regular neuropil contamination may have biased the activity vectors of proximate neurons within columns. For example, Lee et al. (2017) reported that local neuropil activity in V1 was highly correlated and could accurately decode the direction of moving gratings. However, this explanation seems unlikely not only because the estimated neuropil contribution was subtracted during image processing (Pachitariu et al., 2016) but because there was no relationship between lateral distance and the pairwise correlation between the activity vectors of proximate neurons.

Other rodent studies have also reported a weak functional micro-architecture underlying the spatially-intermingled organization of individual cells with dissimilar tuning profiles. Ringach et al. (2016) found that joint tuning of orientation and spatial frequency in V1 was also weakly clustered within cortical distances below 50 μm. In primary auditory cortex, Bandyopadhyay et al. (2010) demonstrated fractured tonotopy for supra-threshold responses among proximate neurons, whereas the inclusion of temporally-coupled sub-threshold inputs revealed spatial clustering of similar mean response properties. Similarly, "noise correlation"—which is equivalent to the pairwise trial-by-trial correlation of activity traces in this study—has been previously shown to be elevated between neighbouring neurons at the same cortical depth in auditory and visual cortices, despite the local diversity of tuning (Kondo et al., 2016; Rothschild et al., 2010). Altogether, these findings suggest that proximate cortical neurons in rodents may share input selectivity but perform independent computational roles. Indeed, response preferences have been reported to be more clustered according to thalamocortical input in L4 (LeMessurier et al., 2019; Winkowski & Kanold, 2013) and L1 (D'Souza et al., 2019; Ji et al., 2015). While no depth-dependent clustering was observed in this study, this could likely be attributed to anatomical differences in the middle layers of M1 relative to primary sensory regions. Thalamocortical synapses are halved in L4 of M1 relative to S1, with no direct input to inhibitory interneurons (Bopp et al., 2017), and arborization extends broadly beyond columnar boundaries (Kuramoto et al., 2009). Instead, top-down feedback via L1 afferents to apical dendrite bundles may more strongly modulate columnar activity in M1 (and patchy expression of muscarinic acetylcholine receptors has indeed been observed in L1 of M1; van der Zee & Luiten, 1999), although this remains to be further explored.

The lack of pervasive functional minicolumnar architecture in the rodent cortex may be the consequence of a developmental idiosyncrasy. Although it conforms to the same general radial organizational principles observed in other mammals, there appears to be a more significant tangential dispersion of clonally-related neurons between neighbouring radial glial fibres in rodent cortex (Ohtsuki et al., 2012; Tan & Breen, 1993; Torii et al., 2009). Considering that clonally-related cells are more likely to be interconnected during development (Yu et al., 2009, 2012) and share functional preferences (Li et al., 2012; Ohtsuki et al., 2012), this increased horizontal migration may underlie both the spatial intermingling of cells with different tuning and the reduced evidence of functional columnar clustering. However, lineage is not the only determinant of functional connectivity. For example, subcortical projection neurons in L5 form periodic radially-oriented cellular arrays that are not clonally-related, yet show preferential post-natal electrical coupling and correlated activity in maturity (Maruoka et al., 2011, 2017). Moreover, although the cortex exhibits substantial intrinsic functional selectivity, complete maturation depends on experience-dependent synaptic plasticity (Hubel & Wiesel, 1963; Ko et al., 2013, 2014). Altogether, clonally-related cells may form a crude structural and functional scaffold that is refined by synaptic remodeling and sensory experience to form dedicated microcircuits for processing related information.

In higher mammals, distinct co-tuned minicolumns may have emerged as an evolutionary consequence of cortical expansion (Kriegstein et al., 2006; Rakic, 1995). It is plausible that rodents simply lack the cortical volume and complexity that warrants increased selective local connectivity and parallel computations among cells with similar tuning. In a brain with reduced cell numbers, proximate cells with shared input but heterogenous stimulus tuning may minimize cortical wiring for more efficient information

processing (Koulakov & Chklovskii, 2001). In fact, small subsets of cells within a rodent "minicolumn" could plausibly function as fine-scale competitive subcircuits (Yoshimura et al., 2005), mimicking the function of minicolumns within a macrocolumn in mammals with larger cortices.

6. REPRESENTATIONAL DRIFT IS A CONSEQUENCE OF PROBABILISTIC CELL DYNAMICS

6.1 ABSTRACT

Recent long-term calcium imaging studies have demonstrated that hippocampal and cortical spatial representations dynamically change with recurrent exposures to a familiar environment, a finding that is in apparent contrast to the notion of a stable engram. Considering the critical role of the hippocampus in spatiotemporal memory encoding, the progressive reorganization of hippocampal memory representations may reflect—or be actively driving—the temporal distinction of events. By extension, ongoing hippocampal modulation of cortical spatial representations may also underlie temporal drift in the neocortex. To examine the influence of the hippocampus on cortical dynamics over time, *in vivo* two-photon microscopy of genetically encoded calcium indicator mice was used to longitudinally image neurons in CA1, as well as retrosplenial and motor cortices, before and after bilateral hippocampal lesions. Consistent with previous studies, hippocampal and cortical spatial representations exhibited regular turnover of active spatially selective cells and drifting place fields both within and across experimental days. However, temporal drift in the cortex did not depend on an intact hippocampus, and stable spatial representations could be derived from mean population activity across days. Over weeks of repeated experience, population activity gradually became more correlated in RSC—but not motor cortex—in both sham and lesioned mice. These results support that representational drift in the hippocampus and cortex is predominantly a consequence of intrinsic single-cell dynamics and that a spatial map is locally stabilized in the RSC by ongoing experience.

6.2 INTRODUCTION

The stable engram

The *systems* (circuit-level) consolidation of a distributed memory representation is likely the consequence of *synaptic* consolidation mechanisms. Donald Hebb (1949) first proposed that "when an axon of cell A is near enough to excite a cell B and repeatedly or persistently takes part in firing it, some growth process or metabolic change takes place in one or both cells such that A's efficiency, as one of the cells firing B, is increased". This concept was famously paraphrased as "cells that fire together, wire together" (Shatz, 1992) and the mechanism by which synaptic efficacy is strengthened between glutamatergic neurons—dubbed long-term potentiation (LTP)—was experimentally resolved (for review see Bliss et al., 2018; Bliss & Lømo, 1973). Since its discovery, a number of parallels have been drawn between LTP and many types of learning, and it is now generally accepted that LTP is the cellular correlate of long-term memory (Morris et al., 1986; Whitlock et al., 2006). The most well-studied form of LTP is mediated by N-methyl-D-aspartate (NMDA)-type glutamate receptors, which are abundantly distributed among neurons in the hippocampus, cerebellum, and layers 2/3 and 5 of the neocortex (Brose et al., 1993; Monaghan & Cotman, 1985; Moriyoshi et al., 1991). In general, NMDA receptor-mediated LTP is characterized by intracellular signalling cascades that culminate in post-synaptic transcription upregulation (Bourtchuladze et al., 1994; Nguyen et al., 1994), functional changes resulting from the trafficking of additional α-amino-3-hydroxy-5-methyl-4-isoxazole propionic acid (AMPA)-type glutamate receptors to the post-synaptic density (Hayashi et al., 2000; Shi et al., 1999), and structural modifications to dendritic spines (Engert & Bonhoeffer, 1999; Ma et al., 1999). Accordingly, the stability of learned

behaviours and the permanence of long-term memory have been attributed to the persistence of these functional connections between the neurons that constitute a distinct memory trace (Abdou et al., 2018; Kentros et al., 1998; Thompson & Best, 1990), which are often referred to as an "engram" (Semon, 1921).

There is an inherent trade-off between the stability of connections necessary for long-term memory maintenance and the experience-dependent plasticity required for ongoing learning. The adaptive remodelling of memory circuits is facilitated by the sprouting of new dendritic spines and the balanced elimination of pre-existing synapses, processes that are governed by the dynamic (and often probabilistic) expression of CREB (Han et al., 2007), CaMKIIα (Lisman et al., 2012), IEGs (Guzowski et al., 1999), and other synaptic plasticity molecules (Silva, 2007). In the CA1 subregion of the hippocampus, spines are strikingly impermanent, exhibiting a mean lifetime of only 1-2 weeks (Attardo et al., 2015). Assuming complete turnover of synaptic connectivity within 3-6 weeks, this finding is consistent with the duration of time that some memories have been experimentally determined to remain hippocampus-dependent in rodents (e.g. Anagnostaras et al., 1999; Kim & Fanselow, 1992; Ross & Eichenbaum, 2006). Although synapses in the cortex are also in constant flux, a small proportion of the spines formed during initial learning are preferentially stabilized during repeated training, even after long intertrial intervals, and the majority of cortical spines have been shown to persist for months in the adult cortex (Grutzendler et al., 2002; Holtmaat et al., 2005; Trachtenberg et al., 2002; Xu et al., 2009; Yang et al., 2009). Thus, Holtmaat et al. (2005) proposed that there may be two distinct populations of synapses with complementary functions: persistent spines that reliably encode experience and more transient spines that facilitate network plasticity. Moreover, theoretical work has substantiated that both fast learning and robust

memory storage ("slow forgetting") can be supported by a network with stochastic formation and elimination of redundant synaptic connections (Fauth et al., 2015; Fusi, 2002). Thus, synaptic turnover does not necessarily undermine the concept of a generally stable engram in the neocortex, and differences in circuit plasticity between the hippocampus and cortex support complementary learning systems theories (Marr, 1971; McClelland et al., 1995; Squire & Alvarez, 1995).

Updating spatiotemporal representations in the hippocampus

A key property of hippocampal place codes is their ability to distinguish contexts through a process called "remapping". Stable place cells can undergo *rate* remapping where the integrity of the spatial code is preserved but changes in mean firing rate convey task-related information (Allen et al., 2012), the direction of navigation (Navratilova et al., 2012), or changes to sensory cues in the environment (Leutgeb et al., 2005). During episodes where select features of an environment are manipulated, such as the colour of the enclosure or the orientation of cues, a spatial representation may undergo *partial* remapping. In this case, a significant portion of place cells and their fields remain unaltered while others become inactive or exhibit new place fields (Anderson & Jeffery, 2003; Quirk et al., 1990; Tanila et al., 1997), which may actually be the observable result of profound rate remapping in some instances. Finally, the active subset of hippocampal place cells and their spatial tuning in two environments is largely orthogonal as a consequence of *global* remapping (Alme et al., 2014; Leutgeb et al., 2004; Muller & Kubie, 1987). That is, two uncorrelated spatial representations emerge to distinguish two environments due to the stochastic allocation of place fields at distances that exceed the intrinsic scale of the path

integration system (Rich et al., 2014). Altogether, various degrees of population remapping can robustly distinguish both small- and large-scale changes to a spatial context.

It seems that a similar hippocampal mechanism may exist to reflect the passage of time (for review see Eichenbaum, 2014). Just as place cells have place fields that completely tile a given environment, MacDonald et al. (2011) identified time cells that had "time fields" collectively spanning a delay period separating the presentation of distinct objects and their associated odor-cued rewards. Analogous to place cell remapping, time cells "re-timed" when the delay period was extended and distinct time ensembles emerged to disambiguate different sequences of events. Importantly, place and time cells arise from the same population, and many cells conjunctively encode place and time, suggesting a common mechanism for their allocation (Kraus et al., 2013). This finding suggests that both place and time cells share a general computational function, consistent with the view that episodic memory requires binding content to a spatiotemporal framework.

Over extended timescales or during repeated exploration of a familiar environment, there must be a mechanism for disambiguating distinct episodes that have occurred within a single spatiotemporal context. Much like the extent of environmental change can influence place field remapping in the hippocampus, the elapsed time between episodes may also dictate the scale to which reactivated memory representations are re-timed (though it should be noted that this effect might not be restricted to time cells *per se*). Recent chronic calcium imaging studies have demonstrated that place codes in mouse hippocampal subregions CA3 and CA1 dynamically change with recurrent exposures to the same context (Dong et al., 2021; Hainmueller & Bartos, 2018; Levy et al., 2020; Ziv et al., 2013). Moreover, greater temporal proximity between successive exploration of two environments has been shown to increase the overlap of contextual memory representations in CA1,

regardless of whether the two environments were identical or distinct (Cai et al., 2016; Ludvig, 1999; Mankin et al., 2012; Manns et al., 2007; Rubin et al., 2015). Thus, re-timing across episodes might appear as cumulative modifications to the population code for a particular context (Manns et al., 2007).

Representational drift in the neocortex

Akin to the temporal dynamics observed in the hippocampus, the mouse posterior parietal (Driscoll et al., 2017), vibrissal M1 (Huber et al., 2012), piriform (Schoonover et al., 2021), retrosplenial (Mao et al., 2018), auditory (Aschauer et al., 2022), and visual cortices (Deitch et al., 2021; Marks & Goard, 2021) each also exhibit progressive drift in the population representations of recurring experiences or behaviors. Representational drift is also conspicuous in studies that are touted as evidence for a persistent neural correlate of memory. For example, a fear conditioning study that employed genetic tagging of cell assemblies demonstrated that, although the hippocampal and cortical neurons active during fear conditioning were significantly more likely to be recruited again during subsequent memory retrieval, only ~40% of tagged neurons in CA1 and RSC were reactivated either two days or two weeks later (Tayler et al., 2013). Thus, the engram may actually be a moving target, where single-cell tuning, firing rate, and/or local connections are adjusted dynamically with time or ongoing experience.

It is tempting to speculate that this progressive engram reorganization is the consequence of "reconsolidation" processes initiated by memory retrieval (for reviews see Nader et al., 2000; Sara, 2000). Stimulus conditioning studies in rodents have revealed that a "reminder cue" or re-exposure to a context can temporarily render a memory labile and susceptible to amnesic treatments (Misanin et al., 1968), enhancement (Inda et al., 2011;

Lee, 2008), or accelerated extinction (Berman & Dudai, 2001; Vianna et al., 2001). During this transient window of instability after reactivation—a period of approximately six hours—the persistence of the memory depends on new protein synthesis (Nader et al., 2000a). Although not identical to the original consolidation process, this finding suggests that reconsolidation similarly involves the restructuring and/or strengthening of established synaptic connections. Importantly, reactivation of remote (i.e. hippocampus-independent) contextual memories can return them to a hippocampus-dependent state for a short period of time (1-2 days; Debiec et al., 2002), but this effect appears restricted to reminder events that restore the context-specificity of the memory (Winocur et al., 2009; Winters et al., 2011). Thus, it is conceivable that back-projections from the hippocampus mediate the restructuring of existing cortical memory traces for the purpose of updating and disambiguating similar spatiotemporal memories.

Study objectives

Considering the prominent role of the hippocampus in the encoding and consolidation of spatiotemporal memories, one questions if the hippocampus also directly facilitates representational dynamics in the cortex. Indeed, the progressive reorganization of hippocampal synapses and memory representations may reflect—or be actively driving—the temporal distinction of events, which may also modulate downstream context-dependent cortical representations. However, there are currently no published studies that directly examine the influence of the hippocampus on cortical dynamics over time. Furthermore, existing studies of representational drift fail to adequately explore the alternative explanation: that temporal drift may be largely the consequence of probabilistic cell dynamics. To address this gap in the literature, *in vivo* two-photon microscopy of

genetically encoded Thy1-GCaMP6s calcium indicator mice was used to longitudinally image neurons in CA1, as well as retrosplenial and motor cortices, both before and after bilateral dorsal hippocampal lesions. Mice ran on a familiar treadmill belt for ten consecutive days and, during a subset of those days, two added obstacles interchanged positions at the mid-point of the behavioural session which enabled dissociation of spatial remapping from temporal effects within days. This behavioural paradigm was repeated for each imaged region of interest, enabling examination of both the single-cell dynamics within and across days (amid stable and unstable cue configurations), as well as population dynamics over several weeks of repeated context exposures.

6.3 RESULTS

Spatially selective cell characteristics were stable over time

First, the stability of spatially selective cell characteristics (refer to Figure 3.1) across days with added obstacles was examined in CA1 (n=3) and cortical regions (RSC, M2, and M1) both before (n=11) and after sham (n=5) or bilateral dorsal hippocampal lesions (n=4; refer to Figure 2.4). There were no significant differences detected across days 3-8 in the mean proportion of cells that were classified as spatially selective in CA1 and all cortical treatment groups (two-way repeated measures ANOVA & Tukey's test, $F(3.9,192.2)=1.566$, $p=0.19$; Figure 6.1A) and no effect of treatment group ($F(3,49)=1.566$, $p=0.39$). The distribution of place fields across the length of the treadmill belt remained consistent across days with added obstacles (two-sample Chi-squared tests between pairs of consecutive days, $p=0.05$-0.42; Figure 6.1B) in CA1 and across cortical treatment groups. There *was* a main effect of time on median place field width (two-way repeated measures ANOVA & Tukey's test, $F(3.9,189)=5.652$, $p<0.001$; Figure 6.1C) but there were no discernable trends underlying the pairs of days that were identified as significantly different and no effect of cortical treatment group ($F(3,49)=0.6288$, $p=0.60$). Moreover, the median place field width on any given day (and from any given region or treatment group) was consistently within 36-42 cm. There was no main effect of time on the fraction of spatially selective cells that exhibited only one place field (or, conversely, multiple place fields; two-way repeated measures ANOVA, $F(3.8,185.6)=2.245$, $p=0.07$; Figure 6.1D) across CA1 and all cortical treatment groups. However, the main effect of treatment on the number of place fields exhibited by spatially selective cells persisted ($F(3,49)=4.659$, $p<0.01$; refer to Figure 3.4E).

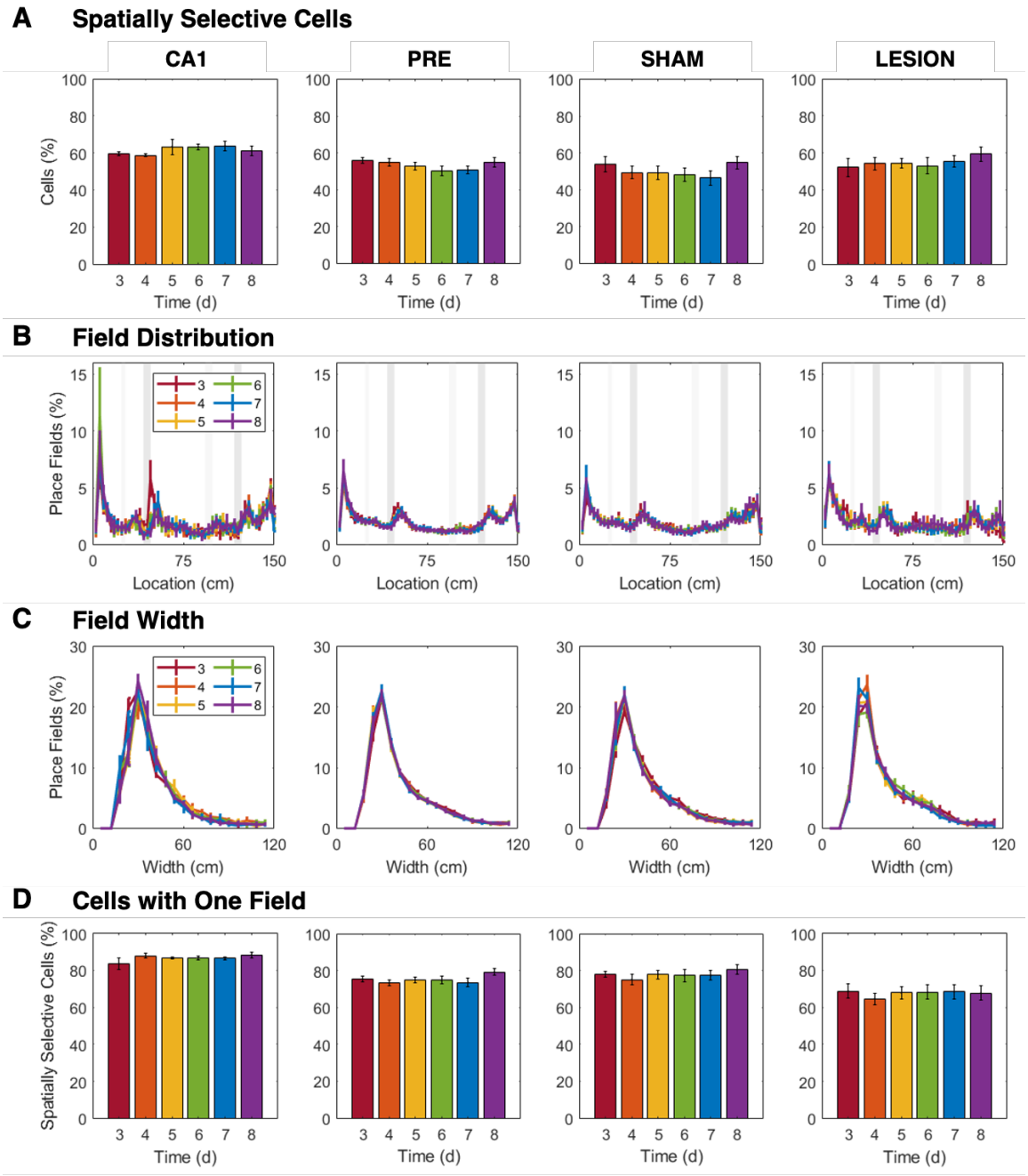

Figure 6.1: The characteristics of spatially selective cells in CA1 and the neocortex were generally stable across days with added cues. Cells from RSC, M2, and M1 were grouped together by treatment: pre-surgery (PRE), sham lesion (SHAM), or bilateral lesion of the hippocampus (LESION). (A) Proportion of spatially selective cells detected across experimental days 3-8. (B) Distributions of place field locations across the length of the treadmill belt across experimental days 3-8. Gray bars indicate positions of stable cues (light gray) and interchangeable obstacles (dark gray). (C) Histogram of place field widths for spatially selective cells detected across experimental days 3-8. (D) Fraction of spatially selective cells that exhibited one place field (as opposed to multiple place fields) across experimental days 3-8. For all plots, error bars are SEM.

Finally, to ensure mice were trained to asymptote in the familiar spatial context, spatial information was compared across cells from regions imaged within the first ten days, the following ten days, and the final ten days both before and after sham or bilateral hippocampal lesions. There were no significant differences in the median spatial information across the experimental paradigm over extended time periods, regardless of treatment (Figure 6.2; Kruskal-Wallis, p=0.15-0.62). Note that, while the addition of interchangeable obstacles increased the spatial information encoded by cortical cells (particularly on cue-swap days 4-7; refer to Figure 3.5B), the baseline spatial information on any given day remained consistent over the course of the experiment.

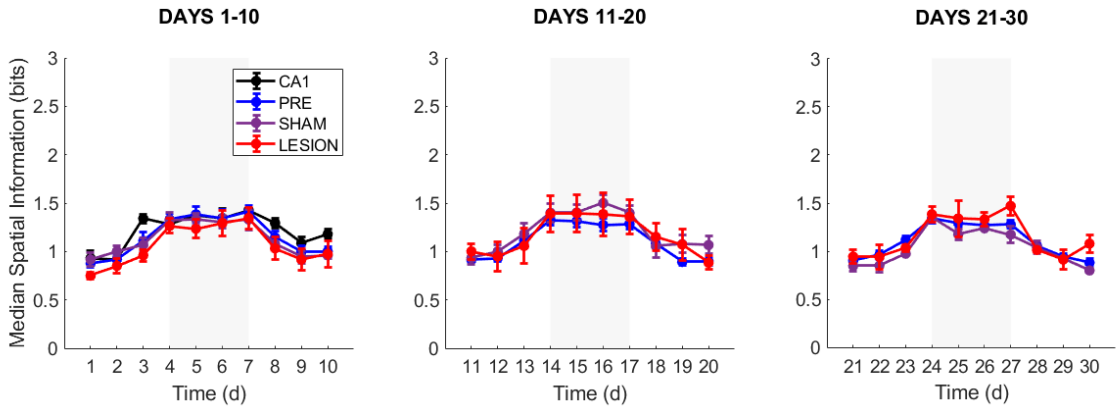

Figure 6.2: Median spatial information was increased by unstable sensory cues in the neocortex but otherwise stable throughout the experimental timeline. Three cortical regions (RSC, M2, and M1) were sequentially imaged in each mouse both before (PRE) and after sham (SHAM) or bilateral hippocampal lesion (LESION) surgeries. All detected cells were pooled across cortical regions according to their order of imaging (left: days 1-10; middle: days 11-20; right: days 21-30) and median spatial information was averaged across mice for each day of the ten-day paradigm. CA1, which was only assessed for ten days, is shown for comparison. Cue-swap days are indicated by gray background. Note that the obstacles were also added to the treadmill on the days flanking the four cue-swap days but in a stable orientation. Error bars are SEM.

Population activity correlation increased in RSC with time or recurrent experience

On any given day, the spatially selective cells in the hippocampus and the cortex exhibited place fields that offered a uniform representation of the spatial environment. Consistent with previous studies (Hainmueller & Bartos, 2018; Huber et al., 2012; Mao et al., 2018; Ziv et al., 2013), these spatial representations transformed across days such that they appeared to decay over time (Figure 6.3A-B). This temporal drift in the representations of the spatial environment persisted after bilateral lesions of the dorsal hippocampus (Figure 6.3C). However, the RSC exhibited increased population stability across days relative to both the hippocampus and motor cortices, regardless of treatment.

To further examine population activity patterns across the ten day paradigm, the mean normalized activity vectors for each cell were cross-correlated (within a range of +/- 9 cm to account for place field drift) and averaged to obtain the Pearson's correlation co-efficient for the population for each pair of days. For cue-swap days (4-7), the pre- and post-swap trials were counterbalanced such that half of the neurons were always sampled from orientation A and the other half from orientation B across days. Within days, the mean correlation between odd and even trials was used as the starting (t = 0 d) correlation. In motor cortices, there were no significant differences in the mean population activity vector correlations between the first ten days of exposure to the experimental paradigm relative to later pre-surgery trials (experimental days 11-30; Kruskal-Wallis & Dunn–Šidák, M2: p=0.63, M1: p=1), after sham surgeries (experimental days 31-60; M2: p=0.63, M1: p=0.28), or after bilateral lesions of the dorsal hippocampus (experimental days 31-60; M2: p=0.63, M1: p=0.98; Figure 6.4A). However, in RSC, the mean population activity vector correlations were significantly higher in pre-surgery trials (Kruskal-Wallis & Dunn–Šidák,

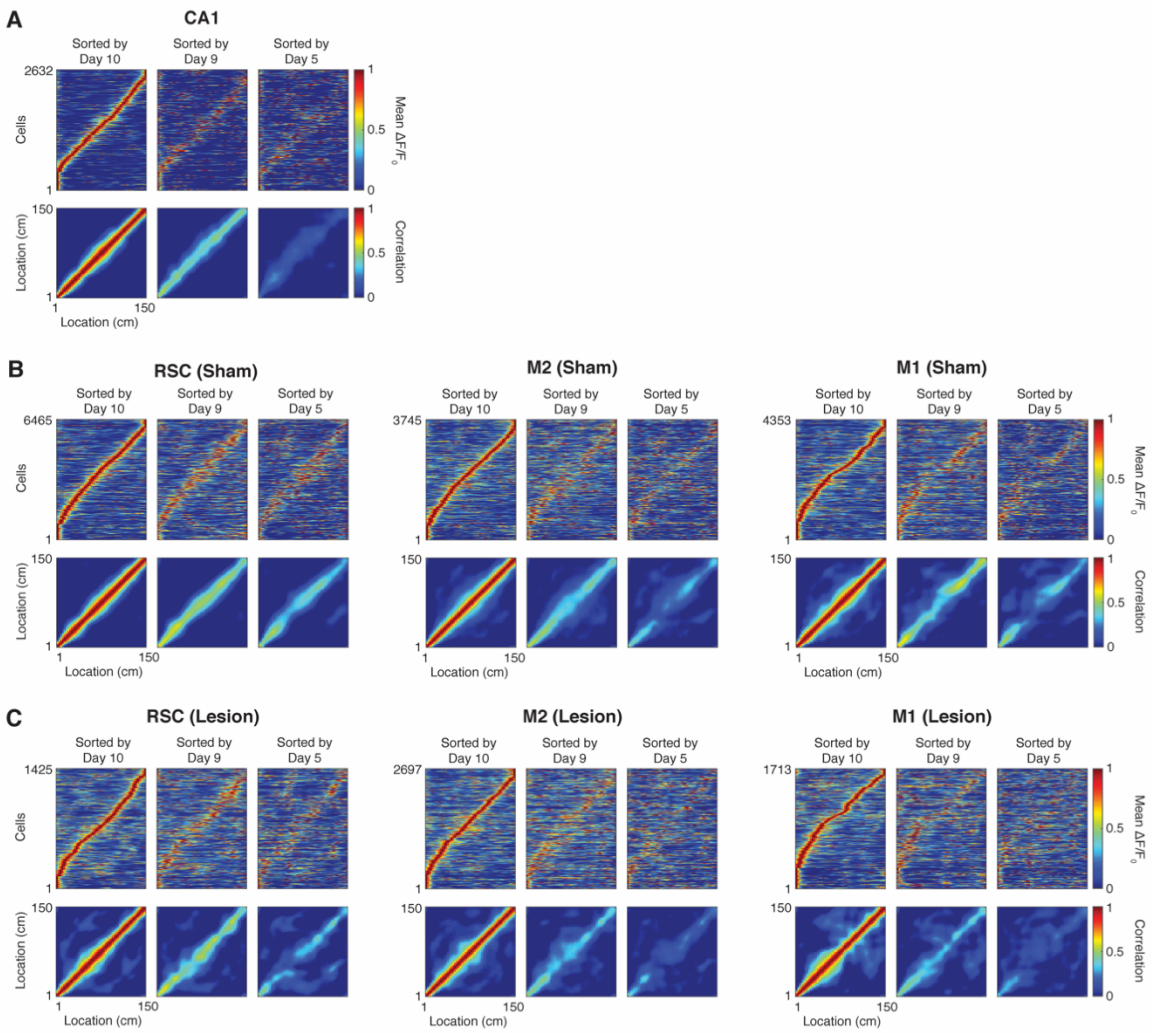

Figure 6.3: Spatial representations were temporally dynamic in hippocampal CA1 and in RSC, M2, and M1 after sham and dorsal hippocampal lesions. For (A) CA1 and each cortical region in the (B) sham and (C) lesion treatment groups, top panels: mean normalized $\Delta F/F_0$ of all neurons detected on day 10 (pooled across animals), sorted by the location of maximum firing on day 10 (left), day 9 (center), and day 5 (right). Bottom panels: corresponding Pearson's correlation matrices comparing sorted population activity on day 10 with that of day 10 (left), day 9 (center), and day 5 (right).

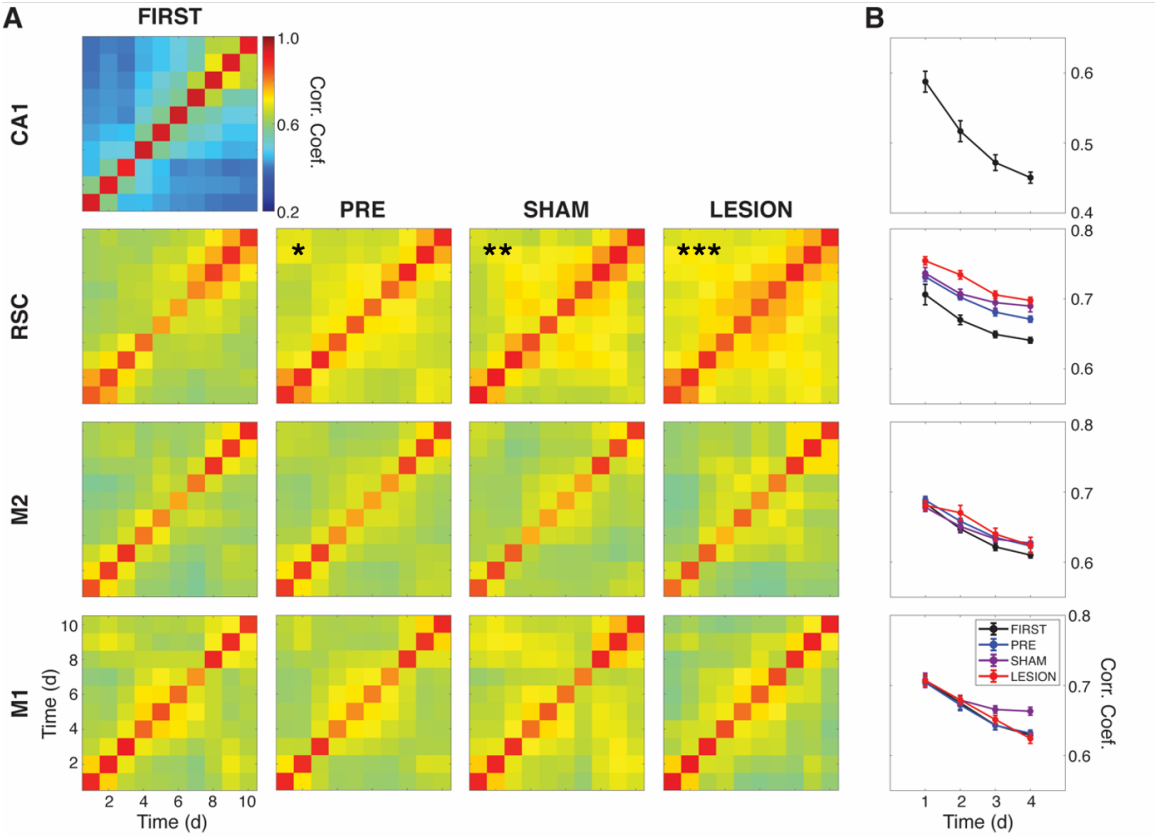

Figure 6.4: Correlation of population activity increased with time or repeated context exposures in RSC. (A) For each pair of days, the mean normalized activity vectors for each cell were cross-correlated (within a range of +/- 9 cm to account for the majority of place field drift) and averaged to obtain the Pearson's correlation co-efficient for the population. For cue-swap days (4-7), the pre- and post-swap trials were counterbalanced such that half of the neurons were always sampled from orientation A and the other half from orientation B across days. The diagonal represents the mean correlation between odd and even trials within one day (*p<0.05, **p<0.01, ***p<0.001, relative to FIRST, Kruskal-Wallis and Dunn–Šidák). (B) Rate of decay of mean correlation in the 1-4 days surrounding a context exposure. Error bars are SEM between sliding windows.

$p<0.05$) and after subsequent sham surgeries ($p<0.01$) or hippocampal lesions ($p<0.001$) relative to the first ten days of exposure to the paradigm (Figure 6.4A). Although there is a trend towards increased population correlation in mice with hippocampal lesions relative to sham controls, the difference between those two conditions was not significant (Kruskal-Wallis & Dunn–Šidák, $p=0.66$). Despite increased population stability, RSC representations decayed across four consecutive days at only slightly reduced rates across conditions (r = -0.052 to -0.062) relative to representations in M2 (r = -0.064 to -0.071) and M1 (r = -0.063 to -0.082). In contrast, the decay rate of the mean population activity correlation over four days after each behavioural episode was more than doubled in CA1 (r = -0.182) relative to mean first exposure (r = -0.072), pre-surgery (r = -0.071), post-sham (r = -0.068), and post-lesion (r = -0.063) decay rates in the cortex (Figure 6.4B).

Representational drift compounded over time and did not depend on an intact hippocampus

Measures of temporal drift—such as changes in spatial tuning or cell activity—were highly consistent across cortical regions. Therefore, cortical cells from RSC, M2, and M1 were grouped together for all subsequent analyses. Between consecutive behavioural sessions, the distributions of place field shifts were highly peaked around 0 cm and 54-59% of all place field drift occurred within 15 cm of the previous place field location. The distributions of place field shifts were not significantly different between CA1 or any cortical experimental groups (two-sample Chi-square tests, $p=0.45$; Figure 6.5A). Thus, although some large shifts in spatial tuning did occur, place fields typically did not randomly relocate.

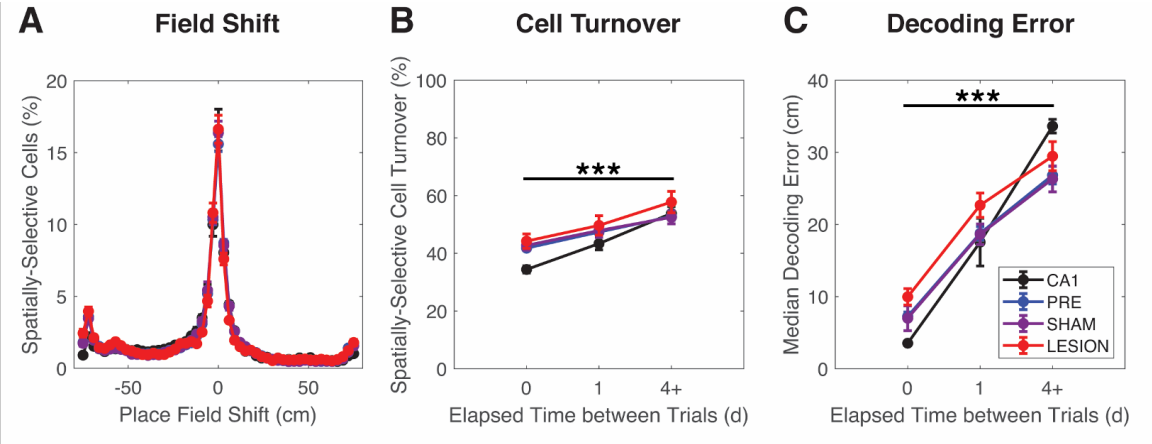

Figure 6.5: Representational drift increased with elapsed time and did not depend on an intact hippocampus. Pre-surgery (PRE), post-sham (SHAM), and post-lesion (LESION) data was pooled across all cortical regions (RSC, M2, and M1). (A) The shift in the location of maximum firing of spatially selective cells between consecutive days, shown as a proportion of total detected place fields. Error bars are SEM. (B) The proportion of spatially selective cells that gain or lose place fields (i.e. active cell turnover) between the first and last halves of an experimental session (0d), between consecutive days (1d), or between distant days (4+d). Error bars are SEM. (C) Median position decoding error using a Bayesian decoder trained on trials from the same day (0d), the previous day (1d), or distant days prior (4+d). Error bars are SEM. For (B) and (C), there was a main effect of time (***$p<0.001$, two-way mixed measures ANOVA).

The turnover of active spatially selective cells was next compared within sessions, between consecutive days, and between distant (4+) days. For within-day comparisons, trials were divided into the first (10 min) and last (10 min) halves, which coincided with the timing of the cue-swap on days 4-7, and spatially selective cell detection was done independently for each half of the behavioural sessions. Altogether, there was a main effect of time such that there was less overlap in the active population of spatially selective cells with increasing intervals of intervening time (two-way mixed measures ANOVA, $F(1.342,65.74)=113.5$, $p<0.001$; Figure 6.5B).

Although physical distortion of the cortical volume after hippocampal lesions prevented image alignment between pre-surgery and post-lesion conditions, turnover in the active cell population could also be examined pre- and post-surgery in sham controls. When the active population of spatially selective cells from the last day of pre-surgery behaviour was compared to that of the first day of post-sham surgery behaviour, the pattern of increasing active cell turnover was extended across the three week recovery interval ($M\pm SEM$: 60±3%) from that observed between distant (4+) experimental days in sham controls ($M\pm SEM$: 50±2%; refer to Figure 6.5B). Therefore, reorganization of cortical spatial representations appears to be contingent on passing time (or ongoing experience in the home cage) rather than recurrent experience in the experimental context.

Finally, a Bayesian decoder was trained with the mean population activity from individual days (or odd trials for within-day comparisons), which was used to decode location from the population activity from within an experimental session (even laps), the subsequent day, or distant (4+) days. In CA1 and across all cortical conditions, median Bayesian decoding error significantly increased with increasing intervals separating the training and test datasets (two-way mixed measures ANOVA, $F(1.6,80)=302.3$, $p<0.001$; Figure 6.5C). In fact, the median decoding error for all regions and conditions was only below 10 cm for within-day comparisons. Thus, the day-to-day predictive capacity of the population activity was limited at greater intervals of passing time, presumably as a consequence of active spatially selective cell turnover.

Highly active spatially selective cells were more likely to exhibit fields across days

Larger synapses—an outcome of consolidation processes—are correlated with increased stability over time (Holtmaat et al., 2005; Trachtenberg et al., 2002). Both dendritic spine size (Loewenstein et al., 2011) and the firing rates of pyramidal neurons (Mizuseki & Buzsáki, 2013) show a log-normal distribution, suggesting these might be interrelated indicators of synaptic efficacy. Thus, more highly excitable cells may similarly prove to be more stable over time. To test this assumption, the characteristics of spatially selective cells that were reactivated across consecutive days were compared with those that gained or lost fields (i.e. "turned over"). Across all experimental groups, there was a main effect of field stability across days on peak non-normalized activity (two-way repeated measures ANOVA & Tukey's test, $F(1,47)=278.9$, $p<0.0001$; Figure 6.6A), encoded spatial information (two-way repeated measures ANOVA & Tukey's test, $F(1,47)=506.1$, $p<0.0001$; Figure 6.6B), and lifetime sparsity (two-way repeated measures ANOVA & Tukey's test, $F(1,47)=700.9$, $p<0.0001$; Figure 6.6C). Specifically, spatially selective cells that were reactivated across consecutive days had significantly higher peak activity, encoded higher spatial information, and exhibited lower sparsity indices relative to cells that gained or lost fields between consecutive days. Relative to pre-surgery and sham controls, there was no effect of dorsal hippocampal lesions on the peak activity (two-way repeated measures ANOVA, $F(2,47)=1.033$, $p=0.36$), median encoded spatial information (two-way repeated measures ANOVA, $F(2,47)=0.6826$, $p=0.51$), or median lifetime sparsity (two-way repeated measures ANOVA, $F(2,47)=0.9531$, $p=0.39$; sham and lesion data not shown) of cells with stable or unstable fields across days (data not shown).

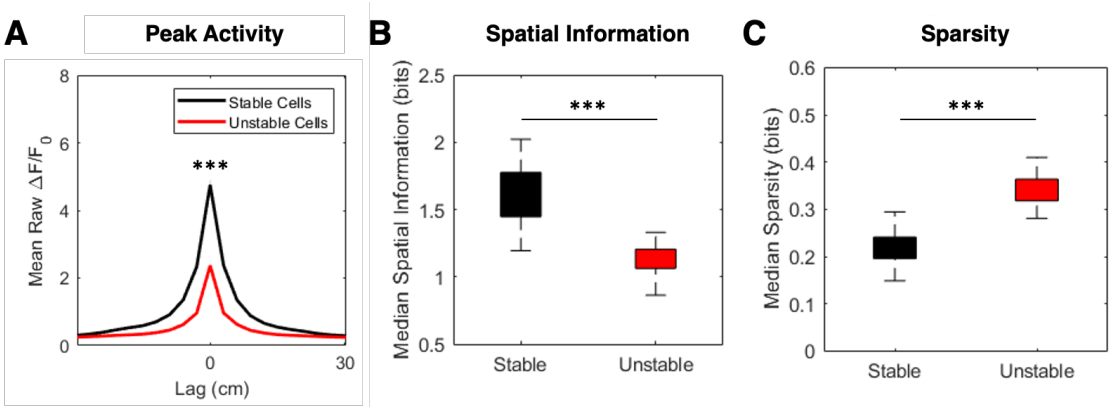

Figure 6.6: Spatially selective cells that were reactivated across consecutive days exhibited higher peak activity, encoded higher spatial information, and had lower lifetime sparsity indices relative to cells that gained or lost fields. Pre-surgery data was pooled across all cortical regions (RSC, M2, and M1). Note that sham and dorsal hippocampal lesion data are not shown. "Stable" spatially selective cells exhibited fields on two consecutive days (black) whereas "unstable" spatially selective cells gained or lost fields between those two days (red). (A) Aligned peak non-normalized $\Delta F/F_0$ of stable and unstable spatially selective cells. Shaded area is SEM. (B) Spatial information encoded by stable and unstable spatially selective cells. For all boxplots, line: median; box: 25th and 75th percentiles; whiskers: minimum and maximum values; + signs: outliers. (C) Lifetime sparsity indices of stable and unstable spatially selective cells.

Time, not remapping, governed reorganization of spatial representations during recurrent experience in the same environment

To determine the relative contributions of temporal reorganization and spatial remapping during cue-swap events, the turnover of active spatially selective cells between stable (e.g. A/B → A/B) or unstable (e.g. A/B → B/A) cue configuration transitions was compared within sessions, between consecutive days, and between distant (4+) days. There was no significant difference in active population turnover between stable or unstable cue transitions at any time interval (two-way ANOVA, $F(1,52)=0.48$, $p=0.49$) and the main effect of time persisted such that there was less overlap in the active population with increasing intervals of intervening time (two-way ANOVA, $F(2,104)=131.9$, $p<0.001$;

Figure 6.7A). The distributions of place field turnover—that is, place fields that were gained or lost during transitions—were also not significantly different between stable or unstable cue orientation transitions (two-sample Chi-square test, p=0.33; Figure 6.7B), and was proportionate to the mean distribution of all detected place fields across days (refer to Figure 3.1). Moreover, the distributions of place field shifts between stable or unstable cue orientations were not significantly different (two-sample Chi-square test, p=0.28; Figure 6.7C), suggesting that individual place fields tended to subside and re-emerge in the same general location despite the local changes to the environment. During unstable transitions, only 5% of all spatially selective cells exhibited place field remapping consistent with the distance between the interchanging obstacle positions (~75 cm). Altogether, time—not spatial remapping—appears to be the main determinant of changes in the active population of cells and their spatial tuning during recurrent experience within a familiar context.

Stable spatial representations could be decoded from mean population activity across days

Considering that the absence of an intact hippocampus did not significantly impact temporal drift, an alternative explanation is that "noisy" probabilistic cell dynamics underlies the day-to-day variability of an otherwise stable spatial representation. To examine this possibility, the mean population activity across days was compared to that on individual days. On any given day, the location of maximum firing for the majority of cells could be reliably predicted from the mean preferred location across days in all examined regions of interest (Figure 6.8). Notably, the correlation between the mean normalized population activity across days and that on individual test days was higher than between two consecutive days (refer to Figure 6.3).

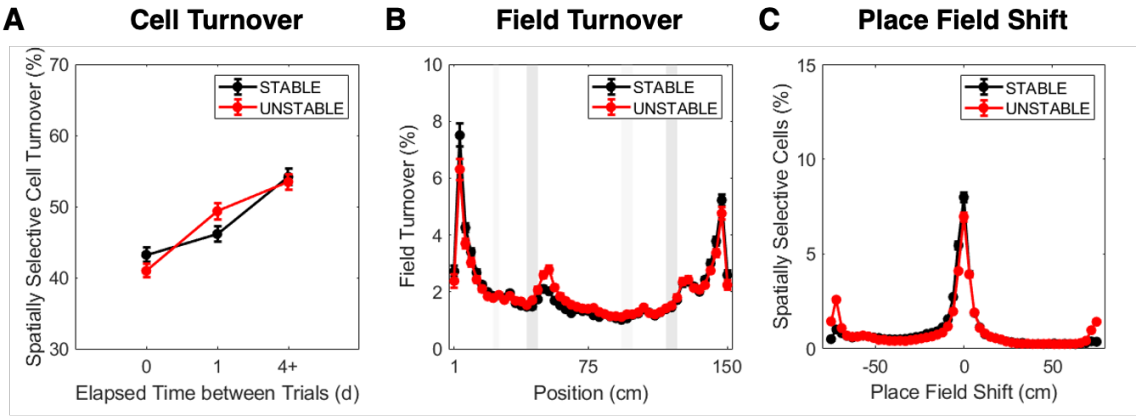

Figure 6.7: Time, not spatial remapping, was the main determinant of population drift during transitions between both stable and unstable cue transitions. Data was pooled across all regions (CA1, RSC, M2, and M1) and treatments (pre-surgery, sham controls, and mice with bilateral lesions of the dorsal hippocampus). (A) The proportions of spatially selective cells that gained or lost place fields (i.e. turnover) during stable or unstable transitions in cue orientations. The proportion is shown between the first and last halves of an experimental session (0d), between consecutive days (1d), or between distant days (4+d). Error bars are SEM. (B) Distributions of place fields that were gained or lost during transitions between stable or unstable cue orientations. Gray bars indicate positions of stable cues (light gray) and interchangeable obstacles (dark gray). Error bars are SEM. (C) The mean shifts in the location of maximum firing of cells during the transitions between stable or unstable cue configurations, shown as a proportion of total detected spatially selective cells. Error bars are SEM.

The Bayesian decoder was next trained with the mean normalized population activity across all days excluding individual test days. Although there was elevated decoding error around the locations of the interchangeable obstacles as a result of shifting place fields on cue-swap days (Figure 6.9A), the median decoding error was, nevertheless, reduced on days with added cues (Figure 6.9B). The median decoding error for any given day was typically below 10 cm in pre-surgery and sham lesioned animals, making it comparable with the median decoding error within days when the decoder was trained with odd trials (refer to Figure 6.5C).

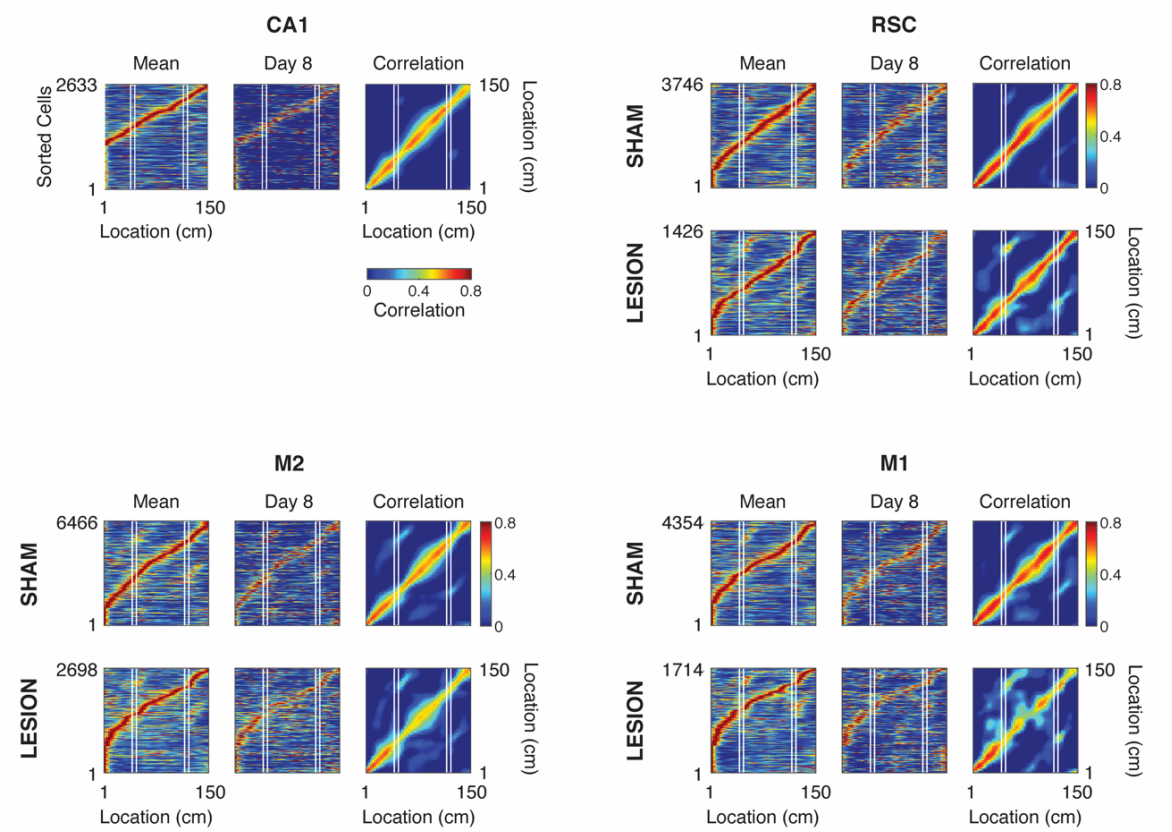

Figure 6.8: Population activity on individual days could be derived from mean population activity across days. For each region, spatially selective cells were pooled across mice for sham controls and mice with bilateral dorsal hippocampal lesions. White lines indicate boundaries of interchangeable obstacle positions. Left panels ("Mean"): mean normalized activity vectors were averaged across experimental days (excluding test day 8) and sorted by the order of maximum activity. Center panels ("Day 8"): mean normalized activity vectors from day 8 were sorted by the order of mean population activity across days. Note: comparable results were obtained for all other experimental days (data not shown). Right panels ("Correlation"): Pearson's correlation matrices comparing the mean population activity across experimental days (excluding day 8) with that of test day 8 for each location on the treadmill belt.

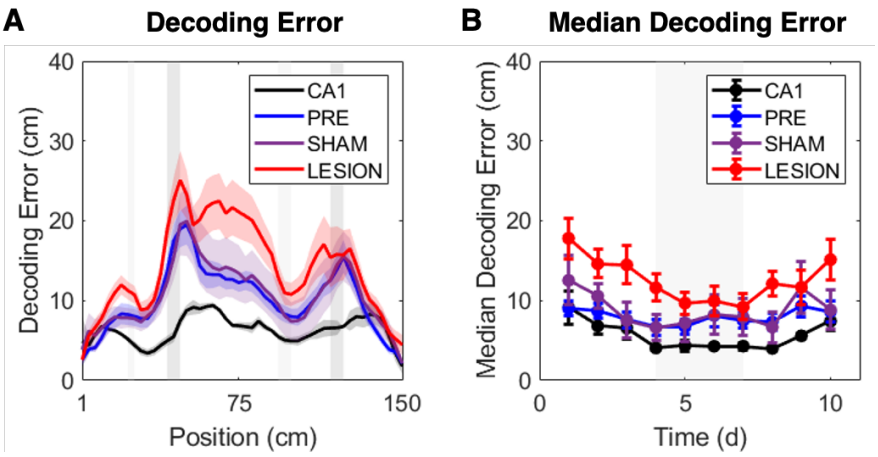

Figure 6.9: Accuracy of Bayesian decoding of mouse position across days was improved by training the decoder with mean population activity. Spatially selective cortical cells were grouped by treatment across cortical regions. Decoder was trained with normalized population activity, averaged across all experimental days excluding the test day. (A) Mean Bayesian decoding error across the length of the treadmill belt, averaged across all experimental days. Shaded area is SEM. Grey bars indicate interchangeable obstacle positions. (B) Median decoding error for each experimental day, averaged across mice. Error bars are SEM. Grey bar indicates cue-swap days.

6.4 DISCUSSION

This study assessed if the temporal drift of neocortical spatial representations is a consequence of hippocampus-mediated restructuring or intrinsic cell dynamics. Consistent with previous studies (Hainmueller & Bartos, 2018; Huber et al., 2012; Mao et al., 2018; Ziv et al., 2013), both hippocampal and cortical representations of a familiar environment demonstrated progressive reorganization both within experimental sessions and between days, regardless of whether local cues were stable or unstable. In the cortex, this drift in the active subset of spatially selective cells was largely unaffected by dorsal hippocampal lesions. Instead, the mean population activity across days could be used to reliably decode the activity on individual days, supporting that spatial representations in both the hippocampus and cortex are redundant, relatively stable, and only *appear* to drift as a consequence of probabilistic single cell dynamics. Nevertheless, representational drift exhibited a degree of temporal regularity because (1) active cell turnover compounded across days and (2) the normalized population vector on any given day became an increasingly unreliable estimate of spatial position with passing time. Thus, it is plausible that both homeostatic changes in intrinsic excitability and gradual synaptic remodeling during ongoing experience (outside of the experimental context) contribute to representational drift over extended timescales.

Previous findings that temporal proximity increased the overlap of contextual representations in CA1 (Cai et al., 2016; Ludvig, 1999; Mankin et al., 2012; Manns et al., 2007; Rubin et al., 2015) are reminiscent of IEG studies that failed to demonstrate a proportionate increase in the number of hippocampal neurons recruited following successive exploration of multiple familiar and novel environments (Alme et al., 2014; Witharana et al., 2016). In both instances, the non-random probability of allocation to a

spatial representation is almost certainly a reflection of non-uniform neural excitability. Place cells exhibit intrinsically lower spike thresholds than silent cells from the onset of spatial exploration and future place cells display higher burst propensities than silent cells even prior to sensory input (Epsztein et al., 2011; Mizuseki & Buzsáki, 2013). The firing rates of hippocampal neurons follow a persistent, highly skewed distribution (Mizuseki & Buzsáki, 2013), as does dendritic spine size (Loewenstein et al., 2011), and the number of place fields expressed in a given environment or over multiple environments (Maurer et al., 2006; Rich et al., 2014). Taken together, propensity for activation appears relatively constrained to a more excitable subset of the neuronal population during allocation to a spatial representation (Cai et al., 2016; Rashid et al., 2016; Yiu et al., 2014) and these conditions appear to similarly bias the likelihood of *reactivation* in response to a stimulus (Pignatelli et al., 2019).

Neurons exploit homeostatic plasticity mechanisms to maintain synaptic weights and intrinsic excitability within a physiologically-relevant range. In the absence of such processes, Hebbian plasticity during recurrent experience would continuously compound, resulting in the unhindered potentiation of synapses and destabilization of the network. There are a number of plausible—and not mutually exclusive—mechanisms for adjusting the response properties of a cell, which would also influence the probability of reactivation over time. For homeostatic regulation of firing rate, the Bienenstock-Cooper-Munro (BCM) theory posits that a sliding threshold between synaptic potentiation and depression is adjusted dynamically with the mean activity of the post-synaptic cell (Bienenstock et al., 1982), a model that is supported by considerable experimental and computational evidence (for review see Cooper & Bear, 2012). The strength of connections can also be locally and globally scaled, constraining dendritic spine size while preserving relative synaptic weights

(Turrigiano et al., 1998). In addition to activity-dependent synaptic potentiation and depression, the sizes of individual synapses fluctuate substantially in response to both spontaneous neural activity and when synaptic activity is blocked, while the mean synapse size remains constant (Loewenstein et al., 2011; Minerbi et al., 2009; Yasumatsu et al., 2008). Notably, many of these mechanisms operate on the scale of days, supporting that these changes could underlie gradual changes in excitability and, therefore, systematic drift in the active cell population.

An important caveat is that the degree of representational drift observed in this study may not necessarily pertain to other species. Although studies of representational drift in rats are limited, electrophysiological studies suggest that rats demonstrate higher long-term reproducibility of both CA1 (Thompson & Best, 1990) and CA3 (Mankin et al., 2012) activity than what has been observed using calcium imaging of mice (Hainmueller & Bartos, 2018; Ziv et al., 2013). One possible explanation may be that cell detection and spike sorting in electrophysiological studies are inherently biased towards cells with the highest firing rates, which also appear to exhibit the most stable activity over time. However, Kentros et al. (2004) also observed enhanced place field stability among CA1 cells of mice using long-term multiple single-unit recordings, leading the authors to suggest that mice might simply pay less attention to distal environmental cues than rats. The visual acuity of rats is approximately twice that of mice (Prusky et al., 2000), which may explain why rats tend to use distal cues for navigation whereas mice rely predominantly on local or idiothetic cues (Cho et al., 1998) and perform worse on spatial tasks that necessitate the use of distal cues (Whishaw, 1995; Whishaw & Tomie, 1996). Therefore, with the addition of local cues, mice might be more likely to perceive the same treadmill environment as a different one, impacting the stability of place cells and place fields across days. Although

some remapping was indeed evident during cue-swaps in this study, spatially selective cell turnover was equivalent over time between stable and unstable cue orientations, and the locations of shifting place fields were proportionately distributed throughout the environment. Instead, variability in temporal drift between species might emerge as a result of inherent differences in the relative expression of potassium channels or plasticity proteins (Koopmans et al., 2018) and, therefore, species-specific differences in intrinsic excitability and synaptic stability.

Despite consistent turnover of the active cells allocated to the spatial representation across days, the population activity in RSC, but not motor cortices, gradually became more correlated with recurrent experience. While RSC inactivation and lesion studies have previously implicated the RSC in spatial learning and navigation (Czajkowski et al., 2014; Nelson et al., 2015; Vann & Aggleton, 2002, 2004, 2005), this study provides evidence that, after hippocampal-mediated encoding (Esteves et al., 2021; Mao et al., 2018), a cortical correlate of the spatial map is stored and locally strengthened within the RSC. Notably, this finding is consistent with reports of increased IEG expression in the RSC during remote memory retrieval (Maviel et al., 2004; Milczarek et al., 2018; Tayler et al., 2013) and a recent study that demonstrated persistence of a pre-operatively learned spatial representation in the RSC after bilateral lesions of the dorsal hippocampus (Esteves et al., 2023). However, unlike the current study, Esteves et al. (2023) reported a substantial decline in spatial tuning for a familiar environment over the thirty day recovery interval separating behavioural sessions before and after lesion surgeries. Nevertheless, the loss of encoded spatial information was gradually restored with recurrent behaviour in the familiar context, but not a novel context, suggesting that re-exposure to the environment facilitated re-strengthening of established connections in the cortex. Several experimental factors may

have contributed to both the prolonged maintenance of encoded spatial information among cortical spatially selective cells in this study and the enhanced population correlation in RSC over time. First, in this study, mouse behaviour was motivated with an aversive air stimulus, an acute stressor that was limited to the duration of a behavioural session. In contrast, Esteves et al. (2023) employed chronic water restriction (coupled with sucrose water rewards as behavioural motivation), a long-term stressor that may have augmented corticosterone levels and impacted learning and memory throughout the course of their study. Second, in this study, the same cued treadmill belt was used for the duration of both training and experiments and the addition of unstable cues may have served to enhance attention during recurrent behaviour (Kentros et al., 2004). Thus, although synaptic size was not directly monitored in this study, it is plausible that many connections in the RSC may have reached the upper limits of potentiation and dendritic spine size with prolonged experience (Matsuzaki et al., 2004; O'Donnell et al., 2011). Larger synapses are correlated with increased stability (Holtmaat et al., 2005; Trachtenberg et al., 2002) and, therefore, less variability in excitatory post-synaptic potential amplitudes over time (Aitchison et al., 2021). In contrast, in the study performed by Esteves et al. (2023), mice were extensively trained in a one context and then exposed to *two* unique, stably cued environments in each of the thirteen days prior to surgery. In addition, the timespan of behaviour per day within any given environment was halved relative to the current study. Therefore, mice not only had reduced experience with the familiar treadmill belt, but the temporal proximity between the successive exploration of the two environments may have also caused representational overlap during memory consolidation and reduced the fidelity of subsequent retrieval (Cai et al., 2016; Ludvig, 1999; Mankin et al., 2012; Manns et al., 2007; Rubin et al., 2015).

Future studies might directly examine the relationship between measures of excitability (including firing rate or IEG expression) with synapse size, number, and long-term stability.

The results of this study are consistent with a model proposed by Rokni et al. (2007) to explain the unstable tuning curves of cells in the motor cortex. While sensory feedback produces behaviourally-relevant synaptic changes to minimize errors over time, this plasticity mechanism is noisy and behaviourally-irrelevant changes in tuning can occur randomly and independently at individual synapses. Thus, they suggested that a continuum of redundant synaptic configurations converge on an "optimal manifold" to produce a dominant pattern of population activity covariation, which generates consistent behaviours in response to variable sensory-evoked activity. In the context of an attractor neural network framework (Amari, 1972; Amit, 1989; Rolls & Treves, 1998), memory or action selection could be achieved when network dynamics settle into a stable local minima (akin to the "valley" of the optimal manifold). In this case, stochastic noise or homeostatic fluctuations in synaptic strengths would not only prevent the network from perseverating in an attractor state but would also prevent novel learning from overriding existing memory representations (Fusi, 2002). In fact, random synaptic drift within existing, interconnected circuits may underlie the finding that schema-consistent information is much more rapidly consolidated than novel, uncorrelated inputs (McClelland, 2013; Tse et al., 2007, 2011; van Kesteren et al., 2012). Altogether, it is likely that the biological basis of the engram is indeed rooted in synaptic connectivity. However, it appears that the dynamic state of the network supports stable behaviour, rather than any single cell assembly.

7. GENERAL CONCLUSIONS

The results of these studies collectively support that, while the hippocampus may not be essential for the retrieval or temporal restructuring of cortical spatial representations of familiar environments, it enduringly supports the online binding of unreliable sensory attributes to a coherent contextual framework during behaviour. Adhering to regional and laminar hierarchies of top-down information flow, the hippocampus appears to suppress sensory-evoked signals in the cortex that are congruent with the current internal model of the environment, perhaps through coordinated activation of a distributed cortical network that can locally modulate the balance between excitation and inhibition. Importantly, the concept that descending feedback functions to suppress or "explain away" ascending sensory inputs in lower cortices is a central hypothesis of the predictive coding theoretical framework (e.g. Friston, 2005; Rao & Ballard, 1999; Srinivasan et al., 1982). Thus, at the apex of the cortical hierarchy, the hippocampus is poised to facilitate both the coordinated reinstatement of distributed cortical memory representations and the propagation of top-down predictions to improve the efficiency of cortical information processing (Barron et al., 2020).

8. APPENDICES

8.1 SUPPLEMENTARY DATA

Qualitative prediction of dorsal hippocampal lesion extent

In these studies, mice were imaged longitudinally before and after bilateral dorsal hippocampal lesions. However, because magnetic resonance imaging was not feasible, the accuracy and extent of the lesions remained unknown throughout several weeks of data collection. Previous studies in mice (Deacon et al., 2002), rats (Kim, 1960; Kimble et al., 1967), and gerbils (Antonawich et al., 1997; Glickman et al., 1970) have demonstrated that nest building behaviours are impaired by bilateral dorsal hippocampal damage. Thus, this qualitative measure was tested as a method of predicting the *extent* of bilateral dorsal hippocampal lesions.

Intact mice typically construct cup or ball-shaped nests surrounded by shredded cotton and paper in a shallow crater of sawdust bedding (Figure 8.1A). Compared to this standard, nest construction was scored in sham and lesioned mice according to the following scale: 1=nesting materials were distributed without shredding (e.g. Figure 8.1B); 2=nesting materials were gathered to form an open cup-shaped nest without shredding OR nesting materials were shredded but distributed; 3=nesting materials were shredded and gathered to form an open cup-shaped nest; 4=nesting materials were shredded and gathered to form a ball-shaped nest.

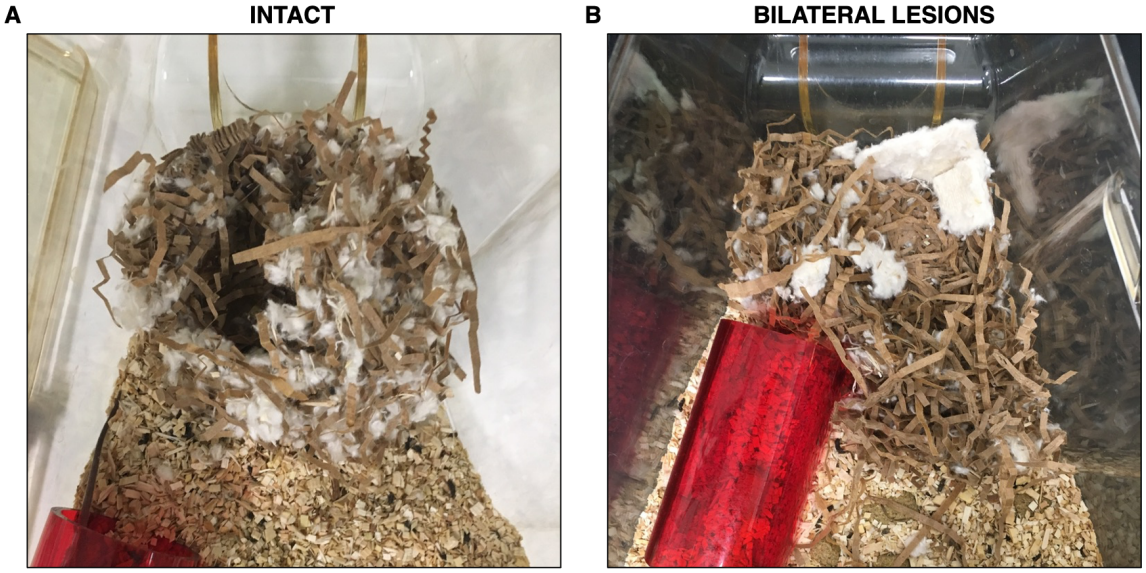

Figure 8.1: Nest construction was impaired by bilateral lesions of the dorsal hippocampus. (A) Example of a ball-shaped nest constructed by an intact mouse. (B) Impoverished nest constructed by a mouse with bilateral dorsal hippocampal lesions. Note the distributed bed of nesting materials, including intact compressed cotton squares.

Consistent with Deacon et al. (2002), mice with bilateral dorsal hippocampal lesions demonstrated a significantly reduced median nest construction score relative to sham controls, indicating impaired nesting behaviours (Wilcoxon Rank-Sum test, p=0.02; Figure 8.1B; Table 8.1). On the other hand, mice with unilateral or incomplete bilateral dorsal hippocampal lesions demonstrated nesting behaviours that were largely indistinguishable from sham controls (Wilcoxon Rank-Sum test, p=0.55; Table 8.1). Only one mouse in the incomplete lesion group exhibited reduced nesting behaviours. Notably, this mouse also had the largest *bilateral* lesion (31% of left and 48% of right hippocampus) in the group. For comparison, another mouse with the same total hippocampal volume loss owing to a more extensive *unilateral* lesion did not exhibit reduced nesting behaviours relative to controls. Overall, nest construction score was highly positively correlated with the volume of intact hippocampus (R=0.83; Figure 8.2), supporting that nesting behaviours are a simple and reliable qualitative predictor of bilateral hippocampal lesion extent.

Table 8.1: Nest construction scores for mice with sham hippocampal lesions, incomplete or unilateral dorsal hippocampal lesions, and bilateral dorsal hippocampal lesions. * indicates a significant difference ($p < 0.05$, Wilcoxon Rank-Sum Test) when compared to the sham control group.

Dorsal Hippocampal Lesion Group	*n*	Median Nest Score	Inter-quartile Range	Volume of Intact Hippocampus $M \pm SD$ (mm^3)	*p*
Sham Control	5	3	0	23.3 ± 0.9	–
Incomplete/Unilateral	6	3	0	17.4 ± 3.6	0.55
Complete Bilateral	4	1	0	10.1 ± 1.5	0.02*

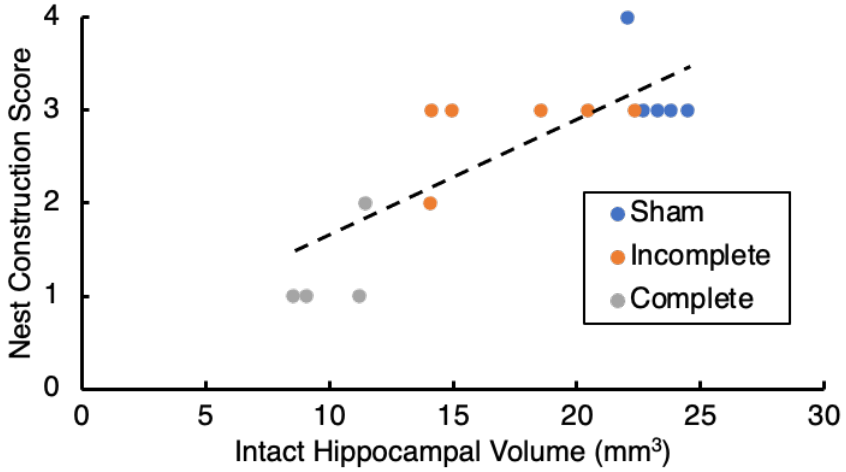

Figure 8.2: Volume of intact hippocampus was positively correlated (R=0.83) with nest construction score.

Aversive air stimulus improved performance

Previous studies have relied on reward-motivated training to encourage treadmill running (e.g. Esteves et al., 2021, 2023; Mao et al., 2017, 2018). Alternatively, an aversive air stimulus can be used to greatly reduce training time while also eliminating the need for chronic water restriction. To assess relative treadmill running performance, mice trained to run in response to the air stimulus were tested for three consecutive days in the absence of the air stimulus (i.e. reward motivated only).

In the presence of only the static cues, there was no significant difference (two-tailed *t*-test, $t(9) = 0.76$, $p = 0.464$) in performance between reward-driven mice ($M \pm SD$ = 35±17 laps) and air stimulus-motivated mice ($M \pm SD$ = 41±9 laps). When obstacles were added to the belt, the performance of reward-driven mice ($M \pm SD$ = 20±6 laps) was significantly reduced (two-tailed *t*-test, $t(11) = 4.05$, $p = 0.002$) compared to air stimulus-motivated mice ($M \pm SD$ = 35±8 laps; Figure 8.3A), justifying the use of an aversive stimulus in these studies. Consistent with previous findings (Dr. Samsoon Inayat, personal communication), place fields were overrepresented near the location of the air stimulus onset suggesting that this sensory cue was utilized as a salient contextual landmark (Figure 8.3B).

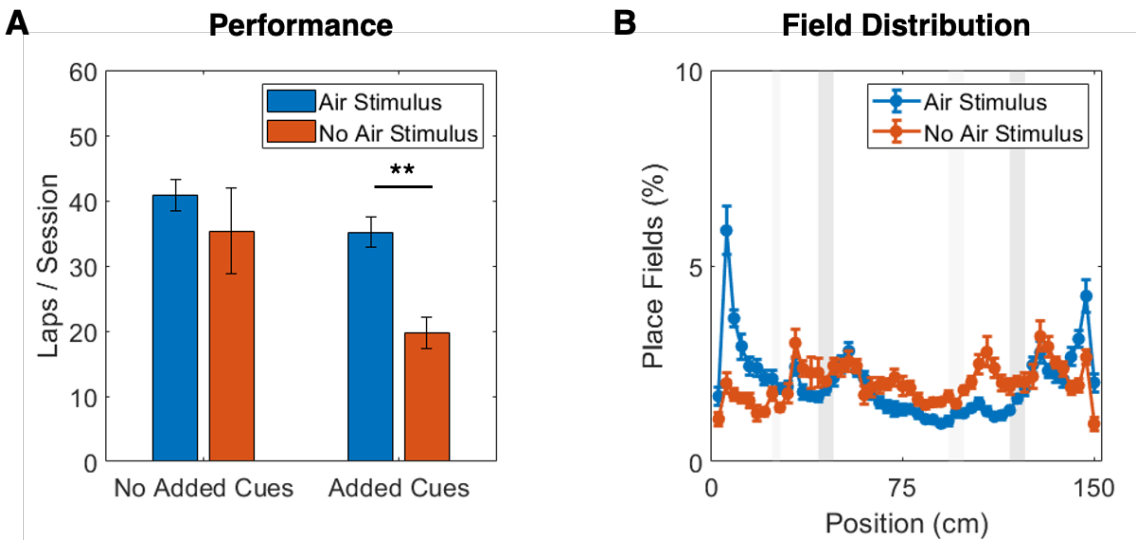

Figure 8.3: An aversive air stimulus improved running performance in physically-demanding environments and stimulus onset was overrepresented as a salient sensory cue. (A) Number of laps run by mice in response to an aversive air stimulus (blue) relative to reward motivation only (orange) in the presence and absence of the added interchangeable obstacles. Error bars are SEM. (B) Distributions of place field locations across the binned length of the treadmill belt in mice running in response to an aversive air stimulus (blue) relative to reward motivation only (orange). Air stimulus onset is located at the first binned position in the treadmill environment. Gray bars indicate positions of stable cues (light gray) and interchangeable obstacles (dark gray). Error bars are SEM.

9. REFERENCES

Abdou, K., Shehata, M., Choko, K., Nishizono, H., Matsuo, M., Muramatsu, S., & Inokuchi, K. (2018). Synapse-specific representation of the identity of overlapping memory engrams. *Science*, *360*(6394), 1227–1231. https://doi.org/10.1126/science.aat3810

Addis, D. R., Moscovitch, M., Crawley, A. P., & McAndrews, M. P. (2004). Recollective qualities modulate hippocampal activation during autobiographical memory retrieval. *Hippocampus*, *14*(6), 752–762. https://doi.org/10.1002/hipo.10215

Aitchison, L., Jegminat, J., Menendez, J. A., Pfister, J. P., Pouget, A., & Latham, P. E. (2021). Synaptic plasticity as Bayesian inference. *Nature Neuroscience*, *24*(4), 565–571. https://doi.org/10.1038/s41593-021-00809-5

Alexander, A. S., Carstensen, L. C., Hinman, J. R., Raudies, F., Chapman, G. W., & Hasselmo, M. E. (2020). Egocentric boundary vector tuning of the retrosplenial cortex. *Science Advances*, *6*(8), eaaz2322. https://doi.org/10.1126/sciadv.aaz2322

Alexander, A. S., & Nitz, D. A. (2015). Retrosplenial cortex maps the conjunction of internal and external spaces. *Nature Neuroscience*, *18*(8), 1143–1151. https://doi.org/10.1038/nn.4058

Alink, A., & Blank, H. (2021). Can expectation suppression be explained by reduced attention to predictable stimuli? *NeuroImage*, *231*, 117824. https://doi.org/https://doi.org/10.1016/j.neuroimage.2021.117824

Allen Brain Institute for Science. (2011). *Allen Reference Atlas – Mouse Brain*. atlas.brain-map.org

Allen, K., Rawlins, J. N. P., Bannerman, D. M., & Csicsvari, J. (2012). Hippocampal place cells can encode multiple trial-dependent features through rate remapping. *Journal of Neuroscience*, *32*(42), 14752–14766. https://doi.org/10.1523/JNEUROSCI.6175-11.2012

Alme, C. B., Miao, C., Jezek, K., Treves, A., Moser, E. I., & Moser, M.-B. (2014). Place cells in the hippocampus: eleven maps for eleven rooms. *Proceedings of the National Academy of Sciences*, *111*(52), 18428–18435. https://doi.org/10.1073/pnas.1421056111

Alstermark, B., Ogawa, J., & Isa, T. (2004). Lack of monosynaptic corticomotoneuronal EPSPs in rats: disynaptic EPSPs mediated via reticulospinal neurons and

polysynaptic EPSPs via segmental interneurons. *Journal of Neurophysiology*, *91*(4), 1832–1839. https://doi.org/10.1152/jn.00820.2003

Amari, S.-I. (1972). Learning patterns and pattern sequences by self-organizing nets of threshold elements. *Institute of Electrical and Electronics Engineers Transactions on Computers*, *C–21*(11), 1197–1206. https://doi.org/10.1109/T-C.1972.223477

Amit, D. J. (1989). *Modelling brain function: the world of attractor neural networks*. Cambridge University Press.

Anagnostaras, S. G., Maren, S., & Fanselow, M. S. (1999). Temporally graded retrograde amnesia of contextual fear after hippocampal damage in rats: within-subjects examination. *The Journal of Neuroscience*, *19*(3), 1106–1114.

Andermann, M. L., Gilfoy, N. B., Goldey, G. J., Sachdev, R. N. S., Wölfel, M., McCormick, D. A., Reid, R. C., & Levene, M. J. (2013). Chronic cellular imaging of entire cortical columns in awake mice using microprisms. *Neuron*, *80*(4), 900–913. https://doi.org/10.1016/j.neuron.2013.07.052

Anderson, M. I., & Jeffery, K. J. (2003). Heterogeneous modulation of place cell firing by changes in context. *The Journal of Neuroscience*, *23*(26), 8827–8835.

Anderson, S. A., Eisenstat, D. D., Shi, L., & Rubenstein, J. L. (1997). Interneuron migration from basal forebrain to neocortex: dependence on Dlx genes. *Science*, *278*(5337), 474–476. https://doi.org/10.1126/science.278.5337.474

Antonawich, F. J., Melton, C. S., Wu, P., & Davis, J. N. (1997). Nesting and shredding behavior as an indicator of hippocampal ischemic damage. *Brain Research*, *764*(1–2), 249–252.

Aronoff, R., Matyas, F., Mateo, C., Ciron, C., Schneider, B., & Petersen, C. C. H. (2010). Long-range connectivity of mouse primary somatosensory barrel cortex. In *European Journal of Neuroscience* (Vol. 31, Issue 12, pp. 2221–2233). https://doi.org/10.1111/j.1460-9568.2010.07264.x

Aschauer, D. F., Eppler, J.-B., Ewig, L., Chambers, A. R., Pokorny, C., Kaschube, M., & Rumpel, S. (2022). Learning-induced biases in the ongoing dynamics of sensory representations predict stimulus generalization. *Cell Reports*, *38*(6), 110340. https://doi.org/https://doi.org/10.1016/j.celrep.2022.110340

Attardo, A., Fitzgerald, J. E., & Schnitzer, M. J. (2015). Impermanence of dendritic spines in live adult CA1 hippocampus. *Nature*, *523*(7562), 592–596. https://doi.org/10.1038/nature14467

Auger, S. D., Mullally, S. L., & Maguire, E. A. (2012). Retrosplenial cortex codes for permanent landmarks. *PLoS ONE*, *7*(8), e43620. https://doi.org/10.1371/journal.pone.0043620

Auger, S. D., Zeidman, P., & Maguire, E. A. (2015). A central role for the retrosplenial cortex in de novo environmental learning. *eLife*, *4*, e09031. https://doi.org/10.7554/eLife.09031

Austin, C. P., & Cepko, C. L. (1990). Cellular migration patterns in the developing mouse cerebral cortex. *Development*, *110*(3), 713–732.

Ayaz, A., Stäuble, A., Hamada, M., Wulf, M.-A., Saleem, A. B., & Helmchen, F. (2019). Layer-specific integration of locomotion and sensory information in mouse barrel cortex. *Nature Communications*, *10*(1), 2585. https://doi.org/10.1038/s41467-019-10564-8

Bakker, R., Tiesinga, P., & Kötter, R. (2015). The Scalable Brain Atlas: instant web-based access to public brain atlases and related content. *Neuroinformatics*, *13*(3), 353–366. https://doi.org/10.1007/s12021-014-9258-x

Bandyopadhyay, S., Shamma, S. A., & Kanold, P. O. (2010). Dichotomy of functional organization in the mouse auditory cortex. *Nature Neuroscience*, *13*(3), 361–368. https://doi.org/10.1038/nn.2490

Barlow, H. B. (1972). Single units and sensation: A neuron doctrine for perceptual psychology? *Perception*, *1*, 371–394.

Barnes, C. A., McNaughton, B. L., Mizumori, S. J. Y., Leonard, B. W., & Lin, L.-H. (1990). Comparison of spatial and temporal characteristics of neuronal activity in sequential stages of hippocampal processing. In J. Storm-Mathisen, J. Zimmer, & O. P. Ottersen (Eds.), *Progress in Brain Research* (Vol. 83, pp. 287–300). Elsevier. https://doi.org/https://doi.org/10.1016/S0079-6123(08)61257-1

Barron, H. C., Auksztulewicz, R., & Friston, K. (2020). Prediction and memory: A predictive coding account. *Progress in Neurobiology*, *192*, 101821. https://doi.org/https://doi.org/10.1016/j.pneurobio.2020.101821

Barth, A. L., & Poulet, J. F. A. (2012). Experimental evidence for sparse firing in the neocortex. *Trends in Neurosciences*, *35*(6), 345–355. https://doi.org/10.1016/j.tins.2012.03.008

Barthas, F., & Kwan, A. C. (2017). Secondary motor cortex: where "sensory" meets "motor" in the rodent frontal cortex. *Trends in Neurosciences*, *40*(3), 181–193. https://doi.org/10.1016/j.tins.2016.11.006

Beaulieu, C. (1993). Numerical data on neocortical neurons in adult rat, with special reference to the GABA population. *Brain Research*, *609*(1), 284–292. https://doi.org/https://doi.org/10.1016/0006-8993(93)90884-P

Belgard, T. G., Marques, A. C., Oliver, P. L., Abaan, H. O., Sirey, T. M., Hoerder-Suabedissen, A., García-Moreno, F., Molnár, Z., Margulies, E. H., & Ponting, C. P. (2011). A transcriptomic atlas of mouse neocortical layers. *Neuron*, *71*(4), 605–616. https://doi.org/10.1016/j.neuron.2011.06.039

Berman, D. E., & Dudai, Y. (2001). Memory extinction, learning anew, and learning the new: dissociations in the molecular machinery of learning in cortex. *Science*, *291*(5512), 2417–2419. https://doi.org/10.1126/science.1058165

Bienenstock, E. L., Cooper, L. N., & Munro, P. W. (1982). Theory for the development of neuron selectivity: orientation specificity and binocular interaction in visual cortex. *The Journal of Neuroscience*, *2*(1), 32. https://doi.org/10.1523/JNEUROSCI.02-01-00032.1982

Blasdel, G. G., & Salama, G. (1986). Voltage-sensitive dyes reveal a modular organization in monkey striate cortex. *Nature*, *321*(6070), 579–585. https://doi.org/10.1038/321579a0

Bliss, T. V. P., Collingridge, G. L., Morris, R. G. M., & Reymann, K. G. (2018). Long-term potentiation in the hippocampus: discovery, mechanisms and function. *Neuroforum*, *24*(3), A103–A120. https://doi.org/doi:10.1515/nf-2017-A059

Bliss, T. V. P., & Lømo, T. (1973). Long-lasting potentiation of synaptic transmission in the dentate area of the anaesthetized rabbit following stimulation of the perforant path. *The Journal of Physiology*, *232*(2), 331–356. https://doi.org/https://doi.org/10.1113/jphysiol.1973.sp010273

Bolhuis, J. J., Stewart, C. A., & Forrest, E. M. (1994). Retrograde amnesia and memory reactivation in rats with ibotenate lesions to the hippocampus or subiculum. *Quarterly Journal of Experimental Psychology B*, *47*(2), 129–150.

Bonin, V., Histed, M. H., Yurgenson, S., & Reid, R. C. (2011). Local diversity and fine-scale organization of receptive fields in mouse visual cortex. *The Journal of Neuroscience*, *31*(50), 18506–18521. https://doi.org/10.1523/JNEUROSCI.2974-11.2011

Bopp, R., Holler-Rickauer, S., Martin, K. A. C., & Schuhknecht, G. F. P. (2017). An ultrastructural study of the thalamic input to layer 4 of primary motor and primary somatosensory cortex in the mouse. *The Journal of Neuroscience*, *37*(9), 2435–2448. https://doi.org/10.1523/JNEUROSCI.2557-16.2017

Bourboulou, R., Marti, G., Michon, F.-X., El Feghaly, E., Nouguier, M., Robbe, D., Koenig, J., & Epsztein, J. (2019). Dynamic control of hippocampal spatial coding resolution by local visual cues. *eLife*, *8*, e44487. https://doi.org/10.7554/eLife.44487

Bourtchuladze, R., Frenguelli, B., Blendy, J., Cioffi, D., Schutz, G., & Silva, A. J. (1994). Deficient long-term memory in mice with a targeted mutation of the cAMP-responsive element-binding protein. *Cell*, *79*(1), 59–68. https://doi.org/10.1016/0092-8674(94)90400-6

Brecht, M., Krauss, A., Muhammad, S., Sinai-Esfahani, L., Bellanca, S., & Margrie, T. W. (2004). Organization of rat vibrissa motor cortex and adjacent areas according to cytoarchitectonics, microstimulation, and intracellular stimulation of identified cells. *Journal of Comparative Neurology*, *479*(4), 360–373. https://doi.org/10.1002/cne.20306

Brose, N., Gasic, G. P., Vetter, D. E., Sullivan, J. M., & Heinemann, S. F. (1993). Protein chemical characterization and immunocytochemical localization of the NMDA receptor subunit NMDA R1. *Journal of Biological Chemistry*, *268*(30), 22663–22671. https://doi.org/10.1016/s0021-9258(18)41579-7

Buldyrev, S. V., Cruz, L., Gomez-Isla, T., Gomez-Tortosa, E., Havlin, S., Le, R., Stanley, H. E., Urbanc, B., & Hyman, B. T. (2000). Description of microcolumnar ensembles in association cortex and their disruption in Alzheimer and Lewy body dementias. *Proceedings of the National Academy of Sciences of the United States of America*, *97*(10), 5039–5043. https://doi.org/10.1073/pnas.060009897

Burke, S. N., Chawla, M. K., Penner, M. R., Crowell, B. E., Worley, P. F., Barnes, C. A., & McNaughton, B. L. (2005). Differential encoding of behavior and spatial context in deep and superficial layers of the neocortex. *Neuron*, *45*(5), 667–674. https://doi.org/https://doi.org/10.1016/j.neuron.2005.01.042

Burke, S. N., Maurer, A. P., Nematollahi, S., Uprety, A. R., Wallace, J. L., & Barnes, C. A. (2011). The influence of objects on place field expression and size in distal hippocampal CA1. *Hippocampus*, *21*(7), 783–801. https://doi.org/10.1002/hipo.20929

Burkhalter, A. (1989). Intrinsic connections of rat primary visual cortex: Laminar organization of axonal projections. *Journal of Comparative Neurology*, *279*(2), 171–186. https://doi.org/https://doi.org/10.1002/cne.902790202

Bush, P. C., & Mainen, Z. F. (2015). Columnar architecture improves noise robustness in a model cortical network. *PLoS ONE*, *10*(3), e0119072. https://doi.org/10.1371/journal.pone.0119072

Buxhoeveden, D., Fobbs, A., Roy, E., & Casanova, M. (2002). Quantitative comparison of radial cell columns in children with Down's syndrome and controls. *Journal of Intellectual Disability Research*, *46*, 76–81. https://doi.org/10.1046/j.1365-2788.2002.00362.x

Buxhoeveden, D. P., & Casanova, M. F. (2002). The minicolumn hypothesis in neuroscience. *Brain*, *125*(5), 935–951. https://doi.org/10.1093/brain/awf110

Buxhoeveden, D. P., & Casanova, M. F. (2005). Encephalization, minicolumns, and hominid evolution. In M. F. Casanova (Ed.), *Neocortical Modularity and the Cell Minicolumn* (pp. 117–136). Nova Science Publishers.

Buxhoeveden, D. P., Hasselrot, U., Buxhoeveden, N. E., Booze, R. M., & Mactutus, C. F. (2006). Microanatomy in 21 day rat brains exposed prenatally to cocaine. *International Journal of Developmental Neuroscience*, *24*(5), 335–341. https://doi.org/10.1016/j.ijdevneu.2006.04.004

Buzsáki, G. (1986). Hippocampal sharp waves: their origin and significance. *Brain Research*, *398*(2), 242–252. https://doi.org/10.1016/0006-8993(86)91483-6

Buzsáki, G. (1989). Two-stage model of memory trace formation: a role for "noisy" brain states. *Neuroscience*, *31*(3), 551–570. https://doi.org/10.1016/0306-4522(89)90423-5

Byrne, P., Becker, S., & Burgess, N. (2007). Remembering the past and imagining the future: A neural model of spatial memory and imagery. *Psychological Review*, *114*(2), 340–375. https://doi.org/10.1037/0033-295X.114.2.340

Cai, D. J., Aharoni, D., Shuman, T., Shobe, J., Biane, J., Song, W., Wei, B., Veshkini, M., La-Vu, M., Lou, J., Flores, S. E., Kim, I., Sano, Y., Zhou, M., Baumgaertel, K., Lavi, A., Kamata, M., Tuszynski, M., Mayford, M., … Silva, A. J. (2016). A shared neural ensemble links distinct contextual memories encoded close in time. *Nature*, *534*(7605), 115–118. https://doi.org/10.1038/nature17955

Cameron, R. S., & Rakic, P. (1991). Glial cell lineage in the cerebral cortex: a review and synthesis. *Glia*, *4*(2), 124–137. https://doi.org/10.1002/glia.440040204

Cao, V. Y., Ye, Y., Mastwal, S., Ren, M., Coon, M., Liu, Q., Costa, R. M., & Wang, K. H. (2015). Motor learning consolidates Arc-expressing neuronal ensembles in secondary motor cortex. *Neuron*, *86*(6), 1385–1392. https://doi.org/https://doi.org/10.1016/j.neuron.2015.05.022

Carpenter-Hyland, E. P., Plummer, T. K., Vazdarjanova, A., & Blake, D. T. (2010). Arc expression and neuroplasticity in primary auditory cortex during initial learning are inversely related to neural activity. *Proceedings of the National Academy of Sciences*

of the United States of America, *107*(33), 14828–14832. https://doi.org/10.1073/pnas.1008604107

Casanova, M. F. (2007). Schizophrenia seen as a deficit in the modulation of cortical minicolumns by monoaminergic systems. *International Review of Psychiatry*, *19*(4), 361–372. https://doi.org/10.1080/09540260701486738

Casanova, M. F. (2013). The minicolumnopathy of autism spectrum disorders. In J. D. Buxbaum & P. R. Hof (Eds.), *The Neuroscience of Autism Spectrum Disorders* (pp. 327–333). Academic Press.

Casanova, M. F., Buxhoeveden, D., & Gomez, J. (2003). Disruption in the inhibitory architecture of the cell minicolumn: implications for autism. *Neuroscientist*, *9*(6), 496–507. https://doi.org/10.1177/1073858403253552

Casanova, M. F., Buxhoeveden, D. P., Cohen, M., Switala, A. E., & Roy, E. L. (2002). Minicolumnar pathology in dyslexia. *Annals of Neurology*, *52*(1), 108–110. https://doi.org/10.1002/ana.10226

Casanova, M. F., de Zeeuw, L., Switala, A., Kreczmanski, P., Korr, H., Ulfig, N., Heinsen, H., Steinbusch, H. W. M., & Schmitz, C. (2005). Mean cell spacing abnormalities in the neocortex of patients with schizophrenia. *Psychiatry Research*, *133*(1), 1–12. https://doi.org/10.1016/j.psychres.2004.11.004

Casanova, M. F., El-Baz, A., Vanbogaert, E., Narahari, P., & Switala, A. (2010). A topographic study of minicolumnar core width by lamina comparison between autistic subjects and controls: possible minicolumnar disruption due to an anatomical element in-common to multiple laminae. *Brain Pathology*, *20*(2), 451–458. https://doi.org/10.1111/j.1750-3639.2009.00319.x

Casanova, M. F., Kreczmanski, P., Trippe, J., Switala, A., Heinsen, H., Steinbusch, H. W. M., & Schmitz, C. (2008). Neuronal distribution in the neocortex of schizophrenic patients. *Psychiatry Research*, *158*(3), 267–277. https://doi.org/10.1016/j.psychres.2006.12.009

Casanova, M. F., van Kooten, I. A. J., Switala, A. E., van Engeland, H., Heinsen, H., Steinbusch, H. W. M., Hof, P. R., Trippe, J., Stone, J., & Schmitz, C. (2006). Minicolumnar abnormalities in autism. *Acta Neuropathologica*, *112*(3), 287–303. https://doi.org/10.1007/s00401-006-0085-5

Cauller, L. J., & Connors, B. W. (1994). Synaptic physiology of horizontal afferents to layer I in slices of rat SI neocortex. *The Journal of Neuroscience*, *14*(2), 751–762.

Cenquizca, L. A., & Swanson, L. W. (2007). Spatial organization of direct hippocampal field CA1 axonal projections to the rest of the cerebral cortex. *Brain Research Reviews*, *56*(1), 1–26. https://doi.org/10.1016/j.brainresrev.2007.05.002

Cermak, L. S., & O'Connor, M. (1983). The anterograde and retrograde retrieval ability of a patient with amnesia due to encephalitis. *Neuropsychologia*, *21*(3), 213–234. https://doi.org/10.1016/0028-3932(83)90039-8

Chance, S. A. (2006). Subtle changes in the ageing human brain. *Nutrition and Health*, *18*(3), 217–224. https://doi.org/10.1177/026010600601800303

Chance, S. A., Casanova, M. F., Switala, A. E., & Crow, T. J. (2008). Auditory cortex asymmetry, altered minicolumn spacing and absence of ageing effects in schizophrenia. *Brain*, *131*, 3178–3192. https://doi.org/10.1093/brain/awn211

Chance, S. A., Casanova, M. F., Switala, A. E., Crow, T. J., & Esiri, M. M. (2006). Minicolumn thinning in temporal lobe association cortex but not primary auditory cortex in normal human ageing. *Acta Neuropathologica*, *111*(5), 459–464. https://doi.org/10.1007/s00401-005-0014-z

Chance, S. A., Clover, L., Cousijn, H., Currah, L., Pettingill, R., & Esiri, M. M. (2011). Microanatomical correlates of cognitive ability and decline: normal ageing, MCI, and Alzheimer's disease. *Cerebral Cortex*, *21*(8), 1870–1878. https://doi.org/10.1093/cercor/bhq264

Chang, H. R., Esteves, I. M., Neumann, A. R., Sun, J., Mohajerani, M. H., & McNaughton, B. L. (2020). Coordinated activities of retrosplenial ensembles during resting-state encode spatial landmarks. *Philosophical Transactions of the Royal Society B: Biological Sciences*, *375*(1799), 20190228. https://doi.org/10.1098/rstb.2019.0228

Chen, L. L., Lin, L. H., Green, E. J., Barnes, C. A., & McNaughton, B. L. (1994). Head-direction cells in the rat posterior cortex. I. Anatomical distribution and behavioral modulation. *Experimental Brain Research*, *101*(1), 8–23. https://doi.org/10.1007/BF00243212

Chen, Q., Cichon, J., Wang, W., Qiu, L., Lee, S. J. R., Campbell, N. R., DeStefino, N., Goard, M. J., Fu, Z., Yasuda, R., Looger, L. L., Arenkiel, B. R., Gan, W. B., & Feng, G. (2012). Imaging neural activity using Thy1-GCaMP transgenic mice. *Neuron*, *76*(2), 297–308. https://doi.org/10.1016/j.neuron.2012.07.011

Chen, T.-W., Li, N., Daie, K., & Svoboda, K. (2017). A map of anticipatory activity in mouse motor cortex. *Neuron*, *94*(4), 866-879.e4. https://doi.org/https://doi.org/10.1016/j.neuron.2017.05.005

Cho, J., & Sharp, P. E. (2001). Head direction, place, and movement correlates for cells in the rat retrosplenial cortex. *Behavioral Neuroscience*, *115*(1), 3–25. https://doi.org/10.1037/0735-7044.115.1.3

Cho, Y. H., Giese, K. P., Tanila, H., Silva, A. J., & Eichenbaum, H. (1998). Abnormal hippocampal spatial representations in αCaMKIIT286A and CREBαΔ− mice. *Science*, *279*(5352), 867–869. https://doi.org/10.1126/science.279.5352.867

Churchland, M. M., Santhanam, G., & Shenoy, K. V. (2006). Preparatory activity in premotor and motor cortex reflects the speed of the upcoming reach. *Journal of Neurophysiology*, *96*(6), 3130–3146. https://doi.org/10.1152/jn.00307.2006

Clark, B. J., Simmons, C. M., Berkowitz, L. E., & Wilber, A. A. (2018). The retrosplenial-parietal network and reference frame coordination for spatial navigation. *Behavioral Neuroscience*, *132*(5), 416–429. https://doi.org/10.1037/bne0000260

Clark, R. E., Broadbent, N. J., & Squire, L. R. (2005). Hippocampus and remote spatial memory in rats. *Hippocampus*, *15*(2), 260–272. https://doi.org/10.1002/hipo.20056

Clark, R. E., Broadbent, N. J., Zola, S. M., & Squire, L. R. (2002). Anterograde amnesia and temporally graded retrograde amnesia for a nonspatial memory task after lesions of hippocampus and subiculum. *The Journal of Neuroscience*, *22*(11), 4663–4669.

Cooper, B. G., & Mizumori, S. J. (1999). Retrosplenial cortex inactivation selectively impairs navigation in darkness. *Neuroreport*, *10*(3), 625–630. https://doi.org/10.1097/00001756-199902250-00033

Cooper, L. N., & Bear, M. F. (2012). The BCM theory of synapse modification at 30: interaction of theory with experiment. *Nature Reviews Neuroscience*, *13*(11), 798–810.

Corcoran, K. A., Donnan, M. D., Tronson, N. C., Guzmán, Y. F., Gao, C., Jovasevic, V., Guedea, A. L., & Radulovic, J. (2011). NMDA receptors in retrosplenial cortex are necessary for retrieval of recent and remote context fear memory. *The Journal of Neuroscience*, *31*(32), 11655. https://doi.org/10.1523/JNEUROSCI.2107-11.2011

Cossart, R., Aronov, D., & Yuste, R. (2003). Attractor dynamics of network UP states in the neocortex. *Nature*, *423*(6937), 283–288. https://doi.org/10.1038/nature01614

Cowansage, K. K., Shuman, T., Dillingham, B. C., Chang, A., Golshani, P., & Mayford, M. (2014). Direct reactivation of a coherent neocortical memory of context. *Neuron*, *84*(2), 432–441. https://doi.org/https://doi.org/10.1016/j.neuron.2014.09.022

Cruikshank, S. J., Ahmed, O. J., Stevens, T. R., Patrick, S. L., Gonzalez, A. N., Elmaleh, M., & Connors, B. W. (2012). Thalamic control of layer 1 circuits in prefrontal cortex. *The Journal of Neuroscience*, *32*(49), 17813–17823. https://doi.org/10.1523/JNEUROSCI.3231-12.2012

Cruz, L., Roe, D. L., Urbanc, B., Cabral, H., Stanley, H. E., & Rosene, D. L. (2004). Age-related reduction in microcolumnar structure in area 46 of the rhesus monkey correlates with behavioral decline. *Proceedings of the National Academy of Sciences of the United States of America*, *101*(45), 15846–15851. https://doi.org/10.1073/pnas.0407002101

Cruz, L., Roe, D. L., Urbanc, B., Inglis, A., Stanley, H. E., & Rosene, D. L. (2009). Age-related reduction in microcolumnar structure correlates with cognitive decline in ventral but not dorsal area 46 of the rhesus monkey. *Neuroscience*, *158*(4), 1509–1520. https://doi.org/10.1016/j.neuroscience.2008.11.033

Cruz, L., Urbanc, B., Inglis, A., Rosene, D. L., & Stanley, H. E. (2008). Generating a model of the three-dimensional spatial distribution of neurons using density maps. *NeuroImage*, *40*(3), 1105–1115. https://doi.org/10.1016/j.neuroimage.2007.12.042

Czajkowski, R., Jayaprakash, B., Wiltgen, B., Rogerson, T., Guzman-Karlsson, M. C., Barth, A. L., Trachtenberg, J. T., & Silva, A. J. (2014). Encoding and storage of spatial information in the retrosplenial cortex. *Proceedings of the National Academy of Sciences*, *111*(23), 8661–8666. https://doi.org/10.1073/pnas.1313222111

Damasio, A. R., Eslinger, P. J., Damasio, H., Van Hoesen, G. W., & Cornell, S. (1985). Multimodal amnesic syndrome following bilateral temporal and basal forebrain damage. *Archives of Neurology*, *42*(3), 252–259. https://doi.org/10.1001/archneur.1985.04060030070012

Dana, H., Mohar, B., Sun, Y., Narayan, S., Gordus, A., Hasseman, J. P., Tsegaye, G., Holt, G. T., Hu, A., Walpita, D., Patel, R., Macklin, J. J., Bargmann, C. I., Ahrens, M. B., Schreiter, E. R., Jayaraman, V., Looger, L. L., Svoboda, K., & Kim, D. S. (2016). Sensitive red protein calcium indicators for imaging neural activity. *eLife*, *5*, e12727. https://doi.org/10.7554/eLife.12727

Danielson, N. B., Zaremba, J. D., Kaifosh, P., Bowler, J., Ladow, M., & Losonczy, A. (2016). Sublayer-specific coding dynamics during spatial navigation and learning in hippocampal area CA1. *Neuron*, *91*(3), 652–665. https://doi.org/https://doi.org/10.1016/j.neuron.2016.06.020

de Kock, C. P. J., Bruno, R. M., Spors, H., & Sakmann, B. (2007). Layer- and cell-type-specific suprathreshold stimulus representation in rat primary somatosensory cortex.

The Journal of Physiology, *581*(Pt 1), 139–154. https://doi.org/10.1113/jphysiol.2006.124321

de Kock, C. P. J., & Sakmann, B. (2009). Spiking in primary somatosensory cortex during natural whisking in awake head-restrained rats is cell-type specific. *Proceedings of the National Academy of Sciences of the United States of America*, *106*(38), 16446–16450. https://doi.org/10.1073/pnas.0904143106

Deacon, R. M. J., Croucher, A., Nicholas, J., & Rawlins, P. (2002). Hippocampal cytotoxic lesion effects on species-typical behaviours in mice. *Behavioural Brain Research*, *132*, 203–213.

Debiec, J., LeDoux, J. E., & Nader, K. (2002). Cellular and systems reconsolidation in the hippocampus. *Neuron*, *36*(3), 527–538. https://doi.org/https://doi.org/10.1016/S0896-6273(02)01001-2

Deitch, D., Rubin, A., & Ziv, Y. (2021). Representational drift in the mouse visual cortex. *Current Biology*, *31*(19), 4327–4339. https://doi.org/https://doi.org/10.1016/j.cub.2021.07.062

Di Rosa, E., Crow, T. J., Walker, M. A., Black, G., & Chance, S. A. (2009). Reduced neuron density, enlarged minicolumn spacing and altered ageing effects in fusiform cortex in schizophrenia. *Psychiatry Research*, *166*(2–3), 102–115. https://doi.org/10.1016/j.psychres.2008.04.007

Dong, C., Madar, A. D., & Sheffield, M. E. J. (2021). Distinct place cell dynamics in CA1 and CA3 encode experience in new environments. *Nature Communications*, *12*(1), 2977. https://doi.org/10.1038/s41467-021-23260-3

Donoghue, J. P., & Wise, S. P. (1982). The motor cortex of the rat: cytoarchitecture and microstimulation mapping. *The Journal of Comparative Neurology*, *212*(1), 76–88. https://doi.org/10.1002/cne.902120106

Douglas, R. J., & Martin, K. A. C. (2004). Neuronal circuits of the neocortex. *Annual Review of Neuroscience*, *27*, 419–451. https://doi.org/10.1146/annurev.neuro.27.070203.144152

Douglas, R. J., Martin, K. A. C., & Whitteridge, D. (1989). A canonical microcircuit for neocortex. *Neural Computation*, *1*(4), 480–488. https://doi.org/10.1162/neco.1989.1.4.480

Driscoll, L. N., Pettit, N. L., Minderer, M., Chettih, S. N., & Harvey, C. D. (2017). Dynamic reorganization of neuronal activity patterns in parietal cortex. *Cell*, *170*(5), 986-999.e16. https://doi.org/10.1016/j.cell.2017.07.021

D'Souza, R. D., Bista, P., Meier, A. M., Ji, W., & Burkhalter, A. (2019). Spatial clustering of inhibition in mouse primary visual cortex. *Neuron*, *104*(3), 588-600.e5. https://doi.org/10.1016/j.neuron.2019.09.020

Dupret, D., O'Neill, J., Pleydell-Bouverie, B., & Csicsvari, J. (2010). The reorganization and reactivation of hippocampal maps predict spatial memory performance. *Nature Neuroscience*, *13*(8), 995–1002. https://doi.org/10.1038/nn.2599

Ego-Stengel, V., & Wilson, M. A. (2010). Disruption of ripple-associated hippocampal activity during rest impairs spatial learning in the rat. *Hippocampus*, *20*(1), 1–10. https://doi.org/10.1002/hipo.20707

Eichenbaum, H. (2014). Time cells in the hippocampus: a new dimension for mapping memories. *Nature Reviews Neuroscience*, *15*(11), 732–744. https://doi.org/10.1038/nrn3827

Engert, F., & Bonhoeffer, T. (1999). Dendritic spine changes associated with hippocampal long-term synaptic plasticity. *Nature*, *399*(6731), 66–70. https://doi.org/10.1038/19978

Epsztein, J., Brecht, M., & Lee, A. K. (2011). Intracellular determinants of hippocampal CA1 place and silent cell activity in a novel environment. *Neuron*, *70*(1), 109–120. https://doi.org/10.1016/j.neuron.2011.03.006

Escobar, M. I., Pimienta, H., Caviness, V. S., Jacobson, M., Crandall, J. E., & Kosik, K. S. (1986). Architecture of apical dendrites in the murine neocortex: dual apical dendritic systems. *Neuroscience*, *17*(4), 975–989. https://doi.org/10.1016/0306-4522(86)90074-6

Esteves, I. M., Chang, H., Neumann, A. R., & McNaughton, B. L. (2023). Consolidation of cellular memory representations in superficial neocortex. *iScience*, *26*(2), 105970. https://doi.org/https://doi.org/10.1016/j.isci.2023.105970

Esteves, I. M., Chang, H., Neumann, A. R., Sun, J., Mohajerani, M. H., & McNaughton, B. L. (2021). Spatial information encoding across multiple neocortical regions depends on an intact hippocampus. *Journal of Neuroscience*, *41*(2), 307–319. https://doi.org/10.1523/JNEUROSCI.1788-20.2020

Euston, D. R., Tatsuno, M., & McNaughton, B. L. (2007). Fast-forward playback of recent memory sequences in prefrontal cortex during sleep. *Science*, *318*(5853), 1147–1150. https://doi.org/10.1126/science.1148979

Evarts, E. V. (1968). Relation of pyramidal tract activity to force exerted during voluntary movement. *Journal of Neurophysiology*, *31*(1), 14–27. https://doi.org/10.1152/jn.1968.31.1.14

Farr, T. D., Liu, L., Colwell, K. L., Whishaw, I. Q., & Metz, G. A. (2006). Bilateral alteration in stepping pattern after unilateral motor cortex injury: A new test strategy for analysis of skilled limb movements in neurological mouse models. *Journal of Neuroscience Methods*, *153*(1), 104–113. https://doi.org/https://doi.org/10.1016/j.jneumeth.2005.10.011

Fauth, M., Wörgötter, F., & Tetzlaff, C. (2015). Formation and maintenance of robust long-term information storage in the presence of synaptic turnover. *PLoS Computational Biology*, *11*(12), e1004684. https://doi.org/10.1371/journal.pcbi.1004684

Favorov, O. V, & Diamond, M. E. (1990). Demonstration of discrete place-defined columns--segregates--in the cat SI. *Journal of Comparative Neurology*, *298*(1), 97–112. https://doi.org/10.1002/cne.902980108

Favorov, O. V, Diamond, M. E., & Whitsel, B. L. (1987). Evidence for a mosaic representation of the body surface in area 3b of the somatic cortex of cat. *Proceedings of the National Academy of Sciences of the United States of America*, *84*(18), 6606–6610. https://doi.org/10.1073/pnas.84.18.6606

Favorov, O. V, & Whitsel, B. L. (1988). Spatial organization of the peripheral input to area 1 cell columns. I. The detection of "segregates". *Brain Research*, *472*(1), 25–42. https://doi.org/10.1016/0165-0173(88)90003-3

Favorov, O. V., Whitsel, B. L., & Tommerdahl, M. (2015). Discrete, place-defined macrocolumns in somatosensory cortex: lessons for modular organization of the cerebral cortex. In M. F. Casanova & I. Opris (Eds.), *Recent Advances on the Modular Organization of the Cortex* (pp. 143–179). Springer Science + Business Media.

Felleman, D. J., & Van Essen, D. C. (1991). Distributed hierarchical processing in the primate cerebral cortex. *Cerebral Cortex*, *1*(1), 1–47. https://academic.oup.com/cercor/article/1/1/1/408896

Ferbinteanu, J., Kennedy, P. J., & Shapiro, M. L. (2006). Episodic memory - From brain to mind. *Hippocampus*, *16*(9), 691–703. https://doi.org/10.1002/hipo.20204

Ferezou, I., Haiss, F., Gentet, L. J., Aronoff, R., Weber, B., & Petersen, C. C. H. (2007). Spatiotemporal dynamics of cortical sensorimotor integration in behaving mice. *Neuron*, *56*(5), 907–923. https://doi.org/10.1016/j.neuron.2007.10.007

Fischer, L. F., Mojica Soto-Albors, R., Buck, F., & Harnett, M. T. (2020). Representation of visual landmarks in retrosplenial cortex. *eLife*, *9*, e51458. https://doi.org/10.7554/eLife.51458

Fleischmann, A., Hvalby, O., Jensen, V., Strekalova, T., Zacher, C., Layer, L. E., Kvello, A., Reschke, M., Spanagel, R., Sprengel, R., Wagner, E. F., & Gass, P. (2003). Impaired long-term memory and NR2A-type NMDA receptor-dependent synaptic plasticity in mice lacking c-Fos in the CNS. *The Journal of Neuroscience*, *23*(27), 9116–9122.

Friedrich, J., Zhou, P., & Paninski, L. (2017). Fast online deconvolution of calcium imaging data. *PLoS Computational Biology*, *13*(3), e1005423. https://doi.org/10.1371/journal.pcbi.1005423

Friston, K. (2005). A theory of cortical responses. *Philosophical Transactions of the Royal Society B: Biological Sciences*, *360*(1456), 815–836.

Fritsch, G. (1870). Uber die elektrische Erregbarkeit des Grosshirns. *Arch, Anat. Physiol. Wiss. Med.*, *37*, 300–332.

Fujisawa, S., Amarasingham, A., Harrison, M. T., & Buzsáki, G. (2008). Behavior-dependent short-term assembly dynamics in the medial prefrontal cortex. *Nature Neuroscience*, *11*(7), 823–833. https://doi.org/10.1038/nn.2134

Fulvi Mari, C. (2004). Extremely dilute modular neuronal networks: neocortical memory retrieval dynamics. *Journal of Computational Neuroscience*, *17*(1), 57–79. https://doi.org/10.1023/B:JCNS.0000023871.60959.88

Fulvi Mari, C., & Treves, A. (1998). Modeling neocortical areas with a modular neural network. *BioSystems*, *48*(1–3), 47–55. https://doi.org/10.1016/s0303-2647(98)00049-5

Fusi, S. (2002). Hebbian spike-driven synaptic plasticity for learning patterns of mean firing rates. *Biological Cybernetics*, *87*, 459–470. https://doi.org/10.1007/s00422-002-0356-8

Gal, J. S., Morozov, Y. M., Ayoub, A. E., Chatterjee, M., Rakic, P., & Haydar, T. F. (2006). Molecular and morphological heterogeneity of neural precursors in the mouse neocortical proliferative zones. *Journal of Neuroscience*, *26*(3), 1045–1056. https://doi.org/10.1523/JNEUROSCI.4499-05.2006

Garner, A. R., Rowland, D. C., Hwang, S. Y., Baumgaertel, K., Roth, B. L., Kentros, C., & Mayford, M. (2012). Generation of a synthetic memory trace. *Science*, *335*(6075), 1513–1516. https://doi.org/10.1126/science.1214985

Garraghty, P. E., & Sur, M. (1990). Morphology of single intracellularly stained axons terminating in area 3b of macaque monkeys. *Journal of Comparative Neurology*, *294*(4), 583–593. https://doi.org/10.1002/cne.902940406

Gauthier, J. L., & Tank, D. W. (2018). A dedicated population for reward coding in the hippocampus. *Neuron*, *99*(1), 179-193.e7. https://doi.org/10.1016/j.neuron.2018.06.008

Geiller, T., Fattahi, M., Choi, J. S., & Royer, S. (2017). Place cells are more strongly tied to landmarks in deep than in superficial CA1. *Nature Communications*, *8*, 14531. https://doi.org/10.1038/ncomms14531

Georgopoulos, A. P., Kalaska, J. F., Caminiti, R., & Massey, J. T. (1982). On the relations between the direction of two-dimensional arm movements and cell discharge in primate motor cortex. *The Journal of Neuroscience*, *2*(11), 1527–1537.

Ghandour, K., Ohkawa, N., Fung, C. C. A., Asai, H., Saitoh, Y., Takekawa, T., Okubo-Suzuki, R., Soya, S., Nishizono, H., Matsuo, M., Osanai, M., Sato, M., Ohkura, M., Nakai, J., Hayashi, Y., Sakurai, T., Kitamura, T., Fukai, T., & Inokuchi, K. (2019). Orchestrated ensemble activities constitute a hippocampal memory engram. *Nature Communications*, *10*(1), 2637. https://doi.org/10.1038/s41467-019-10683-2

Gilbert, C. D., & Wiesel, T. N. (1983). Functional organization of the visual cortex. *Progress in Brain Research*, *58*, 209–218. https://doi.org/10.1016/S0079-6123(08)60022-9

Gilboa, A., Winocur, G., Grady, C. L., Hevenor, S. J., & Moscovitch, M. (2004). Remembering our past: functional neuroanatomy of recollection of recent and very remote personal events. *Cerebral Cortex*, *14*(11), 1214–1225. https://doi.org/10.1093/cercor/bhh082

Girardeau, G., Benchenane, K., Wiener, S. I., Buzsáki, G., & Zugaro, M. B. (2009). Selective suppression of hippocampal ripples impairs spatial memory. *Nature Neuroscience*, *12*(10), 1222–1223. https://doi.org/10.1038/nn.2384

Girman, S. V, Sauvé, Y., & Lund, R. D. (1999). Receptive field properties of single neurons in rat primary visual cortex. *Journal of Neurophysiology*, *82*(1), 301–311. https://doi.org/10.1152/jn.1999.82.1.301

Glickman, S. E., Higgins, T. J., Isaacson, R. L., Higgins, T. J., & Isaacson, R. L. (1970). Some effects of hippocampal lesions on the behavior of Mongolian gerbils. *Physiology and Behavior*, *5*(8), 931–938.

Gothard, K. M., Skaggs, W. E., Moore, K. M., & McNaughton, B. L. (1996). Binding of hippocampal CA1 neural activity to multiple reference frames in a landmark-based navigation task. *The Journal of Neuroscience*, *16*(2), 823–835.

Götz, M., & Barde, Y.-A. (2005). Radial glial cells defined and major intermediates between embryonic stem cells and CNS neurons. *Neuron*, *46*(3), 369–372. https://doi.org/10.1016/j.neuron.2005.04.012

Gremel, C. M., & Costa, R. M. (2013). Premotor cortex is critical for goal-directed actions. *Frontiers in Computational Neuroscience*, *7*, 110. https://doi.org/10.3389/fncom.2013.00110

Gressens, P., & Evrard, P. (1993). The glial fascicle: an ontogenic and phylogenic unit guiding, supplying and distributing mammalian cortical neurons. *Brain Research. Developmental Brain Research*, *76*(2), 272–277. https://doi.org/10.1016/0165-3806(93)90218-y

Grutzendler, J., Kasthuri, N., & Gan, W.-B. (2002). Long-term dendritic spine stability in the adult cortex. *Nature*, *420*(6917), 812–816. https://doi.org/10.1038/nature01276

Guo, J.-Z., Graves, A. R., Guo, W. W., Zheng, J., Lee, A., Rodríguez-González, J., Li, N., Macklin, J. J., Phillips, J. W., Mensh, B. D., Branson, K., & Hantman, A. W. (2015). Cortex commands the performance of skilled movement. *eLife*, *4*, e10774–e10774. https://doi.org/10.7554/eLife.10774

Guo, K., Yamawaki, N., Svoboda, K., & Shepherd, G. M. G. (2018). Anterolateral motor cortex connects with a medial subdivision of ventromedial thalamus through cell type-specific circuits, forming an excitatory thalamo-cortico-thalamic loop via layer 1 apical tuft dendrites of layer 5B pyramidal tract type neurons. *The Journal of Neuroscience*, *38*(41), 8787–8797. https://doi.org/10.1523/JNEUROSCI.1333-18.2018

Guo, Z. V., Li, N., Huber, D., Ophir, E., Gutnisky, D., Ting, J. T., Feng, G., & Svoboda, K. (2014). Flow of cortical activity underlying a tactile decision in mice. *Neuron*, *81*(1), 179–194. https://doi.org/https://doi.org/10.1016/j.neuron.2013.10.020

Gupta, A. S., van der Meer, M. A. A., Touretzky, D. S., & Redish, A. D. (2010). Hippocampal replay is not a simple function of experience. *Neuron*, *65*(5), 695–705. https://doi.org/10.1016/j.neuron.2010.01.034

Guzowski, J. F., Lyford, G. L., Stevenson, G. D., Houston, F. P., McGaugh, J. L., Worley, P. F., & Barnes, C. A. (2000). Inhibition of activity-dependent arc protein expression in the rat hippocampus impairs the maintenance of long-term potentiation

and the consolidation of long-term memory. *The Journal of Neuroscience*, *20*(11), 3993–4001.

Guzowski, J. F., McNaughton, B. L., Barnes, C. A., & Worley, P. F. (1999). Environment-specific expression of the immediate-early gene Arc in hippocampal neuronal ensembles. *Nature Neuroscience*, *2*(12), 1120–1124. https://doi.org/10.1038/16046

Guzowski, J. F., Miyashita, T., Chawla, M. K., Sanderson, J., Maes, L. I., Houston, F. P., Lipa, P., McNaughton, B. L., Worley, P. F., & Barnes, C. A. (2006). Recent behavioral history modifies coupling between cell activity and Arc gene transcription in hippocampal CA1 neurons. *Proceedings of the National Academy of Sciences of the United States of America*, *103*(4), 1077. https://doi.org/10.1073/pnas.0505519103

Haggerty, D. C., & Ji, D. (2015). Activities of visual cortical and hippocampal neurons co-fluctuate in freely moving rats during spatial behavior. *eLife*, *4*, e08902. https://doi.org/10.7554/eLife.08902

Hainmueller, T., & Bartos, M. (2018). Parallel emergence of stable and dynamic memory engrams in the hippocampus. *Nature*, *558*(7709), 292–296. https://doi.org/10.1038/s41586-018-0191-2

Hall, R. D., & Lindholm, E. P. (1974). Organization of motor and somatosensory neocortex in the albino rat. *Brain Research*, *66*(1), 23–38. https://doi.org/10.1016/0006-8993(74)90076-6

Han, J.-H., Kushner, S. A., Yiu, A. P., Cole, C. J., Matynia, A., Brown, R. A., Neve, R. L., Guzowski, J. F., Silva, A. J., & Josselyn, S. A. (2007). Neuronal competition and selection during memory formation. *Science*, *316*(5823), 457–460. https://doi.org/10.1126/science.1139438

Han, S., Yang, W., & Yuste, R. (2019). Two-color volumetric imaging of neuronal activity of cortical columns. *Cell Reports*, *27*(7), 2229-2240.e4. https://doi.org/10.1016/j.celrep.2019.04.075

Harand, C., Bertran, F., La Joie, R., Landeau, B., Mézenge, F., Desgranges, B., Peigneux, P., Eustache, F., & Rauchs, G. (2012). The hippocampus remains activated over the long term for the retrieval of truly episodic memories. *PloS ONE*, *7*(8), e43495. https://doi.org/10.1371/journal.pone.0043495

Harris, J. A., Mihalas, S., Hirokawa, K. E., Whitesell, J. D., Choi, H., Bernard, A., Bohn, P., Caldejon, S., Casal, L., Cho, A., Feiner, A., Feng, D., Gaudreault, N., Gerfen, C. R., Graddis, N., Groblewski, P. A., Henry, A. M., Ho, A., Howard, R., … Zeng, H.

(2019). Hierarchical organization of cortical and thalamic connectivity. *Nature*, *575*(7781), 195–202. https://doi.org/10.1038/s41586-019-1716-z

Harris, K. D., & Mrsic-Flogel, T. D. (2013). Cortical connectivity and sensory coding. *Nature*, *503*(7474), 51–58. https://doi.org/10.1038/nature12654

Harris, K. D., & Shepherd, G. M. G. (2015). The neocortical circuit: themes and variations. *Nature Neuroscience*, *18*(2), 170–181. https://doi.org/10.1038/nn.3917

Hassabis, D., Kumaran, D., Vann, S. D., & Maguire, E. A. (2007). Patients with hippocampal amnesia cannot imagine new experiences. *Proceedings of the National Academy of Sciences*, *104*(5), 1726–1731. https://doi.org/10.1073/pnas.0610561104

Hasselmo, M. E. (2006). The role of acetylcholine in learning and memory. *Current Opinion in Neurobiology*, *16*(6), 710–715.

Hatsopoulos, N. G., Xu, Q., & Amit, Y. (2007). Encoding of movement fragments in the motor cortex. *The Journal of Neuroscience*, *27*(19), 5105. https://doi.org/10.1523/JNEUROSCI.3570-06.2007

Hayashi, Y., Shi, S. H., Esteban, J. A., Piccini, A., Poncer, J. C., & Malinow, R. (2000). Driving AMPA receptors into synapses by LTP and CaMKII: requirement for GluR1 and PDZ domain interaction. *Science*, *287*(5461), 2262–2267. https://doi.org/10.1126/science.287.5461.2262

He, S., Li, Z., Ge, S., Yu, Y. C., & Shi, S. H. (2015). Inside-out radial migration facilitates lineage-dependent neocortical microcircuit assembly. *Neuron*, *86*(5), 1159–1166. https://doi.org/10.1016/j.neuron.2015.05.002

Hebb, D. O. (1949). *The organization of behavior: a neuropsychological theory*. John Wiley & Sons, Inc.

Henriksen, E. J., Colgin, L. L., Barnes, C. A., Witter, M. P., Moser, M.-B., & Moser, E. I. (2010). Spatial representation along the proximodistal axis of CA1. *Neuron*, *68*(1), 127–137. https://doi.org/10.1016/j.neuron.2010.08.042

Henson, R., Shallice, T., & Dolan, R. (2000). Neuroimaging evidence for dissociable forms of repetition priming. *Science*, *287*(5456), 1269–1272. https://doi.org/10.1126/science.287.5456.1269

Hetherington, P. A., & Shapiro, M. L. (1997). Hippocampal place fields are altered by the removal of single visual cues in a distance-dependent manner. *Behavioral Neuroscience*, *111*(1), 20–34. https://doi.org/10.1037//0735-7044.111.1.20

Hollup, S. A., Molden, S., Donnett, J. G., Moser, M.-B., & Moser, E. I. (2001). Accumulation of hippocampal place fields at the goal location in an annular watermaze task. *The Journal of Neuroscience*, *21*(5), 1635. https://doi.org/10.1523/JNEUROSCI.21-05-01635.2001

Holmgren, C., Harkany, T., Svennenfors, B., & Zilberter, Y. (2003). Pyramidal cell communication within local networks in layer 2/3 of rat neocortex. *The Journal of Physiology*, *551*(Pt 1), 139–153. https://doi.org/10.1113/jphysiol.2003.044784

Holthoff, K., & Witte, O. W. (1996). Intrinsic optical signals in rat neocortical slices measured with near-infrared dark-field microscopy reveal changes in extracellular space. *Journal of Neuroscience*, *16*(8), 2740–2749.

Holtmaat, A. J. G. D., Trachtenberg, J. T., Wilbrecht, L., Shepherd, G. M., Zhang, X., Knott, G. W., & Svoboda, K. (2005). Transient and persistent dendritic spines in the neocortex in vivo. *Neuron*, *45*(2), 279–291. https://doi.org/10.1016/j.neuron.2005.01.003

Hooks, B. M., Hires, S. A., Zhang, Y.-X., Huber, D., Petreanu, L., Svoboda, K., & Shepherd, G. M. G. (2011). Laminar analysis of excitatory local circuits in vibrissal motor and sensory cortical areas. *PLoS Biology*, *9*(1), e1000572. https://doi.org/10.1371/journal.pbio.1000572

Hooks, B. M., Mao, T., Gutnisky, D. A., Yamawaki, N., Svoboda, K., & Shepherd, G. M. G. (2013). Organization of cortical and thalamic input to pyramidal neurons in mouse motor cortex. *The Journal of Neuroscience*, *33*(2), 748–760. https://doi.org/10.1523/JNEUROSCI.4338-12.2013

Hoover, W. B., & Vertes, R. P. (2007). Anatomical analysis of afferent projections to the medial prefrontal cortex in the rat. *Brain Structure & Function*, *212*(2), 149–179. https://doi.org/10.1007/s00429-007-0150-4

Horton, J. G., & Adams, D. L. (2005). The cortical column: A structure without a function. *Philosophical Transactions of the Royal Society B: Biological Sciences*, *360*(1456), 837–862. https://doi.org/10.1098/rstb.2005.1623

Horton, N. G., Wang, K., Kobat, D., Clark, C. G., Wise, F. W., Schaffer, C. B., & Xu, C. (2013). In vivo three-photon microscopy of subcortical structures within an intact mouse brain. *Nature Photonics*, *7*(3), 205–209. https://doi.org/10.1038/nphoton.2012.336

Hubel, D. H. (1982). Cortical neurobiology: a slanted historical perspective. *Annual Review of Neuroscience*, *5*, 363–370. https://doi.org/10.1146/annurev.ne.05.030182.002051

Hubel, D. H., & Wiesel, T. N. (1962). Receptive fields, binocular interaction and functional architecture in the cat's visual cortex. *Journal of Physiology*, *160*(1), 106–154. https://doi.org/10.1113/jphysiol.1962.sp006837

Hubel, D. H., & Wiesel, T. N. (1963). Receptive fields of cells in striate cortex of very young, visually inexperienced kittens. *Journal of Neurophysiology*, *26*, 994–1002. https://doi.org/10.1152/jn.1963.26.6.994

Hubel, D. H., & Wiesel, T. N. (1968). Receptive fields and functional architecture of monkey striate cortex. *Journal of Physiology*, *195*(1), 215–243. https://doi.org/10.1113/jphysiol.1968.sp008455

Hubel, D. H., & Wiesel, T. N. (1974). Sequence regularity and geometry of orientation columns in the monkey striate cortex. *Journal of Comparative Neurology*, *158*(3), 267–293. https://doi.org/10.1002/cne.901580304

Hubel, D. H., & Wiesel, T. N. (1977). Functional architecture of macaque monkey visual cortex. *Proceedings of the Royal Society of London B*, *198*, 1–59.

Hubel, D. H., Wiesel, T. N., LeVay, S., Barlow, H. B., & Gaze, R. M. (1977). Plasticity of ocular dominance columns in monkey striate cortex. *Philosophical Transactions of the Royal Society of London. Series B, Biological Sciences*, *278*(961), 377–409. https://doi.org/10.1098/rstb.1977.0050

Huber, D., Gutnisky, D. A., Peron, S., O'Connor, D. H., Wiegert, J. S., Tian, L., Oertner, T. G., Looger, L. L., & Svoboda, K. (2012). Multiple dynamic representations in the motor cortex during sensorimotor learning. *Nature*, *484*(7395), 473–478. https://doi.org/10.1038/nature11039

Huttner, W. B., & Kosodo, Y. (2005). Symmetric versus asymmetric cell division during neurogenesis in the developing vertebrate central nervous system. *Current Opinion in Cell Biology*, *17*(6), 648–657. https://doi.org/10.1016/j.ceb.2005.10.005

Hwang, E. J., Dahlen, J. E., Hu, Y. Y., Aguilar, K., Yu, B., Mukundan, M., Mitani, A., & Komiyama, T. (2022). Disengagement of motor cortex from movement control during long-term learning. *Science Advances*, *5*(10), eaay0001. https://doi.org/10.1126/sciadv.aay0001

Inayat, S., McAllister, B. B., Whishaw, I. Q., & Mohajerani, M. H. (2023). Hippocampal conjunctive and complementary CA1 populations relate sensory events to movement. *iScience*, *26*(4), 106481. https://doi.org/10.1016/j.isci.2023.106481

Inda, M. C., Muravieva, E. V, & Alberini, C. M. (2011). Memory retrieval and the passage of time: from reconsolidation and strengthening to extinction. *The Journal*

of Neuroscience, *31*(5), 1635–1643. https://doi.org/10.1523/JNEUROSCI.4736-10.2011

Insausti, R., Herrero, M. T., & Witter, M. P. (1997). Entorhinal cortex of the rat: cytoarchitectonic subdivisions and the origin and distribution of cortical efferents. *Hippocampus*, *7*(2), 146–183.

Iriki, A., Pavlides, C., Keller, A., & Asanuma, H. (1989). Long-term potentiation in the motor cortex. *Science*, *245*(4924), 1385–1387. https://doi.org/10.1126/science.2551038

Ito, H. T., & Schuman, E. M. (2012). Functional division of hippocampal area CA1 via modulatory gating of entorhinal cortical inputs. *Hippocampus*, *22*(2), 372–387. https://doi.org/10.1002/hipo.20909

Jadhav, S. P., Kemere, C., German, P. W., & Frank, L. M. (2012). Awake hippocampal sharp-wave ripples support spatial memory. *Science*, *336*(6087), 1454–1458. https://doi.org/10.1126/science.1217230

Ji, D., & Wilson, M. A. (2007). Coordinated memory replay in the visual cortex and hippocampus during sleep. *Nature Neuroscience*, *10*(1), 100–107. https://doi.org/10.1038/nn1825

Ji, W., Gămănuţ, R., Bista, P., D'Souza, R. D., Wang, Q., & Burkhalter, A. (2015). Modularity in the organization of mouse primary visual cortex. *Neuron*, *87*(3), 632–643. https://doi.org/https://doi.org/10.1016/j.neuron.2015.07.004

Johansson, C., & Lansner, A. (2007). Imposing biological constraints onto an abstract neocortical attractor network model. *Neural Computation*, *19*(7), 1871–1896. https://doi.org/10.1162/neco.2007.19.7.1871

Johnson, A., & Redish, A. D. (2007). Neural ensembles in CA3 transiently encode paths forward of the animal at a decision point. *The Journal of Neuroscience*, *27*(45), 12176–12189. https://doi.org/10.1523/JNEUROSCI.3761-07.2007

Jones, E. G. (2000). Microcolumns in the cerebral cortex. *Proceedings of the National Academy of Sciences of the United States of America*, *97*(10), 5019–5021. https://doi.org/10.1073/pnas.97.10.5019

Jones, E. G., Friedman, D. P., & Hendry, S. H. (1982). Thalamic basis of place- and modality-specific columns in monkey somatosensory cortex: a correlative anatomical and physiological study. *Journal of Neurophysiology*, *48*(2), 545–568. https://doi.org/10.1152/jn.1982.48.2.545

Jung, M. W., & McNaughton, B. L. (1993). Spatial selectivity of unit activity in the hippocampal granular layer. *Hippocampus*, *3*(2), 165–182. https://doi.org/10.1002/hipo.450030209

Jung, M. W., Wiener, S. I., & McNaughton, B. L. (1994). Comparison of spatial firing characteristics of units in dorsal and ventral hippocampus of the rat. *The Journal of Neuroscience*, *14*(12), 7347. https://doi.org/10.1523/JNEUROSCI.14-12-07347.1994

Kaas, J. H., & Balaram, P. (2015). The types of functional and structural subdivisions of cortical areas. In M. F. Casanova & I. Opris (Eds.), *Recent Advances on the Modular Organization of the Cortex* (pp. 35–62). Springer Science + Business Media.

Kaas, J. H., Nelson, R. J., Sur, M., & Merzenich, M. M. (1981). Organization of somatosensory cortex in primates. In F. O. Schmitt, F. G. Worder, G. Adelman, & S. G. Dennis (Eds.), *The Organization of the Cerebral Cortex* (pp. 237–261). MIT Press.

Kakei, S., Hoffman, D. S., & Strick, P. L. (1999). Muscle and movement representations in the primary motor cortex. *Science*, *285*(5436), 2136–2139. https://doi.org/10.1126/science.285.5436.2136

Karimi Abadchi, J., Nazari-Ahangarkolaee, M., Gattas, S., Bermudez-Contreras, E., Luczak, A., McNaughton, B. L., & Mohajerani, M. H. (2020). Spatiotemporal patterns of neocortical activity around hippocampal sharp-wave ripples. *eLife*, *9*, e51972. https://doi.org/10.7554/eLife.51972

Katche, C., Dorman, G., Slipczuk, L., Cammarota, M., & Medina, J. H. (2013). Functional integrity of the retrosplenial cortex is essential for rapid consolidation and recall of fear memory. *Learning & Memory*, *20*(4), 170–173. https://doi.org/10.1101/lm.030080.112

Kawaguchi, Y., & Kubota, Y. (1997). GABAergic cell subtypes and their synaptic connections in rat frontal cortex. *Cerebral Cortex*, *7*(6), 476–486. https://doi.org/10.1093/cercor/7.6.476

Kawai, R., Markman, T., Poddar, R., Ko, R., Fantana, A. L., Dhawale, A. K., Kampff, A. R., & Ölveczky, B. P. (2015). Motor cortex is required for learning but not for executing a motor skill. *Neuron*, *86*(3), 800–812. https://doi.org/10.1016/j.neuron.2015.03.024

Keene, C. S., & Bucci, D. J. (2008a). Contributions of the retrosplenial and posterior parietal cortices to cue-specific and contextual fear conditioning. *Behavioral Neuroscience*, *122*(1), 89–97. https://doi.org/10.1037/0735-7044.122.1.89

Keene, C. S., & Bucci, D. J. (2008b). Neurotoxic lesions of retrosplenial cortex disrupt signaled and unsignaled contextual fear conditioning. *Behavioral Neuroscience*, *122*(5), 1070–1077. https://doi.org/10.1037/a0012895

Keller, D., Erö, C., & Markram, H. (2018). Cell densities in the mouse brain: a systematic review. *Frontiers in Neuroanatomy*, *12*, 83. https://doi.org/10.3389/fnana.2018.00083

Kelly, M. P., & Deadwyler, S. A. (2003). Experience-dependent regulation of the immediate-early gene arc differs across brain regions. *The Journal of Neuroscience*, *23*(16), 6443–6451.

Kentros, C. G., Agnihotri, N. T., Streater, S., Hawkins, R. D., & Kandel, E. R. (2004). Increased attention to spatial context increases both place field stability and spatial memory. *Neuron*, *42*(2), 283–295. https://doi.org/10.1016/S0896-6273(04)00192-8

Kentros, C. G., Hargreaves, E., Hawkins, R. D., Kandel, E. R., Shapiro, M., & Muller, R. V. (1998). Abolition of long-term stability of new hippocampal place cell maps by NMDA receptor blockade. *Science*, *280*(5372), 2121–2126. https://doi.org/10.1126/science.280.5372.2121

Kim, C. (1960). Nest building, general activity, and salt preference of rats following hippocampal ablation. *Journal of Comparative and Physiological Psychology*, *53*, 11–16. https://doi.org/https://doi.org/10.1037/h0038350

Kim, J. J., & Fanselow, M. S. (1992). Modality-specific retrograde amnesia of fear. *Science*, *256*(5057), 675–677. https://doi.org/10.1126/science.1585183

Kim, S. M., & Frank, L. M. (2009). Hippocampal lesions impair rapid learning of a continuous spatial alternation task. *PLoS ONE*, *4*(5), e5494-. https://doi.org/10.1371/journal.pone.0005494

Kim, S. M., Ganguli, S., & Frank, L. M. (2012). Spatial information outflow from the hippocampal circuit: distributed spatial coding and phase precession in the subiculum. *The Journal of Neuroscience*, *32*(34), 11539. https://doi.org/10.1523/JNEUROSCI.5942-11.2012

Kimble, D. P., Rogers, L., & Hendrickson, C. W. (1967). Hippocampal lesions disrupt maternal, not sexual, behavior in the albino rat. *Journal of Comparative and Physiological Psychology*, *63*(3), 401–407. https://doi.org/https://doi.org/10.1037/h0024605

Kirkcaldie, M. T. K. (2012). Neocortex. In *The Mouse Nervous System* (pp. 52–111). Elsevier Inc. https://doi.org/10.1016/B978-0-12-369497-3.10004-4

Kirwan, C. B., Bayley, P. J., Galván, V. V, & Squire, L. R. (2008). Detailed recollection of remote autobiographical memory after damage to the medial temporal lobe. *Proceedings of the National Academy of Sciences of the United States of America*, *105*(7), 2676–2680. https://doi.org/10.1073/pnas.0712155105

Knierim, J. J., Kudrimoti, H. S., & McNaughton, B. L. (1995). Place cells, head direction cells, and the learning of landmark stability. *The Journal of Neuroscience*, *15*(3 Pt 1), 1648–1659.

Ko, H., Cossell, L., Baragli, C., Antolik, J., Clopath, C., Hofer, S. B., & Mrsic-Flogel, T. D. (2013). The emergence of functional microcircuits in visual cortex. *Nature*, *496*(7443), 96–100. https://doi.org/10.1038/nature12015

Ko, H., Mrsic-Flogel, T. D., & Hofer, S. B. (2014). Emergence of feature-specific connectivity in cortical microcircuits in the absence of visual experience. *The Journal of Neuroscience*, *34*(29), 9812. https://doi.org/10.1523/JNEUROSCI.0875-14.2014

Kohn, A., Pinheiro, A., Tommerdahl, M. A., & Whitsel, B. L. (1997). Optical imaging in vitro provides evidence for the minicolumnar nature of cortical response. *Neuroreport*, *8*(16), 3513–3518. https://doi.org/10.1097/00001756-199711100-00019

Kok, P., Rahnev, D., Jehee, J. F. M., Lau, H. C., & De Lange, F. P. (2012). Attention reverses the effect of prediction in silencing sensory signals. *Cerebral Cortex*, *22*(9), 2197–2206. https://doi.org/10.1093/cercor/bhr310

Kondo, M., & Matsuzaki, M. (2021). Neuronal representations of reward-predicting cues and outcome history with movement in the frontal cortex. *Cell Reports*, *34*(5). https://doi.org/10.1016/j.celrep.2021.108704

Kondo, S., Yoshida, T., & Ohki, K. (2016). Mixed functional microarchitectures for orientation selectivity in the mouse primary visual cortex. *Nature Communications*, *7*. https://doi.org/10.1038/ncomms13210

Koopmans, F., Pandya, N. J., Franke, S. K., Phillippens, I. H. C. M. H., Paliukhovich, I., Li, K. W., & Smit, A. B. (2018). Comparative hippocampal synaptic proteomes of rodents and primates: differences in neuroplasticity-related proteins. *Frontiers in Molecular Neuroscience*, *11*, 364. https://doi.org/10.3389/fnmol.2018.00364

Kornack, D. R., & Rakic, P. (1995). Radial and horizontal deployment of clonally related cells in the primate neocortex: relationship to distinct mitotic lineages. *Neuron*, *15*(2), 311–321. https://doi.org/10.1016/0896-6273(95)90036-5

Koulakov, A. A., & Chklovskii, D. B. (2001). Orientation preference patterns in mammalian visual cortex: a wire length minimization approach. *Neuron*, *29*(2), 519–527. https://doi.org/https://doi.org/10.1016/S0896-6273(01)00223-9

Kraus, B. J., Robinson, R. J., White, J. A., Eichenbaum, H., & Hasselmo, M. E. (2013). Hippocampal "time cells": time versus path integration. *Neuron*, *78*(6), 1090–1101. https://doi.org/10.1016/j.neuron.2013.04.015

Kriegstein, A., Noctor, S., & Martínez-Cerdeño, V. (2006). Patterns of neural stem and progenitor cell division may underlie evolutionary cortical expansion. *Nature Reviews Neuroscience*, *7*(11), 883–890. https://doi.org/10.1038/nrn2008

Kudrimoti, H. S., Barnes, C. A., & McNaughton, B. L. (1999). Reactivation of hippocampal cell assemblies: effects of behavioral state, experience, and EEG dynamics. *The Journal of Neuroscience*, *19*(10), 4090–4101.

Kuramoto, E., Furuta, T., Nakamura, K. C., Unzai, T., Hioki, H., & Kaneko, T. (2009). Two types of thalamocortical projections from the motor thalamic nuclei of the rat: a single neuron-tracing study using viral vectors. *Cerebral Cortex*, *19*(9), 2065–2077. https://doi.org/10.1093/cercor/bhn231

Landry, P., & Deschênes, M. (1981). Intracortical arborizations and receptive fields of identified ventrobasal thalamocortical afferents to the primary somatic sensory cortex in the cat. *Journal of Comparative Neurology*, *199*(3), 345–371. https://doi.org/10.1002/cne.901990304

Landry, P., Diadori, P., Leclerc, S., & Dykes, R. W. (1987). Morphological and electrophysiological characteristics of somatosensory thalamocortical axons studied with intra-axonal staining and recording in the cat. *Experimental Brain Research*, *65*(2), 317–330. https://doi.org/10.1007/BF00236304

Lawrence, D. G., & Kuypers, H. G. J. M. (1968). The functional organization of the motor system in the monkey: I. The effects of bilateral pyramidal lesions. *Brain*, *91*(1), 1–14.

Lee, J. L. C. (2008). Memory reconsolidation mediates the strengthening of memories by additional learning. *Nature Neuroscience*, *11*(11), 1264–1266. https://doi.org/10.1038/nn.2205

Lee, S., Meyer, J. F., Park, J., & Smirnakis, S. M. (2017). Visually driven neuropil activity and information encoding in mouse primary visual cortex. *Frontiers in Neural Circuits*, *11*. https://doi.org/10.3389/fncir.2017.00050

Lein, E. S., Hawrylycz, M. J., Ao, N., Ayres, M., Bensinger, A., Bernard, A., Boe, A. F., Boguski, M. S., Brockway, K. S., Byrnes, E. J., Chen, L., Chen, L., Chen, T.-M., Chi Chin, M., Chong, J., Crook, B. E., Czaplinska, A., Dang, C. N., Datta, S., … Jones, A. R. (2007). Genome-wide atlas of gene expression in the adult mouse brain. *Nature*, *445*(7124), 168–176. https://doi.org/10.1038/nature05453

LeMessurier, A. M., Laboy-Juárez, K. J., McClain, K., Chen, S., Nguyen, T., & Feldman, D. E. (2019). Enrichment drives emergence of functional columns and improves sensory coding in the whisker map in L2/3 of mouse S1. *eLife*, *8*, e46321. https://doi.org/10.7554/eLife.46321

Letzkus, J. J., Wolff, S. B. E., Meyer, E. M. M., Tovote, P., Courtin, J., Herry, C., & Lüthi, A. (2011). A disinhibitory microcircuit for associative fear learning in the auditory cortex. *Nature*, *480*(7377), 331–335. https://doi.org/10.1038/nature10674

Leutgeb, S., Leutgeb, J. K., Barnes, C. A., Moser, E. I., McNaughton, B. L., & Moser, M.-B. (2005). Independent codes for spatial and episodic memory in hippocampal neuronal ensembles. *Science*, *309*(5734), 619–623. https://doi.org/10.1126/science.1114037

Leutgeb, S., Leutgeb, J. K., Treves, A., Moser, M.-B., & Moser, E. I. (2004). Distinct ensemble codes in hippocampal areas CA3 and CA1. *Science*, *305*(5688), 1295–1298. https://doi.org/10.1126/science.1100265

Lev, D. L., & White, E. L. (1997). Organization of pyramidal cell apical dendrites and composition of dendritic clusters in the mouse: emphasis on primary motor cortex. *The European Journal of Neuroscience*, *9*(2), 280–290. https://doi.org/10.1111/j.1460-9568.1997.tb01398.x

Levy, S. J., Kinsky, N. R., Mau, W., Sullivan, D. W., & Hasselmo, M. E. (2020). Hippocampal spatial memory representations in mice are heterogeneously stable. *Hippocampus*, *31*(3), 244–260. https://doi.org/10.1002/hipo.23272

Li, N., Daie, K., Svoboda, K., & Druckmann, S. (2016). Robust neuronal dynamics in premotor cortex during motor planning. *Nature*, *532*(7600), 459–464. https://doi.org/10.1038/nature17643

Li, Y., Lu, H., Cheng, P. L., Ge, S., Xu, H., Shi, S. H., & Dan, Y. (2012). Clonally related visual cortical neurons show similar stimulus feature selectivity. *Nature*, *486*(7401), 118–121. https://doi.org/10.1038/nature11110

Lisman, J., & Redish, A. D. (2009). Prediction, sequences and the hippocampus. *Philosophical Transactions of the Royal Society B: Biological Sciences*, *364*(1521), 1193–1201. https://doi.org/10.1098/rstb.2008.0316

Lisman, J., Yasuda, R., & Raghavachari, S. (2012). Mechanisms of CaMKII action in long-term potentiation. *Nature Reviews. Neuroscience*, *13*(3), 169–182. https://doi.org/10.1038/nrn3192

Liu, X., Ramirez, S., Pang, P. T., Puryear, C. B., Govindarajan, A., Deisseroth, K., & Tonegawa, S. (2012). Optogenetic stimulation of a hippocampal engram activates fear memory recall. *Nature*, *484*(7394), 381–385. https://doi.org/10.1038/nature11028

Loewenstein, Y., Kuras, A., & Rumpel, S. (2011). Multiplicative dynamics underlie the emergence of the log-normal distribution of spine sizes in the neocortex in vivo. *The Journal of Neuroscience*, *31*(26), 9481–9488. https://doi.org/10.1523/JNEUROSCI.6130-10.2011

Long, X., & Zhang, S.-J. (2021). A novel somatosensory spatial navigation system outside the hippocampal formation. *Cell Research*, *31*(6), 649–663. https://doi.org/10.1038/s41422-020-00448-8

Lorente de Nó, R. (1938). Architectonics and structure of the cerebral cortex. In J. F. Fulton (Ed.), *Physiology of the Nervous System* (pp. 291–330). Oxford University Press.

Lücke, J., & von der Malsburg, C. (2004). Rapid processing and unsupervised learning in a model of the cortical macrocolumn. *Neural Computation*, *16*(3), 501–533. https://doi.org/10.1162/089976604772744893

Ludvig, N. (1999). Place cells can flexibly terminate and develop their spatial firing. A new theory for their function. *Physiology & Behavior*, *67*(1), 57–67. https://doi.org/10.1016/s0031-9384(99)00048-7

Lundqvist, M., Rehn, M., Djurfeldt, M., & Lansner, A. (2006). Attractor dynamics in a modular network model of neocortex. *Network: Computation in Neural Systems*, *17*(3), 253–276. https://doi.org/10.1080/09548980600774619

Ma, L., Zablow, L., Kandel, E. R., & Siegelbaum, S. A. (1999). Cyclic AMP induces functional presynaptic boutons in hippocampal CA3-CA1 neuronal cultures. *Nature Neuroscience*, *2*(1), 24–30. https://doi.org/10.1038/4525

Ma, Y., Hu, H., Berrebi, A. S., Mathers, P. H., & Agmon, A. (2006). Distinct subtypes of somatostatin-containing neocortical interneurons revealed in transgenic mice. *The Journal of Neuroscience*, *26*(19), 5069–5082. https://doi.org/10.1523/JNEUROSCI.0661-06.2006

MacDonald, C. J., Lepage, K. Q., Eden, U. T., & Eichenbaum, H. (2011). Hippocampal "time cells" bridge the gap in memory for discontiguous events. *Neuron*, *71*(4), 737–749. https://doi.org/10.1016/j.neuron.2011.07.012

Maeda, H., Fukuda, S., Kameda, H., Murabe, N., Isoo, N., Mizukami, H., Ozawa, K., & Sakurai, M. (2016). Corticospinal axons make direct synaptic connections with spinal motoneurons innervating forearm muscles early during postnatal development in the rat. *The Journal of Physiology*, *594*(1), 189–205. https://doi.org/10.1113/JP270885

Maguire, E. A., Henson, R. N., Mummery, C. J., & Frith, C. D. (2001). Activity in prefrontal cortex, not hippocampus, varies parametrically with the increasing remoteness of memories. *Neuroreport*, *12*(3), 441–444. https://doi.org/10.1097/00001756-200103050-00004

Maguire, E. A., Nannery, R., & Spiers, H. J. (2006). Navigation around London by a taxi driver with bilateral hippocampal lesions. *Brain*, *129*, 2894–2907. https://doi.org/10.1093/brain/awl286

Makino, H., & Komiyama, T. (2015). Learning enhances the relative impact of top-down processing in the visual cortex. *Nature Neuroscience*, *18*(8), 1116–1122. https://doi.org/10.1038/nn.4061

Mankin, E. A., Sparks, F. T., Slayyeh, B., Sutherland, R. J., Leutgeb, S., & Leutgeb, J. K. (2012). Neuronal code for extended time in the hippocampus. *Proceedings of the National Academy of Sciences of the United States of America*, *109*(47), 19462–19467. https://doi.org/10.1073/pnas.1214107109

Manns, I. D., Sakmann, B., & Brecht, M. (2004). Sub- and suprathreshold receptive field properties of pyramidal neurones in layers 5A and 5B of rat somatosensory barrel cortex. *The Journal of Physiology*, *556*(Pt 2), 601–622. https://doi.org/10.1113/jphysiol.2003.053132

Manns, J. R., Howard, M. W., & Eichenbaum, H. (2007). Gradual changes in hippocampal activity support remembering the order of events. *Neuron*, *56*(3), 530–540. https://doi.org/10.1016/j.neuron.2007.08.017

Mao, D., Kandler, S., McNaughton, B. L., & Bonin, V. (2017). Sparse orthogonal population representation of spatial context in the retrosplenial cortex. *Nature Communications*, *8*(1). https://doi.org/10.1038/s41467-017-00180-9

Mao, D., Molina, L. A., Bonin, V., & McNaughton, B. L. (2020). Vision and locomotion combine to drive path integration sequences in mouse retrosplenial cortex. *Current Biology*, *30*(9), 1680–1688. https://doi.org/10.1016/j.cub.2020.02.070

Mao, D., Neumann, A. R., Sun, J., Bonin, V., Mohajerani, M. H., & McNaughton, B. L. (2018). Hippocampus-dependent emergence of spatial sequence coding in retrosplenial cortex. *Proceedings of the National Academy of Sciences of the United States of America*, *115*(31), 8015–8018. https://doi.org/10.1073/pnas.1803224115

Mao, T., Kusefoglu, D., Hooks, B. M., Huber, D., Petreanu, L., & Svoboda, K. (2011). Long-range neuronal circuits underlying the interaction between sensory and motor cortex. *Neuron*, *72*(1), 111–123. https://doi.org/10.1016/j.neuron.2011.07.029

Maren, S., Aharonov, G., & Fanselow, M. S. (1997). Neurotoxic lesions of the dorsal hippocampus and Pavlovian fear conditioning in rats. *Behavioural Brain Research*, *88*(2), 261–274. https://doi.org/10.1016/s0166-4328(97)00088-0

Markram, H., Muller, E., Ramaswamy, S., Reimann, M. W., Abdellah, M., Sanchez, C. A., Ailamaki, A., Alonso-Nanclares, L., Antille, N., Arsever, S., Kahou, G. A. A., Berger, T. K., Bilgili, A., Buncic, N., Chalimourda, A., Chindemi, G., Courcol, J.-D., Delalondre, F., Delattre, V., … Schürmann, F. (2015). Reconstruction and simulation of neocortical microcircuitry. *Cell*, *163*(2), 456–492. https://doi.org/https://doi.org/10.1016/j.cell.2015.09.029

Marks, T. D., & Goard, M. J. (2021). Stimulus-dependent representational drift in primary visual cortex. *Nature Communications*, *12*, 5169. https://doi.org/10.1038/s41467-021-25436-3

Marr, D. (1970). A theory for cerebral neocortex. *Proceedings of the Royal Society of London. Series B. Biological Sciences*, *176*(43), 161–234. https://doi.org/10.1098/rspb.1970.0040

Marr, D. (1971). Simple memory: a theory for archicortex. *Philosophical Transactions of the Royal Society of London. Series B, Biological Sciences*, *262*(841), 23–81. https://doi.org/10.1098/rstb.1971.0078

Martin, S. J., de Hoz, L., & Morris, R. G. M. (2005). Retrograde amnesia: neither partial nor complete hippocampal lesions in rats result in preferential sparing of remote spatial memory, even after reminding. *Neuropsychologia*, *43*(4), 609–624. https://doi.org/10.1016/j.neuropsychologia.2004.07.007

Maruoka, H., Kubota, K., Kurokawa, R., Tsuruno, S., & Hosoya, T. (2011). Periodic organization of a major subtype of pyramidal neurons in neocortical layer V. *The Journal of Neuroscience*, *31*(50), 18522–18542. https://doi.org/10.1523/JNEUROSCI.3117-11.2011

Maruoka, H., Nakagawa, N., Tsuruno, S., Sakai, S., Yoneda, T., & Hosoya, T. (2017). Lattice system of functionally distinct cell types in the neocortex. *Science*, *358*, 610–615. http://science.sciencemag.org/

Masurkar, A. V, Srinivas, K. V, Brann, D. H., Warren, R., Lowes, D. C., & Siegelbaum, S. A. (2017). Medial and lateral entorhinal cortex differentially excite deep versus superficial CA1 pyramidal neurons. *Cell Reports*, *18*(1), 148–160. https://doi.org/10.1016/j.celrep.2016.12.012

Matsuzaki, M., Honkura, N., Ellis-Davies, G. C. R., & Kasai, H. (2004). Structural basis of long-term potentiation in single dendritic spines. *Nature*, *429*(6993), 761–766. https://doi.org/10.1038/nature02617

Matus-Amat, P., Higgins, E. A., Barrientos, R. M., & Rudy, J. W. (2004). The role of the dorsal hippocampus in the acquisition and retrieval of context memory representations. *The Journal of Neuroscience*, *24*(10), 2431–2439. https://doi.org/10.1523/JNEUROSCI.1598-03.2004

Maurer, A. P., Cowen, S. L., Burke, S. N., Barnes, C. A., & McNaughton, B. L. (2006). Organization of hippocampal cell assemblies based on theta phase precession. *Hippocampus*, *16*(9), 785–794. https://doi.org/10.1002/hipo.20202

Maviel, T., Durkin, T. P., Menzaghi, F., & Bontempi, B. (2004). Sites of neocortical reorganization critical for remote spatial memory. *Science*, *305*(5680), 96–99. https://doi.org/10.1126/science.1098180

McClelland, J. L. (2013). Incorporating rapid neocortical learning of new schema-consistent information into complementary learning systems theory. *Journal of Experimental Psychology: General*, *142*(4), 1190–1210. https://doi.org/10.1037/a0033812

McClelland, J. L., McNaughton, B. L., & O'Reilly, R. C. (1995). Why there are complementary learning systems in the hippocampus and neocortex: insights from the successes and failures of connectionist models of learning and memory. *Psychological Review*, *102*(3), 419–457.

McIntyre, D. C., Kelly, M. E., & Staines, W. A. (1996). Efferent projections of the anterior perirhinal cortex in the rat. *Journal of Comparative Neurology*, *369*(2), 302–318.

McNaughton, B. L., Barnes, C. A., Gerrard, J. L., Gothard, K., Jung, M. W., Knierim, J. J., Kudrimoti, H., Qin, Y., Skaggs, W. E., Suster, M., & Weaver, K. L. (1996). Deciphering the hippocampal polyglot: the hippocampus as a path integration system. *The Journal of Experimental Biology*, *199*, 173–185.

McNaughton, B. L., Battaglia, F. P., Jensen, O., Moser, E. I., & Moser, M.-B. (2006). Path integration and the neural basis of the "cognitive map." *Nature Reviews Neuroscience*, *7*(8), 663–678. https://doi.org/10.1038/nrn1932

McNaughton, B. L., Leonard, B., & Chen, L. (1989). Cortical-hippocampal interactions and cognitive mapping: a hypothesis based on reintegration of the parietal and inferotemporal pathways for visual processing. *Psychobiology*, *17*(3), 230–235.

Mehta, M. R., Barnes, C. A., & McNaughton, B. L. (1997). Experience-dependent, asymmetric expansion of hippocampal place fields. *Proceedings of the National Academy of Sciences*, *94*(16), 8918–8921.

Merlin, S., Horng, S., Marotte, L. R., Sur, M., Sawatari, A., & Leamey, C. A. (2013). Deletion of Ten-m3 induces the formation of eye dominance domains in mouse visual cortex. *Cerebral Cortex*, *23*(4), 763–774. https://doi.org/10.1093/cercor/bhs030

Milczarek, M. M., Vann, S. D., & Sengpiel, F. (2018). Spatial memory engram in the mouse retrosplenial cortex. *Current Biology*, *28*(12), 1975–1980. https://doi.org/10.1016/j.cub.2018.05.002

Minerbi, A., Kahana, R., Goldfeld, L., Kaufman, M., Marom, S., & Ziv, N. E. (2009). Long-term relationships between synaptic tenacity, synaptic remodeling, and network activity. *PLOS Biology*, *7*(6), e1000136-. https://doi.org/10.1371/journal.pbio.1000136

Misanin, J. R., Miller, R. R., & Lewis, D. J. (1968). Retrograde amnesia produced by electroconvulsive shock after reactivation of a consolidated memory trace. *Science*, *160*(3827), 554–555. https://doi.org/10.1126/science.160.3827.554

Miyashita, T., & Rockland, K. S. (2007). GABAergic projections from the hippocampus to the retrosplenial cortex in the rat. *European Journal of Neuroscience*, *26*(5), 1193–1204. https://doi.org/10.1111/j.1460-9568.2007.05745.x

Mizuseki, K., & Buzsáki, G. (2013). Preconfigured, skewed distribution of firing rates in the hippocampus and entorhinal cortex. *Cell Reports*, *4*(5), 1010–1021. https://doi.org/10.1016/j.celrep.2013.07.039

Mizuseki, K., Diba, K., Pastalkova, E., & Buzsáki, G. (2011). Hippocampal CA1 pyramidal cells form functionally distinct sublayers. *Nature Neuroscience*, *14*(9), 1174–1181. https://doi.org/10.1038/nn.2894

Monaghan, D. T., & Cotman, C. W. (1985). Distribution of N-methyl-D-aspartate-sensitive L-[3H]glutamate-binding sites in rat brain. *The Journal of Neuroscience*, *5*(11), 2909–2919. https://doi.org/10.1523/JNEUROSCI.05-11-02909.1985

Moran, D. W., & Schwartz, A. B. (1999). Motor cortical representation of speed and direction during reaching. *Journal of Neurophysiology*, *82*(5), 2676–2692. https://doi.org/10.1152/jn.1999.82.5.2676

Moriyoshi, K., Masu, M., Ishii, T., Shigemoto, R., Mizuno, N., & Nakanishi, S. (1991). Molecular cloning and characterization of the rat NMDA receptor. *Nature*, *354*(6348), 31–37. https://doi.org/10.1038/354031a0

Morris, R. G., Garrud, P., Rawlins, J. N., & O'Keefe, J. (1982). Place navigation impaired in rats with hippocampal lesions. *Nature*, *297*(5868), 681–683. https://doi.org/10.1038/297681a0

Morris, R. G. M. (1981). Spatial localization does not require the presence of local cues. *Learning and Motivation*, *12*(2), 239–260. https://doi.org/https://doi.org/10.1016/0023-9690(81)90020-5

Morris, R. G. M., Anderson, E., Lynch, G. S., & Baudry, M. (1986). Selective impairment of learning and blockade of long-term potentiation by an N-methyl-D-aspartate receptor antagonist, AP5. *Nature*, *319*(6056), 774–776. https://doi.org/10.1038/319774a0

Morrow, M. M., Jordan, L. R., & Miller, L. E. (2007). Direct comparison of the task-dependent discharge of M1 in hand space and muscle space. *Journal of Neurophysiology*, *97*(2), 1786–1798.

Mountcastle, V. B. (1957). Modality and topographic properties of single neurons of cat's somatic sensory cortex. *Journal of Neurophysiology*, *20*(4), 408–434.

Mountcastle, V. B. (1997). The columnar organization of the neocortex. *Brain*, *120*, 701–722.

Mountcastle, V. B. (2003). Introduction. Computation in cortical columns. *Cerebral Cortex*, *13*(1), 2–4. https://doi.org/10.1093/cercor/13.1.2

Muller, R. U., & Kubie, J. L. (1987). The effects of changes in the environment on the spatial firing of hippocampal complex-spike cells. *The Journal of Neuroscience*, *7*(7), 1951–1988.

Mumby, D. G., Astur, R. S., Weisend, M. P., & Sutherland, R. J. (1999). Retrograde amnesia and selective damage to the hippocampal formation: memory for places and

object discriminations. *Behavioural Brain Research*, *106*(1–2), 97–107. https://doi.org/10.1016/s0166-4328(99)00097-2

Murayama, M., Pérez-Garci, E., Nevian, T., Bock, T., Senn, W., & Larkum, M. E. (2009). Dendritic encoding of sensory stimuli controlled by deep cortical interneurons. *Nature*, *457*(7233), 1137–1141. https://doi.org/10.1038/nature07663

Murray, E. A., Bussey, T. J., & Wise, S. P. (2000). Role of prefrontal cortex in a network for arbitrary visuomotor mapping. In W. X. Schneider, A. M. Owen, & J. Duncan (Eds.), *Executive Control and the Frontal Lobe: Current Issues* (pp. 114–129). Springer Berlin Heidelberg. https://doi.org/10.1007/978-3-642-59794-7_13

Murray, E. A., & Wise, S. P. (1996). Role of the hippocampus plus subjacent cortex but not amygdala in visuomotor conditional learning in Rhesus monkeys. *Behavioral Neuroscience*, *110*(6), 1261–1270. https://doi.org/10.1037/0735-7044.110.6.1261

Nadel, L., & Moscovitch, M. (1997). Memory consolidation, retrograde amnesia and the hippocampal complex. *Current Opinion in Neurobiology*, *7*(2), 217–227. https://doi.org/10.1016/s0959-4388(97)80010-4

Nadel, L., & Willner, J. (1980). Context and conditioning: A place for space. *Physiological Psychology*, *8*(2), 218–228. https://doi.org/10.3758/BF03332853

Nader, K., Schafe, G. E., & LeDoux, J. E. (2000a). Fear memories require protein synthesis in the amygdala for reconsolidation after retrieval. *Nature*, *406*(6797), 722–726. https://doi.org/10.1038/35021052

Nader, K., Schafe, G. E., & LeDoux, J. E. (2000b). The labile nature of consolidation theory. *Nature Reviews Neuroscience*, *1*(3), 216–219. https://doi.org/10.1038/35044580

Nauhaus, I., Nielsen, K. J., Disney, A. A., & Callaway, E. M. (2012). Orthogonal micro-organization of orientation and spatial frequency in primate primary visual cortex. *Nature Neuroscience*, *15*(12), 1683–1690. https://doi.org/10.1038/nn.3255

Navratilova, Z., Hoang, L. T., Schwindel, C. D., Tatsuno, M., & McNaughton, B. L. (2012). Experience-dependent firing rate remapping generates directional selectivity in hippocampal place cells. *Frontiers in Neural Circuits*, *6*, 6. https://doi.org/10.3389/fncir.2012.00006

Neafsey, E. J., Bold, E. L., Haas, G., Hurley-Gius, K. M., Quirk, G., Sievert, C. F., & Terreberry, R. R. (1986). The organization of the rat motor cortex: A microstimulation mapping study. *Brain Research Reviews*, *11*(1), 77–96. https://doi.org/10.1016/0165-0173(86)90011-1

Nelson, A. J. D., Hindley, E. L., Pearce, J. M., Vann, S. D., & Aggleton, J. P. (2015). The effect of retrosplenial cortex lesions in rats on incidental and active spatial learning. *Frontiers in Behavioral Neuroscience*, *9*, 11. https://doi.org/10.3389/fnbeh.2015.00011

Nguyen, P. V., Abel, T., & Kandel, E. R. (1994). Requirement of a critical period of transcription for induction of a late phase of LTP. *Science*, *265*(5175), 1104–1107. https://doi.org/10.1126/science.8066450

Nieuwenhuys, R. (1994). The neocortex. An overview of its evolutionary development, structural organization and synaptology. *Anatomy and Embryology*, *190*(4), 307–337. https://doi.org/10.1007/BF00187291

Nitz, D. (2009). Parietal cortex, navigation, and the construction of arbitrary reference frames for spatial information. *Neurobiology of Learning and Memory*, *91*(2), 179–185. https://doi.org/10.1016/j.nlm.2008.08.007

Niwa, M., Kamiya, A., Murai, R., Kubo, K., Gruber, A. J., Tomita, K., Lu, L., Tomisato, S., Jaaro-Peled, H., Seshadri, S., Hiyama, H., Huang, B., Kohda, K., Noda, Y., O'Donnell, P., Nakajima, K., Sawa, A., & Nabeshima, T. (2010). Knockdown of DISC1 by in utero gene transfer disturbs postnatal dopaminergic maturation in the frontal cortex and leads to adult behavioral deficits. *Neuron*, *65*(4), 480–489. https://doi.org/10.1016/j.neuron.2010.01.019

Noctor, S. C., Flint, A. C., Weissman, T. A., Dammerman, R. S., & Kriegstein, A. R. (2001). Neurons derived from radial glial cells establish radial units in neocortex. *Nature*, *409*(6821), 714–720. https://doi.org/10.1038/35055553

Noctor, S. C., Martínez-Cerdeño, V., Ivic, L., & Kriegstein, A. R. (2004). Cortical neurons arise in symmetric and asymmetric division zones and migrate through specific phases. *Nature Neuroscience*, *7*(2), 136–144. https://doi.org/10.1038/nn1172

Obermayer, J., Heistek, T. S., Kerkhofs, A., Goriounova, N. A., Kroon, T., Baayen, J. C., Idema, S., Testa-Silva, G., Couey, J. J., & Mansvelder, H. D. (2018). Lateral inhibition by Martinotti interneurons is facilitated by cholinergic inputs in human and mouse neocortex. *Nature Communications*, *9*(1), 4101. https://doi.org/10.1038/s41467-018-06628-w

O'Connor, D. H., Peron, S. P., Huber, D., & Svoboda, K. (2010). Neural activity in barrel cortex underlying vibrissa-based object localization in mice. *Neuron*, *67*(6), 1048–1061. https://doi.org/10.1016/j.neuron.2010.08.026

O'Donnell, C., Nolan, M. F., & van Rossum, M. C. W. (2011). Dendritic spine dynamics regulate the long-term stability of synaptic plasticity. *The Journal of Neuroscience*, *31*(45), 16142–16156. https://doi.org/10.1523/JNEUROSCI.2520-11.2011

Ohkawa, N., Saitoh, Y., Suzuki, A., Tsujimura, S., Murayama, E., Kosugi, S., Nishizono, H., Matsuo, M., Takahashi, Y., Nagase, M., Sugimura, Y. K., Watabe, A. M., Kato, F., & Inokuchi, K. (2015). Artificial association of pre-stored information to generate a qualitatively new memory. *Cell Reports*, *11*(2), 261–269. https://doi.org/10.1016/j.celrep.2015.03.017

Ohki, K., Chung, S., Ch'ng, Y. H., Kara, P., & Reid, R. C. (2005). Functional imaging with cellular resolution reveals precise micro-architecture in visual cortex. *Nature*, *433*(7026), 597–603. https://doi.org/10.1038/nature03274

Ohtsuki, G., Nishiyama, M., Yoshida, T., Murakami, T., Histed, M., Lois, C., & Ohki, K. (2012). Similarity of visual selectivity among clonally related neurons in visual cortex. *Neuron*, *75*(1), 65–72. https://doi.org/https://doi.org/10.1016/j.neuron.2012.05.023

Okada, S., Igata, H., Sasaki, T., & Ikegaya, Y. (2017). Spatial representation of hippocampal place cells in a T-maze with an aversive stimulation. *Frontiers in Neural Circuits*, *11*, 101. https://doi.org/10.3389/fncir.2017.00101

O'Kane, D., & Treves, A. (1992a). Short- and long-range connections in autoassociative memory. *Journal of Physics A: Mathematical and General*, *25*(19), 5055–5069. https://doi.org/10.1088/0305-4470/25/19/018

O'Kane, D., & Treves, A. (1992b). Why the simplest notion of neocortex as an autoassociative memory would not work. *Network: Computation in Neural Systems*, *3*(4), 379–384. https://doi.org/10.1088/0954-898X_3_4_002

O'Keefe, J. (1976). Place units in the hippocampus of the freely moving rat. *Experimental Neurology*, *51*(1), 78–109. https://doi.org/10.1016/0014-4886(76)90055-8

O'Keefe, J., & Dostrovsky, J. (1971). The hippocampus as a spatial map. Preliminary evidence from unit activity in the freely-moving rat. *Brain Research*, *34*(1), 171–175. https://doi.org/10.1016/0006-8993(71)90358-1

O'Keefe, J., & Nadel, L. (1978). *The hippocampus as a cognitive map*. Clarendon Press.

O'Keefe, J., & Speakman, A. (1987). Single unit activity in the rat hippocampus during a spatial memory task. *Experimental Brain Research*, *68*(1), 1–27. https://doi.org/10.1007/BF00255230

Olsen, G. M., Hovde, K., Kondo, H., Sakshaug, T., Sømme, H. H., Whitlock, J. R., & Witter, M. P. (2019). Organization of posterior parietal–frontal connections in the rat. *Frontiers in Systems Neuroscience*, *13*, 38. https://www.frontiersin.org/article/10.3389/fnsys.2019.00038

Olson, J. M., Li, J. K., Montgomery, S. E., & Nitz, D. A. (2020). Secondary motor cortex transforms spatial information into planned action during navigation. *Current Biology*, *30*(10), 1845-1854.e4. https://doi.org/https://doi.org/10.1016/j.cub.2020.03.016

Omlor, W., Wahl, A.-S., Sipilä, P., Lütcke, H., Laurenczy, B., Chen, I.-W., Sumanovski, L. T., van 't Hoff, M., Bethge, P., Voigt, F. F., Schwab, M. E., & Helmchen, F. (2019). Context-dependent limb movement encoding in neuronal populations of motor cortex. *Nature Communications*, *10*(1), 4812. https://doi.org/10.1038/s41467-019-12670-z

Onodera, K., & Kato, H. K. (2022). Translaminar recurrence from layer 5 suppresses superficial cortical layers. *Nature Communications*, *13*(1), 2585. https://doi.org/10.1038/s41467-022-30349-w

O'Rourke, N. A., Sullivan, D. P., Kaznowski, C. E., Jacobs, A. A., & McConnell, S. K. (1995). Tangential migration of neurons in the developing cerebral cortex. *Development*, *121*(7), 2165–2176.

Ouzounov, D. G., Wang, T., Wang, M., Feng, D. D., Horton, N. G., Cruz-Hernández, J. C., Cheng, Y.-T., Reimer, J., Tolias, A. S., Nishimura, N., & Xu, C. (2017). In vivo three-photon imaging of activity of GCaMP6-labeled neurons deep in intact mouse brain. *Nature Methods*, *14*(4), 388–390. https://doi.org/10.1038/nmeth.4183

Pachitariu, M., Stringer, C., Dipoppa, M., Schröder, S., Rossi, L. F., Dalgleish, H., Carandini, M., & Harris, K. (2016). Suite2p: beyond 10,000 neurons with standard two-photon microscopy. *BioRxiv*, 061507. https://doi.org/10.1101/061507

Packard, M. G., & McGaugh, J. L. (1996). Inactivation of hippocampus or caudate nucleus with lidocaine differentially affects expression of place and response learning. *Neurobiology of Learning and Memory*, *65*(1), 65–72. https://doi.org/10.1006/nlme.1996.0007

Passingham, R. E., Myers, C., Rawlins, N., Lightfoot, V., & Fearn, S. (1988). Premotor cortex in the rat. *Behavioral Neuroscience*, *102*(1), 101–109. https://doi.org/10.1037//0735-7044.102.1.101

Pastalkova, E., Itskov, V., Amarasingham, A., & Buzsáki, G. (2008). Internally generated cell assembly sequences in the rat hippocampus. *Science*, *321*(5894), 1322–1327. https://doi.org/10.1126/science.1159775

Pavlides, C., Miyashita, E., & Asanuma, H. (1993). Projection from the sensory to the motor cortex is important in learning motor skills in the monkey. *Journal of Neurophysiology*, *70*(2), 733–741. https://doi.org/10.1152/jn.1993.70.2.733

Paxinos, G., & Franklin, K. B. J. (2001). *The mouse brain in stereotaxic coordinates* (2nd ed.). Academic Press. https://books.google.ca/books?id=8RJZLwEACAAJ

Penfield, W., & Milner, B. (1958). Memory deficit produced by bilateral lesions in the hippocampal zone. *American Medical Association Archives of Neurology and Psychiatry*, *79*(5), 475–497. https://doi.org/10.1001/archneurpsyc.1958.02340050003001

Pereira, A., Ribeiro, S., Wiest, M., Moore, L. C., Pantoja, J., Lin, S.-C., & Nicolelis, M. A. L. (2007). Processing of tactile information by the hippocampus. *Proceedings of the National Academy of Sciences*, *104*(46), 18286–18291. www.pnas.orgcgidoi10.1073pnas.0708611104

Peters, A., & Sethares, C. (1996). Myelinated axons and the pyramidal cell modules in monkey primary visual cortex. *Journal of Comparative Neurology*, *365*(2), 232–255.

Petersen, C. C. H., & Crochet, S. (2013). Synaptic computation and sensory processing in neocortical layer 2/3. *Neuron*, *78*(1), 28–48. https://doi.org/10.1016/j.neuron.2013.03.020

Petreanu, L., Gutnisky, D. A., Huber, D., Xu, N., O'Connor, D. H., Tian, L., Looger, L., & Svoboda, K. (2012). Activity in motor–sensory projections reveals distributed coding in somatosensation. *Nature*, *489*(7415), 299–303. https://doi.org/10.1038/nature11321

Petreanu, L., Mao, T., Sternson, S., & Svoboda, K. (2009). The subcellular organization of neocortical excitatory connections. *Nature*, *457*(7233), 1142–1145. www.nature.com/nature.

Peyrache, A., Khamassi, M., Benchenane, K., Wiener, S. I., & Battaglia, F. P. (2009). Replay of rule-learning related neural patterns in the prefrontal cortex during sleep. *Nature Neuroscience*, *12*(7), 919–926. https://doi.org/10.1038/nn.2337

Pfeiffer, B. E., & Foster, D. J. (2013). Hippocampal place-cell sequences depict future paths to remembered goals. *Nature*, *497*(7447), 74–79. https://doi.org/10.1038/nature12112

Pignatelli, M., Ryan, T. J., Roy, D. S., Lovett, C., Smith, L. M., Muralidhar, S., & Tonegawa, S. (2019). Engram cell excitability state determines the efficacy of memory retrieval. *Neuron*, *101*(2), 274-284.e5. https://doi.org/10.1016/j.neuron.2018.11.029

Pluta, S., Naka, A., Veit, J., Telian, G., Yao, L., Hakim, R., Taylor, D., & Adesnik, H. (2015). A direct translaminar inhibitory circuit tunes cortical output. *Nature Neuroscience*, *18*(11), 1631–1640. https://doi.org/10.1038/nn.4123

Pluta, S. R., Telian, G. I., Naka, A., & Adesnik, H. (2019). Superficial layers suppress the deep layers to fine-tune cortical coding. *The Journal of Neuroscience*, *39*(11), 2052. https://doi.org/10.1523/JNEUROSCI.1459-18.2018

Pnevmatikakis, E. A., Soudry, D., Gao, Y., Machado, T. A., Merel, J., Pfau, D., Reardon, T., Mu, Y., Lacefield, C., Yang, W., Ahrens, M., Bruno, R., Jessell, T. M., Peterka, D. S., Yuste, R., & Paninski, L. (2016). Simultaneous denoising, deconvolution, and demixing of calcium imaging data. *Neuron*, *89*(2), 285–299. https://doi.org/10.1016/j.neuron.2015.11.037

Poorthuis, R. B., Enke, L., & Letzkus, J. J. (2014). Cholinergic circuit modulation through differential recruitment of neocortical interneuron types during behaviour. *The Journal of Physiology*, *592*(19), 4155–4164. https://doi.org/https://doi.org/10.1113/jphysiol.2014.273862

Powell, T. P., & Mountcastle, V. B. (1959). Some aspects of the functional organization of the cortex of the postcentral gyrus of the monkey: a correlation of findings obtained in a single unit analysis with cytoarchitecture. *Bulletin of the Johns Hopkins Hospital*, *105*, 133–162.

Pronichev, I. V, & Lenkov, D. N. (1998). Functional mapping of the motor cortex of the white mouse by a microstimulation method. *Neuroscience and Behavioral Physiology*, *28*(1), 80–85. https://doi.org/10.1007/BF02461916

Prusky, G. T., West, P. W. R., & Douglas, R. M. (2000). Behavioral assessment of visual acuity in mice and rats. *Vision Research*, *40*(16), 2201–2209. https://doi.org/https://doi.org/10.1016/S0042-6989(00)00081-X

Purves, D., Riddle, D. R., & LaMantia, A. S. (1992). Iterated patterns of brain circuitry (or how the cortex gets its spots). *Trends in Neurosciences*, *15*(10), 362–368. https://doi.org/10.1016/0166-2236(92)90180-g

Qin, Y.-L., McNaughton, B. L., Skaggs, W. E., & Barnes, C. A. (1997). Memory reprocessing in corticocortical and hippocampocortical neuronal ensembles. *Philosophical Transactions of the Royal Society of London B*, *352*, 1525–1533.

Quirk, G. J., Muller, R. U., & Kubie, J. L. (1990). The firing of hippocampal place cells in the dark depends on the rat's recent experience. *The Journal of Neuroscience*, *7*(6), 2008–2017.

Race, E., Keane, M. M., & Verfaellie, M. (2011). Medial temporal lobe damage causes deficits in episodic memory and episodic future thinking not attributable to deficits in narrative construction. *Journal of Neuroscience*, *31*(28), 10262–10269. https://doi.org/10.1523/JNEUROSCI.1145-11.2011

Rakic, P. (1978). Neuronal migration and contact guidance in the primate telencephalon. *Postgraduate Medical Journal*, *54*, 25–40.

Rakic, P. (1988). Specification of cerebral cortical areas. *Science*, *241*(4862), 170–176. https://doi.org/10.1126/science.3291116

Rakic, P. (1995). A small step for the cell, a giant leap for mankind: a hypothesis of neocortical expansion during evolution. *Trends in Neurosciences*, *18*(9), 383–388. https://doi.org/https://doi.org/10.1016/0166-2236(95)93934-P

Rakic, P. (2003). Elusive radial glial cells: historical and evolutionary perspective. *Glia*, *43*(1), 19–32. https://doi.org/10.1002/glia.10244

Rakic, P. (2007). The radial edifice of cortical architecture: from neuronal silhouettes to genetic engineering. *Brain Research Reviews*, *55*(2), 204–219. https://doi.org/10.1016/j.brainresrev.2007.02.010

Rakic, P. (2009). Evolution of the neocortex: a perspective from developmental biology. *Nature Reviews Neuroscience*, *10*(10), 724–735. https://doi.org/10.1038/nrn2719

Ramirez, S., Liu, X., Lin, P.-A., Suh, J., Pignatelli, M., Redondo, R. L., Ryan, T. J., & Tonegawa, S. (2013). Creating a false memory in the hippocampus. *Science*, *341*(6144), 387–391. https://doi.org/10.1126/science.1239073

Rao, R. P. N., & Ballard, D. H. (1999). Predictive coding in the visual cortex: a functional interpretation of some extra-classical receptive-field effects. *Nature Neuroscience*, *2*(1), 79–87.

Rashid, A. J., Yan, C., Mercaldo, V., Hsiang, H.-L. L., Park, S., Cole, C. J., De Cristofaro, A., Yu, J., Ramakrishnan, C., Lee, S. Y., Deisseroth, K., Frankland, P. W., & Josselyn, S. A. (2016). Competition between engrams influences fear memory formation and recall. *Science*, *353*(6297), 383–387. https://doi.org/10.1126/science.aaf0594

Rausell, E., & Jones, E. G. (1995). Extent of intracortical arborization of thalamocortical axons as a determinant of representational plasticity in monkey somatic sensory cortex. *Journal of Neuroscience*, *15*(6), 4270–4288.

Reep, R. L., & Corwin, J. V. (1999). Topographic organization of the striatal and thalamic connections of rat medial agranular cortex. *Brain Research*, *841*(1–2), 43–52. https://doi.org/10.1016/s0006-8993(99)01779-5

Reep, R. L., Corwin, J. V, Hashimoto, A., & Watson, R. T. (1987). Efferent connections of the rostral portion of medial agranular cortex in rats. *Brain Research Bulletin*, *19*(2), 203–221. https://doi.org/10.1016/0361-9230(87)90086-4

Reep, R. L., Goodwin, G. S., & Corwin, J. V. (1990). Topographic organization in the corticocortical connections of medial agranular cortex in rats. *The Journal of Comparative Neurology*, *294*(2), 262–280. https://doi.org/10.1002/cne.902940210

Reid, C. B., Liang, I., & Walsh, C. (1995). Systematic widespread clonal organization in cerebral cortex. *Neuron*, *15*, 299–310.

Reijmers, L. G., Perkins, B. L., Matsuo, N., & Mayford, M. (2007). Localization of a stable neural correlate of associative memory. *Science*, *317*(5842), 1230–1233. https://doi.org/10.1126/science.1143839

Rich, P. D., Liaw, H.-P., & Lee, A. K. (2014). Large environments reveal the statistical structure governing hippocampal representations. *Science*, *345*(6198), 814–817. https://doi.org/10.1126/science.1255635

Richter, D., Ekman, M., & de Lange, F. P. (2018). Suppressed sensory response to predictable object stimuli throughout the ventral visual stream. *The Journal of Neuroscience*, *38*(34), 7452. https://doi.org/10.1523/JNEUROSCI.3421-17.2018

Ringach, D. L., Mineault, P. J., Tring, E., Olivas, N. D., Garcia-Junco-Clemente, P., & Trachtenberg, J. T. (2016). Spatial clustering of tuning in mouse primary visual cortex. *Nature Communications*, *7*(1), 12270. https://doi.org/10.1038/ncomms12270

Rinkus, G. J. (2010). A cortical sparse distributed coding model linking mini- and macrocolumn-scale functionality. *Frontiers in Neuroanatomy*, *4*, 1–13. https://doi.org/10.3389/fnana.2010.00017

Robinson, N. T. M., Descamps, L. A. L., Russell, L. E., Buchholz, M. O., Bicknell, B. A., Antonov, G. K., Lau, J. Y. N., Nutbrown, R., Schmidt-Hieber, C., & Häusser, M. (2020). Targeted activation of hippocampal place cells drives memory-guided spatial behavior. *Cell*, *183*(6), 1586-1599.e10. https://doi.org/https://doi.org/10.1016/j.cell.2020.09.061

Rokni, U., Richardson, A. G., Bizzi, E., & Seung, H. S. (2007). Motor learning with unstable neural representations. *Neuron*, *54*(4), 653–666. https://doi.org/https://doi.org/10.1016/j.neuron.2007.04.030

Rolls, E. T. (2013). The mechanisms for pattern completion and pattern separation in the hippocampus. *Frontiers in Systems Neuroscience*, *7*, 74. https://doi.org/10.3389/fnsys.2013.00074

Rolls, E. T. (2016). *Cerebral cortex: principles of operation*. Oxford University Press.

Rolls, E. T., & Treves, A. (1998). *Neural networks and brain function.* Oxford University Press.

Rosenbaum, R. S., Köhler, S., Schacter, D. L., Moscovitch, M., Westmacott, R., Black, S. E., Gao, F., & Tulving, E. (2005). The case of K.C.: contributions of a memory-impaired person to memory theory. *Neuropsychologia*, *43*(7), 989–1021. https://doi.org/10.1016/j.neuropsychologia.2004.10.007

Ross, R. S., & Eichenbaum, H. (2006). Dynamics of hippocampal and cortical activation during consolidation of a nonspatial memory. *The Journal of Neuroscience*, *26*(18), 4852–4859. https://doi.org/10.1523/JNEUROSCI.0659-06.2006

Rothschild, G., Eban, E., & Frank, L. M. (2017). A cortical-hippocampal-cortical loop of information processing during memory consolidation. *Nature Neuroscience*, *20*(2), 251–259. https://doi.org/10.1038/nn.4457

Rothschild, G., Nelken, I., & Mizrahi, A. (2010). Functional organization and population dynamics in the mouse primary auditory cortex. *Nature Neuroscience*, *13*(3), 353–360. https://doi.org/10.1038/nn.2484

Rousseeuw, P. J. (1987). Silhouettes: a graphical aid to the interpretation and validation of cluster analysis. *Journal of Computational and Applied Mathematics*, *20*, 53–65. https://doi.org/https://doi.org/10.1016/0377-0427(87)90125-7

Rubin, A., Geva, N., Sheintuch, L., & Ziv, Y. (2015). Hippocampal ensemble dynamics timestamp events in long-term memory. *eLife*, *4*, e12247. https://doi.org/10.7554/eLife.12247.001

Ryan, L., Nadel, L., Keil, K., Putnam, K., Schnyer, D., Trouard, T., & Moscovitch, M. (2001). Hippocampal complex and retrieval of recent and very remote autobiographical memories: evidence from functional magnetic resonance imaging in neurologically intact people. *Hippocampus*, *11*(6), 707–714. https://doi.org/10.1002/hipo.1086

Sakata, S., & Harris, K. D. (2009). Laminar structure of spontaneous and sensory-evoked population activity in auditory cortex. *Neuron*, *64*(3), 404–418. https://doi.org/10.1016/j.neuron.2009.09.020

Saleem, A. B., Diamanti, E. M., Fournier, J., Harris, K. D., & Carandini, M. (2018). Coherent encoding of subjective spatial position in visual cortex and hippocampus. *Nature*, *562*(7725), 124–127. https://doi.org/10.1038/s41586-018-0516-1

Saleh, M., Takahashi, K., & Hatsopoulos, N. G. (2012). Encoding of coordinated reach and grasp trajectories in primary motor cortex. *The Journal of Neuroscience*, *32*(4), 1220. https://doi.org/10.1523/JNEUROSCI.2438-11.2012

Sara, S. J. (2000). Retrieval and reconsolidation: toward a neurobiology of remembering. *Learning & Memory*, *7*(2), 73–84. https://doi.org/10.1101/lm.7.2.73

Sato, M., Mizuta, K., Islam, T., Kawano, M., Sekine, Y., Takekawa, T., Gomez-Dominguez, D., Schmidt, A., Wolf, F., Kim, K., Yamakawa, H., Ohkura, M., Lee, M. G., Fukai, T., Nakai, J., & Hayashi, Y. (2020). Distinct mechanisms of over-representation of landmarks and rewards in the hippocampus. *Cell Reports*, *32*(1), 107864. https://doi.org/10.1016/j.celrep.2020.107864

Sato, T. R., Gray, N. W., Mainen, Z. F., & Svoboda, K. (2007). The functional microarchitecture of the mouse barrel cortex. *PLOS Biology*, *5*(7), e189-. https://doi.org/10.1371/journal.pbio.0050189

Save, E., Cressant, A., Thinus-Blanc, C., & Poucet, B. (1998). Spatial firing of hippocampal place cells in blind rats. *The Journal of Neuroscience*, *18*(5), 1818–1826.

Schmitzer-Torbert, N. (2007). Place and response learning in human virtual navigation: Behavioral measures and gender differences. *Behavioral Neuroscience*, *121*(2), 277–290. https://doi.org/10.1037/0735-7044.121.2.277

Schnepel, P., Kumar, A., Zohar, M., Aertsen, A., & Boucsein, C. (2015). Physiology and impact of horizontal connections in rat neocortex. *Cerebral Cortex*, *25*(10), 3818–3835. https://doi.org/10.1093/cercor/bhu265

Schoonover, C. E., Ohashi, S. N., Axel, R., & Fink, A. J. P. (2021). Representational drift in primary olfactory cortex. *Nature*, *594*(7864), 541–546. https://doi.org/10.1038/s41586-021-03628-7

Schubert, D., Staiger, J. F., Cho, N., Kötter, R., Zilles, K., & Luhmann, H. J. (2001). Layer-specific intracolumnar and transcolumnar functional connectivity of layer V

pyramidal cells in rat barrel cortex. *The Journal of Neuroscience*, *21*(10), 3580–3592.

Schwindel, C. D., & McNaughton, B. L. (2011). Hippocampal–cortical interactions and the dynamics of memory trace reactivation. In E. J. W. Van Someren, Y. D. Van Der Werf, P. R. Roelfsema, H. D. Mansvelder, & F. H. Lopes Da Silva (Eds.), *Slow Brain Oscillations of Sleep, Resting State and Vigilance* (Vol. 193, pp. 163–177). Elsevier. https://doi.org/https://doi.org/10.1016/B978-0-444-53839-0.00011-9

Scoville, W. B., & Milner, B. (1957). Loss of recent memory after bilateral hippocampal lesions. *Journal of Neurology, Neurosurgery, & Psychiatry*, *20*, 11–21. https://doi.org/https://doi.org/10.1136/jnnp.20.1.11

Seamans, J. K., & Yang, C. R. (2004). The principal features and mechanisms of dopamine modulation in the prefrontal cortex. *Progress in Neurobiology*, *74*(1), 1–58. https://doi.org/10.1016/j.pneurobio.2004.05.006

Semon, R. W. (1921). *The mneme*. George Allen & Unwin Ltd.

Senzai, Y., Fernandez-Ruiz, A., & Buzsáki, G. (2019). Layer-specific physiological features and interlaminar interactions in the primary visual cortex of the mouse. *Neuron*, *101*(3), 500-513.e5. https://doi.org/10.1016/j.neuron.2018.12.009

Sermet, B. S., Truschow, P., Feyerabend, M., Mayrhofer, J. M., Oram, T. B., Yizhar, O., Staiger, J. F., & Petersen, C. C. H. (2019). Pathway-, layer- and cell-type-specific thalamic input to mouse barrel cortex. *eLife*, *8*, e52665. https://doi.org/10.7554/eLife.52665

Shamma, S. A., Fleshman, J. W., Wiser, P. R., & Versnel, H. (1993). Organization of response areas in ferret primary auditory cortex. *Journal of Neurophysiology*, *69*(2), 367–383. https://doi.org/10.1152/jn.1993.69.2.367

Shatz, C. J. (1992). The developing brain. *Scientific American*, *267*(3), 60–67. https://doi.org/10.1038/scientificamerican0992-60

Shepherd, G. M., & Rowe, T. B. (2017). Neocortical lamination: insights from neuron types and evolutionary precursors. *Frontiers in Neuroanatomy*, *11*, 100. https://doi.org/10.3389/fnana.2017.00100

Shi, S. H., Hayashi, Y., Petralia, R. S., Zaman, S. H., Wenthold, R. J., Svoboda, K., & Malinow, R. (1999). Rapid spine delivery and redistribution of AMPA receptors after synaptic NMDA receptor activation. *Science*, *284*(5421), 1811–1816. https://doi.org/10.1126/science.284.5421.1811

Shibata, H. (1993). Efferent projections from the anterior thalamic nuclei to the cingulate cortex in the rat. *The Journal of Comparative Neurology*, *330*(4), 533–542. https://doi.org/10.1002/cne.903300409

Shibata, H., Honda, Y., Sasaki, H., & Naito, J. (2009). Organization of intrinsic connections of the retrosplenial cortex in the rat. *Anatomical Science International*, *84*(4), 280–292. https://doi.org/10.1007/s12565-009-0035-0

Silberberg, G., & Markram, H. (2007). Disynaptic inhibition between neocortical pyramidal cells mediated by Martinotti cells. *Neuron*, *53*(5), 735–746. https://doi.org/https://doi.org/10.1016/j.neuron.2007.02.012

Silva, A. J. (2007). Consolidation: molecular restlessness. In H. L. Roediger, Y. Dudai, & S. M. Fitzpatrick (Eds.), *Science of Memory Concepts* (pp. 167–170).

Siniscalchi, M. J., Phoumthipphavong, V., Ali, F., Lozano, M., & Kwan, A. C. (2016). Fast and slow transitions in frontal ensemble activity during flexible sensorimotor behavior. *Nature Neuroscience*, *19*(9), 1234–1242. https://doi.org/10.1038/nn.4342

Skaggs, W. E., & McNaughton, B. L. (1996). Replay of neuronal firing sequences in rat hippocampus during sleep following spatial experience. *Science*, *271*(5257), 1870–1873. https://doi.org/10.1126/science.271.5257.1870

Skaggs, W. E., McNaughton, B. L., Gothard, K. M., & Markus, E. J. (1993). An information-theoretic approach to deciphering the hippocampal code. In S. J. Hanson, J. D. Cowan, & C. L. Giles (Eds.), *Advances in Neural Information Processing Systems 5* (pp. 1030–1037). Morgan-Kaufmann.

Skaggs, W. E., McNaughton, B. L., Wilson, M. A., & Barnes, C. A. (1996). Theta phase precession in hippocampal neuronal populations and the compression of temporal sequences. *Hippocampus*, *6*(2), 149–172.

Skoglund, T. S., Pascher, R., & Berthold, C. H. (1997). The existence of a layer IV in the rat motor cortex. *Cerebral Cortex*, *7*(2), 178–180. https://doi.org/10.1093/cercor/7.2.178

Smith, C. N., & Squire, L. R. (2009). Medial temporal lobe activity during retrieval of semantic memory is related to the age of the memory. *The Journal of Neuroscience*, *29*(4), 930. https://doi.org/10.1523/JNEUROSCI.4545-08.2009

Smith, D. M., Barredo, J., & Mizumori, S. J. Y. (2012). Complimentary roles of the hippocampus and retrosplenial cortex in behavioral context discrimination. *Hippocampus*, *22*(5), 1121–1133. https://doi.org/10.1002/hipo.20958

Sparks, F. T., Lehmann, H., Hernandez, K., & Sutherland, R. J. (2011). Suppression of neurotoxic lesion-induced seizure activity: evidence for a permanent role for the hippocampus in contextual memory. *PloS ONE*, *6*(11), e27426. https://doi.org/10.1371/journal.pone.0027426

Squire, L. R., & Alvarez, P. (1995). Retrograde amnesia and memory consolidation: a neurobiological perspective. *Current Opinion in Neurobiology*, *5*(2), 169–177. https://doi.org/https://doi.org/10.1016/0959-4388(95)80023-9

Srinivasan, M. V., Laughlin, S. B., & Dubs, A. (1982). Predictive coding: a fresh view of inhibition in the retina. *Proceedings of the Royal Society of London. Series B. Biological Sciences*, *216*(1205), 427–459.

Steinvorth, S., Levine, B., & Corkin, S. (2005). Medial temporal lobe structures are needed to re-experience remote autobiographical memories: evidence from H.M. and W.R. *Neuropsychologia*, *43*(4), 479–496. https://doi.org/10.1016/j.neuropsychologia.2005.01.001

Steward, O. (1976). Topographic organization of the projections from the entorhinal area to the hippocampal formation of the rat. *The Journal of Comparative Neurology*, *167*(3), 285–314. https://doi.org/10.1002/cne.901670303

Stuesse, S. L., & Newman, D. B. (1990). Projections from the medial agranular cortex to brain stem visuomotor centers in rats. *Experimental Brain Research*, *80*(3), 532–544. https://doi.org/10.1007/BF00227994

Sugar, J., Witter, M. P., van Strien, N. M., & Cappaert, N. L. M. (2011). The retrosplenial cortex: intrinsic connectivity and connections with the (para)hippocampal region in the rat. An interactive connectome. *Frontiers in Neuroinformatics*, *5*, 7. https://doi.org/10.3389/fninf.2011.00007

Sugimoto, S., Sakurada, M., Horikawa, J., & Taniguchi, I. (1997). The columnar and layer-specific response properties of neurons in the primary auditory cortex of Mongolian gerbils. *Hearing Research*, *112*(1–2), 175–185. https://doi.org/10.1016/s0378-5955(97)00119-6

Sul, J. H., Jo, S., Lee, D., & Jung, M. W. (2011). Role of rodent secondary motor cortex in value-based action selection. *Nature Neuroscience*, *14*(9), 1202–1208. https://doi.org/10.1038/nn.2881

Summerfield, C., Trittschuh, E. H., Monti, J. M., Mesulam, M.-M., & Egner, T. (2008). Neural repetition suppression reflects fulfilled perceptual expectations. *Nature Neuroscience*, *11*(9), 1004–1006. https://doi.org/10.1038/nn.2163

Sun, Y., Jin, S., Lin, X., Chen, L., Qiao, X., Jiang, L., Zhou, P., Johnston, K. G., Golshani, P., Nie, Q., Holmes, T. C., Nitz, D. A., & Xu, X. (2019). CA1-projecting subiculum neurons facilitate object–place learning. *Nature Neuroscience*, *22*(11), 1857–1870. https://doi.org/10.1038/s41593-019-0496-y

Suter, B. A., & Shepherd, G. M. G. (2015). Reciprocal interareal connections to corticospinal neurons in mouse M1 and S2. *The Journal of Neuroscience*, *35*(7), 2959–2974. https://doi.org/10.1523/JNEUROSCI.4287-14.2015

Sutherland, R. J., Weisend, M. P., Mumby, D., Astur, R. S., Hanlon, F. M., Koerner, A., Thomas, M. J., Wu, Y., Moses, S. N., Cole, C., Hamilton, D. A., & Hoesing, J. M. (2001). Retrograde amnesia after hippocampal damage: recent vs. remote memories in two tasks. *Hippocampus*, *11*(1), 27–42. https://doi.org/10.1002/1098-1063(2001)11:1<27::AID-HIPO1017>3.0.CO;2-4

Sutherland, R. J., Whishaw, I. Q., & Kolb, B. (1988). Contributions of cingulate cortex to two forms of spatial learning and memory. *The Journal of Neuroscience*, *8*(6), 1863–1872.

Swanson, L. W., & Köhler, C. (1986). Anatomical evidence for direct projections from the entorhinal area to the entire cortical mantle in the rat. *The Journal of Neuroscience*, *6*(10), 3010–3023.

Swindale, N. V. (1990). Is the cerebral cortex modular? *Trends in Neurosciences*, *13*(12), 487–492. https://doi.org/10.1016/0166-2236(90)90082-l

Takehara-Nishiuchi, K., Insel, N., Hoang, L. T., Wagner, Z., Olson, K., Chawla, M. K., Burke, S. N., & Barnes, C. A. (2013). Activation patterns in superficial layers of neocortex change between experiences independent of behavior, environment, or the hippocampus. *Cerebral Cortex*, *23*(9), 2225–2234. https://doi.org/10.1093/cercor/bhs209

Takehara-Nishiuchi, K., & McNaughton, B. L. (2008). Spontaneous changes of neocortical code for associative memory during consolidation. *Science*, *322*(5903), 960–963. https://doi.org/10.1126/science.1161299

Tamamaki, N., & Nojyo, Y. (1995). Preservation of topography in the connections between the subiculum, field CA1, and the entorhinal cortex in rats. *The Journal of Comparative Neurology*, *353*(3), 379–390. https://doi.org/10.1002/cne.903530306

Tan, S. S., & Breen, S. (1993). Radial mosaicism and tangential cell dispersion both contribute to mouse neocortical development. *Nature*, *362*(6421), 638–640. https://doi.org/10.1038/362638a0

Tanaka, K. Z., He, H., Tomar, A., Niisato, K., Y Huang, A. J., & McHugh, T. J. (2018). The hippocampal engram maps experience but not place. *Science*, *361*, 392–397. http://science.sciencemag.org/

Tanaka, K. Z., Pevzner, A., Hamidi, A. B., Nakazawa, Y., Graham, J., & Wiltgen, B. J. (2014). Cortical representations are reinstated by the hippocampus during memory retrieval. *Neuron*, *84*(2), 347–354. https://doi.org/10.1016/j.neuron.2014.09.037

Tanila, H., Shapiro, M. L., & Eichenbaum, H. (1997). Discordance of spatial representation in ensembles of hippocampal place cells. *Hippocampus*, *7*(6), 613–623. https://doi.org/10.1002/(SICI)1098-1063(1997)7:6<613::AID-HIPO4>3.0.CO;2-F

Tanji, J., & Evarts, E. V. (1976). Anticipatory activity of motor cortex neurons in relation to direction of an intended movement. *Journal of Neurophysiology*, *39*(5), 1062–1068. https://doi.org/10.1152/jn.1976.39.5.1062

Tayler, K. K., Tanaka, K. Z., Reijmers, L. G., & Wiltgen, B. J. (2013). Reactivation of neural ensembles during the retrieval of recent and remote memory. *Current Biology*, *23*(2), 99–106. https://doi.org/10.1016/j.cub.2012.11.019

Teng, E., & Squire, L. R. (1999). Memory for places learned long ago is intact after hippocampal damage. *Nature*, *400*(6745), 675–677. https://doi.org/10.1038/23276

Tennant, K. A., Adkins, D. L., Donlan, N. A., Asay, A. L., Thomas, N., Kleim, J. A., & Jones, T. A. (2011). The organization of the forelimb representation of the C57BL/6 mouse motor cortex as defined by intracortical microstimulation and cytoarchitecture. *Cerebral Cortex*, *21*(4), 865–876. https://doi.org/10.1093/cercor/bhq159

Teyler, T. J., & DiScenna, P. (1986). The hippocampal memory indexing theory. *Behavioral Neuroscience*, *100*(2), 147–154. https://doi.org/10.1037//0735-7044.100.2.147

Thapa, R., Sparks, F. T., Hanif, W., Gulbrandsen, T., & Sutherland, R. J. (2014). Recent memory for socially transmitted food preferences in rats does not depend on the hippocampus. *Neurobiology of Learning and Memory*, *114*, 113–116. https://doi.org/https://doi.org/10.1016/j.nlm.2014.05.006

Thompson, L. T., & Best, P. J. (1990). Long-term stability of the place-field activity of single units recorded from the dorsal hippocampus of freely behaving rats. *Brain Research*, *509*, 299–308.

Thomson, A. M., & Lamy, C. (2007). Functional maps of neocortical local circuitry. *Frontiers in Neuroscience*, *1*(1), 19–42. https://doi.org/10.3389/neuro.01.1.1.002.2007

Todd, T. P., Mehlman, M. L., Keene, C. S., DeAngeli, N. E., & Bucci, D. J. (2016). Retrosplenial cortex is required for the retrieval of remote memory for auditory cues. *Learning & Memory*, *23*(6), 278–288. https://doi.org/10.1101/lm.041822.116

Todorovic, A., van Ede, F., Maris, E., & de Lange, F. P. (2011). Prior expectation mediates neural adaptation to repeated sounds in the auditory cortex: an MEG study. *The Journal of Neuroscience*, *31*(25), 9118. https://doi.org/10.1523/JNEUROSCI.1425-11.2011

Tolman, E. C. (1948). Cognitive maps in rats and men. *Psychological Review*, *55*(4), 189–208. https://doi.org/10.1037/h0061626

Tommerdahl, M., Favorov, O., Whitsel, B. L., Nakhle, B., & Gonchar, Y. A. (1993). Minicolumnar activation patterns in cat and monkey SI cortex. *Cerebral Cortex*, *3*(5), 399–411. https://doi.org/10.1093/cercor/3.5.399

Torii, M., Hashimoto-Torii, K., Levitt, P., & Rakic, P. (2009). Integration of neuronal clones in the radial cortical columns by EphA and ephrin-A signalling. *Nature*, *461*(7263), 524–528. https://doi.org/10.1038/nature08362

Trachtenberg, J. T., Chen, B. E., Knott, G. W., Feng, G., Sanes, J. R., Welker, E., & Svoboda, K. (2002). Long-term in vivo imaging of experience-dependent synaptic plasticity in adult cortex. *Nature*, *420*(6917), 788–794. https://doi.org/10.1038/nature01273

Treves, A. (2005). Frontal latching networks: a possible neural basis for infinite recursion. *Cognitive Neuropsychology*, *22*(3), 276–291. https://doi.org/10.1080/02643290442000329

Treves, A., & Rolls, E. T. (1994). Computational analysis of the role of the hippocampus in memory. *Hippocampus*, *4*(3), 374–391. https://doi.org/doi.org/10.1002/hipo.450040319

Tse, D., Langston, R. F., Kakeyama, M., Bethus, I., Spooner, P. A., Wood, E. R., Witter, M. P., & Morris, R. G. M. (2007). Schemas and memory consolidation. *Science*, *316*(5821), 76–82. https://doi.org/10.1126/science.1135935

Tse, D., Takeuchi, T., Kakeyama, M., Kajii, Y., Okuno, H., Tohyama, C., Bito, H., & Morris, R. G. M. (2011). Schema-dependent gene activation and memory encoding in neocortex. *Science*, *333*(6044), 891–895. https://doi.org/10.1126/science.1205274

Tulving, E. (1972). Episodic and semantic memory. In E. Tulving & W. Donaldson (Eds.), *Organization of Memory* (pp. 381–403). Academic Press.

Tulving, E., Schacter, D. L., McLachlan, D. R., & Moscovitch, M. (1988). Priming of semantic autobiographical knowledge: a case study of retrograde amnesia. *Brain and Cognition*, *8*(1), 3–20. https://doi.org/10.1016/0278-2626(88)90035-8

Turrigiano, G. G., Leslie, K. R., Desai, N. S., Rutherford, L. C., & Nelson, S. B. (1998). Activity-dependent scaling of quantal amplitude in neocortical neurons. *Nature*, *391*(6670), 892–896. https://doi.org/10.1038/36103

Ueta, Y., Otsuka, T., Morishima, M., Ushimaru, M., & Kawaguchi, Y. (2014). Multiple layer 5 pyramidal cell subtypes relay cortical feedback from secondary to primary motor areas in rats. *Cerebral Cortex*, *24*(9), 2362–2376. https://doi.org/10.1093/cercor/bht088

Umbach, G., Kantak, P., Jacobs, J., Kahana, M., Pfeiffer, B. E., Sperling, M., & Lega, B. (2020). Time cells in the human hippocampus and entorhinal cortex support episodic memory. *Proceedings of the National Academy of Sciences of the United States of America*, *117*(45), 28463–28474. https://doi.org/10.1073/pnas.2013250117

van der Zee, E. A., & Luiten, P. G. (1999). Muscarinic acetylcholine receptors in the hippocampus, neocortex and amygdala: a review of immunocytochemical localization in relation to learning and memory. *Progress in Neurobiology*, *58*(5), 409–471. https://doi.org/10.1016/s0301-0082(98)00092-6

van Groen, T., & Wyss, J. M. (1990a). The connections of presubiculum and parasubiculum in the rat. *Brain Research*, *518*(1–2), 227–243. https://doi.org/10.1016/0006-8993(90)90976-i

van Groen, T., & Wyss, J. M. (1990b). The postsubicular cortex in the rat: characterization of the fourth region of the subicular cortex and its connections. *Brain Research*, *529*(1–2), 165–177. https://doi.org/10.1016/0006-8993(90)90824-u

van Groen, T., & Wyss, J. M. (1992a). Connections of the retrosplenial dysgranular cortex in the rat. *The Journal of Comparative Neurology*, *315*(2), 200–216. https://doi.org/10.1002/cne.903150207

van Groen, T., & Wyss, J. M. (1992b). Projections from the laterodorsal nucleus of the thalamus to the limbic and visual cortices in the rat. *The Journal of Comparative Neurology*, *324*(3), 427–448. https://doi.org/10.1002/cne.903240310

van Groen, T., & Wyss, J. M. (2003). Connections of the retrosplenial granular b cortex in the rat. *The Journal of Comparative Neurology*, *463*(3), 249–263. https://doi.org/10.1002/cne.10757

van Kesteren, M. T. R., Ruiter, D. J., Fernández, G., & Henson, R. N. (2012). How schema and novelty augment memory formation. *Trends in Neurosciences*, *35*(4), 211–219. https://doi.org/10.1016/j.tins.2012.02.001

van Wijngaarden, J. B., Babl, S. S., & Ito, H. T. (2020). Entorhinal-retrosplenial circuits for allocentric-egocentric transformation of boundary coding. *eLife*, *9*, e59816. https://doi.org/10.7554/eLife.59816

Vann, S. D., & Aggleton, J. P. (2002). Extensive cytotoxic lesions of the rat retrosplenial cortex reveal consistent deficits on tasks that tax allocentric spatial memory. *Behavioral Neuroscience*, *116*(1), 85–94.

Vann, S. D., & Aggleton, J. P. (2004). Testing the importance of the retrosplenial guidance system: effects of different sized retrosplenial cortex lesions on heading direction and spatial working memory. *Behavioural Brain Research*, *155*(1), 97–108. https://doi.org/10.1016/j.bbr.2004.04.005

Vann, S. D., & Aggleton, J. P. (2005). Selective dysgranular retrosplenial cortex lesions in rats disrupt allocentric performance of the radial-arm maze task. *Behavioral Neuroscience*, *119*(6), 1682–1686. https://doi.org/10.1037/0735-7044.119.6.1682

Vattikuti, S., & Chow, C. C. (2010). A computational model for cerebral cortical dysfunction in autism spectrum disorders. *Biological Psychiatry*, *67*(7), 672–678. https://doi.org/10.1016/j.biopsych.2009.09.008

Vazdarjanova, A., Ramirez-Amaya, V., Insel, N., Plummer, T. K., Rosi, S., Chowdhury, S., Mikhael, D., Worley, P. F., Guzowski, J. F., & Barnes, C. A. (2006). Spatial exploration induces ARC, a plasticity-related immediate-early gene, only in calcium/calmodulin-dependent protein kinase II-positive principal excitatory and inhibitory neurons of the rat forebrain. *The Journal of Comparative Neurology*, *498*(3), 317–329. https://doi.org/10.1002/cne.21003

Vedder, L. C., Miller, A. M. P., Harrison, M. B., & Smith, D. M. (2017). Retrosplenial cortical neurons encode navigational cues, trajectories and reward locations during goal directed navigation. *Cerebral Cortex*, *27*(7), 3713–3723. https://doi.org/10.1093/cercor/bhw192

Vianna, M. R. M., Szapiro, G., McGaugh, J. L., Medina, J. H., & Izquierdo, I. (2001). Retrieval of memory for fear-motivated training initiates extinction requiring protein

synthesis in the rat hippocampus. *Proceedings of the National Academy of Sciences*, *98*(21), 12251–12254. https://doi.org/10.1073/pnas.211433298

Viard, A., Piolino, P., Desgranges, B., Chételat, G., Lebreton, K., Landeau, B., Young, A., De La Sayette, V., & Eustache, F. (2007). Hippocampal activation for autobiographical memories over the entire lifetime in healthy aged subjects: an fMRI study. *Cerebral Cortex*, *17*(10), 2453–2467. https://doi.org/10.1093/cercor/bhl153

Vogt, B. A., & Miller, M. W. (1983). Cortical connections between rat cingulate cortex and visual, motor, and postsubicular cortices. *The Journal of Comparative Neurology*, *216*(2), 192–210. https://doi.org/10.1002/cne.902160207

Wang, C., Chen, X., & Knierim, J. J. (2020). Egocentric and allocentric representations of space in the rodent brain. *Current Opinion in Neurobiology*, *60*, 12–20. https://doi.org/10.1016/j.conb.2019.11.005

Weiler, N., Wood, L., Yu, J., Solla, S. A., & Shepherd, G. M. G. (2008). Top-down laminar organization of the excitatory network in motor cortex. *Nature Neuroscience*, *11*(3), 360–366. https://doi.org/10.1038/nn2049

Whishaw, I. Q. (1995). A comparison of rats and mice in a swimming pool place task and matching to place task: Some surprising differences. *Physiology & Behavior*, *58*(4), 687–693. https://doi.org/https://doi.org/10.1016/0031-9384(95)00110-5

Whishaw, I. Q. (2000). Loss of the innate cortical engram for action patterns used in skilled reaching and the development of behavioral compensation following motor cortex lesions in the rat. *Neuropharmacology*, *39*(5), 788–805. https://doi.org/10.1016/s0028-3908(99)00259-2

Whishaw, I. Q., Maaswinkel, H., Gonzalez, C. L., & Kolb, B. (2001). Deficits in allothetic and idiothetic spatial behavior in rats with posterior cingulate cortex lesions. *Behavioural Brain Research*, *118*(1), 67–76. https://doi.org/10.1016/s0166-4328(00)00312-0

Whishaw, I. Q., & Tomie, J.-A. (1996). Of mice and mazes: similarities between mice and rats on dry land but not water mazes. *Physiology & Behavior*, *60*(5), 1191–1197. https://doi.org/10.1016/S0031-9384(96)00176-X

White, E. L., & Peters, A. (1993). Cortical modules in the posteromedial barrel subfield (Sml) of the mouse. *The Journal of Comparative Neurology*, *334*(1), 86–96. https://doi.org/10.1002/cne.903340107

White, N. M., & McDonald, R. J. (2002). Multiple parallel memory systems in the brain of the rat. *Neurobiology of Learning and Memory*, *77*(2), 125–184. https://doi.org/https://doi.org/10.1006/nlme.2001.4008

Whitlock, J. R., Heynen, A. J., Shuler, M. G., & Bear, M. F. (2006). Learning induces long-term potentiation in the hippocampus. *Science*, *313*(5790), 1093–1097. https://doi.org/10.1126/science.1128134

Wiener, S. I., Paul, C. A., & Eichenbaum, H. (1989). Spatial and behavioral correlates of hippocampal neuronal activity. *The Journal of Neuroscience*, *9*(8), 2737. https://doi.org/10.1523/JNEUROSCI.09-08-02737.1989

Wilber, A. A., Clark, B. J., Forster, T. C., Tatsuno, M., & McNaughton, B. L. (2014). Interaction of egocentric and world-centered reference frames in the rat posterior parietal cortex. *Journal of Neuroscience*, *34*(16), 5431–5446.

Wilson, M. A., & McNaughton, B. L. (1993). Dynamics of the hippocampal ensemble code for space. *Science*, *261*(5124), 1055–1058. https://doi.org/10.1126/science.8351520

Wilson, M. A., & McNaughton, B. L. (1994). Reactivation of hippocampal ensemble memories during sleep. *Science*, *265*(5172), 676–679. https://doi.org/10.1126/science.8036517

Wiltgen, B. J., & Silva, A. J. (2007). Memory for context becomes less specific with time. *Learning & Memory*, *14*(4), 313–317. https://doi.org/10.1101/lm.430907

Wiltgen, B. J., Zhou, M., Cai, Y., Balaji, J., Karlsson, M. G., Parivash, S. N., Li, W., & Silva, A. J. (2010). The hippocampus plays a selective role in the retrieval of detailed contextual memories. *Current Biology*, *20*(15), 1336–1344. https://doi.org/10.1016/j.cub.2010.06.068

Winkowski, D. E., & Kanold, P. O. (2013). Laminar transformation of frequency organization in auditory cortex. *The Journal of Neuroscience*, *33*(4), 1498. https://doi.org/10.1523/JNEUROSCI.3101-12.2013

Winocur, G. (1990). Anterograde and retrograde amnesia in rats with dorsal hippocampal or dorsomedial thalamic lesions. *Behavioural Brain Research*, *38*(2), 145–154. https://doi.org/10.1016/0166-4328(90)90012-4

Winocur, G., Frankland, P. W., Sekeres, M., Fogel, S., & Moscovitch, M. (2009). Changes in context-specificity during memory reconsolidation: Selective effects of hippocampal lesions. *Learning and Memory*, *16*(11), 722–729. https://doi.org/10.1101/lm.1447209

Winocur, G., Moscovitch, M., & Sekeres, M. (2007). Memory consolidation or transformation: context manipulation and hippocampal representations of memory. *Nature Neuroscience*, *10*(5), 555–557. https://doi.org/10.1038/nn1880

Winters, B. D., Tucci, M. C., Jacklin, D. L., Reid, J. M., & Newsome, J. (2011). On the dynamic nature of the engram: evidence for circuit-level reorganization of object memory traces following reactivation. *The Journal of Neuroscience*, *31*(48), 17719. https://doi.org/10.1523/JNEUROSCI.2968-11.2011

Wise, S. P., & Murray, E. A. (1999). Role of the hippocampal system in conditional motor learning: mapping antecedents to action. *Hippocampus*, *9*(2), 101–117. https://doi.org/10.1002/(SICI)1098-1063(1999)9:2<101::AID-HIPO3>3.0.CO;2-L

Witharana, W. K. L., Cardiff, J., Chawla, M. K., Xie, J. Y., Alme, C. B., Eckert, M., Lapointe, V., Demchuk, A., Maurer, A. P., Trivedi, V., Sutherland, R. J., Guzowski, J. F., Barnes, C. A., & McNaughton, B. L. (2016). Nonuniform allocation of hippocampal neurons to place fields across all hippocampal subfields. *Hippocampus*, *26*(10), 1328–1344. https://doi.org/10.1002/hipo.22609

Woolsey, T. A., & Van der Loos, H. (1970). The structural organization of layer IV in the somatosensory region (SI) of mouse cerebral cortex. The description of a cortical field composed of discrete cytoarchitectonic units. *Brain Research*, *17*(2), 205–242. https://doi.org/10.1016/0006-8993(70)90079-x

Wyss, J. M., & van Groen, T. (1992). Connections between the retrosplenial cortex and the hippocampal formation in the rat: a review. *Hippocampus*, *2*(1), 1–11. https://doi.org/10.1002/hipo.450020102

Xu, H., Jeong, H.-Y., Tremblay, R., & Rudy, B. (2013). Neocortical somatostatin-expressing GABAergic interneurons disinhibit the thalamorecipient layer 4. *Neuron*, *77*(1), 155–167. https://doi.org/https://doi.org/10.1016/j.neuron.2012.11.004

Xu, T., Yu, X., Perlik, A. J., Tobin, W. F., Zweig, J. A., Tennant, K., Jones, T., & Zuo, Y. (2009). Rapid formation and selective stabilization of synapses for enduring motor memories. *Nature*, *462*(7275), 915–919. https://doi.org/10.1038/nature08389

Yamawaki, N., Borges, K., Suter, B. A., Harris, K. D., & Shepherd, G. M. G. (2014). A genuine layer 4 in motor cortex with prototypical synaptic circuit connectivity. *eLife*, *3*, e05422. https://doi.org/10.7554/eLife.05422

Yamawaki, N., Li, X., Lambot, L., Ren, L. Y., Radulovic, J., & Shepherd, G. M. G. (2019). Long-range inhibitory intersection of a retrosplenial thalamocortical circuit by apical tuft-targeting CA1 neurons. *Nature Neuroscience*, *22*(4), 618–626. https://doi.org/10.1038/s41593-019-0355-x

Yamawaki, N., Radulovic, J., & Shepherd, G. M. G. (2016). A corticocortical circuit directly links retrosplenial cortex to M2 in the mouse. *The Journal of Neuroscience*, *36*(36), 9365. https://doi.org/10.1523/JNEUROSCI.1099-16.2016

Yang, G., Pan, F., & Gan, W. B. (2009). Stably maintained dendritic spines are associated with lifelong memories. *Nature*, *462*(7275), 920–924. https://doi.org/10.1038/nature08577

Yasumatsu, N., Matsuzaki, M., Miyazaki, T., Noguchi, J., & Kasai, H. (2008). Principles of long-term dynamics of dendritic spines. *Journal of Neuroscience*, *28*(50), 13592–13608. https://doi.org/10.1523/jneurosci.0603-08.2008

Yin, H. (2009). The role of the murine motor cortex in action duration and order. *Frontiers in Integrative Neuroscience*, *3*. https://www.frontiersin.org/article/10.3389/neuro.07.023.2009

Yiu, A. P., Mercaldo, V., Yan, C., Richards, B., Rashid, A. J., Hsiang, H.-L. L., Pressey, J., Mahadevan, V., Tran, M. M., Kushner, S. A., Woodin, M. A., Frankland, P. W., & Josselyn, S. A. (2014). Neurons are recruited to a memory trace based on relative neuronal excitability immediately before training. *Neuron*, *83*(3), 722–735. https://doi.org/10.1016/j.neuron.2014.07.017

Yoshimura, Y., Dantzker, J. L. M., & Callaway, E. M. (2005). Excitatory cortical neurons form fine-scale functional networks. *Nature*, *433*(7028), 868–873. https://doi.org/10.1038/nature03252

Yu, Y. C., Bultje, R. S., Wang, X., & Shi, S. H. (2009). Specific synapses develop preferentially among sister excitatory neurons in the neocortex. *Nature*, *458*(7237), 501–504. https://doi.org/10.1038/nature07722

Yu, Y. C., He, S., Chen, S., Fu, Y., Brown, K. N., Yao, X. H., Ma, J., Gao, K. P., Sosinsky, G. E., Huang, K., & Shi, S. H. (2012). Preferential electrical coupling regulates neocortical lineage-dependent microcircuit assembly. *Nature*, *486*(7401), 113–117. https://doi.org/10.1038/nature10958

Zhang, K., Ginzburg, I., McNaughton, B. L., & Sejnowski, T. J. (1998). Interpreting neuronal population activity by reconstruction: unified framework with application to hippocampal place cells. *Journal of Neurophysiology*, *79*(2), 1017–1044. https://doi.org/10.1152/jn.1998.79.2.1017

Zielinski, M. C., Shin, J. D., & Jadhav, S. P. (2019). Coherent coding of spatial position mediated by theta oscillations in the hippocampus and prefrontal cortex. *Journal of Neuroscience*, *39*(23), 4550–4565. https://doi.org/10.1523/JNEUROSCI.0106-19.2019

Ziv, Y., Burns, L. D., Cocker, E. D., Hamel, E. O., Ghosh, K. K., Kitch, L. J., Gamal, A. El, & Schnitzer, M. J. (2013). Long-term dynamics of CA1 hippocampal place codes. *Nature Neuroscience*, *16*(3), 264–266. https://doi.org/10.1038/nn.3329